Green Optical Networks

Xiaowen Dong

Submitted in accordance with the requirements for the degree of
Doctor of Philosophy

The University of Leeds
School of Electronic and Electrical Engineering

November 2012

The candidate confirms that the work submitted is his own, except where work which has formed part of jointly-authored publications has been included. The contribution of the candidate and the other authors to this work has been explicitly indicated below. The candidate confirms that appropriate credit has been given within the thesis where reference has been made to the work of others.

Chapter 4 is based on the work from:

Xiaowen Dong, Taisir El-Gorashi and Jaafar M. H. Elmirghani "IP Over WDM Networks Employing Renewable Energy Sources," IEEE/OSA Journal of Lightwave Technology, vol. 29, No. 1, pp. 3-14, 2011.

This paper has been published jointly with my supervisor Prof. Jaafar Elmirghani and Dr. Taisir Elgorashi.

Chapter 5 is based on the work from:

Xiaowen Dong, Taisir El-Gorashi and Jaafar M. H. Elmirghani, "Green IP Over WDM Networks with Data Centres", IEEE/OSA Journal of Lightwave Technology vol. 29, Issue: 12, pp. 1861 – 1880, 2011.

This paper has been published jointly with my supervisor Prof. Jaafar Elmirghani and Dr. Taisir Elgorashi.

Chapter 6 is based on the work from:

Xiaowen Dong, Taisir El-Gorashi and Jaafar M. H. Elmirghani, "On the Energy Efficiency of Physical Topology Design for IP over WDM Networks," IEEE/OSA Journal of Lightwave Technology, vol. 30, pp. 1931-1942, Issue: 12, 2012.

This paper has been published jointly with my supervisor Prof. Jaafar Elmirghani and Dr. Taisir Elgorashi.

Chapter 8 is based on the work from:

Xiaowen Dong, Ahamd Lawey, Taisir El-Gorashi and Jaafar M. H. Elmirghani, "Energy-efficient core networks," Optical Network Design and Modeling (ONDM), pp. 1-9, 2012.

This paper has been published jointly with my supervisor Prof. Jaafar Elmirghani, Dr. Taisir Elgorashi and Mr. Ahamd Lawey who is a PhD student in our research group. This paper includes three parts: energy efficient peer-to-peer networks, energy efficient data compression in optical networks and energy efficient topology design considering embodied energy in optical networks. I contributed these two parts: energy efficient data compression in optical networks and energy efficient topology design considering embodied energy in optical networks.

Acknowledgements

I would like to sincerely thank my supervisor, Prof. J. M. H. Elmirghani for his abundantly helpful and invaluable assistance, support, guidance and encouragement.

Also I would like to acknowledge Dr. T. H. Elgorashi, my academic advisor for about three years, for her useful advice and fruitful discussions.

Furthermore I would like to thank the students of the Communication Systems and Networks group in the School of Electronic and Electronic Engineering for their friendship and support.

I wish to express my love and gratitude to my beloved families. I am indebted to my parents, Hong Dong and Yuanzheng Shen for giving me the opportunity of studying aboard and their understanding and endless love, through the duration of my studies.

Finally, I would like to offer my regards to all of those who have supported and inspired me in any respect during the completion of this thesis. Special thanks go to my girlfriend Shanqing Dai for her patience, understanding, and support.

Abstract

In the last decade, the bandwidth of the Internet has grown by 50-100 times, thus more power consuming equipment (for example severs, amplifiers, routers, storage devices and communication links) has been deployed, which has led to an increase in the power consumption. It is expected that one of the bottlenecks in the development of ICT will be its power consumption. In order to overcome these problems, the "Green ICT" concept has been proposed which refers to attempts to achieve more energy efficiency and less pollution in the ICT industry.

Here, I focus on the design of optical networks taking power consumption into account, and develop new architectures, protocols, and algorithms to reduce the power consumption of the network.

In this thesis, a novel Mixed Integer Linear Programming (MILP) mathematical model and a novel Renewable Energy Optimisation routing heuristic (REO-hop) were proposed for the energy efficient optical network employing both renewable energy and non-renewable energy. Furthermore, to reduce the power consumption of wavelength division multiplexing (WDM) networks that serve data centres, novel MILP models were proposed to optimise the locations of data centres with and without renewable energy respectively. Moreover to exploit energy reduction in content distribution networks, we also proposed and evaluated a new approach (Energy Delay Optimisation Routing-EDOR). To incorporate the impact of topology, we studied energy efficient physical topologies design, considering operational and embodied energy of network devices, by proposing a novel MILP model. The Routing and Wavelength Assignment (RWA) problem in WDM networks was reconsidered by jointly optimising delay, power consumption and electricity cost using novel MILP models. To further reduce the power consumption of optical networks, novel MILP models for data compression and a novel routing algorithm were proposed. In addition, a novel MILP model to investigate the energy efficiency of orthogonal frequency division multiplexing (OFDM) based optical networks was also proposed. Extensive simulations and analysis is provided and novel observations are presented in this thesis.

Table of Contents

List of Figures

List of Tables

List of Abbreviations

ACK	Acknowledgement
ALR	Adaptive Link Rate
ASON	Automatic Switched Optical Network
ATM	Asynchronous Transfer Mode
BBN	Bayesian Belief Network
BER	Bit Error Rate
BS	Base Stations
CO-D	Coherent Detection
CPE	Customer Premises Equipment
CP	Cyclic Prefix
CST	Central Standard Time
DAC	Digital-to-Analog Conversion
DD	Direct Detection
DFS	Dynamic Frequency Scaling
DIA	Delta-Improvement Algorithm
DML	Directly Modulated Laser
DMS	Decision Management System
DSL	Digital Subscriber Line
DVS	Dynamic Voltage Scaling
EDFA	Erbium Doped Fibre Amplifier
EDOR	Energy-Delay Optimal Routing
EEKM	Energy-Efficient Key Management
EML	Externally Modulated Laser
EPnP	Energy-aware Plug and Play
EST	Eastern Standard Time
ETE	Energy-Aware Traffic Engineering
FC	Fan Controller
FDLs	Fibre Delay Lines
FSO	Free Space Optical

FTTH	Fibre-to-the-Home
GA	Genetic Algorithm
GHG	Green House Gases
GIF	Graphics Interchange Format
GMPLS	Generalised Multiprotocol Label Switching
ICT	Information and Communication Technology
IFFT	Inverse Fast Fourier Transformation
IM	Intensity Modulation
IP	Internet Protocol
IPTV	Internet Protocol Television
ISP	Internet Service Providers
ITU	International Telecommunication Union
JPEG	Joint Photographic Experts Group
LAN	Local Area Network
LCA	Life Cycle Analysis
LCP	Least-Cost Path
LEACH	Low Energy Adaptive Clustering Hierarchy
LFA	Least Flow Algorithm
LFC	Light-Forest Construction
LFM	Linear Field Modulation
LLT	Low-Load Threshold
MAN	Metropolitan Area Network
MECH	Maximum Energy Cluster Head
MEMS	Micro-electromechanical Systems
MIA	Max-Improvement Algorithm
MILP	Mix Integer Linear Programming
MLBs	Multiprocessor-Based Linecards
MLR	Mixed Line Rate
MLTE	Multilayer Traffic Engineering
MPEG	Motion Picture Experts Group
MS	Mobile Stations
MSC	Module Service Card
MST	Mountain Standard Time
MUP	Most-Used Path

MZM	Mach-Zehnder Modulator
NEEM	Network Energy Efficiency Manager
NMS	Network Management System
NSFNET	National Science Foundation network
OADM	Optical Add/drop Multiplexer
OBS	Optical Burst Switching
OCS	Optical Circuit Switching
OEO	Optical-Electrical-Optical
OFDM	Orthogonal Frequency Division Multiplexing
OLMUP	Ordered-Lightpath Most- Used Path
OLT	Optical Line Terminal
ONUs	Optical Network Units
OPS	Optical Packet Switching
ORM	Optical Receiver Module
OSNR	Optical Signal-to-Noise Ratio
OSPF	Open Shortest Path First
OTDM	Optical Time Division Multiplexing
OTM	Optical Transmitter Module
OTN	Optical Transport Network
OXC	Optical Crossconnect
PBT	Polybutylene Terephthalate
PCB	Printed Circuit Board
PEGASIS	Power-efficient Gathering in Sensor Information Systems
PLIM	Physical Layer Interface Module
PNG	Portable Network Graphic
PON	Passive Optical Network
PSK	Phase-Shift Keying
PST	Pacific Standard Time
PUE	Power Usage Effectiveness
QAM	Quadrature Amplitude Modulation
QoS	Quality of Service
QoT	Quality of Transmission
RAM	Random Access Memory

REO-hop	Renewable Energy Optimisation hop
RP	Router Processor
RSOA	Reflective Semiconductor Optical Amplifier
RSVP-TE	Resource Reservation Protocol-Traffic Engineering
RWA	Routing Wavelength Assignment
SCM	Sub-Carrier Multiplexing
SDH	Synchronous Digital Hierarchy
SM	Switch Module
SONET	Synchronous Optical Network
SPF	Shortest Path First
STB	Set-Top Box
TDM	Time Division Multiplexing
TDP	Time-Driven Priority
TDS	Time-Driven Switching
TEEN	Threshold sensitive Energy Efficient Sensor Network
USNET	Unite State network
VoD	Video-on-Demand
WDM	Wavelength Division Multiplexing
WiMAX	IEEE 802.16e
WSNs	Wireless Sensor Networks
WSONs	Wavelength Switched Optical Networks

Chapter 1: Introduction

Information and Communication Technology (ICT) plays an important role in our lives. ICT brings us remarkable advantages and conveniences, helping us to realise the dream of long-distance and high-speed data communication, allowing information to be shared anywhere at any time. The increasing popularity of intensive data applications such as high-definition IPTV video conferencing and data migration is encouraging the development of fast, reliable and efficient ICT infrastructure.

In the last decade, Internet traffic has approximately doubled each year and the bandwidth of the Internet has grown by at least fifty to a hundred percent [1]. Although the development in ICT technologies appeared sufficient to cope with the increasing traffic in networks in the last 10 years; the explosive growth of data traffic has exceeded expectations by far. As early as 2001, it was pointed out that the progress in transmitting technology could probably not be sustained for more than a few years once the growth in data traffic starts leading to traffic tripling (or growing faster) each year [2]. Traffic is currently growing at about 40% per year and therefore is doubling approximately every 2 years [3].

In order to satisfy the sustained growth of data traffic, new network technologies and structures have to be developed. For example, with the evolution of materials for communications, electrical cables have been replaced by optical fibres, thus the bandwidth of the communications channels has increased from kbit/s to Tbit/s. By introducing Wavelength Division Multiplexing (WDM) technology into optical networks, the bandwidth of optical fibre entered a new level. Currently the data transmission speed in a single optical fibre can exceed 100 Tb/s [4].

However to meet demand both new equipment (severs, amplifiers, IP routers, storage devices and transponders) and new network architectures are needed. The additional network equipment consumes significant amounts of energy, which becomes a major contributor to the total energy demand in many developed countries.

For example, in Europe the energy consumption of the Telecom Italia network had reached more than 2 TWh in 2007, which is about 1% of the total Italian energy demand; increasing by 7.95% with respect to the 2005 level [5]. The same problem is faced by British Telecom, who used about 0.7% of the total UK's energy consumption in the winter of 2007, making it the biggest single power consumer in the country [6]. In Asia, a report issued by the Ministry of Internal Affairs and Communications in Japan concluded that ICT equipment (routers, servers, PCs and network systems) consumed 4% of the total electricity generated in Japan in 2006 (45 TWh). Over the past five years the figure has grown by more than 20% [7]. The situation is at its worst in the United States, where Internet equipment consumes roughly 8% of the total electric energy, with a further expected growth of 50% within the next decade [8]. Today, around 1% of the total worldwide energy consumption in broadband-enabled counties is consumed by ICT; the value could rise to 4% in the future [9].

The power consumption of telecommunication equipment has rapidly grown over recent years. The typical router capacity has increased from 100 Gbit/s in 2000 to 10 Tbit/s in 2008, with the power consumption increasing from 1.7 kW to 50 kW [10]. ICT and telecommunications equipment continue to consume significant amounts of power, even in the idle (not the 'sleep') state. The power wastage is significant given that typical router utilisation figures are 20% - 50% in the Internet Service Providers (ISP) backbone, 8% - 25% in enterprise networks and less than 1% in LANs. In ICT equipments, about 20% of the lifetime energy consumption is used in manufacturing and 80% is consumed during the usage of the product in its lifetime [11]. From the data mentioned above, it can be predicted that the bottleneck of ICT development can become its energy consumption rather than its capacity, speed and other elements.

Official studies have shown that the ICT industry is responsible for 2% of the global CO_2 emissions which is on a par with the aviation industry; this proportion is growing rapidly. For instance, more than six million PCs were left on over Christmas 2006; with the inclusion of printers and other hardware, 19,000 tonnes of CO_2 were produced [12]. In practice, approximately 228 grams of CO_2 are produced by a network component that consumes 1 kWh of traditional electricity power produced from coal or natural gas [13]. A family vehicle typically emits 150g of CO_2 perkm. Therefore in a year a 1 kW router port contributes CO_2 pollution equivalent to an approximately 13,000 kilometre journey by a family vehicle. If the network can be designed so that it eliminates 1 kW of non-renewable power consumption, then this will lead to a significant reduction in CO_2 emissions of about 2 tones every year.

All the evidence suggests that the ICT industry is likely to contribute to global warming and environment deterioration. These dangerous signals have wakened the public awareness. Based on these problems, "Green ICT" approaches have started being introduced. Gupta *et al.* pioneered the concept of "greening the Internet" in 2003 [14] Substantial amounts of energy can be saved through the innovative use of renewable sources and the development of new architectures, protocols, and algorithms operating on this hardware. BT has announced plans to develop wind farms to generate 25% of its electricity needs by 2016. This will save 500,000 tonnes of CO_2 each year, the equivalent of a quarter of a million return air trips to New York.

It is encouraging that energy consumption in backbone networks has been receiving attention recently. There are two main reasons: first, the percentage that backbone networks are responsible for of the total network energy consumption is expected to significantly increase with the growing popularity of bandwidth intensive applications such as high-definition IPTV. Secondly, as the energy consumption of the backbone network is limited to a few locations, heat dissipation becomes an important issue to consider. Efforts to reduce the impact of energy consumption in backbone networks have been mostly concentrated on improving the energy efficiency of individual network components or whole network systems. In backbone networks, equipment level techniques are based on using power saving modes when the equipment is underutilised, or in improving the energy efficiency of

hardware parts and operations. Additionally, network level techniques manipulate the energy usage of components by consolidating traffic; achieving energy savings in the system as a whole.

In addition to this, energy consumption and heat dissipation are becoming increasingly primary objectives in large-scale core router design. The energy consumption of data centres is increasing rapidly with the incredible growth of data-intensive applications such as medical informatics, nuclear research, genomics and satellite weather image analysis. The network infrastructure for data centres alone is responsible for 23% of the overall power consumption of networks excluding the energy used for equipment cooling [15].

The "greening" of data centres creates challenges for storage and network designers in reducing energy consumption, while still maintaining the performance and cooling constraints. The primary goal is usually to reduce the ratio of the facility to the IT equipment power usage; called Power Usage Effectiveness (PUE), by increasing the efficiency of the cooling and power distribution systems [16]. Nevertheless, neither the energy efficiency of IT components' nor their level of utilisation is measured by the PUE. The former is improved by technological advancements at the equipment level, while the latter requires the consolidation of resources. Currently, virtualisation is a key tool for achieving this goal through the incorporation of multiple operating environments on the same machine and the migration of workloads inside or between data centres [17].

Although recently significant research efforts have been dedicated to reducing the energy consumption of networks, a large number of energy efficient solutions are concentrating on wireless networks and computer architecture. Therefore, many issues need to be investigated to develop and deploy energy efficient wire-line core networks which typically use optical and IP technologies.

1.1 Research Objectives

The primary research objectives of the work presented in this thesis are as follows:

- To reduce the non-renewable power consumption of backbone IP over WDM networks by employing renewable energy sources and to develop mixed integer linear programming (MILP) models to optimise the utilisation of renewable energy and optimise the location of nodes employing renewable energy,

- Investigate IP over WDM networks with data centres where data centres create a hot node scenario with high energy consumption. Firstly, to determine the optimal location of data centres in an IP over WDM network. Secondly, to study content replication. Thirdly, investigate the problem of whether to locate data centres next to renewable energy sources or to transmit renewable energy to data centres,

- Optimisation the physical topology of IP over WDM networks to minimise the total power consumption of the network considering operational and embodied energy (embodied energy is the energy used to manufacture components),

- To find out the trade-off point among optimising power, delay and electricity cost in IP over WDM networks considering unicasting and anycasting scenarios,

- Investigate the problem of energy efficient data compression for IP over WDM networks while considering the physical optical channel performance and identify the optimum data compression ratio,

- Compare the power consumption of WDM networks to OFDM-based elastic optical networks and optimise both networks.

1.2 Original Contributions

The major contributions of this thesis are summarised as follows:

1. Mixed Integer Linear Programming (MILP) models have been developed for minimising the non-renewable energy consumption and optimising the

location of nodes employing renewable energy in IP over WDM networks. A new routing algorithm (Renewable Energy Optimisation hop, REO-hop) has been set up to minimise the non-renewable energy consumption in the hybrid power IP over WDM network and a simulator has been developed to evaluate the performance the proposed routing algorithm.

2. MILP models have been developed to investigate the optimal locations of data centres in the normal IP over WDM network and hybrid power IP over WDM network, separately. A MILP model for optimising the location of content replication in data centres networks has also been proposed. A new routing algorithm (Energy-delay Optimal Routing, EDOR) has been proposed for minimising the energy consumption of IP over WDM networks with data centres using a replication scheme while maintaining the propagation delay. A simulator has been developed to evaluate the performance of the proposed routing algorithm.

3. The embodied energy of optical network devices has been determined (for the first time) using Life Cycle Analysis (LCA). A useful outcome for the research community, also used in the study in 4 below.

4. MILP models have been proposed for optimising the physical topology in IP over WDM networks considering both the operational and (for the first time in core networks) the embodied energy. The results with two traffic profiles: symmetric and asymmetric (presence of data centres) traffic are compared.

5. MILP models have been developed for jointly optimising the power, delay and electricity cost in IP over WDM networks under a unicasting scenario and an anycasting scenario, separately.

6. The relationships between power consumption and the data compression ratio, between data compression ratio and BER have been investigated. A MILP model has been built for optimising the data compression ratio of IP over WDM networks to minimise the total power consumption of the network. A new energy efficient data compression routing algorithm has also been proposed.

7. The power consumption of optical OFDM-based network devices has been analysed and MILP models have been developed to minimise the power consumption of the optical OFDM-based networks and the spectrum efficiency of these power minimised elastic OFDM based networks has been determined.

1.3 Related Publications

The original contributions of this thesis are supported by the following publications:

- **International Journals**

1. Xiaowen Dong, Taisir El-Gorashi and Jaafar M. H. Elmirghani "IP Over WDM Networks Employing Renewable Energy Sources," *IEEE/OSA Journal of Lightwave Technology,* vol. 29, No. 1, pp. 3-14, 2011.

2. Xiaowen Dong, Taisir El-Gorashi and Jaafar M. H. Elmirghani, "Green IP Over WDM Networks with Data Centres", *IEEE/OSA Journal of Lightwave Technology* vol. 29, Issue: 12, pp. 1861 – 1880, 2011.

3. Xiaowen Dong, Taisir El-Gorashi and Jaafar M. H. Elmirghani, "On the Energy Efficiency of Physical Topology Design for IP over WDM Networks," *IEEE/OSA Journal of Lightwave Technology,* vol. 30, pp. 1931-1942, Issue: 12, 2012.

4. Xiaowen Dong, Taisir El-Gorashi and Jaafar M. H. Elmirghani, "Energy Efficient Optical Networks with Minimised Non-Renewable Power Consumption," *Journal of Network (JNW)*, vol. 7, no. 5, pp. 821-831, 2012.

5. Xiaowen Dong, Taisir El-Gorashi and Jaafar M. H. Elmirghani, "On the use of Renewable Energy in an IP over WDM Network with Data Centres," *IET Optoelectronics*, vol. 6, no. 4, pp. 155-164, 2012.

- **International Conferences**

6. Xiaowen Dong, Taisir El-Gorashi and Jaafar M. H. Elmirghani, "Renewable Energy in IP over WDM Network,", *Proc. 12th International Conference on Transparent Optical Networks (ICTON 2010)*, pp. 1-8, Aug, 2010.

7. Xiaowen Dong, Taisir El-Gorashi and Jaafar M. H. Elmirghani, "Hybird-power IP over WDM network," *Proc. 7th International Conference on Wireless and Optical Communications Networks (WOCN 2010)*, pp. 1-5, Sep, 2010.

8. Xiaowen Dong, Taisir El-Gorashi and Jaafar M. H. Elmirghani, "An Energy Efficient IP over WDM Network," *IEEE/ACM International Conference on Green Computing and Communications (Greencom 2010)*, pp: 292-299, Dec, 2010.

9. Xiaowen Dong, Taisir El-Gorashi and Jaafar M. H. Elmirghani, "Renewable Energy for Low Carbon Emission IP over WDM Networks," *Proc. of 15th Optical Network Design and Modelling (ONDM 2011)*, pp. 1-6, Feb, 2011.

10. Xiaowen Dong, Taisir El-Gorashi and Jaafar M. H. Elmirghani, "Energy-efficient IP over WDM Networks with Data Centres,", *Proc.13h International Conference on Transparent Optical Networks (ICTON 2010)*, pp. 1-8, Jun, 2011.

11. Xiaowen Dong, Taisir El-Gorashi and Jaafar M. H. Elmirghani, "Low Carbon Emission IP over WDM Network," *Proc. of IEEE International Conference on Communication, ICC 2011*, pp. 1-6, Jun, 2011.

12. Xiaowen Dong, Taisir El-Gorashi and Jaafar M. H. Elmirghani, "Green IP over WDM Networks: Solar and Wind Renewable Sources and Data Centres", *Proc. of IEEE Global Communication Conference (GLOBECOM 2011)*, pp. 1-6, Dec, 2011.

13. Xiaowen Dong, Ahmed Lawey, Taisir El-Gorashi and Jaafar M. H. Elmirghani, "Energy-Efficient Core Networks," *Proc. of IEEE Optical Network Design and Modelling (ONDM) conference*, 17-20 April, 2012.

- **Book Chapter**

14. Y. Audzevich, A. Moore, A. Rice, R. Sohan, S. Timotheou, J. Crowcroft, S. Akoush, A. Hopper, A. Wonfor, H. Wang, R. Penty, I. White, X. Dong, T. El-Gorashi and J. Elmirghani, "Intelligent Energy Aware Networks" in the book "Handbook of Energy-Aware and Green Computing," ISBN-10: 1439850402, ISBN-13: 978-1439850404, Chapman and Hall/CRC Press.

1.4 Organisation of the Thesis

Following the introduction in Chapter 1, the remaining parts of this thesis are organised as follows:

Chapter 2 reviews the evolution of optical networks and the three main optical switching techniques. Special attention is given to IP over WDM networks to facilitate understanding the architectures proposed in the following chapters.

Chapter 3 reviews the major energy efficiency approaches proposed for use in communication networks. The current energy efficient solutions for networks are discussed focusing on four aspects: energy efficient topologies, energy efficient protocols, energy efficient architectures and energy efficient network management.

Chapter 4 introduces a new energy efficient hybrid power IP over WDM network architecture. Mathematical models and a new routing algorithm to minimise the non-renewable power consumption of network are presented. In addition to get further non-renewable power reduction in networks, an adaptive link rate technique is introduced. The MILP mathematical model and the heuristic are evaluated considering two different network topologies, NSFNET and USNET.

Chapter 5 investigates the problem of the optimal location of data centres in IP over WDM networks, with and without renewable energy. In addition to the

mathematical models, a replication scheme that replicates the content in different data centres is studied. Due to the popularity of certain content, replication is used to reduce the power consumption of networks. Based on the replication scheme, a new routing algorithm is introduced and shown to reduce the power consumption while maintaining the propagation delay. Simulation results are presented and analysed.

Chapter 6 investigates the optimal physical topologies that minimise the operational energy and embodied energy of the network. Using embodied energies of different materials, the embodied energy of optical network devices is determined. MILP mathematical models are introduced for optimising the physical topology under symmetric and asymmetric traffic.

In Chapter 7 the joint optimisation of power, delay and electricity cost in IP over WDM networks is studied. Both MILP mathematical models and simulation results are discussed under unicasting and anycasting scenarios.

In Chapter 8, a MILP model is given to optimise the data compression ratio along with minimising the total energy consumption of IP over WDM networks as the objective.

Chapter 9 analyses the power consumption of OFDM-based optical networks and introduces a MILP mathematical model to minimise the power consumption of elastic optical networks.

Finally, the thesis is concluded in Chapter 10. The major contributions of this work are summarised and proposals for future works are given.

Chapter 2: Optical Networks and Mixed Integer Linear Programming

2.1 Introduction

In this chapter, we mainly review the evolution of optical networks and introduce the basic concepts of WDM networks. We also discuss the advantages and limitations of the main optical switching techniques. Furthermore, the concept of IP over WDM networks and Mixed Integer Linear Programming (MILP) are presented to help understanding the new mathematic models, new architectures and routing algorithms proposed in the rest of this thesis.

2.2 Evolution of Optical Networks

Since the "optical telegraph" was invented by Claude Chappe in the 1790s, optical communication systems have made significant progress. After centuries of development and in particular the invention of the laser and optical fibres in the 1960s, optical communication became very popular. In 1970 researchers designed single-mode fibres whose loss was below 20 dB/km at 633 nm [18]. Due to high attenuation, such fibres were not used to operate the telephone network. In the 1980s when the attenuation of optical fibres became as low as 0.5 dB/km, long-distance telephone networks and national backbone networks based on optical fibres started to see field deployment [18]. After the opening of the 1310nm and 1550 nm optical communication windows (through the design of optimised fibres, sources and detectors) optical fibre loss was further reduced to 0.2 ~ 0.3 dB/km. Recently

photonic crystal fibres have become attractive in terms of their characteristics which cannot be provided by ordinary optical fibres. Compared to copper cable, optical fibre provides lower error rate and higher capacity. Furthermore copper cables have been replaced by optical fibres. All the improvements in optical fibres motivated the development of optical networks.

In the first generation optical networks, optical devices were only used for information transmission. All switching and other intelligence functions in networks were implemented by electronic devices. A typical example is the Synchronous Optical Network (SONET), which commonly multiplexes channels of 64 kbit/s into data frames with data rates between 155 Mbit/s and 2.5 Gbit/s [19]. In such kinds of optical networks, both the traffic passing by and ending at a node is converted from the optical domain to the electrical domain and switched electronically to an output port (including a port that can drop traffic locally). Following electronic switching, the traffic passing by a node is converted back to the optical domain before departing from the node. With the increase in data transmission rate, electrical switching and optical-electrical-optical (OEO) conversion result in a significant growth in complexity and cost for electronic devices [20]. Therefore, reducing the burden placed on the underlying electronic devices in a node and removing electronic switching for traffic passing by a node became key factors in the development of second generation optical networks.

In order to improve capacity in second generation optical networks different multiplexing strategies were proposed. In optical networks there are two basic multiplexing technologies: Optical Time Division Multiplexing (OTDM) and WDM. In OTDM, lower bit rate optical streams are assigned to different time slots on the multiplexed channel [21]. This is in contrast to Time Division Multiplexing (TDM) which is implemented in electrical domain. OTDM however requires specific optoelectronic devices such as pulsed semiconductor lasers and optical switches. The optical pulses used in OTDM transmission should satisfy several requirements. First the pulse width of the optical signal pulse, which determines the upper bound on the achievable bit rate, must be less than the time slot associated with the desired bit rate. Secondly, the spectral width of the optical signal should be extremely narrow for a given pulse width as the spectral width of the pulse determines the impact of the fibre chromatic dispersion [22]. Currently, using Femtosecond pulses,

OTDM transmission can reach data rates of 1.28 Tb/s over 70 km [23], however single high data rate channels are not very desirable as flexibility/granularity is lost specially that typical individual user rates currently are below 40 Gbit/s.

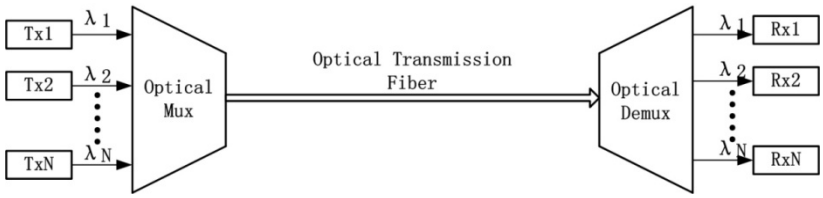

Fig 2 - 1: A point-to-point WDM Transmission Configuration [20]

WDM technology is very similar to Frequency Division Multiplexing (FDM), which can allow multiple non-overlapping wavelength channels to transmit in the same optical fibre link. Each of these channels can operate at a different data rate with typical rates being 10 Gbit/s, 40 Gbit/s and 100 Gbit/s currently [24]. Fig 2-1 shows a basic point-to-point WDM transmission configuration. At the transmitter, different wavelengths ($\lambda_1 \sim \lambda_N$) are multiplexed in the same fibre [20]. At the receiver these wavelengths are split back out, or demultiplexed, into separate fibres. Essentially, the bandwidth capacity of the optical fibre is multiplied by the number of wavelengths multiplexed onto it. Each wavelength being an independent channel can transmit data at a different rate. In addition to increasing the bandwidth, consequently reducing the optical fibre cable cost and use of equipment, WDM also gives the great advantage of transparency which allows different network technologies (SONET, IP, Asynchronous Transfer Mode (ATM), etc) to use the same physical transmission infrastructure [20].

Commonly, WDM is divided into different wavelength density classes: Coarse WDM (CWDM) and Dense WDM (DWDM) [25]. The first generation of WDM technology utilised two wavelengths, 1310 nm and 1550 nm. It was implemented using off-the-shelf optical transmitters (meant for single channel operation at the 1310nm and 1550nm windows) without tight control of wavelengths. Because of the simple implementation and lower number of multiplexed wavelengths, the optical multiplexers and demultiplexers are low cost and low in insertion loss [25]. To further increase the capacity of optical fibres, in 2003 the International Telecommunication Union (ITU) standardised a channel grid for use with CWDM wavelengths, using 18 CWDM wavelengths from 1271 nm to 1611 nm with a

channel spacing of 20 nm [26]. The wavelengths in DWDM, are spaced closer than in CWDM, therefore DWDM offers higher capacity. Currently, DWDM can allow up to 100 wavelengths per fibre (DWDM ITU grid) offering a single fibre capacity beyond 4 Tb/s [27]. However, the requirement of tight control over the wavelengths under all operating temperature conditions result in higher cost for DWDM equipment compared to CWDM.

Combining WDM technology with the adoption of many different mature technologies allowed second generation optical networks to support wavelength-routing. The key components of the second generation networks included: Optical Line Terminals (OLT) [28], Optical Add/drop Multiplexers (OADM) [29], Erbium Doped Fibre Amplifiers (EDFA) [30] and Optical Crossconnects (OXC) [31]. Commonly, OLTs are installed at the end of point-point WDM links. OADMs can drop or add some wavelengths at intermediate nodes without any OEO conversion processing. Similarly to OADMs, OXCs can switch a large number of wavelengths, from tens to thousands. All of the above mentioned components can eliminate OEO conversion and provide lightpaths across the network. Therefore, the second generation optical networks provide much higher bandwidths, larger capacities and also improve the flexibility and transparency of networks.

The third generation of optical networks were developed based on the all-IP and all-optical based approach, i.e. retain the IP layer for applications and the optical layer for capacity and eliminate all the intermediate layers such as SONET, ATM etc. However, packet services, rather than conventional WDM systems that provide fixed bandwidths are needed [32]. Therefore, appropriate optical switching techniques, such as, Optical Packet Switching (OPS) and Optical Burst Switching (OBS) were proposed, although OPS and OBS are not part of the third generation IP over WDM networks and may appear in future generations. In the next section, the main optical switching techniques will be reviewed.

The last section of the network, closest to the users, is the access network. Digital Subscriber Line (DSL) was the first widely used broadband technology to provide Internet access by transmitting digital data over the local telephone network twisted wire pairs. Because the bandwidth of the cable is limited, DSL can provide data rates up to 30 Mbit/s normally [33]. Even current DSL technologies, such as the

latest “NodeScale Vectoring” technology (which enables 100 Mbit/s and higher DSL access speed capability [34]) may not be able to handle the future growth in the number of end users and requirements in terms of network services. To replace DSL technologies, the higher bandwidth Fiber-to-the-Home (FTTH) solution was proposed. It has recently surpassed 75 million users and is continuing to grow at a rapid rate [35]. To realise various FTTH solutions, Passive Optical Networsk (PONs) have been considered the most promising technology. Developing from initial Broadband PON (BPON, 155 Mbit/s to 622 Mbit/s) and Ethernet PON (EPON, 1.2 Gbit/s), next generation Gigabit-Capable PON based on the International Telecommunication Union-Telecommunication Sector (ITU-T) G.987.1 standard is expected to deliver downstream speed at up to 10 Gbit/s [36, 37].

2.3 Optical Switching Techniques

In optical networks, there are three main optical switching techniques: Optical Circuit Switching (OCS), Optical Packet Switching (OPS) and Optical Burst Switching (OBS). OCS and OPS were first developed based on conventional circuit switching and packet switching. Though OCS and OPS have their own particular applications, both techniques have significant drawbacks and limitations. Recently, OBS proposed to combine the advantages of OCS and OPS to overcome their limitations. In this section, the benefits and limitations of these three main optical switching techniques are discussed.

2.3.1 Optical Circuit Switching

OCS was the first optical switching technique used in optical networks. In an OCS based optical network, a dedicated wavelength on each link is used to establish physical connections between pairs of source and destination nodes through switching nodes [20]. Therefore, the end-to-end paths from source nodes to destination nodes are connected sequences of physical links between nodes. At each switching node the incoming data is switched to the appropriate outgoing link. Three phases are involved in an OCS process: circuit establishment, data transfer and

circuit disconnection. The circuit establishment must be finished before data transmission begins [38]. The circuit establishment phase is a two-way reservation overhead for setting up a lightpath. First a source issues a requirement for setting up a circuit link, and then waits for an acknowledgment from the corresponding destination. [20].

OCS is suitable for large data transmissions that need long connection hold times and therefore are widely used in core networks. A key challenge in the practical implementation of OCS based optical networks is the development of efficient algorithms and protocols for establishing lightpaths [39]. To date many Routing and Wavelength Assignment (RWA) algorithms, that select the routes and assign wavelengths to all optical circuits efficiently, have been proposed and developed [40, 41]. Furthermore, dynamic signalling protocols have also been proposed to manage connections, distribute control messages and network state information in SONET and WDM networks. These signalling and control protocols include the Generalised Multiprotocol Label Switching (GMPLS) control plane, which uses the same mechanisms as Multiprotocol Label Switching (MPLS) to manage a circuit [42] and also the Automatic Switched Optical Network (ASON). The goal of these approaches is to specify a common control plane for providing QoS and equipment interoperability across domains and carriers [43].

OCS techniques have some drawbacks. A major issue is that each wavelength must be dedicated between sources and destinations (if no wavelength conversion is used), and cannot allow grooming or statistical multiplexing, which results in low channel efficiency. Another issue is that for bursty traffic, the setup time of a lightpaths can be longer than the burst duration. This results in low bandwidth utilisation. Therefore the development of alternative switching techniques which are suitable for bursty traffic is essential.

2.3.2 Optical Packet Switching

OPS techniques are developed based on mature packet switching concepts, which are widely used in computer networks. It should be noted however that unlike the concepts, some of the optical technologies needed to realise OPS are still lacking.

For example to date there are no viable optical memories [44] Taking full advantage of the available resources and occupying the wavelength only when data has to be sent, a significant statistical multiplexing gain can be provided by OPS as the bandwidth can be shared by multiple data flows. In OPS based optical networks, traffic data is divided and assembled in the payload with a preceding header that contains the destination information. The intermediate nodes function as packet routers, based on the header information, to decide where packets should be forwarded.

However, as mentioned earlier, there are some main reasons that make the implementation of all-optical OPS difficult. The two main obstacles are the need for all-optical packet header processing and the lack of optical Random Access Memory (RAM) [45] Therefore, hybrid OPS approaches, employing OEO conversion have been proposed, such as the relatively complex approach where the packet header is processed in the electrical domain [46]. To attach the header to a packet, different techniques have been proposed; such as transmitting headers and payloads on separate wavelengths, sub-carrier multiplexing (SCM) [47, 48] and serial transmission of headers and payloads on the same wavelength [49]. As the header is separated from the payload and its bit rate is lower than the payloads, electrical processing is feasible. Alternative approaches for the lack of optical RAM have also been proposed based on Fibre Delay Lines (FDLs) [50] and deflection routing [51]. Furthermore, other relevant technologies are needed for OPS and are not fully developed such as burst mode optical packet synchronisation, regeneration, wavelength conversion and packet oriented optical switching fabric [52].

2.3.3 Optical Burst Switching

OBS is proposed to overcome the limitations of OCS and OPS. In OBS, the switching granularity is at the burst level, rather than the wavelength level in OCS (holding time of minutes to months) and the packet level (ms level) in OPS. OBS provides statistical multiplexing and only the wavelength of the control packet (sent ahead of the burst to align switches and reserve wavelengths and other resources) needs OEO conversion at intermediate nodes [53]. Therefore, compared to OPS,

OBS has better transparency. Fig 2-2 gives a simple OBS based optical network architecture.

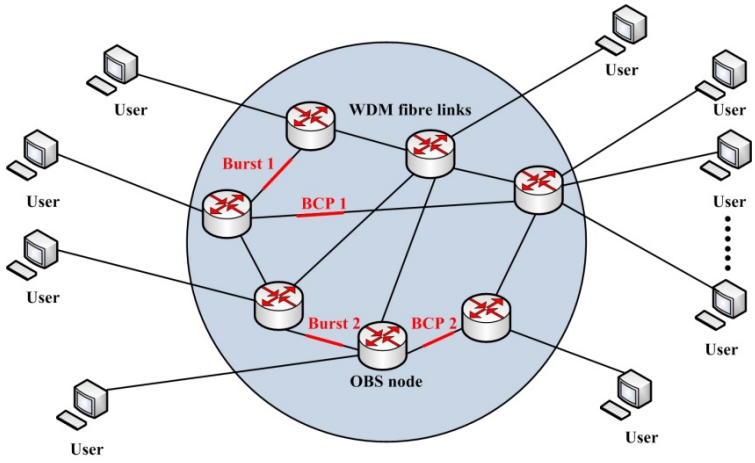

Fig 2 - 2: An OBS based optical network architecture [20]

In the OBS networks proposed in the literature (there are no commercial OPS or OBS networks), there is an OBS interface at the user end, and the OBS node comprises an optical switching fabric, switch control unit and routing processors [54]. There are some key functions in OBS, such as burst assembly, signalling, contention resolution etc. In the following parts, the details of these key functions in OBS will be discussed.

A burst assembly algorithm is used for aggregating traffic into fixed or variable size data bursts. The performance of the OBS network is affected by the choice of this algorithm. There are many different burst assembly algorithms that have been investigated. Typically, based on the time threshold T and the burst length threshold B, these algorithms can be classified into four categories, time-based assembly algorithms, burst length-based assembly algorithms, mixed time/burst length-based assembly algorithms and dynamic assembly algorithms [55]. The first and second categories algorithms use a fixed T or a fixed B respectively as the criterion to send out a burst. The third category algorithms use both T and B as the criterion. The last category of algorithms uses dynamic thresholds. Compared to the first three categories of algorithms, dynamic assembly algorithms are more flexible and therefore improve the performance.

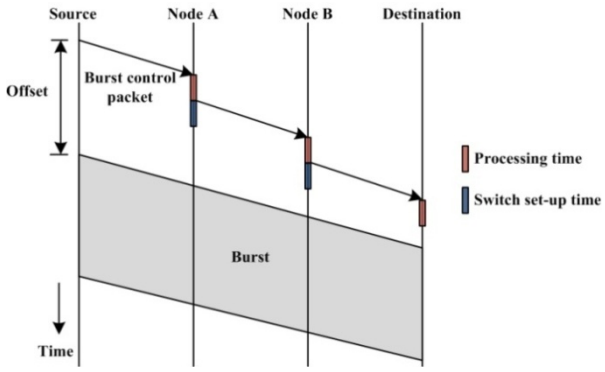

Fig 2 - 3: Distributed OBS signalling with one-way reservation [53]

In the OBS network, signalling is used to build a connection for an assembled optical burst. Distributed signalling with a one-way reservation is the most widely used signalling in proposed OBS network architectures [55]. Fig 2-3 gives the time-space diagram for the distributed signalling with one-way reservation scheme. In the one-way reservation scheme a Burst Control Packet (BCP) containing information about the burst, is used for reserving the required transmission and switching resources and is sent on a separate channel. After a specified time delay (offset), the data burst is sent out without waiting for an acknowledgement (ACK) of the successful establishment of the connection between the source and the destination [53]. The offset offers sufficient time to allow the BCP to be processed at intermediate nodes, plus time to reserve the required resources and configure the switching fabric at each intermediate node.

Contention resolution in OBS has been investigated using different approaches based on time, wavelength, space domains etc. In addition to solutions such as the use of Fibre Delay Lines (FDLs), deflection routing and wavelength conversion, burst segmentation is another way to solve the contention issue. Compared to dropping bursts when there are no sufficient wavelengths and switching resources, burst segmentation which can allow the parts of a burst which overlap with other contending bursts to be dropped, improves packet loss probability in OBS networks [53]. In the process of burst segmentation, a burst is divided into basic transport units called segments. There are two possible burst segment dropping policies; tail dropping and head dropping [56]. Compared to head dropping, prioritised burst segmentation using tail dropping has better successful in-order delivery capabilities.

2.4 IP over WDM Networks

With the development of the Internet, packet-based data traffic is growing rapidly in today's telecommunication networks. While improving the bandwidth of communication channels and transmission speeds of data, many different kinds of networks have been developed that support the Internet Protocol (IP). The routing protocols used in these IP networks can help reduce congestion, delay and deterioration of Quality of Service (QoS) caused by the growth of data traffic. IP based long-haul networks are evolving from an optical layer that implements the Asynchronous Transfer Mode (ATM) and/or Synchronous Digital Hierarchy (SDH) (SONET in the US), to IP over WDM, where IP supports the services and WDM provides the bandwidth. Compared to IP over SDH, the QoS in IP over ATM is better. However in IP over ATM 20% ~ 30% of the bandwidth is wasted by adding a larger amount of header information into an IP package, and ATM itself is technically complex [57]. The layers often do not work in concert because every layer runs at its own speed. In case of failure, different layers compete for protection. To overcome the shortcomings of both IP over ATM and IP over SDH, currently IP packets are carried directly over WDM channels with additional protocol features added, for example from MPLS to maintain quality of service (QoS).

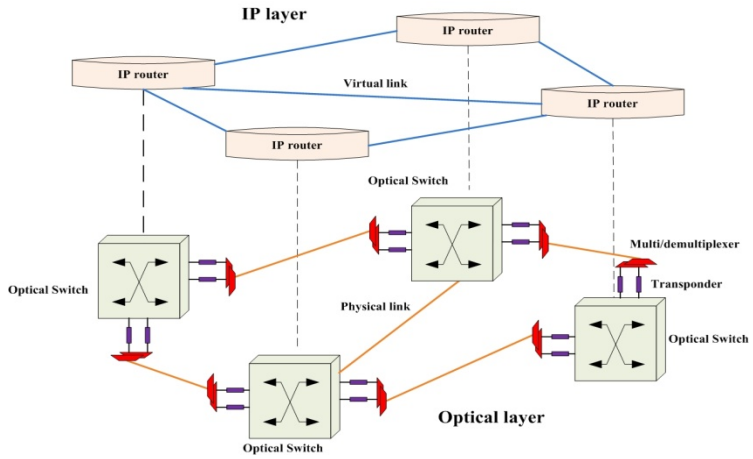

Fig 2 - 4: An IP over WDM network architecture

Fig 2-4 shows the architecture of an IP over WDM network. The IP over the WDM network includes two layers, the IP layer and the optical layer. The IP layer has an IP router in each node connected to an optical switch in the node. The IP

router aggregates data traffic from access networks providing high data rate channels and routes and processes these high speed packets. The optical layer can provide large capacity to support data communication between the IP routers. Optical switches are connected to optical fibre links. On each fibre, a pair of wavelength multiplexers/demultiplexers are used to multiplex/demultiplex wavelengths [58]. The transponders can provide OEO processing for full wavelength conversion at each switching node. In addition to this, for long distance transmission, the EDFAs are used to amplify the optical signals on each fibre.

In the IP over WDM network, virtual lightpaths at different wavelengths are established end-to-end possibly through optical switches to route the data. Fig 2-5 shows the virtual topology in an IP over WDM network. The main advantage of creating virtual topologies in the IP over WDM network is that the lightpath topology is more flexible (than the fixed fibre connections) which enables the network to dynamically respond to changes in the traffic pattern. This allows the load to be balanced and reduces the new connection blocking probability. The reconfiguration of the virtual topology in IP over WDM networks can easily be achieved by changing the lightpath connectivity between IP routers. Similar to WDM networks, the ligthpath is controlled and reconfiguration can be achieved through the tuning of the transmitter wavelength joined with the use of wavelength-selective-switches in the optical level. Alternatively similar functionality can be achieved through the use of fixed tuned transmitters and receivers with optical switches in the nodes.

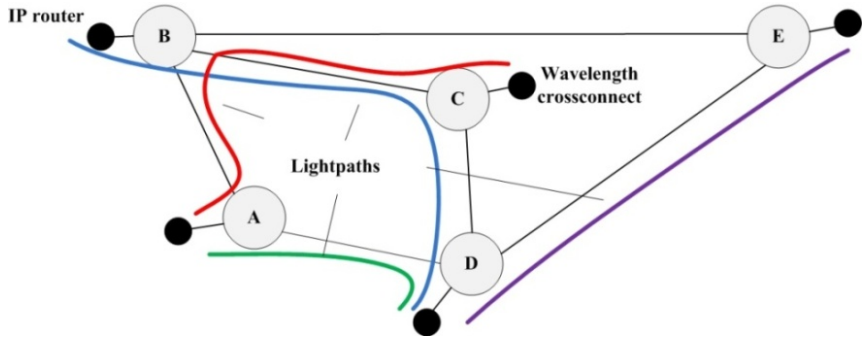

Fig 2 - 5: Virtual topology of IP over WDM network

In an IP over WDM network, the traffic demand can be routed through both the IP layer and the optical layer. In IP layer routing no bandwidth reservation is needed, and the traffic demand is processed and forwarded by IP routers. For long

duration flows and high volume traffic, routing in the optical layer is better, due to the high transmission speeds and the large capacity provided by the wavelengths. Recent research efforts are concentrating on switching all the packets in the optical layer of IP over WDM networks. As mentioned before, OBS is one of the proposals dealing with how to realise this aim. Compared to OCS and OPS, OBS in an IP over WDM network does not need an optical buffer, (optical buffers are hard to implement) and only needs to reserve the bandwidth for the duration of a burst resulting in better bandwidth efficiency. Work on IP over OBS-WDM networks includes routing mechanisms [59] and control architectures [60].

2.5 Mixed Integer Linear Programming

Linear programming (LP) is a mathematical method and a specific case of mathematical optimisation which takes various linear inequalities and linear equalities to meet some conditions and determines the best obtainable result under those conditions. Formally, a LP mathematical model consists of a linear objective function and some linear constraints. The feasible region of a LP model is a set of the intersection of finitely half spaces which compose a convex polyhedron. Each of the intersections is defined by a linear constraint and the objective function is defined on this convex polyhedron [61].

Simplex algorithm and interior-point algorithm are the two most popular algorithms to solve LP problem. In the simplex algorithm, a feasible solution at a vertex of the polypore is constructed for providing the feasible region to search the optimum [62]. In practice, the simplex algorithm can find the global optimum efficiently if the “cycling” problem, even if it is rare, is eliminated. However, the simplex algorithm has poor worst-case behaviour where the number of steps needed by the simplex algorithm is sensitive to the size of the problem [63]. Compared to the simplex algorithm, the interior-point algorithm moves through the interior feasible region and it is worst-case polynomial time algorithm [64].

If some variables in LP need to be integer, then the LP problem becomes a Mixed Integer LP (MILP) problem. MILP is used to solve many practical

optimisation problems, such as economic problems, supply problems and control problems. A special application of MILP is the optimisation of network flow. Most of the research on the optimisation of routing and wavelength assignment in optical networks is based on MILP [58, 65, 66].

Compared to LP, MILP problems are NP-hard in many practical situations, however the MILP problem has the total dual internality property [67]. For the NP-hard MILP problems, linear relaxation is a possible way to get feasible solutions. The main advanced algorithms to solve MILP problems include: cutting-plane, branch and bound, and branch and cut. In a the cutting-plane algorithm, the feasible region is refined by means of linear inequalities until the optimum is found [68]. In a branch-and-bound algorithm, the optimum is found by discarding all infeasible solutions using upper and lower bounds of the quantity being optimized [69]. In a branch and cut algorithm, the branch and bound algorithm is ran first, and then a cutting-plane is used to tighten the LP relaxations [70]. Currently, AMPL and CPLEX are the most popular programming language and solver for MILP respectively. They are used in this thesis to solve the novel MILP models proposed.

2.6 Summary

This chapter has presented a brief review of the evolution of optical networks, advantages and drawbacks of three main optical switching techniques, OCS, OPS and OBS. It was shown that OBS is a compromise between OCS and OPS, has better use of resources than OCS providing a degree of statistical multiplexing gains (lower than those of OPS though) and is easier to implement than OPS. The architecture and multi-layer routing in IP over WDM networks has also been reviewed. As in the rest of this thesis, MILP is adopted as the modelling tool, the concept of MILP is introduced to help understanding the new mathematic models proposed in later chapters.

Chapter 3: Energy Efficiency in Communication Networks

3.1 Introduction

As mentioned in Chapter 1, due to the rapid growth of data traffic, the energy consumption problem can become the bottleneck in the development of networks. Significant efforts has been directed towards reducing the energy consumption of wireless and wired networks recently. In this chapter, the approaches to energy efficiency in communication networks are reviewed based on the following four aspects: energy efficient topologies, energy efficient protocols, energy efficient architectures and energy efficient management. In addition the limitations of current approaches are also discussed in order to guide the research in this thesis.

3.2 Energy Efficient Network Topologies

Conventionally, topology design in networks concentrates on improving capacity and QoS metrics. Even for networks with same node locations, different topologies can result in networks with different performance, for example in terms of propagation delay, congestion, survivability etc.

Topology control is an important approach to conserving energy in wireless networks [71]. With the expansion in the scale and capacity of core networks more energy consuming devices (IP router, transponders etc) are employed. In wavelength

routing optical networks, as mentioned in Chapter 2, the virtual topology is the set of lightpaths [72]. To improve the utilisation of network resources and reduce the number of energy consuming devices, virtual topology design in optical networks has been given more attention. In the following sections, energy efficient network topologies will be discussed and in particular topology control in wireless networks and virtual topology design in optical networks will be described.

3.2.1 Energy Efficient Topology Control in Wireless Networks

In wireless networks, topology control can assign per-node transmission power levels so as to achieve certain network wide goals; such as improving energy efficiency and increasing network lifetime. Several topology control algorithms have been proposed to create power-efficient topologies. In [73], a position-based algorithm is used to set up and maintain a network with minimised energy usage.

In [74], algorithms that improve energy efficiency are introduced based on the underlying assumption that each node is not selfish and collectively completes the global objective of network connectivity while optimising power usage. In [75], the authors developed two distributed algorithms, Max-Improvement Algorithm (MIA) and δ-Improvement Algorithm (DIA), to create topologies that are globally energy efficient, based on selfish algorithms whereby each node selfishly maximises its individual utility. Recently, to address the trade-off between reducing the transmission radius and node degree and cause some links to form an energy-efficient route, the authors in [76] extended the concept of the *r*-neighbourhood graph which is primarily designed for stationary nodes [74] to ad hoc networks.

3.2.2 Energy Efficient Virtual Topology Design in Optical Networks

Designing a virtual topology in an optical network consists of deciding the lightpaths to be set up in terms of their source and destination nodes and the best solution to the routing and wavelength assignment (RWA) problem under the given set of constraints (e.g. delay, available number of wavelengths etc). In general, virtual topology design problems in optical networks can be formulated as

optimisation problems whose aim is to at maximise network throughput, reduce propagation delay, increase utilisation of wavelengths or other performance measures of interest. Recently, due to the increased Internet traffic and energy consumption, virtual topology design has been assigned a new objective namely minimising the power consumption of the core IP over WDM network (and other network segments such as access networks).

In [58], the authors developed an efficient approach using Mixed Integer Linear Programming (MILP) models based on traditional virtual topology and traffic grooming designs to minimise the energy consumption of an IP over WDM network. To overcome the drawbacks of lightpath non-bypass strategies, a multi-hop bypass heuristic was proposed to reduce the network power consumption by staying in the optical layer all the way to the destination node and hence bypassing the power hungry IP routers in the intermediate nodes. Furthermore, in the multi-hop bypass heuristic, the traffic demand between different node pairs can share capacity on common virtual links. The authors in [77] considered holding-time-unaware demands and designed a virtual topology using MILP that minimises power consumption. In [78] the authors focused on the energy consumption minimisation problem of an optical transport network and the problems of power-aware RWA considering a transparent multi-fibre optical network. The static lightpath establishment problem was studied though a MILP formulation. In [66], the authors proposed an MILP formulation to find a power-wise optimal virtual topology. In addition, due to the complexity of the MILP approach, a greedy heuristic and a Genetic Algorithm (GA) were proposed. Similarly in [79], the authors proposed the multi-period power-aware virtual topology design by comparing the Least Flow Algorithm (LFA) [80] and GA exploiting the day-night fluctuations of the traffic.

A novel power-aware RWA algorithm was also proposed for WDM optical networks considering a dynamic lightpath establishment scenario [81]. The proposed algorithm tries to improve the energy efficiency of the optical network by maximising the number of unused optical fibres (by clustering traffic on few routes) in order to minimise the number of optical amplifiers kept active in the network. In essence virtual topology design and traffic clustering on few routes are used to increase the savings obtained through sleep cycles. In [82], the proposed algorithms led to lower power consumption in signal regeneration. The work not only

minimised the power consumption of the optical transport network via energy efficient virtual topology design, but also minimised the power needed in the network by optimising the regenerators placement.

The energy efficient virtual topology designs discussed above considered non-renewable energy sources only. In [83], the authors formulated and compared several energy-aware RWA strategies for WDM networks, whereby optical devices could be powered either by renewable or legacy energy sources. The objectives of such formulations are the minimisation of Green House Gases (GHG) emissions based on MILP.

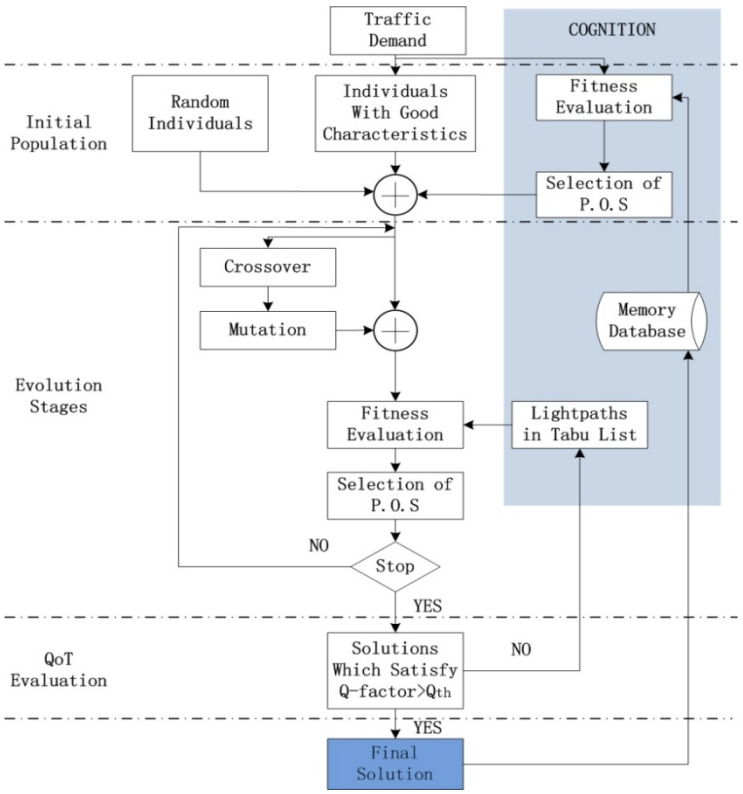

Fig 3 - 1: P-IA-GAPDELT flow diagram and P-SC^T-IA-GAPDELT flow diagram [84]

Other than using MILP to design energy efficient virtual topologies, in [84], two different multi-objective genetic algorithms: P-IA-GAPDELT (Power-optimised Impairment Aware GAPDELT (Genetic Algorithm to Provision the network and to DEsign the Logical Topology)) and P-SC^T-IA-GAPDELT (Power-optimised enhanced with Simple Cognition and Tabu list Impairment Aware GAPDELT) were proposed to minimise both the energy consumption and the network congestion while ensuring that the virtual topologies designed fulfilled the Quality of

Transmission (QoT) requirements. In P-IA-GAPDELT, the initial population is obtained randomly and the fitness of the different solutions found is evaluated in each evolution stage. At the end of the evolution stages, the Q-factors of the lightpaths of the virtual topologies are obtained as solutions, and all the lightpaths that have a Q-factor higher than Q_{th} are considered as valid ones. P-SC^{T}-IA-GAPDELT is an extension of the above algorithm, except it includes cognitive techniques to improve the results [84]. Fig 3-1 gives the flow diagrams for P-IA-GAPDELT and P-SC^{T}-IA-GAPDELT.

3.3 Energy Efficient Network Protocols

With the increase in energy consumption of networks, more and more work on network protocols has begun to focus on energy saving. In the following sections, a review of energy efficient protocols will be given focusing on three aspects; energy efficient routing protocols, energy efficient traffic engineering protocols and energy efficient sleep mode protocols.

3.3.1 Energy Efficient Routing Protocols

In general, the purpose of designing routing protocol is to improve the efficiency of data exchange, reduce propagation delay, increase the stability of the network (among other objectives), regardless of the power consumption.

Work on energy efficient routing protocols has appeared in sensor networks before wired networks. There has been a growing interest in wireless sensor networks that are composed of hundreds or thousands of sensor nodes [85]. Energy efficient routing protocols are proposed due to the node having limited available power and because energy conservation is a critical issue in wireless networks. Low Energy Adaptive Clustering Hierarchy (LEACH) was proposed in [86] as a clustering-based protocol. LEACH utilises randomised rotation of the cluster-heads, to distribute the energy load among the sensors in the network. To improve LEACH, the Threshold sensitive Energy Efficient Sensor Network protocol (TEEN) was

proposed in [87]. In addition to this, another power efficient protocol based on LEACH; Power-efficient Gathering in Sensor Information Systems (PEGASIS) was introduced in [88]. It is a chain-based protocol and it assumes that the location information of all other nodes is known by each node at the first instance. Although LEACH uses a self-configuration approach to reduce energy consumption, it does consider the unequal distribution of nodes in each cluster results in unbalanced energy consumption. This leads to draining of energy quicker at some nodes than others. To overcome the drawback in LEACH, a Maximum Energy Cluster Head (MECH) routing protocol was proposed in [89]. In MECH, the uneven member distribution for clusters is avoided by limiting the cluster range.

Apart from energy efficient routing protocols in wireless networks, new routing protocols considering energy efficiency have also been given much attention in optical networks as of recently. In [90], the authors studied energy efficient routing for the scheduled traffic model and proposed an energy-aware routing algorithm based on traffic grooming in IP over WDM optical networks. In [91], power-awareness was advocated in the design and implementation of the network protocols for IP networks, which considered the potential impact of energy-aware routing protocols. The work in [92] gave a different insight to power aware routing problems in WDM networks. The authors proposed a weighted power-aware routing algorithm, by jointly considering power minimisation and resource blocking in a single cost function. In [93], the authors considered energy-aware routing in WDM core networks to minimise the electricity costs. A MILP model was used to minimise the total electricity costs while optimising the capacity and energy under different network traffic load conditions. Energy efficient multicasting on already dimensioned wavelength routed networks has been investigated in [65] by studying an energy efficient RWA problem while taking optical power impairments into consideration. The authors formulated the problem as a MILP model and a greedy algorithm was also introduced, whose core operation is the Light-Forest Construction (LFC) Stage.

A different approach can be found in [94] where the authors implemented three heuristics considering static traffic demands, which are Least-Cost Path (LCP), Most-Used Path (MUP) and Ordered-Lightpath Most- Used Path (OLMUP). In LCP, for each request, the shortest path is computed as a static routing cost. In MUP, the

current lightpath request was routed by using the shortest path updated routing cost. . In OLMUP, at each iteration, the lightpath that minimises an incremental cost was selected to be routed.

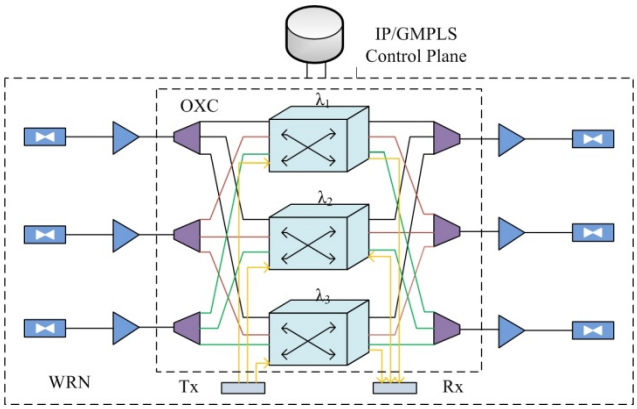

Fig 3 - 2: GMPLS over optical network [95]

Furthermore, energy efficient routing protocols were also designed for Generalised Multi-Protocol Label Switching (GMPLS) optical networks. Fig 3-2 gives an overview of a GMPLS based optical node. In [95], a green Open Shortest Path First (OSPF) protocol was proposed. In this protocol, dynamic routing requests are served both by the routing protocol 'Open Shortest Path First-Traffic Engineering (OSPF-TE)' and the signalling protocol 'Resource Reservation Protocol-Traffic Engineering (RSVP-TE)'. In the routing process, associated with making a routing decision, the OSPF-TE protocol can be extended to distribute energy related information between nodes by adding a new type, length and value to the traffic engineering extension.

In [96], the authors proposed routing optimisations based on energy sources in dynamic GMPLS controlled optical networks and evaluated the influence of re-routing and load balancing factors with different re-routing thresholds. Through applying load balancing criteria, the increased blocking probability caused by using re-routing schemes can be compensated. In Wavelength Switched Optical Networks (WSONs) power-saving engineering extensions have been integrated in GMPLS based on routing protocols. In [97], the authors proposed GMPLS with Power State Engineering (PSE) to control the power using in optoelectronic devices according to the level of data traffic. In [98] a heuristic routing scheme designed for mitigating the power excursion problem that may affect surviving lightpaths in case of the

failure of WDM links in GMPLS-based WSONs was proposed. In addition to the heuristic scheme, the paper also proposed its possible distributed implementation which requires the storage of an L x L matrix in each network node that is dynamically updated by Resource reSerVation Protocol with Traffic Engineering (RSVP-TE) and Open Shortest Path First with Traffic Engineering (OSPF-TE) protocols.

3.3.2 Energy Efficient Traffic Engineering Protocols

Traffic engineering is used to optimise performance of networks, and addresses the problem of efficiently allocating resources. Traditional traffic engineering tries to evenly distribute traffic on all the links in order to reduce the possible congestion induced by traffic bursts. Oppositely, energy efficient traffic engineering has to release some links by migrating their traffic on other links, so that the links without traffic can go to 'sleep' for energy saving. In [99], an intra-domain traffic engineering mechanism, GreenTE, was proposed. The GreenTE approach is formulated as a MILP model which maximises the power saving by turning off line-cards as well as satisfying performance constraints; including link utilisation and packet delay. GreenTE also considered load balancing that is applied on a new set of waking paths. Similar to GreenTE, a distributed Energy-Aware Traffic Engineering (ETE) scheme is proposed in [100]. The status of the network is monitored and automatic decisions are made by ETE through executing a low-complexity heuristic algorithm.

A traffic engineering method, known as Multilayer Traffic Engineering (MLTE), uses an IP layer cost function which is not limited to taking care of IP flow routing. In [101] and [102], the energy efficient MLTE approach through optimised routing and logical topology construction is introduced. In MLTE, traffic is groomed by using the shortest-path routing algorithm onto a subset of virtual full mesh. This is followed by removing unused edges which are identified in the virtual full mesh from the actual logical topology. However, the low-load threshold (LLT) which controls the IP links cost may cause traffic flows to deviate from the links whose traffic load is lower than LLT, until they can be removed from the logical topology.

In [103], traffic shaping was used for increasing bursts and reducing power consumption. A typical example was given by authors as follows: assuming there were three streams to be transmitted in a wireless network. Without traffic shaping, the network card needs to be woken up three times in each period of transmitting packets. If traffic shaping is used for combining all three packets with a certain offset time, the device just needs wake up once to transmit all queued packets, therefore reducing energy consumption. A generalisation of traffic shaping, called, Demand Shaping for Green Communication was proposed in [104]. The basic idea of Demand Shaping is to control the resource usage to ensure that the total demand stays securely below the supply. Through optimising utilisation of network resources, the installation of new cell towers is avoided and the transmitting power is reduced consequently reducing the total energy consumption. In demand shaping, the user should be involved in a closed loop control which is set up between all network components. In order to avoid data loss and to ensure fair sharing of data rates per user, any remaining congestion situations are resolved by wireless flow control and fair scheduling [105].

3.3.3 Energy Efficient Sleep Mode Protocols

In practice, network links are subject to a variation of traffic loads at different times of day. Many studies have investigated energy saving by turning off or putting some network equipment or modules into sleep mode when traffic demands are low. These energy saving schemes are known as ‘sleep mode’ schemes, whereby the entire component or some parts of it are switched off. If a router in the core network is switched to sleep mode, traffic flows passing through this component can be routed to alternative routers in a manner that does not affect the network performance. However, if the network performance deteriorates, some of the sleeping devices will be woken up to reduce the blocking probability, error rate and to enhance the network performance. This process is known as “dynamic sleep mode”.

A typical application of sleep mode protocol in optical networks is described here. The optical crossconnects (OXCs) with an energy consumption of approximately 10nJ per bit dominate the power consumption of a WDM optical

network compared with other components [106]. Hence the energy consumption will be significantly reduced by switching the OXC into sleep mode. In [107], the sleep cycles of OXCs in optical burst switched networks were discussed. For minimising the negative effects brought by sleep mode on QoS, an anycasting scheme was proposed in order to route the node traffic to alternative paths. The active destinations which result in the lowest QoS degradation can be chosen by the user if the original destination is in sleep mode. In [108], three energy-saving paradigms all based on turning off network equipment, were compared. These are (i) turning off the line cards when there is no traffic, without changing the routing of IP traffic and lightpaths, (ii) empty lightpaths, as many as possible, through fixing the vitual topology and rerouting the IP traffic, then switch off the relevant line cards (iii) through optimising lightpaths realisation and rerouting IP traffic to achieve the maximal number of line cards that could be turned off. The first and second strategies serve as a trade-off between energy saving and implementation complexities, while the last strategy may require huge computational complexity in the global optimisation although it is the most energy-saving one.

A novel sleep mode protocol to deliver power reduction through implementation of the "Hibernation" approach was introduced in [109]. The Hibernation mode is based on a Shortest Path First (SPF) approach in terms of reducing the power consumption of each node. During this Hibernation process, the routing and data tables' information of nodes is sent to the control plane with power consumption updates within the network constantly. Sleep mode also is effective for improving the energy efficiency of the GMPLS network, even with the currently standardised GMPLS suite. The support of sleep mode in the links of WSONs with GMPLS control plane had been proposed in [110]. A centralised strategy and a distributed strategy have been used to dynamically select the link to be set to sleep.

Additionally, sleep mode protocols are also used in wireless networks to reduce network power consumption. In [111], a power saving sleep mode was introduced in the IEEE 802.16e standard (WiMAX), in which communication occurs between mobile stations (MS) and base stations (BS) in a metropolitan area generally. In this kind of network, power saving can be achieved by switching off parts of the MS in a controlled manner (switched into sleep mode) when there is neither traffic from MS (uplink) nor to the MS (downlink). In [112], two different extents of 'sleep mode':

idle mode and deep sleep mode were investigated. In the idle mode, the node is neither transmitting nor receiving a packet; however, it is still consuming power because the node listens to the wireless medium continuously in order to detect a packet that it may receive. The deep sleep mode allows the node to be turned off totally and not receive packets, transmit packets or respond to the wireless medium.

3.4 Energy Efficient Network Architectures

Network architecture is another factor which influences the power consumption of networks. To achieve energy efficiency in networks, most of the existing studies on energy efficient network architectures are based on data transmission, structural layout design etc. In the following sections, the details of these studies will be discussed.

3.4.1 Energy Efficient Data Transmission

It is known that the power consumption of processing switches increases when the data is switched at a very high bit rate. Most of the current switches work in asynchronous mode, and the buffers in the switches need to operate faster than the interface rate in order to enable multiple functions to operate simultaneously to access packets stored in the same buffer. The basic principle of pipeline forwarding was introduced in [113] along with a process where the real-time packet advances one hop in each time frame. The time frame can be considered as a virtual container of a constant number of IP packets, which is a basic time period for synchronising the IP packet switches with pipeline forwarding. In addition, time frames are grouped into time cycles in order to provide the basic unit for a periodic repetition of the reservation which is used for the reserved transmission capacity. There are two applications of pipeline forwarding: Time-Driven Switching (TDS) and Time-Driven Priority (TDP). Due to its ability to transmit traffic in large volumes and reduce the total power consumption, TDS is suitable for high speed optical backbones network.

In [114], a parallel network which has the same fibre infrastructure as WDM networks, but is based on pipeline forwarding that coexists with asynchronous IP technology was introduced (as shown in Fig 3-3). As well as carrying traditional traffic, the required signalling for setting up synchronous virtual pipes can be transported by asynchronous IP routers, in the pipeline forwarding parallel network. There are two reasons that pipeline forwarding can be used to reduce the power consumption of networks. First, compared to asynchronous routers, pipeline forwarding significantly reduces the hardware complexity of the switching fabric controllers, because the content of each time frame is switched and forwarded according to its position within the time cycle and therefore there is no need for header processing. Consequently, less process cycles are needed to handle each packet. Secondly, compared to the reconfiguration of switching fabrics before moving each single packet in an asynchronous router, the reconfiguration frequency of the switching fabric of TDS switches can be reduced by using the whole time frames as switching units.

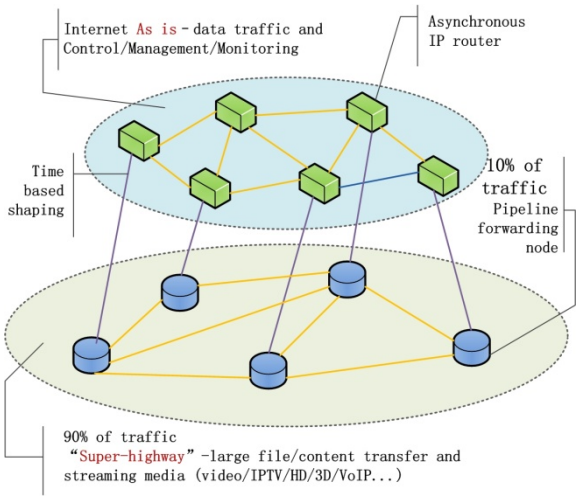

Fig 3 - 3: Parallel network on the same fibre infrastructure with WDM [114]

In IP over WDM optical networks, IP routers consume most of the energy. Thus, it makes sense to minimise the required number of IP router ports in data transmission as a method to reduce energy consumption. Optical bypass can be used to reduce the number of IP router ports in lightpaths for data transmission where the data remains in the optical domain until it reaches the destination node, thus bypassing the IP ports at all the intermediate nodes. In [58], optical bypass was first evaluated both via MILP and simulations showing that it reduces energy

consumption in IP over WDM networks. In addition, it is also observed in that work that an energy-minimised optical network is also cost-minimised. Similar to the optical bypass, end-to-end bypass traffic grooming, which was proposed in [115], reduced power consumption of intermediate nodes in lightpaths compared to conventional data transmission architecture.

3.4.2 Energy Efficient Structural Layout

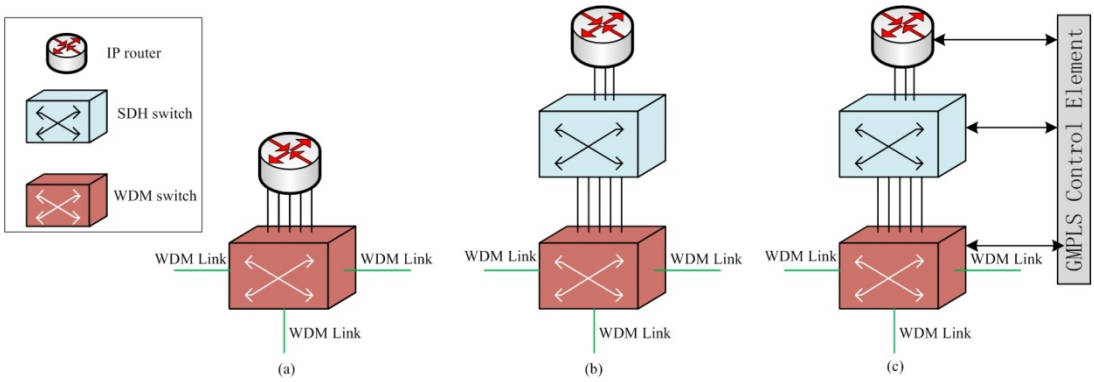

Fig 3 - 4: Node architectures of (a) IP/WDM, (b) IP/SDH/WDM, and (c) GMPLS/ASON [116]

Currently, energy saving for the backbone optical network is not just based on the IP over WDM two-layer architecture. There are several other multi-layer architectures, such as IP over SDH over WDM and OTN (optical transport network) over WDM. The energy consumption of these different types of multi-layer optical networks have been evaluated in several studies recently. In [116], the energy consumption of IP over SDH over WDM was investigated. Compared to the pure IP over WDM optical networks, energy consumption can be saved by introducing the SDH layer. IP routers need to process the data packet by packet and IP layer aggregation in routers results in higher energy consumption. In the underlying SDH and WDM layers, the traffic demands are switched at the SDH layer without IP processing, and electronically bypass the IP router. Thus, energy savings can be made. In [117], similar principles have been extended by including a GMPLS/ASON control plane, where some wavelengths can be switched at the WDM layer; thus optically bypassing all the layers above. This will bring further energy savings, as switches in the WDM layer consumes even less energy than that in the SDH layer. Fig 3-4 gives three different node architectures. In [118], energy efficiency and

CAPEX optimality are studied for IP over OTN over WDM networks via MILP model. Under the specific situation studied, the IP over OTN over WDM has a 30% advantage in energy saving over the IP over WDM architecture [118].

In access networks, energy consumption is dependent on the network structure. Passive optical networks (PONs) consume the smallest energy per transmitted bit, attributed to the proximity of the end user to the exchange and the low power consumption of passive network devices. In PONs, Optical Line Terminal (OLT) and Optical Network Units (ONUs) consume a large portion of the overall energy consumption [119]. Typically, OLT chassis comprise of multiple OLT line cards and each of them communicates with a number of ONUs. All of these OLT line cards in the OLT chassis are usually working in power-on mode to avoid service disruption between ONUs and the central office. To reduce the energy consumption of OLT, a novel energy efficient OLT structure, which adapts the number of power-on OLT line cards in the OLT chassis to the real-time incoming traffic, was proposed in [120]. In [121], the energy consumption of several different PON architecture are compared. Among the considered architectures, WDM-PON based on Reflective Semiconductor Optical Amplifier (RSOA), stacked 10G TDM-PON, and point-to-point fibres offer the lowest power per line potential.

3.4.3 Energy Efficient Caching and Mixed Line Rate

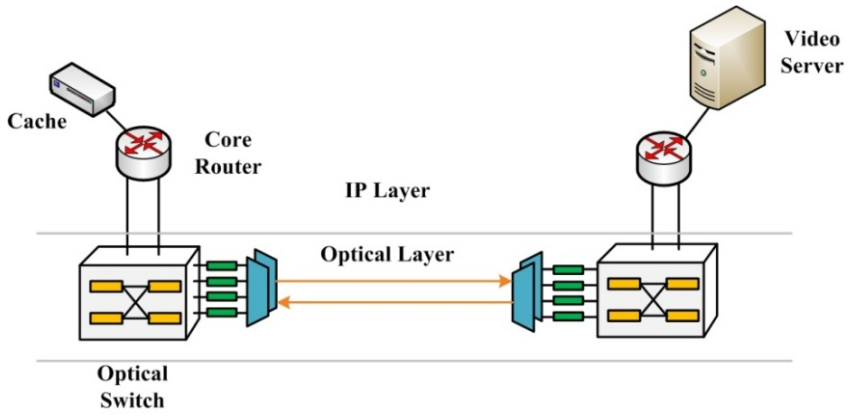

Fig 3 - 5: A cache-based On-Demand Service using IP over WDM [122]

In addition to energy efficient multilayer design in networks, the introduction of caching into current data distribution networks can reduce energy consumption

significantly. In [122], an energy efficient cache-based Video-on-Demand (VoD) service over an IP over WDM network was proposed. Different to a conventional IP over WDM network, the cache-based VoD network architecture shown in Fig 3-5 shows that each node in the network is allocated a limited content caching capacity. In this network, the most popular video content in the video servers are stored by the cache in each node. Video requests can be served by a local node cache, rather than directly from the video server. Compared to the energy consumption associated with routing the video traffic demand in the IP layer all the way from video servers, the cache consumes much less energy. Thus, the energy consumption of the whole network is reduced.

Recently, a popular energy saving architecture design has been proposed that uses a different bit-rate transponder and IP port according to traffic demand. With the support of multi-line-rates, physical ports power consumption can be reduced. In [123], an energy-optimisation framework with mixed line rates has been investigated. By using mixed line rates, energy-efficiency can be improved in three different kinds of optical network architectures: transparent, translucent and opaque, compared to that based on a single line rate. In [124], energy efficiency for IPTV program delivery in optical backbone networks with multiple available line rates was investigated. An energy-efficient flow aggregation was proposed to guarantee minimising the total energy consumption in delivering programs.

3.5 Energy Efficient Network Management

Management in networks uses activities, procedures, and tools to operate, administer, and maintain networked systems [125]. All the actions of network management would consume much more energy under the incredible increase of traffic demand in networks. Therefore, energy efficient management is important. In the following sections, energy efficient management of networks will be discussed in relation to two aspects: energy efficient management at the hardware level and energy efficient management at the network level.

3.5.1 Energy Efficient Management at the Hardware Level

It is known that most network equipment is composed of electrical circuits. If the energy consumption of electrical circuits is reduced, the total power consumption of the network will come down. Prominent examples include the use of clock gating approaches, i.e. the addition of circuits that disable portions of the circuitry when flip-flops do not change their state, and the use of Dynamic Voltage Scaling (DVS) or Dynamic Frequency Scaling (DFS) which are widely used in energy management of modern computer processors [126].

DVS is a power management technique in modern network equipment, whereby the voltage used in a component can be increased or decreased depending on the circumstances. With DVS, reduction of the supply voltage can result in a slower operation of circuits. In this case, in order to adapt the circuit to deliver the appropriate performance while optimising energy consumption [127], a CMOS circuit can be operated at dynamically varying voltage levels. Two external components are required for energy-efficient DVS operation of a processor. The first component is the minimum operating voltage which is predicted based on the deadline for completing the task. With the prediction mechanism, the energy consumption of a processor is reduced without affecting the execution time constraints of the task. The second component required for DVS is a voltage regulator [128], which can change the levels of operating voltage for different clock frequencies, and also can change the operating voltage when a new frequency is determined by the predictor output.

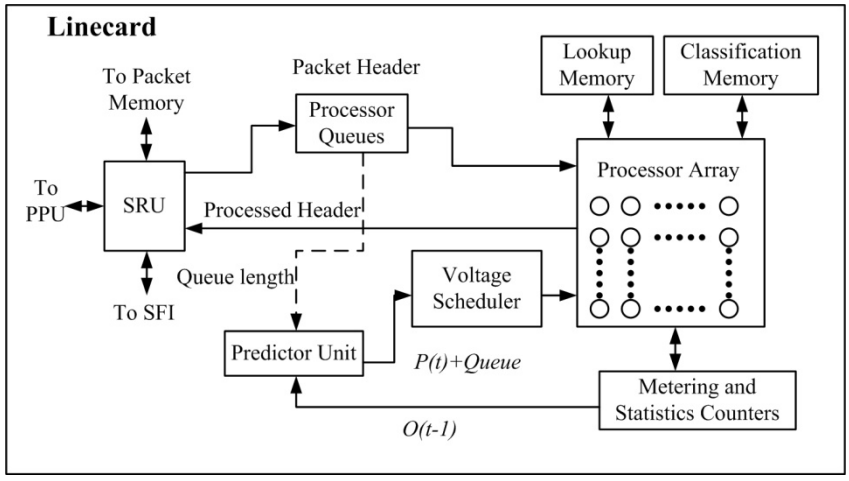

Fig 3 - 6: An energy-efficient multiprocessor based linecard [127]

A typical application of DVS is in Multiprocessor-Based Linecards (MBLs) in order to reduce the power consumption of the network. As the employment of MBLs in next generation routers continues and as the energy consumption due to the increasing number of routers [127] increases, implementing a DVS scheme in an MBL becomes necessary. The architecture of an energy-efficient MBL is shown in Fig 3-6. In Fig 3-6 it is shown that there are two inputs to the predictor: the number of packets and the length of processor queue[127]. The prediction computation level required by the next prediction interval is given by the packets in the processing queue, which are added to the estimated arrival time of the packets. The voltage scheduler unit which is driven by the prediction changes the voltage and frequency settings for the processor array during the next prediction interval.

DFS is another power management technique used in modern network equipment, which includes processors. With DFS, the operating frequency of a microprocessor can be adjusted automatically according to the task loading. In addition of reducing heating problem of chips, the number of processor instructions and the achieved performance also can be reduced by DFS in a given amount of time. Therefore, the trade-off between power consumption and performance is very important when implementing DFS.

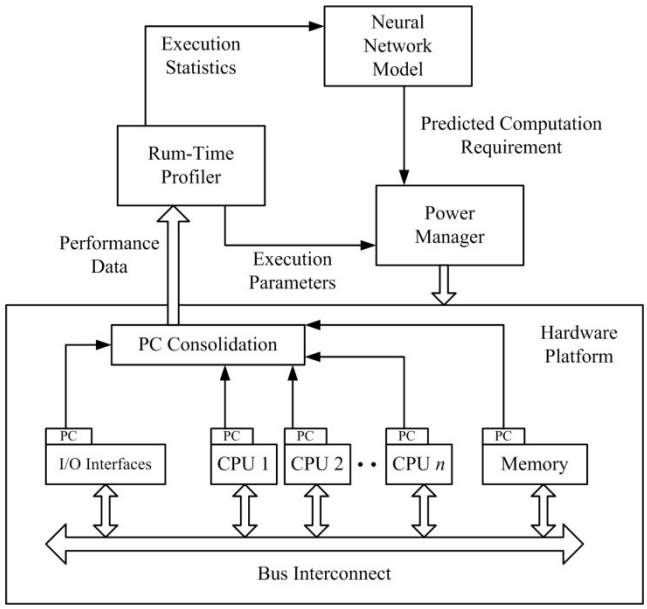

Fig 3 - 7: Block Diagram of The Neural Network Model System [129]

In fact, DFS has a very similar mechanism to DVS. Technology that uses DFS and DVS jointly is known as DVFS. Similar to DVS, DVFS also needs a prediction

mechanism. If the requirements of the applications are known in advance, the DVFS can assign processor voltage and frequency to achieve the maximum power savings. To achieve this aim more accurately, a new prediction mechanism known as neural network model was proposed in [129]. Compared to the normal methods which rely on a history approach for making decisions related to voltage and frequency scaling, a novel neural network based approach for DVFS has two important advantages: first, the effects of the program execution parameters can be captured. Secondly it is not limited to the specific features particular applications and can adapt to many behaviour of applications. The block diagram of the neural network model system is shown in Fig 3-7. In this system, it can be observed that most of the hardware units are linked with the performance counters (PCs). In general, the neural network model can predict the upcoming task load and give advice to the power manager in order to implement DVFS [129].

3.5.2 Energy Efficient Management at the Network Level

At the network level, management deals with controlling the whole network behaviour rather than specifying the hardware's working state. Commonly, this includes monitoring the network, setting parameters, deploying executable code, and logging events that are relevant for the purpose of network management. For the purpose of energy efficiency, several management frameworks have been proposed for networks.

In wireless networks, the energy consumption of the management system itself is very important. To overcome the energy consuming problem caused by the overhead burden which derives from sending, receiving and processing of all management requests and responses in wireless networks, a novel management framework that uses a separate network stack was proposed in [130]. In [131], a more efficient management framework for monitoring a wireless sensor network was proposed. In this proposed framework, the overhead for management purposes (which utilises the unused space in data packets) is reduced significantly. In [132], a new energy efficient management considering overall network resources in wireless sensor networks was proposed. An Energy-Efficient Key Management (EEKM) scheme was designed in [133] to support light-weight rekeying mechanism, which

provided security properties similar to those provided by pair-wise key sharing schemes for large-scale wireless sensor network. In green radio communication networks with sustainable energy supply, an adaptive resource management scheme was proposed in [134] to address the unreliability of renewable energy in QoS provisioning.

In [135], the NEEM (Network Energy Efficiency Manager) was presented. In NEEM, energy saving can be obtained via automating the policy driven analysis and implementing the network changes by adapting to the network traffic dynamics and requirements. A Bayesian Belief Network (BBN) based Decision Management System (DMS) is proposed and evaluated in [136] for IP core networks. The operational modes of the network elements can be changed intelligently by Network Management System (NMS) in order to save energy without compromising the performance and QoS constraints. Fig 3-8 shows an energy aware network management framework. The NMS interacts with the DMS and the Configuration Management System (CMS). The the NMS sends out data relating to energy consumption and QoS to DMS. The policy engine responds to make effective decisions. The configuration changes of actual network elements can be affected when the decision is received by the NMS and translated for the CMS.

In current IP networks, shutting down or turning on links will make link state routing protocols recoverage to a new topology. In [137], the authors proposed a distributed energy-aware link management algorithm to dynamically determine the link states for a router to resolve the disconnection problem of network caused by convergence time. In this management algorithm, the flows will be immediately redirected to their new next hop nodes when the state of link is changed. In addition, an optimisation model has been developed to determine a most power saving network topology and a link metric which is used in the distributed link management algorithm.

In a home network scenario, the studies in [138] proposed a synchronised power management strategy. The authors introduced an energy model to synchronise the behaviour of Home-Gateway (HG) with the Customer Premises Equipment (CPE). In the efficient energy network management model, autonomics between the HG and Set-Top Box (STB) are provided, which allow the HG-STB to register and

synchronise power states. In [139] a network level power management framework based on the Energy-aware Plug and Play (EPnP) for home network devices is proposed. The power consumption of devices with or without user intervention by EPnP technique can be reduced through using the power management by reconfiguring the power control elements of each device in the home network..

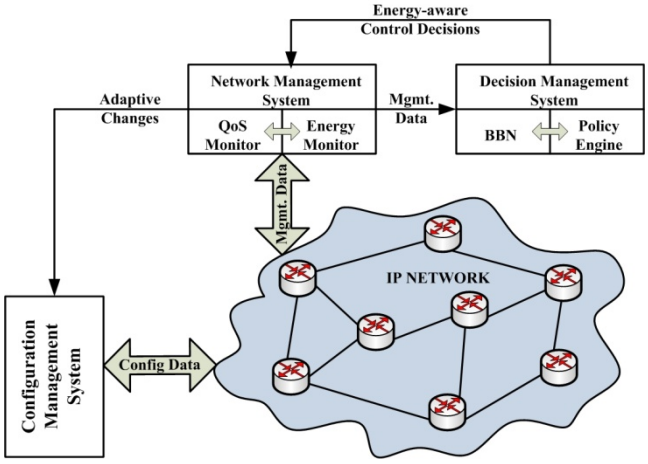

Fig 3 - 8: The energy-aware network management framework [136]

3.6 Summary

This chapter has reviewed a number of approaches to improve the network energy efficiency. It focused on four approaches, namely energy efficient topologies, energy efficient protocols, energy efficient architectures and energy efficient management. It is obvious that current energy efficient network research mainly focuses on wireless networks. However, for the wired networks, such as the optical core network, the energy consumption problem needs to be addressed as well. In addition, some novel ideas for energy saving in networks also need to be investigated, such as employing renewable energy, designing energy efficient physical topology etc. The rest of the chapters of this thesis investigate these areas and make a number of novel proposals.

Chapter 4: Hybrid-power IP over WDM Networks

4.1 Introduction

With network expansion, the energy consumption and CO_2 emissions associated with networks are increasing rapidly. As discussed in Chapter 3, previous research mainly concentrated on networks using pure non-renewable energy. In this chapter, renewable energy combined with non-renewable energy is proposed to reduce the total non-renewable energy consumption, consequently reducing the CO_2 emissions of IP over WDM networks which form the core of current backbone optical networks.

In this chapter, a Mixed Integer Linear Programming (MILP) model is developed for energy minimisation in the network when renewable energy is used and a novel heuristic for improving renewable energy utilisation is proposed. In order to identify the impact of the number and the location of nodes that employ renewable energy on the non-renewable energy consumption of whole network, another MILP model is also constructed. The additional energy savings that can be gained through Adaptive Link Rate (ALR) techniques, where different load dependent energy consumption profiles are considered, have also been investigated. Due to the renewable energy variation in the day and in different seasons, the season and weather effects are also investigated. For the analytic MILP modelling and the simulations, two real topologies National Science Foundation network (NSFNET) and United States NETwork (USNET) are used to evaluate the performance of MILP,

new heuristics and verify the correctness of the MILP models' results through comparison with simulations.

4.2 Hybrid-power IP over WDM Network Architecture

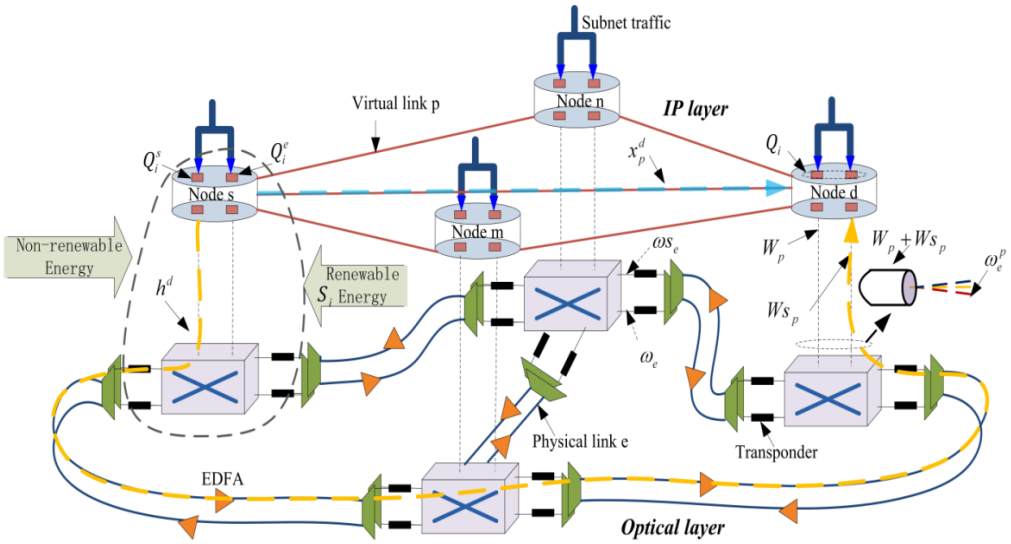

Fig 4 - 1: Structure of the hybrid-power IP over WDM network

Similar to IP over WDM networks, the hybrid-power IP over WDM network architecture is composed of an IP layer and an optical layer. The subnet traffic is aggregated by the IP ports in nodes and then routed through the IP layer. However, the difference between this network and current networks deployed and in most of the literatures [58, 77, 78] is that the power supply of this new network is mixed being composed of non-renewable energy and renewable energy. Fig 4-1 gives the details of the hybrid-power IP over WDM network. The nodes that have access to renewable energy can also be powered by non-renewable energy to guarantee QoS when the renewable energy output becomes low. We assume there are high-speed switches which can switch between non-renewable energy and renewable energy. The renewable energy can power the ports, transponders, optical switches, multiplexers and demultiplexers in a node.

In contrast with previous energy efficient and carbon reduction solutions in IP over WDM networks that use non-renewable energy only, in the hybrid-power IP

over WDM network, the total CO_2 emission of the IP over WDM network will be reduced through network optimisation and by replacing a portion of the non-renewable energy consumption by renewable energy. Therefore, the problem becomes that associated with minimising the non-renewable energy consumption of the hybrid-power IP over WDM network.

4.3 Mathematical Model

In [58], a MILP model was developed for minimising the total energy consumption of IP over WDM networks. We have formulated a model that builds on these concepts but is focused on minimising the non-renewable energy consumption when renewable energy is employed in the hybrid-power network. In this MILP model, we assume the network has the topology $G = (N, E)$ with N nodes and E physical links. The total non-renewable energy consumption of the network is composed of:

1) Non-renewable energy consumption of ports without access to renewable energy

$$\sum_{i \in N} PR \cdot \left(Q_i^e + \sum_{p \in P} \delta_{ip} \cdot W_p \right) \tag{4-1}$$

2) The non-renewable energy consumption of EDFAs

$$\sum_{e \in E} PE \cdot E_e \cdot f_e \tag{4-2}$$

3) The non-renewable energy consumption of router ports that have access to renewable energy (the non-renewable energy may be used for example to guarantee control at all time)

$$\sum_{i \in N} PRS \cdot \left(Q_i^s + \sum_{p \in P} \delta_{ip} \cdot Ws_p \right) \quad (4\text{-}3)$$

4) The non-renewable energy consumption of transponders that have access to renewable energy (again the non-renewable energy may be used for example to guarantee control at all time) and that of the transponders without access to renewable energy

$$\sum_{e \in E} \left(PT \cdot \omega_e + PTS \cdot \omega s_e \right) \quad (4\text{-}4)$$

5) The non-renewable energy consumption of optical switches that have access to renewable energy (similarly the non- renewable energy may be used for example to guarantee control at all time) and that of the optical switches without access to renewable energy

$$\sum_{i \in N} \left(PO_i \cdot (1 - y_i) + POS_i \cdot y_i \right) \quad (4\text{-}5)$$

6) The non-renewable energy consumption of multiplexers and demultiplexers that have access to renewable energy (here also the non-renewable energy may be used for example to guarantee control at all time) and that of the multiplexers and demultiplexers without access to renewable energy

$$\sum_{i \in N} \left(PMD \cdot DMe_i + PMDS \cdot DMs_i \right) \quad (4\text{-}6)$$

The MILP model that minimises the non-renewable energy consumed and obtains the optimal RWA is defined as follows:

Objective: minimise

$$\sum_{i\in N} PR\cdot\left(Q_i^e+\sum_{p\in P}\delta_{ip}\cdot W_p\right)+\sum_{e\in E} PE\cdot E_e\cdot f_e + \sum_{i\in N} PRS\cdot\left(Q_i^s+\sum_{p\in P}\delta_{ip}\cdot Ws_p\right) + \sum_{e\in E}\left(PT\cdot\omega_e+PTS\cdot\omega s_e\right) + \sum_{i\in N}\left(PO_i\cdot(1-y_i)+POS_i\cdot y_i\right) + \sum_{i\in N}\left(PMD\cdot DMe_i+PMDS\cdot DMs_i\right), \tag{4-7}$$

Subject to:

$$\sum_{p\in P} x_p^d = h^d \quad \forall\, d\in D, \tag{4-8}$$

$$\sum_{d\in D} x_p^d \le \left(W_p+Ws_p\right)\cdot B \quad \forall\, p\in P, \tag{4-9}$$

$$\sum_{p\in P}\left(\delta_{ip}\cdot W_p+\delta_{ip}\cdot Ws_p\right)+Q_i \le \nabla^i \quad \forall\, i\in N, \tag{4-10}$$

$$\sum_{e\in E}\delta_{ep}\cdot\omega_e^p = W_p+Ws_p \quad \forall\, p\in P, \tag{4-11}$$

$$PR^s\cdot\left(Q_i^s+\sum_{p\in P}\delta_{ip}\cdot Ws_p\right)+\sum_{e\in E} PT^s\cdot\omega s_e\cdot\delta_{ie}+PMD^s\cdot DMs_i+PO_i^s\cdot y_i \le S_i \quad \forall\, i\in N, \tag{4-12}$$

$$\sum_{p \in P} \omega_e^p \leq W \cdot f_e \quad \forall\, e \in E, \tag{4-13}$$

$$Q_i^e + Q_i^s = Q_i \quad \forall\, i \in N, \tag{4-14}$$

$$\sum_{p \in P} \omega_e^p = \omega_e + \omega s_e \quad \forall\, e \in E, \tag{4-15}$$

$$DMe_i + DMs_i = DM_i, \quad \forall\, i \in N. \tag{4-16}$$

The variables and parameters in the equations above are declared as follows:

$E(Pa)$	Physical link set in optical layer,
$P(Pa)$	Virtual link set in IP layer,
$D(Pa)$	Traffic demand set between node pairs,
$\delta_{ip}(Pa)$	If node *i* belongs to virtual link *p*, δ_{ip} is '1', otherwise it is '0',
$\delta_{ie}(Pa)$	If node *i* belongs to physical link *e*, δ_{ie} is '1', otherwise it is '0',
$\delta_{ep}(Pa)$	If virtual link *p* starts at physical link *e*, δ_{ep} is '1', otherwise it is '0',
$PR(Pa)$ and $PE(Pa)$	Non-renewable energy consumption of a router port and an EDFA respectively both use non-renewable energy,
$PRS(Pa)$	Non-renewable energy consumption of a router port that has access to renewable energy,
PR^s	Renewable energy consumption of a router port that has access to renewable energy,
$PO_i(Pa)$ and $POS_i(Pa)$	Non-renewable energy consumption of an optical switch that has access to non-renewable energy only or has access to renewable energy in node *i,* respectively,
$PO_i^s(Pa)$	Renewable energy consumption of an optical switch that has access to

	renewable energy,
$PMD(Pa)$ and $PMDS(Pa)$	Non-renewable energy consumption of a multi/demultiplexer that has access to non-renewable energy only or has access to renewable energy, respectively,
PMD^s	Renewable energy consumption of a multi/demultiplexer that has access to renewable energy,
$DM_i(Pa)$	The total number of multiplexers and demultiplexers in node *i,*
$DMe_i(Ve)$	Number of multiplexers and demultiplexers in node *i* which use non-renewable energy,
$DMs_i(Ve)$	Number of multiplexers and demultiplexers in node *i* which use renewable energy,
$y_i(Ve)$	If the optical switch in node *i* has access to renewable energy $y_i = 1$, otherwise $y_i = 0$,
ω_e *(Ve)* and $\omega s_e(Ve)$	Number of wavelength channels on physical link *e* in the optical layer which use non-renewable energy and renewable energy respectively,
W_p *(Ve)* and $Ws_p(Ve)$	Number of wavelength channels on virtual link *p* in the IP layer which use non-renewable energy and renewable energy respectively,
$Q_i^e(Ve)$ and $Q_i^s(Ve)$	Number of ports which are powered by non-renewable energy or renewable energy for data aggregation in node *i,*
$x_p^d(Ve)$	Traffic demand *d* between node pairs on virtual link *p,*
$\omega_e^p(Ve)$	Number of wavelength channels of virtual link *p* on physical link *e,*
$f_e(Ve)$	Number of fibers on physical link *e,*
$E_e(Pa)$	Number of EDFAs on each fiber on physical link *e,*
PT(Pa) and *PTS(Pa)*	Non-renewable energy consumption of a transponder that has access to non-renewable energy only or has access to renewable energy respectively,
PT^s	Renewable energy consumption of a transponder that has access to renewable energy,

$W(Pa)$	Number of wavelengths in a fibre,
Q_i (Pa)	Number of ports for assembling data,
$\nabla^i(Pa)$	Maximum number of ports in node *i*,
$S_i(Pa)$	The maximum output power of the renewable energy source in node *i,*
$h^d(Pa)$	Traffic demand *d* between node pairs.
$B(Pa)$	Capacity of each wavelength.

Table 4 - 1: Parameters (Pa) and Variables (Ve) Used for MILP Model

The aim of the objective function (Equation (4-7)) is to minimise the non-renewable energy consumption of the hybrid-power IP over WDM network. Equation (4-8) and Equation (4-11) represent the flow conservation constraint in the IP layer and the optical layer. Equation (4-9) ensures that the traffic flow on each virtual link does not exceed its capacity. The term $(W_p + Ws_p)$ represents the total number of wavelength channels on each virtual link powered by either non-renewable energy or renewable energy. Equation (4-10) ensures that the limit on the number of router ports in each node is not exceeded. Equation (4-12) ensures that the renewable energy consumption of router ports and transponders is not larger than the maximum output power of the renewable energy source in each node. Equation (4-13) and Equation (4-15) give the limit on the number of wavelength channels in each physical link *e.* Equation (4-14) ensures that for each node the total number of ports assembling data is equal to the number of router ports using non-renewable energy and the number of ports using renewable energy. Equation (4-16) gives the limit on the total number of multiplexers and demultiplexers in node *i.*

4.4 Energy Efficient Routing Heuristic

In conventional IP over WDM networks, under the non-bypass heuristic, lightpaths passing through a node must be terminated by OEO processing and all the IP data packets are processed and forwarded by the IP routers [58]. The main disadvantage of non-bypass is that IP router ports are required at each intermediate node between source node and destination node.

To overcome the disadvantage of the non-bypass heuristic, the direct-bypass heuristic is proposed [140]. Under the direct-bypass heuristic, IP traffic is allowed to directly bypass the intermediate router node via a cut-through lightpath. The main benefit of direct-bypass heuristic is that the lightpath bypass strategy can minimise the number of required IP router ports. However, the direct-bypass heuristic is also based on the shortest-path routing method and no matter how much the IP traffic demand is between a node pair, a new virtual lightpaht link will still have to be established. If the traffic demand is lower than the capacity of the lightpath, the bandwidth utilisation will be low.

To overcome these drawbacks, the multi-hop bypass approach is proposed in [58]. Under the Multi-hop bypass heuristic, IP traffic demands between different node pairs are allowed to share capacity on lightpaths common with their routing paths in order to improve the utilisation of bandwidth. Better wavelength bandwidth utilisation will result in fewer virtual links, and therefore fewer IP router ports and lower energy consumption.

4.4.1 The Renewable Energy Optimisation Routing Heuristic (REO-hop)

In the multi-hop bypass heuristic proposed in [58] bandwidth utilisation is improved by allowing traffic demands between different source-destination pairs to share capacity on common virtual links (lightpaths). However, in the hybrid-power IP over WDM network architecture as we assume that renewable energy sources are available on a limited number of nodes, implementing the multi-hop bypass heuristic which is based on shortest-path routing will only minimise the total energy consumption not taking into account whether this energy comes from renewable or

non-renewable sources. To minimise the utilisation of non-renewable energy, we propose a new heuristic where the traffic flows are allowed to traverse as many nodes as possible that use renewable energy to ensure that in addition to reducing the total number of IP router ports and transponders, the non-renewable energy consumption is minimised. This constraint may increase the propagation delay, however to maintain QoS, only the two shortest-path routes are considered. Due to the changing traffic pattern and the fact that the output power of renewable energy sources varies during different times of the day, the routing paths are dynamic. The new heuristic is known as Renewable Energy Optimisation hop (REO-hop). The flowchart of the heuristic is shown in Fig 4-2.

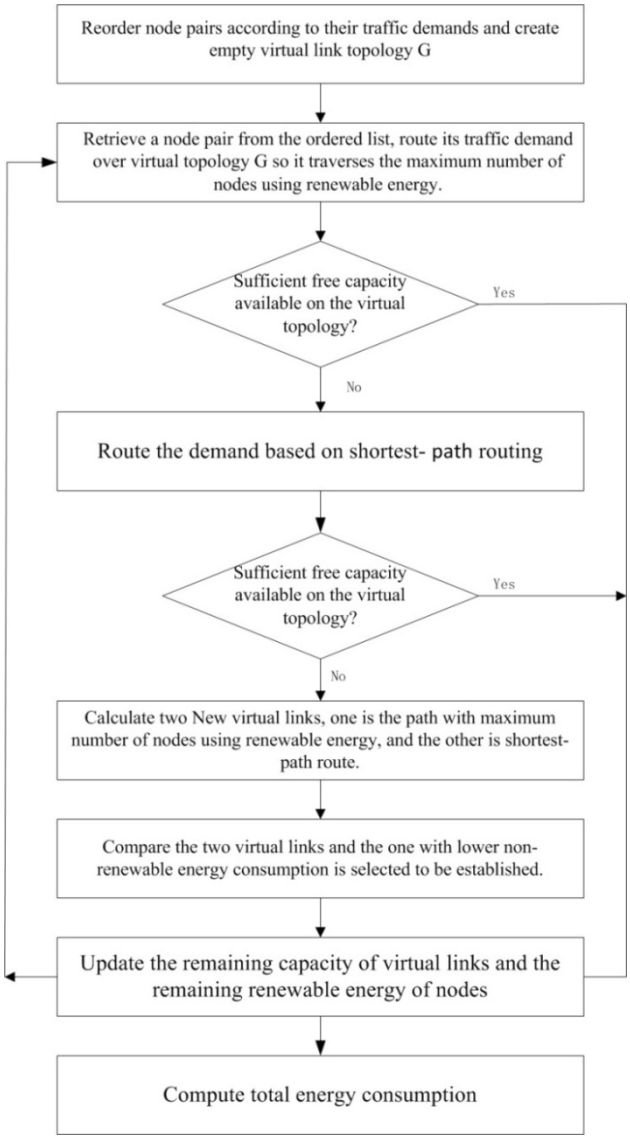

Fig 4 - 2: Flowchart of the REO-hop heuristic

In this heuristic, all the node pairs are reordered based on their traffic demands from highest to lowest and an empty virtual link topology *G* is created. A node pair is then retrieved from the ordered list, and its traffic demand is routed over virtual topology *G* so that it traverses the maximum number of nodes that use renewable energy. As mentioned, only the two routes which are shortest-path routes are considered, i.e. the two shortest-path routes are compared in terms of the number of nodes that use renewable energy and the one with the maximum number is selected. If sufficient free capacity is available on the virtual topology, the selected route is accommodated and the remaining capacity on all the virtual links is updated.

If the selected route with the maximum number of nodes using renewable sources is not available, the other route is selected. In case the virtual topology cannot accommodate either route, a new direct virtual link is established between the node pair. Two virtual links are computed, one is a path with the maximum number of nodes that use renewable energy, and the other is the shortest-path route. The two virtual links are compared and the one with lower non-renewable energy consumption is selected and is established. If the non-renewable energy consumption is the same for both paths, the shortest path is selected in order to minimise the propagation delay. The new virtual link is added to the virtual topology *G*. The above process is repeated for all the node pairs. Then, the remaining renewable energy of each node is checked to determine whether it can support the optical switch and the multiplexers and demultiplexers in a node. When all the traffic demands are routed on the virtual topology *G*, the objective function (Equation (4-7)) is used to calculate the total non-renewable energy consumption of the network.

4.4.2 Network Simulator Design and Implementation

The C programming language is used to develop the simulator for investigating the performance of the REO-hop heuristic. To simplify the development of the simulator, different modules are used to define different objects and function. There are three main objects defined in the simulator: Physical Link, Virtual Link and Node Pairs. Both of Physical Link and Virtual Link objects consist of “ID”, “start nodes”, “end node”, “capacity” and “length”. Physical Link object provides essential information of certain physical link for different functions to calculate the relative

data. Virtual Link object is associated with lightpath and virtual topology. Node Pairs object is used to store the essential traffic demand information between different node pairs, which includes the source node, destination node and amount of traffic demand. Interconnections of different objects and functions are shown in Fig 4-3.

In Fig 4-3, the Traffic Generation function creates the traffic demand between node pairs with a uniform distribution based on a random number generator. The average traffic demand for each node pair is variation in different time of the day with a range from 20 Gb/s to 120 Gb/s. At first, the Node Paris array is reordered according to the traffic demand level of each node pair from high to low. Then Node Pairs object is inputted into the REO-hop function which is used to implement the REO-hop heuristic. In the REO-hop function, after routing the traffic, the relative information (number of IP ports, number of transponders, renewable energy and capacity) will be updated for the nodes and physical links on that path. In this simulator, the shortest routing path is got from a routing table list and the routing path with maximum number of nodes using renewable energy is the output of the Prediction function which is developed to find out the perspective route based on routing table list and a pre-route method. In the pre-route method, after routing traffic traversed enough number of possible paths, the path with maximum number of nodes using renewable energy can be selected.

After finish routing all the traffic demands using the REO-hop function, the number of transponders and ports of each node is used for calculating the power consumption of network. Actually, the number of transponders and ports of each node is stored by Transponder Array and Port Array respectively. In the Physical Link, the link length is used for calculating the average propagation delay and the energy consumption of EDFAs.

A “characteristic capacity” is linked with the available capacity on each virtual link and the characteristic Flag indicates whether the capacity of physical link is fully used or not, i.e. it identifies the link rate which is used as an input to the Adaptive Link Rating (ALR) function. In the ALR function, the power consumption of nodes on the physical links without fully capacity using is calculated based on five different energy profiles: on-off, linear, cubic, log10 and log100.

Finally, the “Calculate Results” function uses all the results from the functions mentioned above as inputs (results of ALR function, Length, Transponder Array and Port Array) to compute the total non-renewable energy consumption of the network and the average propagation delay at one time point.

Under the controlling of time set *T* which consists of time points in a day, the whole simulation process mentioned above is repeated until all the traffic of different time points is routed. These objects and their associated functions compose the core of the simulator. Other modules are created to perform other additional functions.

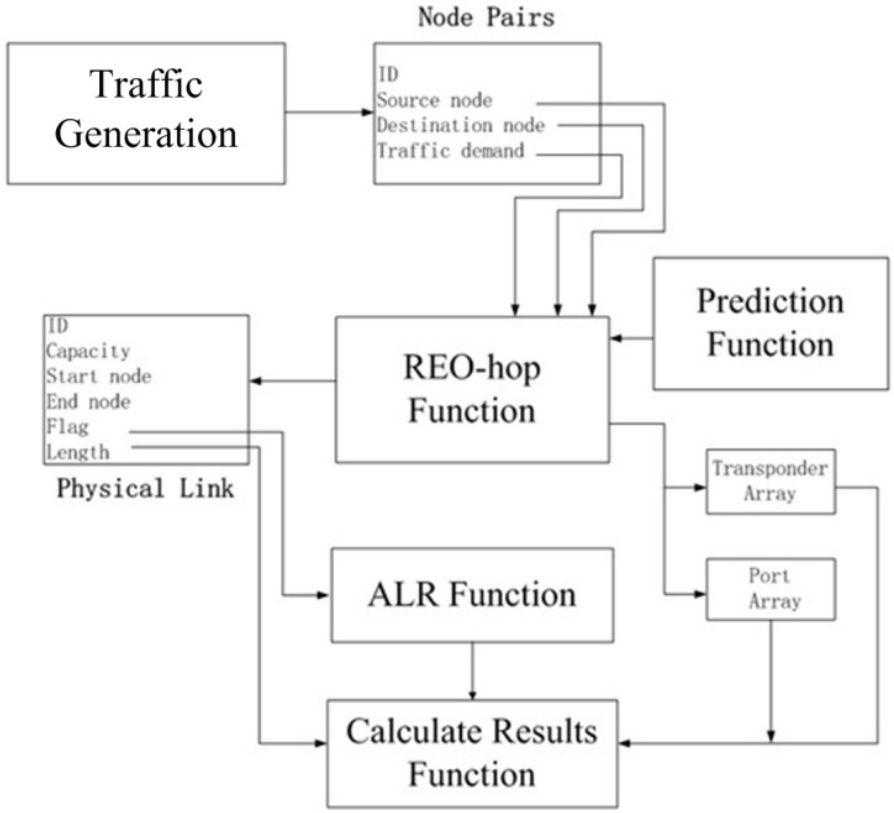

Fig 4 - 3: Interconnections between different objects and functions

4.5 Hybrid-power IP over WDM NSFNET Network results

To test the performance of the REO-hop heuristic and to evaluate the non-renewable energy consumption of the architecture, the NSFNET network, depicted in Fig 4-4, is considered as an example of a real world network.

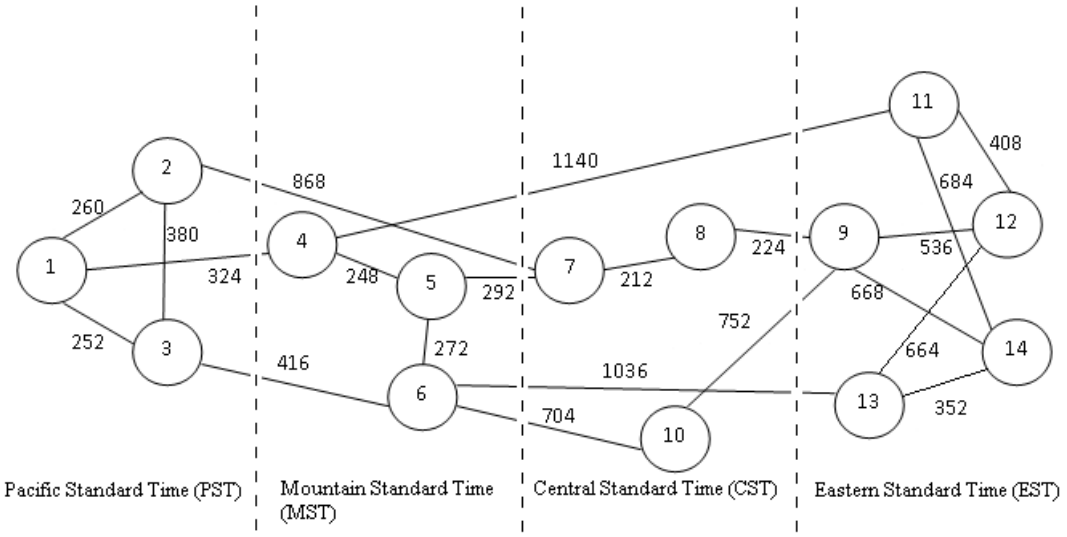

Fig 4 - 4: NSFNET test network with time zones

The NSFNET network consists of 14 nodes and 21 bidirectional links. Solar energy is used as the renewable energy source. As the NFSNET network covers the US, different parts of the network fall in different time zones, i.e., nodes will experience different levels of solar energy and traffic demands at any given point in time. There are four time zones, Eastern Standard Time (EST), Central Standard Time (CST), Mountain Standard Time (MST) and Pacific Standard Time (PST). There is an hour time difference between each time zone and the next, we use EST as the reference time. Note that time zones dictate habits and therefore network utilisation and traffic demands in our case. We however use real sun rise and sun set data to determine the solar energy available in a given city at a given point in time.

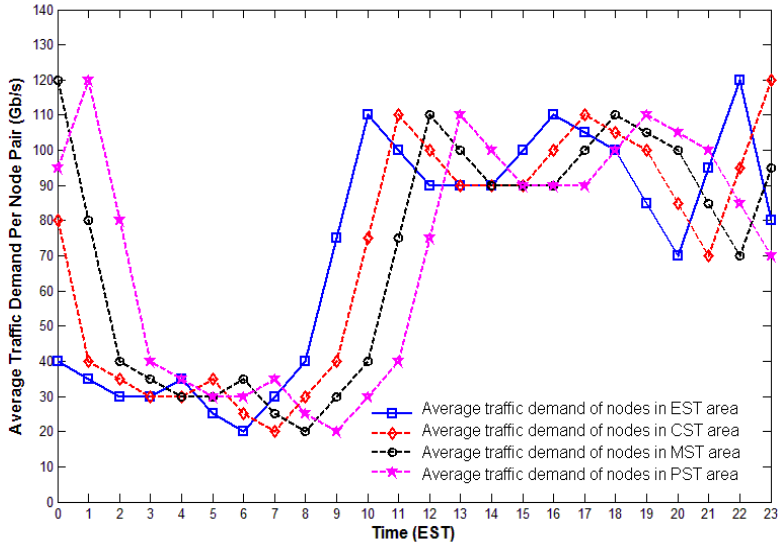

Fig 4 - 5: Average traffic demand in different time zones

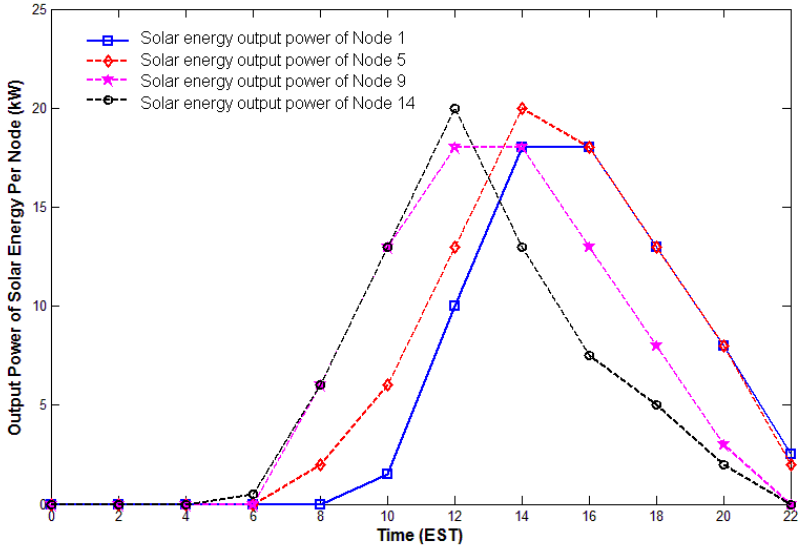

Fig 4 - 6: Solar energy in different nodes in different time zones

Fig 4-5 shows the average traffic demand during different hours of the day [141]. The average traffic demand between each node pair ranges from 20 Gbit/s to 120 Gbit/s and the peak occurs at 22:00 in these traffic profiles. We assume that the traffic demand between each node pair in the same time zone is random with a uniform distribution and no lower than 10 Gbit/s.

The solar energy power [142] available to a node is shown in Fig 4-6. As the output power of solar energy sources varies in different hours of the day, we use the profile in [142] and the sun rise and sun set data associated with each node. The geographical location of nodes affects the sunset and sunrise time, and therefore has

impact on the solar energy generated in each node. Table 4-2 gives the details of the solar energy power available to each node. The solar energy is non-zero from 6:00 to 22:00 and the maximum output power occurs at 12:00.

4.5.1 Non-renewable Power Consumption of the Network

Nodes located at the core of the network with a high nodal degree are selected to use renewable energy as they are expected to consume more power compared to nodes at the edge of the network as more traffic flows are routed through them. Selecting these nodes is expected to maximise the reduction in the non-renewable power consumption. Nodes 4, 5, 6, 7 and 9 are initially selected to use solar energy in our heuristic. Later we study the impact of the location of nodes with solar energy and our MILP model yields the optimum locations.

Typically a one square meter silicon solar cell can produce about 0.28 kW of power [143]. We assume that the maximum solar energy available to a node is 20 kW, therefore a total solar cell area of about 100 m^2 is required. Later we examine the impact of higher solar energy availability per node.

As mentioned under the multi-bypass and REO-hop heuristics, some traffic demands are routed in the optical layer by optical switches. A suitable size optical switch (the Glimmerglass's 192×192 optical switch) is selected based on the maximum number of wavelengths used in each node. Although in the non-bypass heuristic the maximum number of wavelengths used in each node is larger, we still use the same power consumption data for optical switches in the multi-bypass heuristic and REO-hop heuristic due to the negligible difference in energy consumption between different optical switch sizes compared to the power consumption of a router port. Fig 4-7 shows that under the multi-hop bypass (the heuristic requiring fewer wavelengths), the maximum number of wavelengths needed is 109.

(SR: Sunrise, SS: Sunset. SR time and SS time are given in the node's local time in June)

Node ID / Time (EST)	1	2	3	4	5	6	7	8	9	10	11	12	13	14
	SR: 05:43	SR: 05:14	SR: 05:16	SR: 05:54	SR: 05:27	SR: 05:55	SR: 05:51	SR: 05:39	SR: 05:17	SR: 05:53	SR: 05:18	SR: 05:41	SR: 06:27	SR: 05:30
	SS: 20:04	SS: 21:02	SS: 19:34	SS: 20:40	SS: 20:41	SS: 20:10	SS: 20:53	SS: 20:47	SS: 20:24	SS: 19:56	SS: 20:30	SS: 20:29	SS: 20:30	SS: 20:59
00:00	0 kW	0 kW	0 kW	0 kW	0 kW	0 kW	0 kW	0 kW	0 kW	0 kW	0 kW	0 kW	0 kW	0 kW
02:00	0 kW	0 kW	0 kW	0 kW	0 kW	0 kW	0 kW	0 kW	0 kW	0 kW	0 kW	0 kW	0 kW	0 kW
04:00	0 kW	0 kW	0 kW	0 kW	0 kW	0 kW	0 kW	0 kW	0 kW	0 kW	0 kW	0 kW	0 kW	0 kW
06:00	0 kW	0 kW	0 kW	0 kW	0 kW	0 kW	0 kW	0 kW	0 kW	0 kW	2 kW	0.5 kW	0 kW	0.5 kW
08:00	0 kW	0 kW	0 kW	0 kW	2 kW	0.5 kW	0.5 kW	2.5 kW	6 kW	2 kW	6 kW	6 kW	4.5 kW	6 kW
10:00	1.5 kW	2 kW	2 kW	7 kW	6 kW	6 kW	6 kW	6 kW	13 kW	6 kW	13 kW	13 kW	13 kW	13 kW
12:00	10 kW	10 kW	10 kW	13 kW	13 kW	13 kW	13 kW	18 kW	18 kW	18 kW	20 kW	20 kW	20 kW	20 kW
14:00	18 kW	18 kW	18 kW	18 kW	20 kW	20 kW	20 kW	18 kW	18 kW	18 kW	13kW	13kW	13kW	13kW
16:00	18 kW	18 kW	18 kW	18 kW	18 kW	18 kW	18 kW	13kW	13kW	13kW	7.5 kW	7.5 kW	7.5 kW	7.5 kW
18:00	13kW	13kW	13kW	18 kW	13 kW	13 kW	13 kW	8 kW	8 kW	8 kW	5 kW	5 kW	5 kW	5 kW
20:00	8 kW	8 kW	8 kW	8 kW	8 kW	8 kW	8 kW	3kW	3kW	2 kW	2 kW	2 kW	2 kW	2 kW
22:00	2.5 kW	3 kW	0.5 kW	4 kW	2 kW	0.5 kW	3 kW	0 kW	0 kW	0 kW	0 kW	0 kW	0 kW	0 kW

Table 4 - 2: Solar energy output power of each node (20 kW maximum output power)

Table 4-3 shows the MILP optimisation and simulation environment parameters in terms of number of wavelengths, wavelength capacity, distance between two neighbouring EDFAs, and energy consumption of different components in the network. Some of the parameters are similar to those in [58] which are also derived from Cisco's 8-slot CRS-1 data sheets [144], and others are derived from Glimmerglass's 192×192 channels Sytem-600 data sheets [145] and Cisco's ONS 15454 data sheets [146].

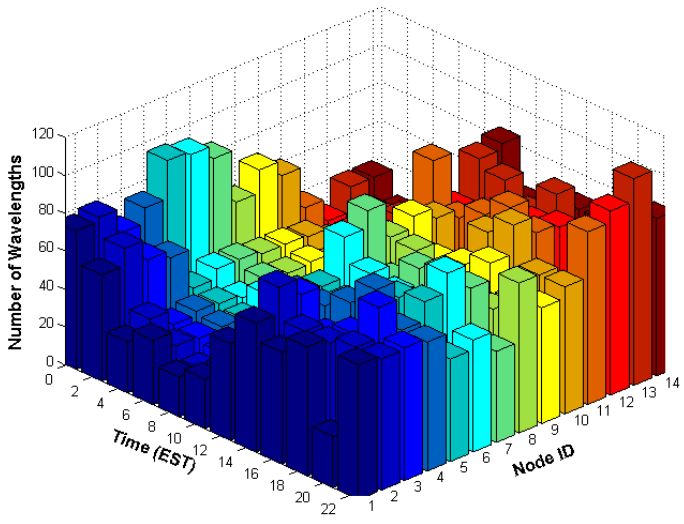

Fig 4 - 7: The number of wavelengths used by each node under the multi-hop-bypass heuristic at different times of the day

The AMPL/LPSOLVE software is used to solve the LP problem. Five different cases are considered: 1) Non-bypass heuristic without renewable energy, 2) Non-bypass heuristic with renewable energy, 3) Multi-hop-bypass heuristic without renewable energy 4) Multi-hop-bypass heuristic with renewable energy, and 5) REO-hop heuristic with renewable energy.

Distance between two neighbouring EDFAs	80 (km)
Number of wavelength in a fibre (W)	16
Capacity of each wavelength (B)	40 (Gbit/s)
Non-renewable power consumption of a router port (PR)	1000 (W)
Renewable power consumption of a router port (PR^s)	1000 (W)
Non-renewable power consumption of an optical switch in node i (PO_i).	85 (W)
Renewable power consumption of an optical switch in node i (PO_i^s).	85 (W)
Non-renewable power consumption of an optical switch that has access to	0 (W)

renewable energy in node i (POS_i)	
Non-renewable power consumption of a router port that has access to renewable energy (*PRS*)	0 (W)
Non-renewable power consumption of a multiplexer or a demultiplexer (*PMD*).	16 (W)
Renewable power consumption of a multiplexer or a demultiplexer (PMD^s).	16 (W)
Non-renewable power consumption of a multiplexer or a demultiplexer that has access to renewable energy (*PMDS*).	0 (W)
Non-renewable power consumption of a transponder (*PT*)	73 (W)
Renewable power consumption of a transponder (PT^s)	73 (W)
Non-renewable power consumption of a transponder that has access to renewable energy (*PTS*)	0 (W)
Non-renewable power consumption of an EDFA (*PE*)	8 (W)

Table 4 - 3: Input data for MILP analytic optimisation and simulation

Fig 4-8 shows the total non-renewable energy consumption. The curves "Non-bypass without solar energy" and "MILP optimal with solar energy" provide the upper and lower bounds on the non-renewable energy consumption. We assume the traffic demands and the output power levels of the solar energy sources given in Fig 4-5 and Table 4-2, respectively. Compared to the "Non-bypass with solar energy" curve, both the multi-hop-bypass and REO-hop heuristics have reduced the non-renewable power consumption. The savings in the non-renewable power consumption, introduced by the REO-hop heuristic, increase at the time of the day when the solar energy is significant (From Fig. 6, this happens between 6:00 and 22:00). Compared with the upper bound, at 12:00, 14:00, 16:00 and 18:00, the REO-hop heuristic saves non-renewable power of about 1000 kW. Furthermore, REO-hop still out- performs the multi-hop-bypass heuristic, from 0:00 to 4:00 when there is no solar energy in the network as REO-hop tries to route demands on virtual links with sufficient capacity rather than using shortest-path routing as with the multi-hop-bypass heuristic.

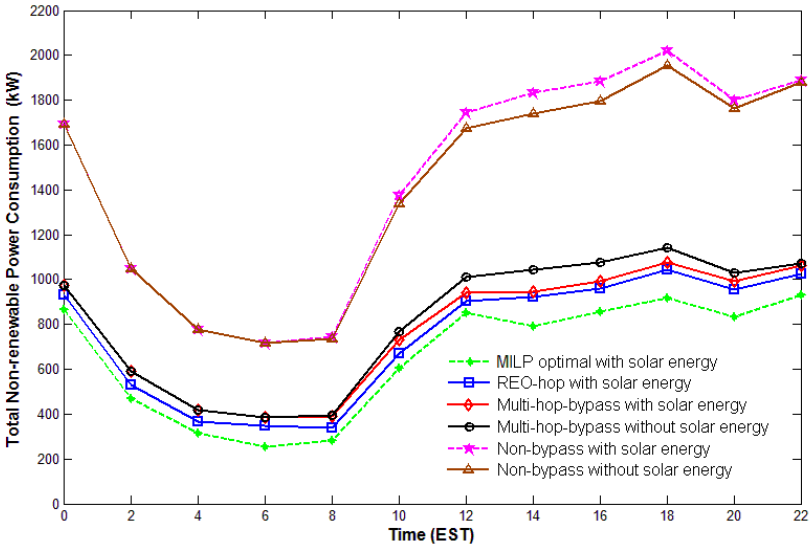

Fig 4 - 8: The total non-renewable power consumption of different heuristics with and without solar energy

We have also examined the impact of different values of the maximum solar energy (40 kW, 60 kW and 80 kW) available per node. A solar cell area of up to 300 m^2 is needed to generate such values (80 kW) [143]. Solar cell cladding with such surface area can be practically built in a typical core routing node location. In Fig 4-9, it is shown that increasing the maximum solar energy output per node has linearly reduced the total non-renewable energy consumption using our algorithms.

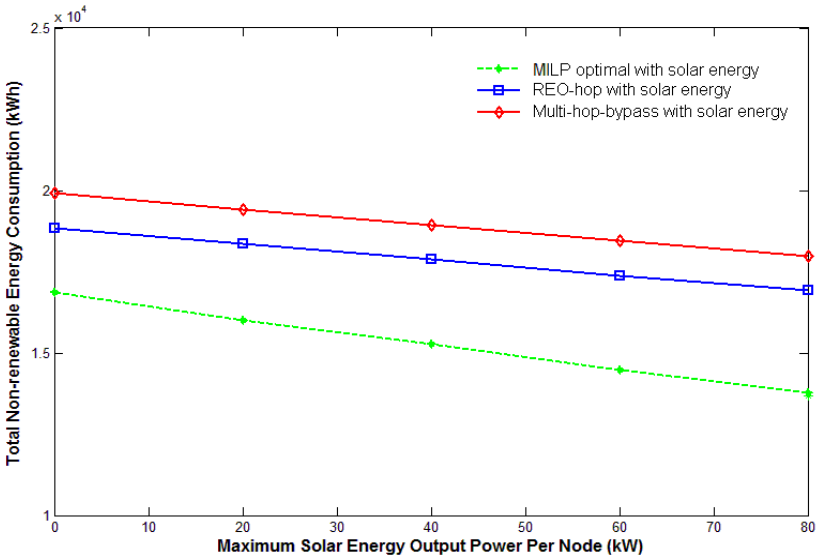

Fig 4 - 9: Total non-renewable energy consumption in 24 hours for different values of the maximum solar energy under different heuristics

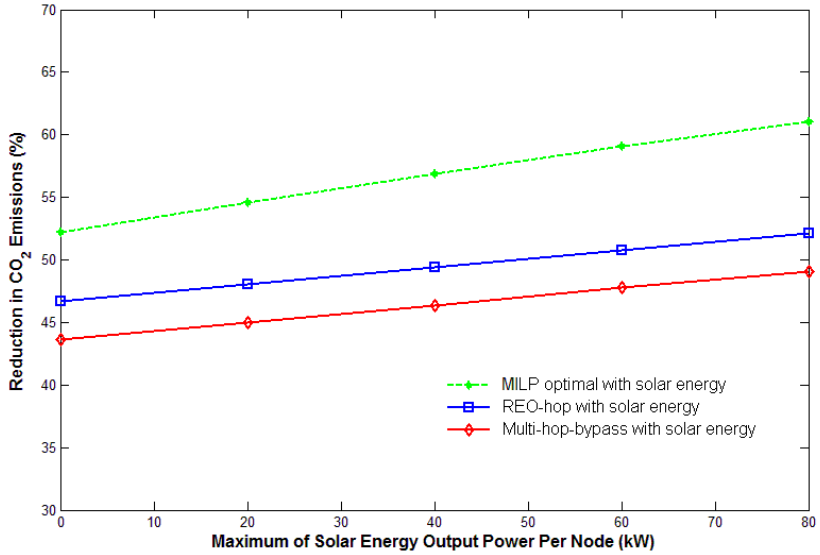

Fig 4 - 10: Reduction in CO_2 emissions in 24 hour period under different heuristics

A similar trend to that observed in Fig 4-9 is noticed for the reduction in CO_2 emissions in Fig 4-10. The total CO_2 emissions during a 24 hour period have been reduced by about 47%~52% and 43%~49% under the REO-hop and multi-hop-bypass heuristics, respectively compared to the non-bypass heuristic without renewable case. As mentioned in Chapter 1, about 228 grams CO_2 are produced through the consumption of 1 kWh of non-renewable energy. We are able to reduce the CO_2 emissions by about 1300 tones every year by using the REO-hop heuristic in NSFNET.

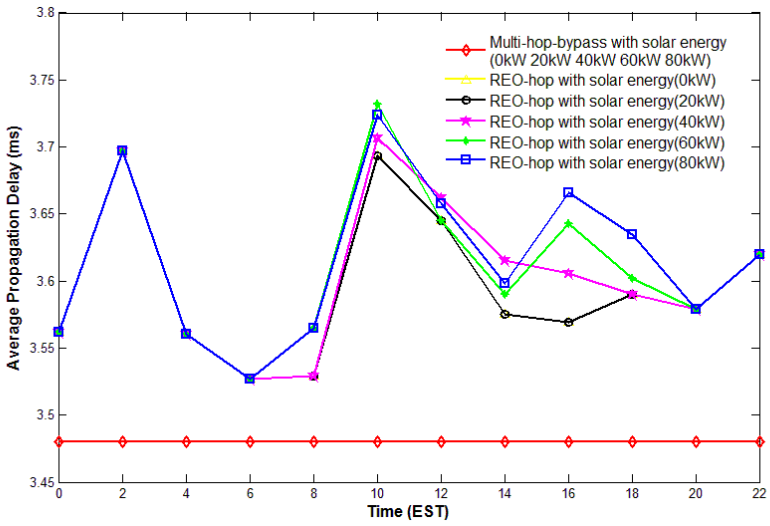

Fig 4 - 11: Average propagation delay of REO-hop and multi-hop-bypass heuristics

As the REO-hop heuristic routes demands dynamically based on the output power of solar energy sources in nodes and the available capacity, the propagation delay under the REO-hop heuristic is expected to increase compared to the multi-hop-bypass heuristic which routes traffic based on the shortest path. However, as the REO-hop heuristic routes demands using only one of the two shortest-path routes, it can be observed in Fig 4-11 that the propagation delay has not increased significantly (the increase is less than 0.3 ms, i.e. less than 10%) maintaining the QoS.

4.5.2 Number and Location of Nodes Using Renewable Energy

In Chapter 4, Section 4.5.1, only the five nodes with the highest nodal degree have been selected in the NSFNET network to use renewable energy. In this section the impact of the number and location of nodes that use renewable energy is studied. First, we investigate how the non-renewable energy consumption is affected by the maximum output power of renewable energy sources and the number of nodes that use renewable energy. In Fig 4-12 the number of nodes with access to renewable energy increases by adding to the list the node with the next larger node ID, i.e. the set of nodes using renewable energy takes the following values: {1}, {1,2}, {1,2,3}, {1,2,3,4}, … {1,2,3…14}. A range of values for the maximum output power of renewable energy sources from 0 kW to 80 kW is examined.

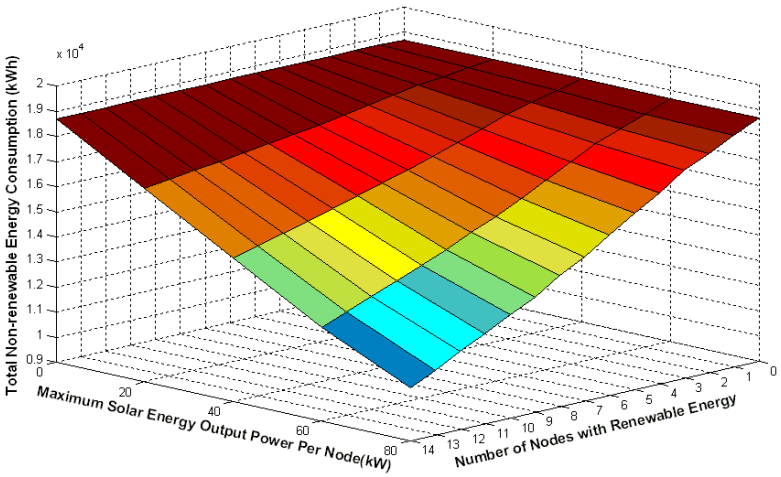

Fig 4 - 12: The total non-renewable energy consumption in 24 hour period under different maximum solar energy power per node and different number of nodes employing solar energy

In Fig 4-12, it is clear that increasing the number of nodes that use renewable energy and increasing the maximum output power per renewable energy source reduces the total non-renewable energy consumption of the network. However, it can be seen from the figure that the relation is not linear between the number of nodes and the non-renewable energy consumption which indicates that some nodes have more impact on the non-renewable energy consumption than others if they are selected to use renewable energy.

To investigate the impact of the location of nodes that use renewable energy on the total non-renewable energy consumption, a new MILP model is developed with the objective of optimising the selection of nodes that use renewable energy such that the non-renewable energy consumption savings are maximised. The new MILP model is subject to the same constraints in Chapter 4, Section 4.3, except that Equation (4-12) is replaced with Equation (4-18) and a new constraint is added (Equation (4-19)).

In this model, time is considered as a variable. Therefore, *t* is added to all the variables in Table 4-1 where *t* is the time point of time set *T*. The new MILP model by which we would be able to obtain optimal node locations employing renewable energy is defined as follows:

Objective: maximise

$$\sum_{t\epsilon T}\sum_{i\epsilon N}\left(PR^{s}\cdot\left(Q_{it}^{s}+\sum_{p\epsilon P}\delta_{ipt}\cdot Ws_{pt}\right)+\sum_{e\epsilon E}PT^{s}\cdot\omega s_{et}\cdot\delta_{iet}+PMD^{s}\cdot DMs_{it}+PO_{i}^{s}\cdot y_{it}\right) \quad (4\text{-}17)$$

Subject to:

Equations: (4-8) (4-9) (4-10) (4-11) (4-13) (4-14) (4-15) (4-16)

(Every variable in the equations above has had the time variable *t* augmented)

$$PR^s \cdot \left(Q_{it}^s + \sum_{p \in P} \delta_{ipt} \cdot Ws_{pt} \right) + \sum_{e \in E} PT^s \cdot \omega s_{et} \cdot \delta_{iet} + PMD^s \cdot DMs_{it} + PO_i^s \cdot y_{it} \leq S_{it} \cdot \varepsilon_i \quad (4\text{-}18)$$

$$\forall\, i \in N, t \in T$$

$$\sum_{i \in N} \varepsilon_i = Ns \quad (4\text{-}19)$$

where ε_i =1 if node i uses renewable energy, otherwise ε_i=0, and Ns is the total number of nodes with access to renewable energy. Equation (4-18) ensures that the renewable energy consumption in each node is within the maximum output power of its associated renewable energy source at any time of the day. Equation (4-19) implies that the total number of nodes that use renewable energy is limited to Ns which is set in advance.

The optimisation results are given in Fig 4-13 under different values of the maximum renewable energy output power (20 kW to 80 kW), assuming Ns=5 and the traffic demand shown in Fig 4-5. We can see that the optimal node selection does not change. To verify the optimisation results, in Fig 4-14 we evaluate the total non-renewable energy consumption in a 24 hour period under the REO-hop heuristic where we assume that only a single node uses renewable energy (note that Fig 4-13 used MILP). We evaluate the performance under different values of the maximum solar energy per node. It is clear that the total non-renewable consumption is lower when the nodes in the centre of the network (4, 5, 6, 7, and 9) use renewable energy.

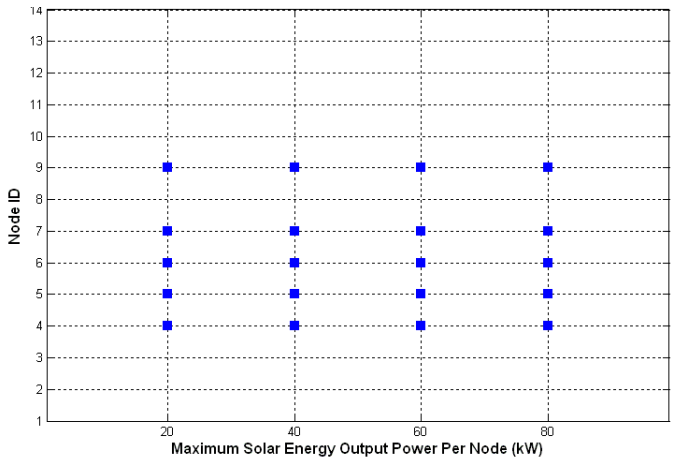

Fig 4 - 13: Optimum node location of nodes with access to renewable energy for different values of maximum available solar energy per node (MILP-optimal)

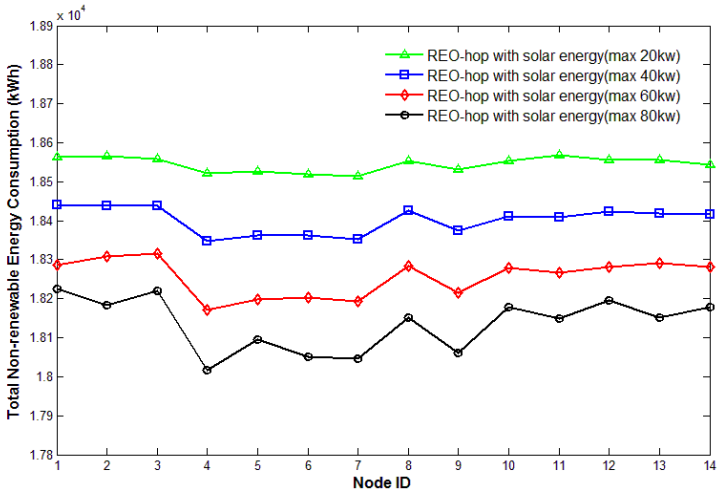

Fig 4 - 14: The total non-renewable energy consumption in 24 hour period with different nodes using renewable energy

In Fig 4-15, the delay and power consumption performance are evaluated under the REO-hop heuristic with a maximum renewable power of 60 kW per node when central network nodes {4, 5, 6, 7, 9} or the periphery nodes {1, 2, 10, 11, 14} are selected to use renewable energy. It is clear that the former node set results in a higher reduction in the non-renewable power consumption compared to the latter node set. Also in Fig 4-15 it is clear that selecting the node set {4, 5, 6, 7, 9} results in a lower average propagation delay compared to the node set {1, 2, 10, 11, 14}. Therefore, the optimal selection of nodes using renewable energy results in better utilisation of the renewable energy resources.

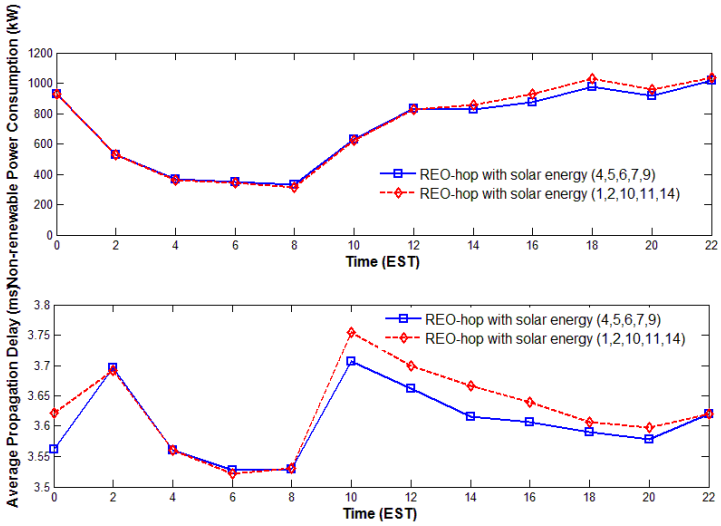

Fig 4 - 15: The non-renewable power consumption and the average propagation delay under two different node selection scenarios using renewable energy

4.5.3 The Non-renewable Energy Consumption of Nodes

In this section we investigate the reduction in the non-renewable energy consumption experienced by each node individually under different heuristics. We compare the scenarios when no renewable energy sources are used and when some nodes use renewable energy (nodes 4, 5, 6, 7 and 9). Assuming the traffic demand in Fig 4-5 and that the maximum solar power is 60 kW, Fig 4-16 shows the non-renewable energy consumption of all nodes in the NSFNET network. It is clear that under both cases the non-renewable energy consumption of nodes with the Non-bypass heuristic has a large variance because nodes at the centre of the network consume more energy as more traffic flows are routed through them. Compared with the Non-bypass heuristic, the multi-hop-bypass and REO-hop heuristics have significantly reduced the non-renewable energy consumption and its variance. However, nodes at the centre of network still have slightly more non-renewable energy consumption than the nodes at the edge of the network. As expected, the REO-hop heuristic results in further reductions compared to the multi-hop-bypass heuristic. It is also clear in the figure that as nodes at the centre of the network use renewable energy, their non-renewable energy consumption is significantly reduced when renewable energy sources are introduced to the network.

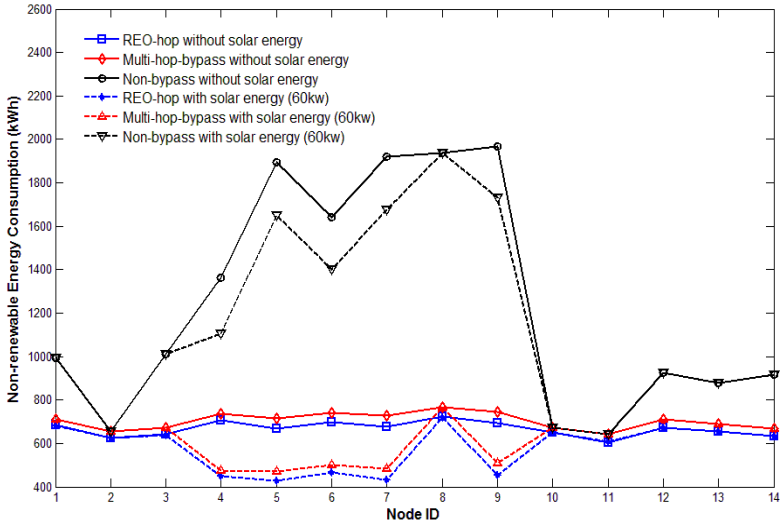

Fig 4 - 16: The non-renewable energy consumption of the nodes in a 24 hour period under different heuristics

4.5.4 The Non-renewable Power Consumption of the REO-hop Heuristic under Adaptive Link Rate

Results were obtained in the previous sections under the assumption that equipment has two energy states (on and off), i.e. the equipment consumes full power when switched-on. However, energy consumption can be decreased by deploying energy-efficient components. Several factors affect the power consumption of telecommunication equipment, such as traffic load, temperature and QoS policies [126]. Load is considered one of the factors that have the highest influence on equipment power consumption. In this section, the effect of ALR on the non-renewable power consumption is investigated.

Different energy profiles are proposed to provide a more accurate definition of the dependency between equipment energy consumption and traffic load. Fig 4-17 shows different energy profiles for telecommunication equipment [126] where energy consumption is a function of the load on the network component. The latter is expressed as a percentage of the total capacity of the network component. We consider (i) 'On-off' energy profile [126] (ii) 'Linear' energy profile: Here the energy consumption depends linearly on the traffic load, e.g. in switch architectures like Batcher, Crossbar and Fully-Connected [126], [147] (iii) 'Log_{10}' energy profile employed in equipment that uses hibernation techniques such as the low-power idle technique for Ethernet [148]. In this approach data is sent as fast as possible to allow the equipment to quickly return to the low-power idle state. (iv) 'Log_{100}' energy profile: This profile is considered as a middle function between the 'On-off' and the 'Log10' profiles. (v) 'Cubic' energy profile: Typical in equipment that uses Dynamic voltage Scaling (DVS) and Dynamic Frequency Scaling (DFS) [126].

Under the same assumptions of Section 4.5.1 and with 20 kW solar power at the five optimum nodes or 80 kW at all nodes, Fig 4-18 shows the non-renewable energy consumption of the REO-hop heuristic where we consider the different energy profiles in Fig 4-17 for router ports and transponders (the two most energy consuming sub-systems in the node). It is clear from Fig 4-18 that the non-renewable energy consumption curves' behaviour is subject to the energy profile curves in Fig 4-17. The largest reduction in non-renewable energy consumption occurred under the 'cubic' profile. Compared to the 'on-off' profile, the 'cubic' profile results in a

reduction in the non-renewable energy consumption by up to 9% between 12:00 and 20:00.

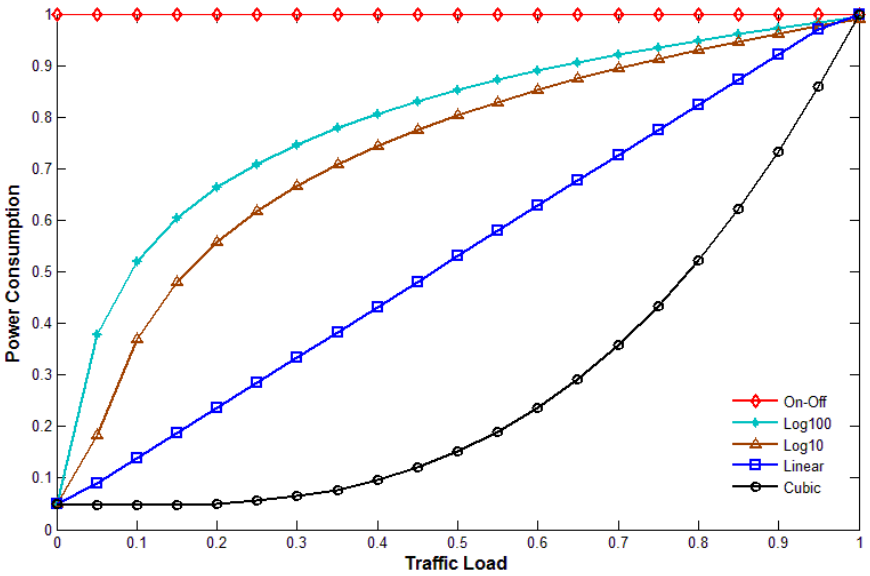

Fig 4 - 17: Different energy profiles

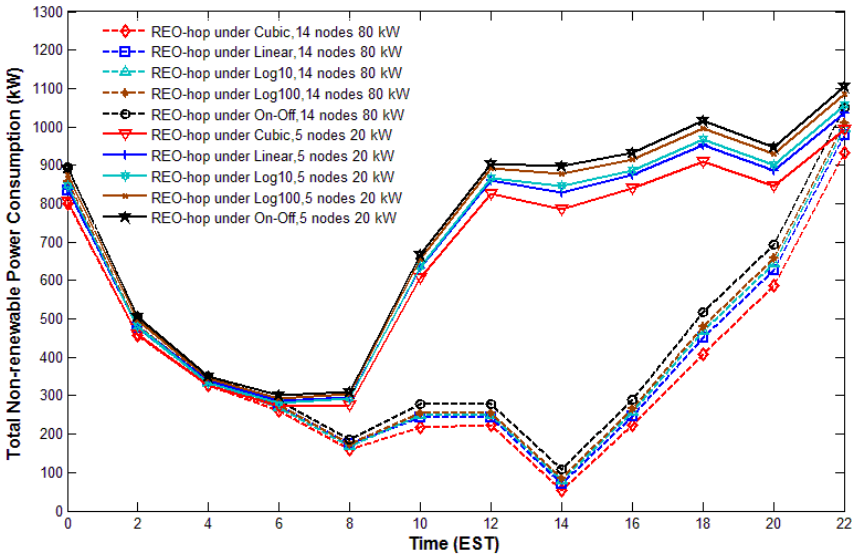

Fig 4 - 18: Total non-renewable power consumption of the REO-hop heuristic under different energy profiles

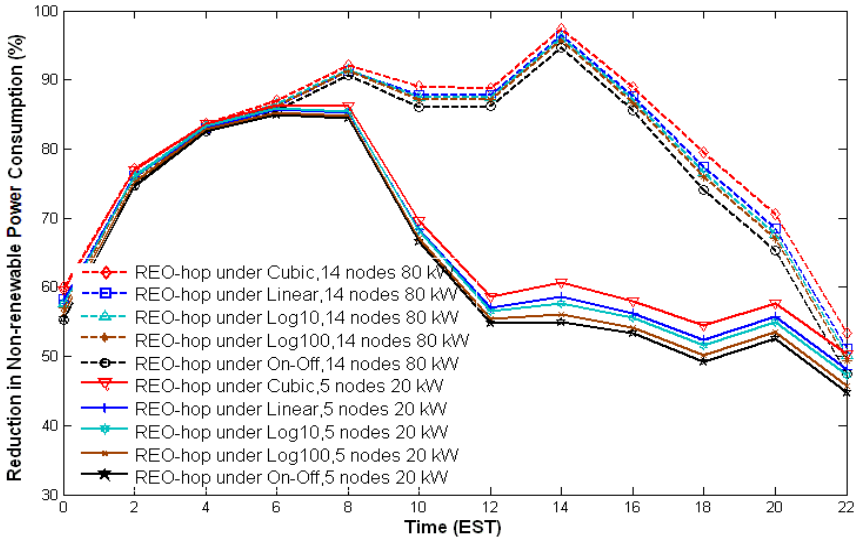

Fig 4 - 19: Reduction in non-renewable power consumption of the REO-hop heuristic under different energy profiles

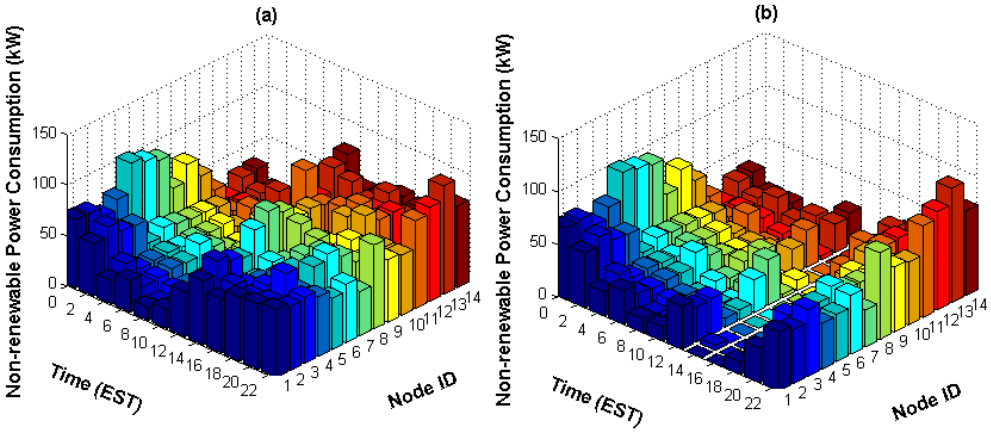

Fig 4 - 20: Non-renewable power consumption at each node under REO-hop heuristic and 'cubic' profile with: (a) 20 kW solar power at nodes (4, 5, 6, 7, 9), (b) 80 kW at all nodes

It should be noted that in Fig 4-18 the energy profiles of Fig 4-17 are only applied to partially loaded wavelengths while an 'on-off' profile is applied to fully loaded wavelengths. For example a traffic demand of 70 Gbit/s between a node pair calls for two wavelengths, one fully loaded, the other partially loaded. The relatively small (9%) reduction in energy consumption associated with ALR is commensurate with this. Note that when all the nodes have access to 80 kW solar power then the power consumption in Fig 4-18 continues to decrease beyond 6 am due to the availability of solar power at the nodes. At 22:00 the two sets of curves converge,

however the total energy consumption is still lower when all nodes have access to solar power due to solar power availability in more nodes.

The sum of the total power consumed by all nodes, where each node is dimensioned based on the largest number of router ports needed over the 24 hour period is 2010 kW which is the peak shown in Fig 4-8 in the non-bypass case without solar energy. The energy saving between such a network and the results in Fig 4-18 (clustered curves where only 5 nodes use 20 kW renewable power) is significant and the maximum is approximately 85%. The average savings in this case are approximately 65% and vary slightly between the five profiles. These savings are shown in Fig 4-19. Note that the 85% and 65% savings are almost real energy savings since the renewable energy is low here and has limited effect. The savings come from our architecture design (photonic switching instead of electronic routing) and powering down unused router ports and transponders. Fig 4-20 shows the non-renewable power consumption of the individual nodes in the network under the REO-hop heuristic when only the 5 optimum nodes have access to 20 kW renewable power each, and when all the nodes have access to 80 kW renewable power each. It helps appreciate the typical power consumption levels per node and the impact of 20 kW renewable power at five nodes (4, 5, 6, 7, 9) and 80 kW renewable at all nodes.

Fig 4-18 also shows the total non renewable power consumption when all the NSFNET nodes have access to 80 kW renewable power each. The maximum reduction in non-renewable power consumption (reduction in CO_2 emissions) in this case compared to the peak in Fig 4-8 is 97%. This is also shown in Fig 4-19. The average savings here are approximately 78% with small variation between the five profiles.

4.6 Hybrid-power IP over WDM Network in the USNET Network

The USNET network, depicted in Fig 4-21, is considered as another (larger scale) example of a real world network to compare with the NSFNET network. The USNET network consists of 24 nodes and 43 bidirectional links. Solar energy is used

as the renewable energy source. As the USNET network covers the US, it is similar to the NSFNET network in terms of time zones. It also has four time zones, Eastern Standard Time (EST), Central Standard Time (CST), Mountain Standard Time (MST) and Pacific Standard Time (PST). We also use EST as the reference time.

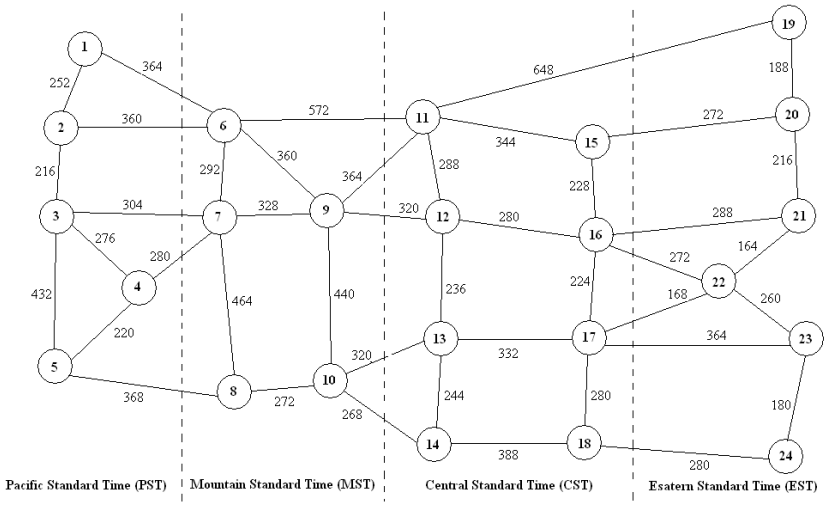

Fig 4 - 21: The USNET network with time zones

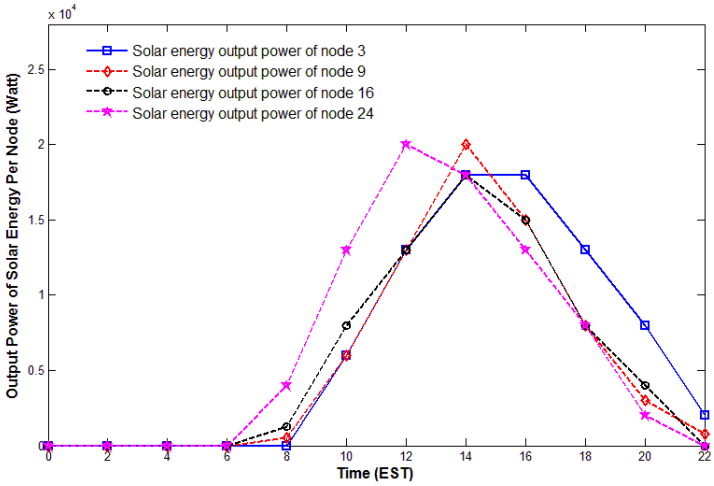

Fig 4 - 22: Solar energy in different nodes in different time zones

The same average traffic demand (Fig 4-5) used in the NSFNET network during different hours of the day is also used in USNET network. The geographical location of nodes affects the sunset and sunrise time, and therefore has impact on the solar energy generated in each node. The solar energy available to different time zones in a typical clear sky day in June are shown in Fig 4-22. Table 4-4 gives the details of the solar power available to each node. This is non-zero from 6:00 to 22:00 and the maximum occurs at 12:00.

(SR: Sunrise, SS: Sunset. SR time and SS time are given in the node's local time in June)

Time(EST) / Node ID		0:00	2:00	4:00	6:00	8:00	10:00	12:00	14:00	16:00	18:00	20:00	22:00
1	SR:5:12 SS: 21:09	0 kW	0 kW	0 kW	0 kW	0 kW	6 kW	13 kW	18 kW	18 kW	13 kW	8kW	4 kW
2	SR:5:27 SS: 21:01	0 kW	0 kW	0 kW	0 kW	0 kW	6 kW	13 kW	18 kW	18 kW	13 kW	8kW	4 kW
3	SR:5:44 SS: 20:10	0 kW	0 kW	0 kW	0 kW	0 kW	6 kW	13 kW	18 kW	18 kW	13 kW	8kW	2 kW
4	SR:5:56 SS: 21:02	0 kW	0 kW	0 kW	0 kW	0 kW	6 kW	13 kW	18 kW	18 kW	13 kW	8kW	4 kW
5	SR:5:42 SS: 20:08	0 kW	0 kW	0 kW	0 kW	0 kW	6 kW	13 kW	18 kW	18 kW	13 kW	8kW	2 kW
6	SR:5:27 SS: 20:47	0 kW	0 kW	0 kW	0 kW	0.5 kW	6 kW	13 kW	20 kW	18 kW	13 kW	8kW	0.6 kW
7	SR:5:57 SS: 21:01	0 kW	0 kW	0 kW	0 kW	0 kW	6 kW	13 kW	20 kW	18 kW	13 kW	8kW	3 kW
8	SR:5:18 SS: 19:34	0 kW	0 kW	0 kW	0 kW	0.8 kW	6 kW	13 kW	20 kW	15 kW	8 kW	3kW	0 kW
9	SR:5:32 SS: 20:31	0 kW	0 kW	0 kW	0 kW	0.5 kW	6 kW	13 kW	20 kW	15 kW	8 kW	3kW	0.8 kW
10	SR:6:01 SS: 20:17	0 kW	0 kW	0 kW	0 kW	0 kW	6 kW	18 kW	20 kW	15 kW	8 kW	2kW	0.5 kW
11	SR:5:55 SS: 21:02	0 kW	0 kW	0 kW	0 kW	0.5k W	8 kW	13 kW	18 kW	15 kW	8 kW	5 kW	0 kW
12	SR:6:12 SS: 21:06	0 kW	0 kW	0 kW	0 kW	0.6k W	8 kW	13 kW	18 kW	15 kW	8 kW	5 kW	0 kW
13	SR:6:13 SS: 20:46	0 kW	0 kW	0 kW	0 kW	0.5k W	8 kW	13 kW	18 kW	15 kW	8 kW	4 kW	0 kW
14	SR:6:35 SS: 20:37	0 kW	0 kW	0 kW	0 kW	0.5k W	8 kW	13 kW	18 kW	15 kW	8 kW	4 kW	0 kW
15	SR:5:27 SS: 20:33	0 kW	0 kW	0 kW	0 kW	1.5k W	8 kW	13 kW	18 kW	15 kW	8 kW	4 kW	0 kW
16	SR:5:46 SS: 20:18	0 kW	0 kW	0 kW	0 kW	1.3k W	8 kW	13 kW	18 kW	15 kW	8 kW	4 kW	0 kW
17	SR:5:54 SS: 20:11	0 kW	0 kW	0 kW	0 kW	1kW	7 kW	13 kW	18 kW	15 kW	8 kW	4 kW	0 kW
18	SR:6:00 SS: 20:04	0 kW	0 kW	0 kW	0 kW	1kW	7 kW	13 kW	18 kW	15 kW	8 kW	4 kW	0 kW
19	SR:5:08 SS: 20:41	0 kW	0 kW	0 kW	1.8 kW	5 kW	15 kW	20 kW	18 kW	13 kW	8 kW	2 kW	0 kW
20	SR:5:14 SS: 20:31	0 kW	0 kW	0 kW	1.5 kW	5 kW	15 kW	20 kW	18 kW	13 kW	8 kW	2 kW	0 kW
21	SR:5:25 SS: 20:32	0 kW	0 kW	0 kW	1 kW	4.5 kW	13 kW	20 kW	18 kW	13 kW	8 kW	2 kW	0 kW
22	SR:5:43 SS: 20:38	0 kW	0 kW	0 kW	0.8 kW	4.3 kW	13 kW	20 kW	18 kW	13 kW	8 kW	2 kW	0 kW
23	SR:5:54 SS: 20:28	0 kW	0 kW	0 kW	0 kW	4 kW	13 kW	20 kW	18 kW	13 kW	8 kW	2 kW	0 kW
24	SR:6:19 SS: 20:34	0 kW	0 kW	0 kW	0 kW	4 kW	13 kW	20 kW	18 kW	13 kW	8 kW	2 kW	0 kW

Table 4 - 4: Solar power available to each node in the USNET (20 kW maximum output power)

4.6.1 The Non-renewable Power Consumption of the Network

In this section the non-renewable power consumption of the network in a clear sky day in June is investigated. Nodes 1, 4, 6, 7, 19, 20 and 22 are selected randomly

to deploy solar energy sources. In Section 4.6.2, the optimisation of the location of nodes deploying solar energy is studied.

As in NSFNET, typically a one square meter silicon solar cell can produce about 0.28kW of power [143] and the maximum solar energy available to a node is 20kW, therefore a total solar cell area of about 100 m^2 is required. We assume the traffic demands and the output power levels of the solar energy sources given in Fig 4-5 and Fig 4-22, respectively. The network parameters are same as in Table 4-3 in Section 4.5.1.

The AMPL/CPLEX software is used to solve the MILP problem. Five different cases are considered: 1) Non-bypass heuristic without renewable energy, 2) Non-bypass heuristic with renewable energy, 3) Multi-hop-bypass heuristic without renewable energy 4) Multi-hop-bypass heuristic with renewable energy, and 5) REO-hop heuristic with renewable energy.

Fig 4-23 shows the total non-renewable power consumption under the assumption that the maximum solar energy available to a node is 20 kW. The curve "Non-bypass without solar energy" provides the upper bound on the non-renewable power consumption. Compared to the upper bound, both the multi-hop-bypass and REO-hop heuristics have reduced the non-renewable power consumption. When the solar energy is significant and the traffic demand is high (between 6:00 and 22:00), the REO-hop heuristic with solar energy slightly outperforms the multi-hop-bypass heuristic. Compared with the upper bound, at 12:00, 14:00, 16:00 and 18:00, the REO-hop heuristic saves non-renewable power of about 3000 kW, i.e. about 50%. Furthermore, the REO-hop heuristic still outperforms the multi-hop-bypass heuristic from 0:00 to 6:00 when there is no solar power and the traffic demand is low as the REO-hop routing algorithm tries to route demands on virtual links with sufficient capacity rather than using shortest-path routing as with the multi-hop-bypass heuristic.

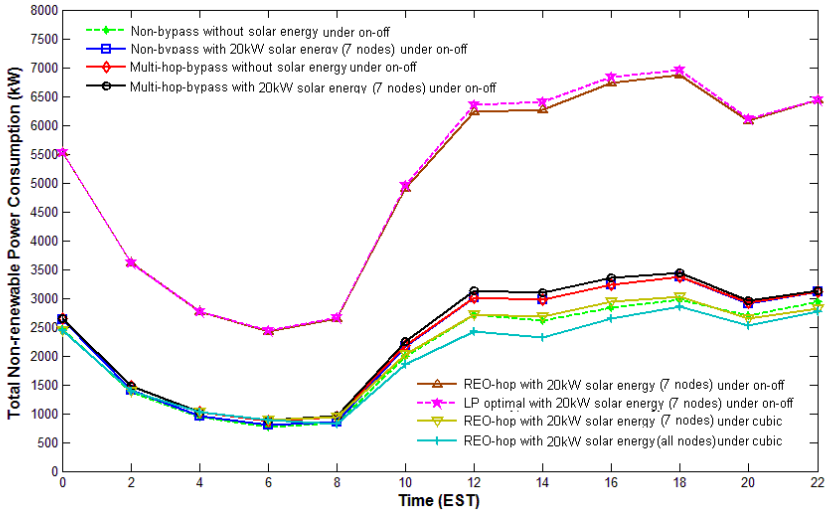

Fig 4 - 23: The total non-renewable power consumption of different heuristics with and without solar energy

Load is one of the factors that influences equipment energy consumption. The results in Fig 4-23 are under the "on-off" energy profile. In Fig 4-23, the total non-renewable power consumption under a "cubic" energy profile is also investigated. Introducing the cubic energy profile has resulted in reducing the total non-renewable power consumption under the REO-hop heuristic by 58%. Further CO_2 reductions can be introduced by deploying solar energy in all the nodes in the network. Compared to the upper bound, the REO-hop heuristic under the cubic energy profile and when all nodes have access to solar energy (see Fig 4-23) has achieved an average non-renewable power reduction (CO_2 reduction) of 69%.

In Fig 4-24, the impact of different values of the maximum solar energy (40 kW, 60 kW and 80 kW) available per node on the total non-renewable energy consumption is examined. A solar cell area of up to 300 m^2 is needed to generate such values (300 m^2 for 80kW). Solar cell cladding with such surface area can be practically built in a typical core routing node location. It is clear that increasing the maximum solar energy output per node has linearly reduced the total non-renewable energy consumption using different algorithms. Using the REO-hop heuristic has resulted in higher reduction in the non-renewable energy consumption compared to the multi-hop heuristic.

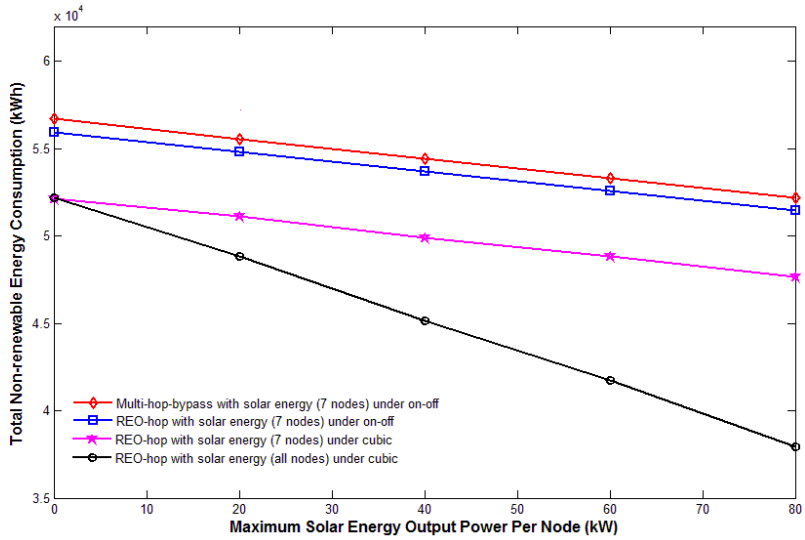

Fig 4 - 24: The total non-renewable energy consumption in a 24 hour period for different values of the maximum solar energy under different heuristics and energy profiles

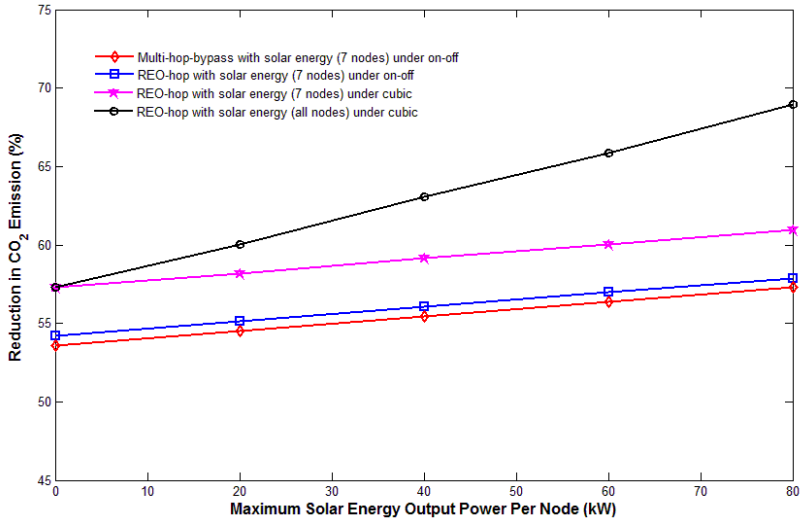

Fig 4 - 25: Reduction in CO_2 emissions in a 24 hour period under different heuristics

Similar trends to those observed in Fig 4-24 are noticed for the reduction in CO_2 emissions in Fig 4-25 The total CO_2 emissions during a 24 hour period have been reduced by about 57%~69% using the REO-hop heuristic with all nodes employing 80 kW solar energy under the cubic energy profile. We are able to reduce the CO_2 emissions by about 4600 tones every year by using the REO-hop heuristic in the USNET network.

It can be seen from Fig 4-10 and Fig 4-25 that the REO-hop heuristic has resulted in higher reductions in the non-renewable energy consumption of the USNET compared to the NSFNET when there is no solar energy or only few nodes

employing solar energy. This can be understood by noting that the REO-hop heuristic is based on bypass and reduces the non-renewable power consumption mainly by reducing the number of IP ports in intermediate nodes between the source node and the destination node. Given that the average hop count is 2.5 and 3.0 in the NSFNET and the USNET, respectively, the REO-hop heuristic will result in higher reductions in the number of IP ports in intermediate nodes in the USNET and therefore a higher percentage reduction in the non-renewable energy consumption in the USNET.

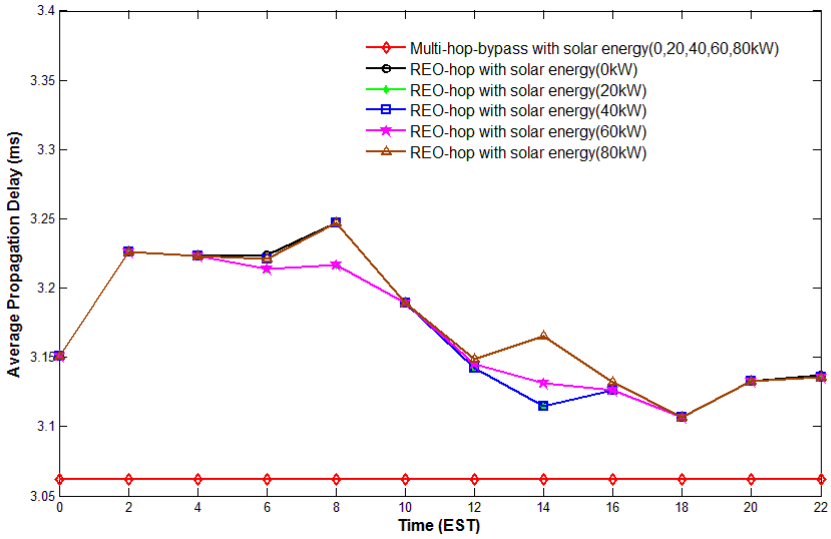

Fig 4 - 26: Average propagation delay of REO-hop and multi-hop-bypass heuristic

As the REO-hop heuristic routes demands dynamically based on the output power of solar energy sources in nodes and the available capacity, it can be seen in Fig 4-26 that the propagation delay has not increased significantly compared to the multi-hop-bypass heuristic which is based on the shortest path (the increase is less than 0.2 ms, i.e. less than 8%) maintaining the QoS.

4.6.2 Number and Location of Nodes Using Renewable Energy in USNET

In Section 4.6.1, 7 nodes randomly in the USNET network have been selected to use renewable energy. To optimise the location of nodes that have access to renewable energy, the MILP model mentioned in Section 4.5.2 is used. The optimisation results are given in Fig 4-27 (a) under different values of the maximum

renewable energy output power (20 kW to 80 kW), assuming Ns=7 and the traffic demand shown in Fig 4-5. The optimal node selection does not change.

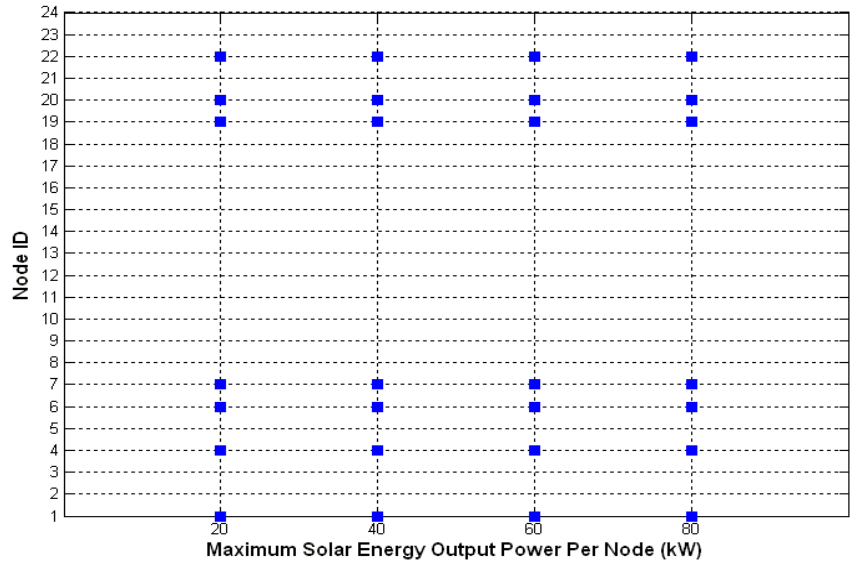

Fig 4 - 27: Optimal location of nodes with access to renewable energy for different values of the maximum available solar energy per node

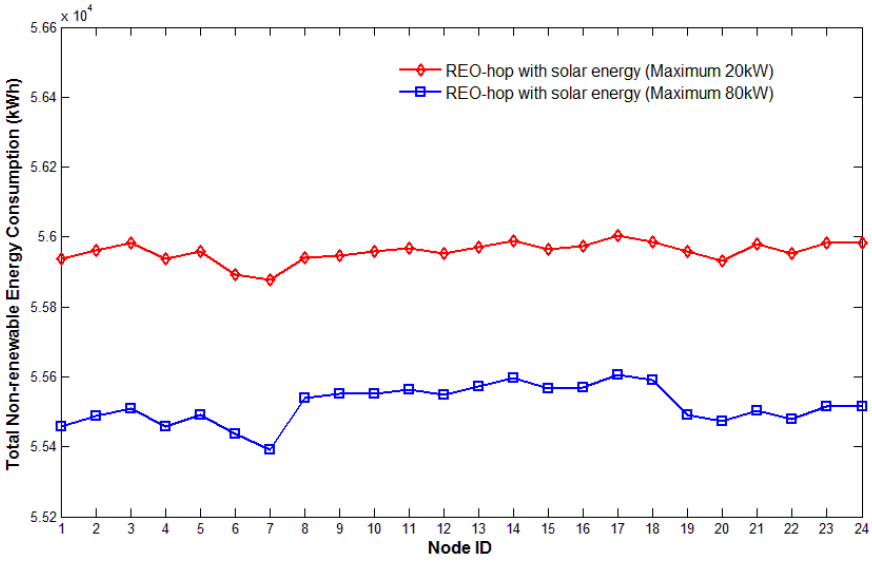

Fig 4 - 28: The total non-renewable energy consumption in a 24 hour period with different nodes using renewable energy

To verify the optimisation results in Fig 4-27, we evaluate the total non-renewable energy consumption in a 24 hour period under the REO-hop heuristic in Fig 4-28 where we assume that only a single node uses renewable energy. We evaluate the performance under different values of the maximum solar energy per

node. It is clear that the total non-renewable consumption is lower when nodes (1, 4, 6, 7, 19, 20 and 22) use renewable energy.

From Fig 4-27 and Fig 4-28, it can be seen that the distribution of optimal node locations is different compared to the NSFNET network as the impact of deploying renewable energy at a node depends on its energy consumption and geographical location. Nodes with larger traffic flows and higher solar energy are expected to have more impact on the total non-renewable energy consumption of the network. Fig 4-29 and Fig 4-31 show the non-renewable energy consumption under the REO-hop heuristic without solar energy and the output power of the solar energy of each node (maximum output power is 80 kW) in the NSFNET network, respectively. The nodes in the centre of the NSFNET network consume more non-renewable energy and have larger solar energy output power in a 24 hour period compared to other nodes. Therefore deploying renewable energy in these nodes will result in larger reduction in the total non-renewable energy consumption of network. Similarly, in the USNET network nodes with the highest non-renewable energy consumption without solar energy (Fig 4-30) and the highest output solar energy (Fig 4-32) are selected to deploy solar energy.

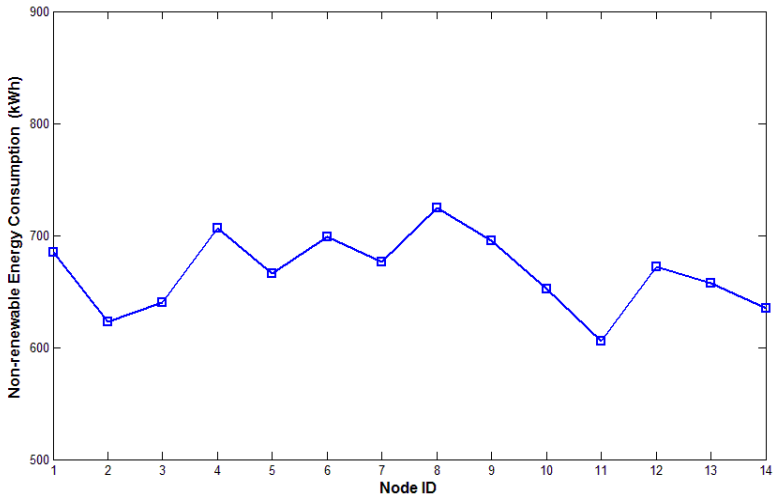

Fig 4 - 29: The non-renewable energy consumption of the NSFNET nodes in a 24 hour period using REO-hop heuristics without solar energy under on-off energy profile in a clear day in June

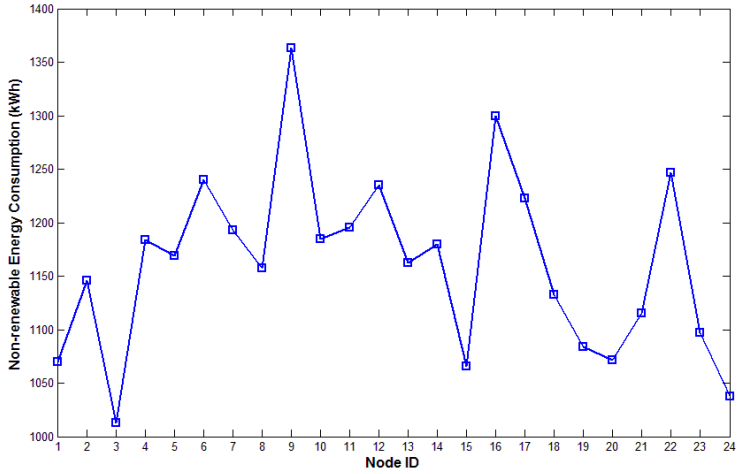

Fig 4 - 30: The non-renewable energy consumption of the USNET nodes in a 24 hour period using REO-hop heuristics without solar energy under on-off energy profile in a clear day in June

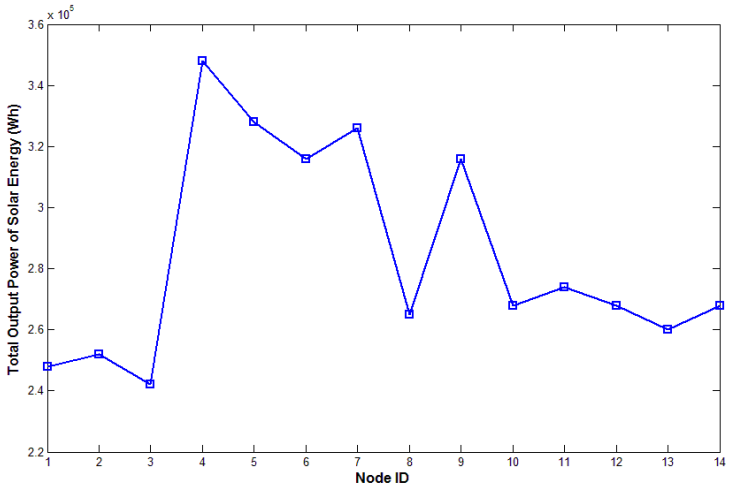

Fig 4 - 31: The solar energy of the NSFNET network nodes in a 24 hour period in a clear day in June

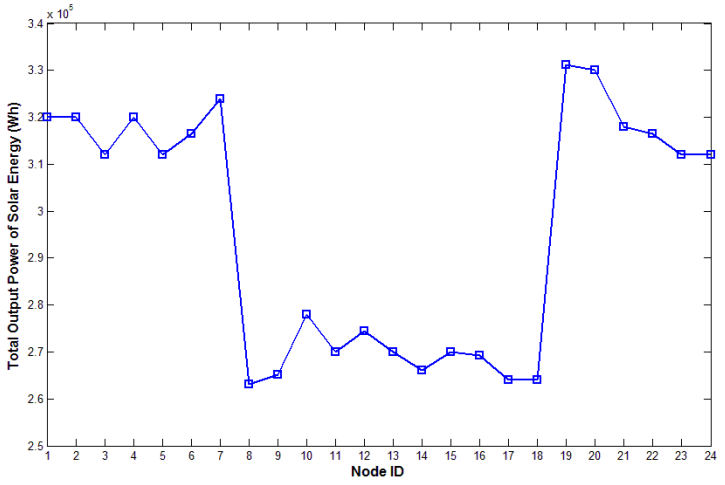

Fig 4 - 32: The solar energy of the USNET network nodes in a 24 hour period in a clear day in June

4.7 Season and Weather Effects

In the previous sections, results were obtained based on the available solar energy in a typical clear sky day in June. However, the available solar energy varies with seasons and weather conditions. In this section the impact of different seasons and weather conditions on the non-renewable power consumption of the network is identified. We consider the larger scale topology, the USNET network. Assuming that the solar cells at a node can produce a maximum of 80 kW, Fig 4-33 [149] and Fig 4-34 [150] show the solar energy in different months of the year and in a cloudy day, respectively. We evaluate the non-renewable power consumption under the different solar energy profiles with the traffic demand in Fig 4-5 and assuming the optimal location of the nodes employing solar energy (1, 4, 6, 7, 19, 20 and 22).

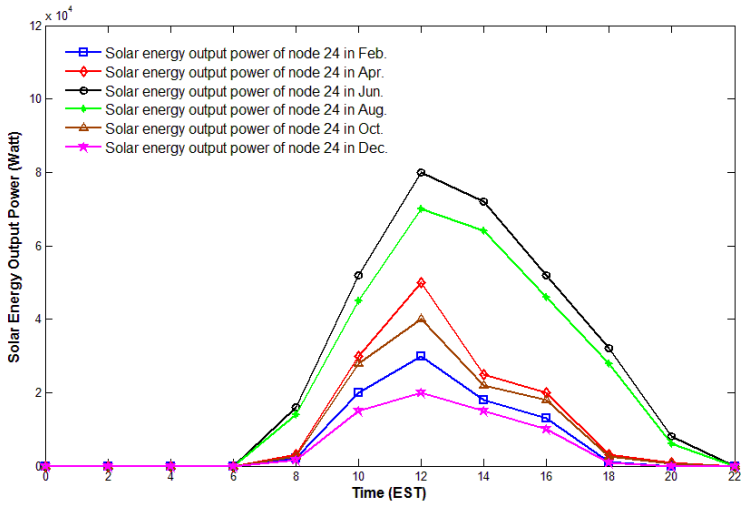

Fig 4 - 33: Solar energy of a node in different months [149]

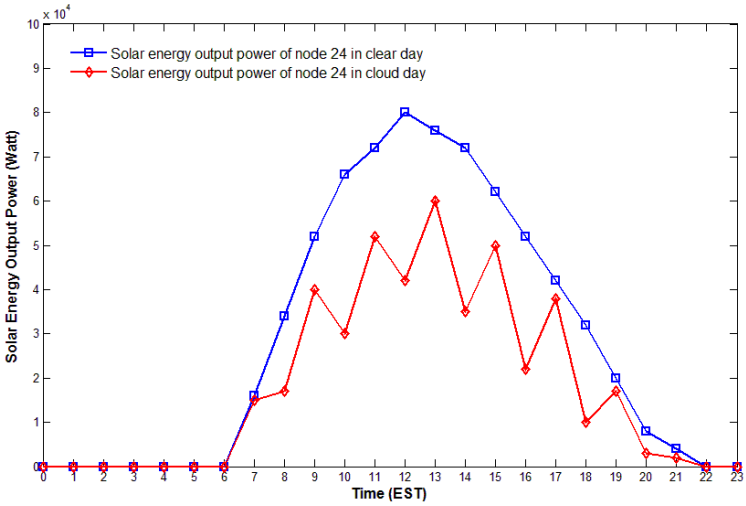

Fig 4 - 34: Output solar energy of a node in different weather conditions [150]

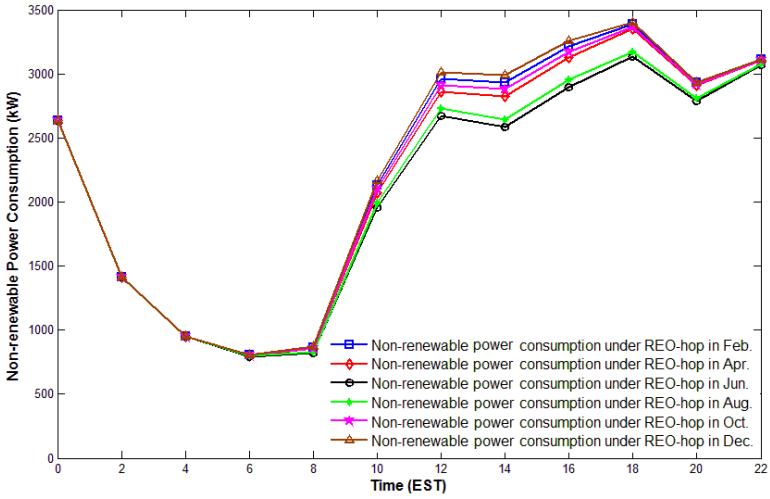

Fig 4 - 35: The non-renewable power consumption of the network with REO-hop heuristic under the on-off energy profile in different months

The non-renewable power consumption of the USNET network with the REO-hop heuristic under an on-off energy profile and in different months is shown in Fig 4-35. As expected in June where the solar radiation is the maximum and the day is longer, the non-renewable power consumption from 6:00 to 20:00 is the lowest compared to other months. The maximum non-renewable energy consumption is experienced in December where the solar radiation is at its lowest and the day is shorter. Compared to June, the non-renewable energy consumption in December has increased by an average of 7%. The total energy consumption of the USNET network in different months of the year is shown in Fig 4-36.

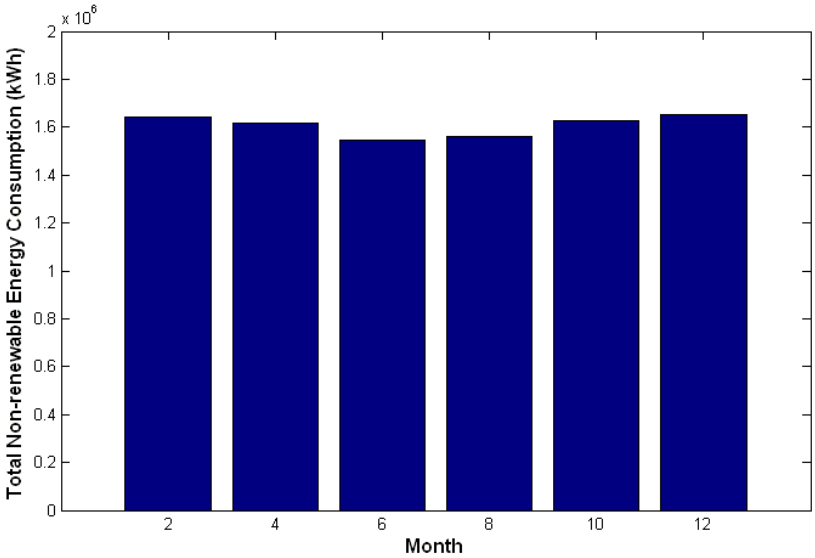

Fig 4 - 36: The total non-renewable energy consumption of the network with the REO-hop heuristic under the on-off energy profile in different months

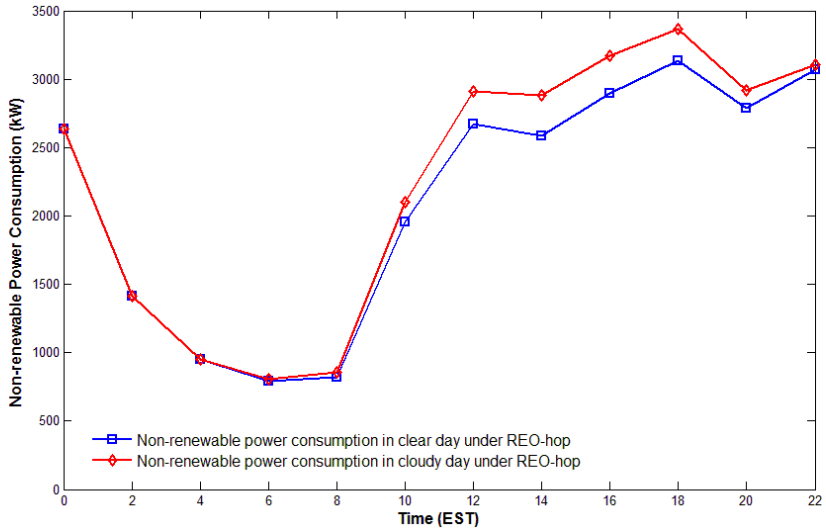

Fig 4 - 37: The non-renewable power consumption of the network with the REO-hop heuristic under the on-off energy profile in different weather conditions in June

Fig 4-37 shows the impact of a cloudy day on the non-renewable power consumption of the USNET network with REO-hop heuristic under on-off energy profile. As expected the non-renewable power consumption is higher in a cloudy day from 6:00 to 20:00 compared to a clear sky day in June. The increase in the non-renewable power consumption is limited to 9%.

4.8 Summary

In this thesis, the use of renewable energy in IP over WDM networks to reduce the non-renewable energy consumption and consequently CO_2 emissions has been proposed. An MILP optimisation model and a highly efficient heuristic based on multi-hop-bypass, known as REO-hop, have been developed to optimise the use of renewable energy in the hybrid-power IP over WDM architecture. The MILP model and the REO-hop heuristic have been investigated assuming solar energy sources under two topologies, the NSFNET and the USNET. For both topologies, the REO-hop heuristic outperforms the multi-hop-bypass. However, the REO-hop heuristic has resulted in higher reductions in the non-renewable energy consumption of the USNET compared to the NSFNET because the REO-hop heuristic will result in higher reductions in the number of ports in intermediate nodes in the USNET as it has a higher average hop number. Compared to the multi-hop-bypass heuristic, the

REO-hop heuristic has reduced the CO_2 emissions by up to 78% in the NSFNET network and 69% in the USNET network while maintaining QoS. An MILP optimisation model has also been developed to optimise the selection of nodes that employ renewable energy. Furthermore, the effects of seasons and weather conditions have been investigated. The results show that the non-renewable energy consumption in December has increased by an average of 7% compared to June, and the increase in the non-renewable energy consumption in a cloudy day is limited to 9% compared to a clear sky day in June.

All the results in this chapter are based on symmetric traffic. To extend, it is also very interesting to optimise the power consumption of the IP over WDM network where network traffic is asymmetric. A general case of a network with asymmetric traffic is that where some nodes are connected to data centres and therefore create traffic on top of the regular traffic. The next chapter will investigate the green optical network with data centres.

Chapter 5: Energy Efficient IP over WDM Networks with Data Centres

5.1 Introduction

The "greening" of data centres creates challenges in attempting to reduce power consumption while maintaining performance. Most of the previous research on data centres power consumption has focused on understanding how to minimise the power consumption inside the data centre. A group known as "Green Grid" was formed to increase the energy efficiency in data centres [151]. However as the networking infrastructure of data centres alone, without considering the cooling equipment energy requirements, is responsible for about 23% of the overall power consumption [15], it is also important to consider the power consumption associated with transporting data between data centres and between data centres and end-users. The total energy consumed by networking elements in data centres in 2006 in the US alone was 3 billion kWh and this continues to rise [152]. In [153] the power consumption of data centres is optimised by powering off unused links and switches while maintaining performance and fault tolerance goals.

The presence of data centres in IP over WDM networks can create a hot node scenario where more traffic is destined to or originates from a data centre node. This can lead to a significant increase in the power consumption of data centre nodes as the number of ports (which are the major power consuming component) increases. In this chapter, the power consumption of IP over WDM networks that contain data centres is studied and in particular three problems are investigated. Firstly, the

optimisation of the data centres locations to minimise the power consumption. A MILP model with this objective is developed. Three factors that affect the optimum location of the data centres in IP over WDM networks are investigated: the IP over WDM routing approach (bypass and non-bypass), the regularity of the network topology and the number of data centres in the network.

Secondly, the energy savings introduced by implementing a data replication scheme [154-156], in the IP over WDM network with data centres are investigated, where frequently accessed data objects are replicated over multiple data centres according to their popularity. Unlike [154-156], the goal here is to minimise power consumption and although delay minimisation is a by-product, it is not the main goal. A novel algorithm, Energy-Delay Optimal Routing (EDOR) is proposed, to minimise the power consumption under the replication scheme while maintaining the QoS. The power savings achieved by the multi-hop bypass and the non-bypass heuristics are investigated.

Thirdly, introducing renewable energy sources (wind and solar energy) to the IP over WDM network with data centres is investigated. The main focus here is to evaluate the merits of transporting bits to where renewable energy is (wind farms), instead of transporting renewable energy to where data centres are. Therefore, we are interested here in the power losses associated with transporting electrical power to data centres and the impact of this on the optimum data centre locations, as well as the impact of the network topology, routing, traffic and other factors on the optimum data centre locations from the power minimisation point of view. A MILP model is set up to optimise the location of data centres by minimising the network non-renewable power consumption taking into account the utilisation of the renewable energy resources and the losses.

5.2 Data Centre Location Optimisation

Fig. 1 shows an IP over WDM network with data centres. In this section IP over WDM networks with data centres are investigated under the lightpath non-bypass and the multi-hop bypass heuristics. The multi-hop bypass heuristic is based on

shortest-path routing. Shortest-path routing is suitable for data centre traffic where end users do not tolerate high delay in accessing data centres. Shortest-path routing is also assumed under the non-bypass heuristic.

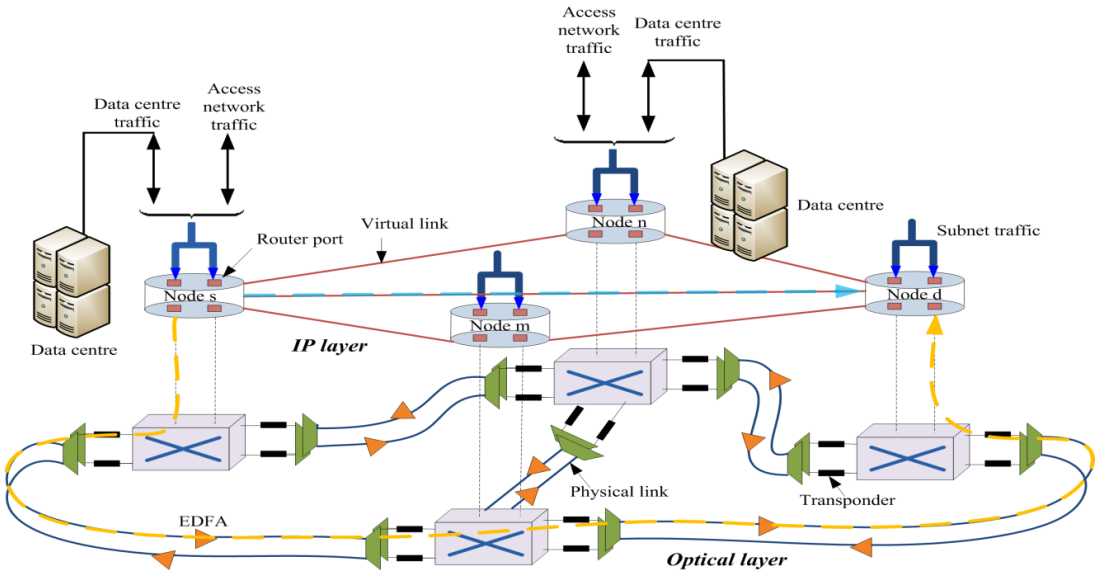

Fig 5 - 1: An IP over WDM network with data centres

5.2.1 Mathematical Model

In this section MILP models are developed to minimise the power consumption of the network by optimising the locations of data centres in the IP over WDM network under the non bypass and the multi-hop bypass approaches. The MILP model for the non bypass approach is developed under the following assumptions:

1. Each node writes and retrieves data from all data centres equally (content popularity is dealt with in Section 5.3).
2. Different data centres have different content.
3. Regular traffic demand is considered, i.e. the traffic demand between regular nodes, and we also consider data centre traffic demands which include the traffic demand between data centres and regular nodes and the traffic demand between data centres (a data centre can access data objects available in another data centre).
4. The traffic demand between data centres and nodes at time t is assumed to be a certain ratio of the regular traffic demand λ^{sdt} between nodes.

5. The uplink traffic demand ratio from nodes to data centres, *Ru,* is smaller than the downlink traffic from data centres to nodes ratio, *Rd* [157].

The total power consumption of the network at time *t* under these assumptions is composed of:

The power consumption of ports in regular nodes and data centres at time *t*

$$\sum_{i\in N}\sum_{j\in N:i\neq j} PR\cdot\omega_{mnt}+\sum_{i\in N} PR\cdot Q_{it}, \tag{5-1}$$

The power consumption of transponders in regular nodes and data centres at time *t*

$$\sum_{m\in N}\sum_{n\in Np_m} PT\cdot\omega_{mnt}, \tag{5-2}$$

The power consumption of EDFAs at time *t*

$$\sum_{m\in N}\sum_{n\in Np_m} PE\cdot EA_{mn}\cdot f_{mn}, \tag{5-3}$$

The power consumption of optical switches in regular nodes and data centres at time *t*

$$\sum_{i\in N} PO_i, \tag{5-4}$$

The power consumption of multiplexers and demultiplexer in regular nodes and data centres at time *t*

$$\sum_{i\in N} PMD\cdot DM_i. \tag{5-5}$$

The MILP model by which we could be able to get the optimal locations of data centres is defined as follows:

Objective: minimise

$$\sum_{t\in T}\left(\sum_{m\in N}\sum_{n\in Np_m} PR\cdot\omega_{mnt}+\sum_{i\in N} PR\cdot Q_{it}+\sum_{m\in N}\sum_{n\in Np_m} PT\cdot\omega_{mnt}\right.$$
$$+\sum_{m\in N}\sum_{n\in Np_m} PE\cdot EA_{mn}\cdot f_{mn}+\sum_{i\in N} PO_i \qquad (5\text{-}6)$$
$$\left.+\sum_{i\in N} PMD\cdot DM_i\right),$$

Subject to:

$$\sum_{j\in N:i\neq j}\lambda\_d_{ijt}^{sd}-\sum_{j\in N:i\neq j}\lambda\_d_{jit}^{sd}=\begin{cases}\lambda^{sdt}\cdot Rd\cdot\delta_s & if\ i=s\\ -\lambda^{sdt}\cdot Rd\cdot\delta_s & if\ i=d\\ 0 & otherwise\end{cases} \qquad (5\text{-}7)$$

$$\forall\ t\in T,\forall\ s,d,i\in N: s\neq d,$$

$$\sum_{j\in N:i\neq j}\lambda\_u_{ijt}^{sd}-\sum_{j\in N:i\neq j}\lambda\_u_{jit}^{sd}=\begin{cases}\lambda^{sdt}\cdot Ru\cdot\delta_d & if\ i=s\\ -\lambda^{sdt}\cdot Ru\cdot\delta_d & if\ i=d\\ 0 & otherwise\end{cases} \qquad (5\text{-}8)$$

$$\forall\ t\in T,\forall\ s,d,i\in N: s\neq d,$$

$$\sum_{j\in N:i\neq j}\lambda\_r_{ijt}^{sd}-\sum_{j\in N:i\neq j}\lambda\_r_{jit}^{sd}=\begin{cases}\lambda^{sdt} & if\ i=s\\ -\lambda^{sdt} & if\ i=d\\ 0 & otherwise\end{cases} \qquad (5\text{-}9)$$

$$\forall\ t\in T,\forall\ s,d,i\in N: s\neq d,$$

$$\sum_{s\in N}\sum_{d\in N:s\neq d}\left(\lambda\_d_{ijt}^{sd}+\lambda\_u_{ijt}^{sd}+\lambda\_r_{ijt}^{sd}\right)\leq C_{ijt}\cdot B \qquad (5\text{-}10)$$

$$\forall\ t\in T,\forall\ i,j\in N: i\neq j,$$

$$\sum_{n\in Np_m} W_{mnt}^{ij}-\sum_{n\in Np_m} W_{nmt}^{ij}=\begin{cases}C_{ijt} & m=i\\ -C_{ijt} & m=j\\ 0 & otherwise\end{cases} \qquad (5\text{-}11)$$

$$\forall\ t \in T, \qquad \forall\ i,j,m \in N: i \neq j,$$

$$\sum_{i \in N} \sum_{j \in N: i \neq j} W_{mnt}^{ij} \leq W \cdot f_{mn} \tag{5-12}$$

$$\forall\ t \in T, \forall\ m \in N, n \in Np_m,$$

$$\sum_{i \in N} \delta_i = Ndc, \tag{5-13}$$

$$\sum_{i \in N} \sum_{j \in N: i \neq j} W_{mnt}^{ij} = \omega_{mnt}, \tag{5-14}$$

$$\forall\ t \in T, \forall\ m \in N, n \in Np_m,$$

$$Q_{it} = \left(\sum_{d \in N: d \neq i} \lambda^{idt} + \sum_{s \in N: s \neq i} \lambda^{sit} \cdot Rd \cdot \delta_s + \sum_{d \in N: n \neq i} \lambda^{idt} \cdot Ru \cdot \delta_d \right) / B \tag{5-15}$$

$$\forall\ t \in T, \forall\ i \in N.$$

In this MILP model, the parameters are defined as:

i and *j*	Denote end points of a virtual link in the IP layer,
s and *d*	Denote source and destination points of regular traffic demand between a node pair,
m and *n*	Denote end points of a physical fibre link in the optical layer,
Np_i	The set of neighbour nodes of node *i* in the optical layer,
L_{mn}	The length of the link between nodes *m* and *n* in the optical layer,
T	The set of time points,

S	Distance between neighbouring EDFAs,
W	Number of wavelengths in a fibre,
N	The set of nodes,
B	The capacity of each wavelength,
EA_{mn}	The number of EDFAs on physical link (*m, n*). Typically $\mathrm{EA_{mn}} = \lfloor \mathrm{L_{mn}}/\mathrm{S} - 1 \rfloor + 2$, where S is the distance between two neighbouring EDFAs,
f_{mn}	The number of fibres on physical link (*m, n*),
PR	Power consumption of a router port,
PT	Power consumption of a transponder,
PE	Power consumption of an EDFA,
POi	Power consumption of an optical switch.,
PMD	Power consumption of a multi/demultiplexer,
Ndc	The total number of data centres.

The following variables are also defined:

C_{ijt}	The number of wavelength channels (integer) in the virtual link (*i, j*) at time *t*,
Cd_{ijt}	The number of wavelength channels (integer) in the virtual link (*i, j*) for downlink traffic at time *t*,
Cu_{ijt}	The number of wavelength channels (integer) in the virtual link (*i, j)* for uplink traffic at time *t*,

Cr_{ijt} The number of wavelength channels (integer) in the virtual link (*i, j*) for regular traffic at time *t*,

ω_{mnt} The number of wavelength channels in the physical link (m, n) at time *t*,

W_{mnt}^{ij} The number of wavelength channels in the virtual link (*i, j*) that traverse physical link (*m, n*) at time *t*,

Q_{it} The number of ports in node i used for data aggregation at time *t*,

δ_i $\delta_i = 1$ if node *i* is a data centre, otherwise $\delta_i = 0$,

δ_s $\delta_s = 1$ if the source of the traffic demand is a data centre, otherwise $\delta_s = 0$,

δ_d $\delta_d = 1$ if the destination of the traffic demand is a data centre, otherwise $\delta_d = 0$,

$\lambda\_d_{ijt}^{sd}$ The downlink traffic flow from data centre *s* to node *d* that traverses the virtual link (*i, j*) at time *t*,

$\lambda\_u_{ij}^{sd}$ The uplink traffic flow from node s to data centre d that traverses the virtual link (*i, j*) at time *t*,

$\lambda\_r_{ijt}^{sd}$ The regular traffic flow from node s to node d that traverses the virtual link (*i, j*) at time *t*.

The above constraints (5-7), (5-8) and (5-9) represent the flow conservation constraints for the downlink, uplink and regular traffic flows, respectively and ensure that traffic flows can be split and transmitted through multiple flow paths in the IP layer. Constraint (5-10) ensures that the downlink, uplink and regular traffic flows in a virtual link do not exceed its capacity. Constraint (5-11) is the flow conservation constraint for data centre traffic and regular traffic in the optical layer. Constraint (5-12) ensures that the limited number of wavelength channels on each physical link is not exceeded. Constraint (5-13) gives the number of data centres. Constraint (5-14)

ensures that the limited number of wavelength channels on a physical link is not exceeded. Constraint (5-15) gives the total number of data aggregation ports in each node.

The model can be extended to represent the bypass approach by redefining the power consumption of ports in regular nodes and data centres at time *t* as follows:

$$\sum_{i\in N}\sum_{j\in N:i\neq j} PR\cdot C_{ijt}+\sum_{i\in N} PR\cdot Q_{it} \tag{5-16}$$

Therefore the objective function becomes:

$$\sum_{t\in T}\left(\sum_{m\in N}\sum_{n\in Np_m} PR\cdot C_{ijt}+\sum_{i\in N} PR\cdot Q_{it}+\sum_{m\in N}\sum_{n\in Np_m} PT\cdot \omega_{mnt} + \sum_{m\in N}\sum_{n\in Np_m} PE\cdot EA_{mn}\cdot f_{mn}+\sum_{i\in N} PO_i + \sum_{i\in N} PMD\cdot DM_i\right) \tag{5-17}$$

5.2.2 Simulation and Results

To evaluate the energy savings introduced by optimising the locations of data centres in IP over WDM networks, the irregular topology depicted in Fig 5-2 is considered (later a more regular topology in the form of NSFNET is considered). The network consists of 10 nodes and 14 bidirectional links. We assume that the network has a single data centre.

Fig 5-3 shows the average traffic demand between regular nodes during different hours of the day [141]. The average traffic demand between each node pair ranges from 20 Gbit/s to 120 Gbit/s and the peak occurs at 22:00. The traffic demand between nodes and data centres is generated based on the regular traffic demand in Fig 5-3 where we assume that *Ru*=0.2 and *Rd*=1.5, these factors specify the data

centre upload and download traffic volumes respectively in relation to regular traffic. For example *Rd*=1.5 specifies data centre download traffic (additional traffic) that is 1.5 times the regular traffic in the network. These *Ru* and *Rd* values match the input and output rates of a typical data centre [158].

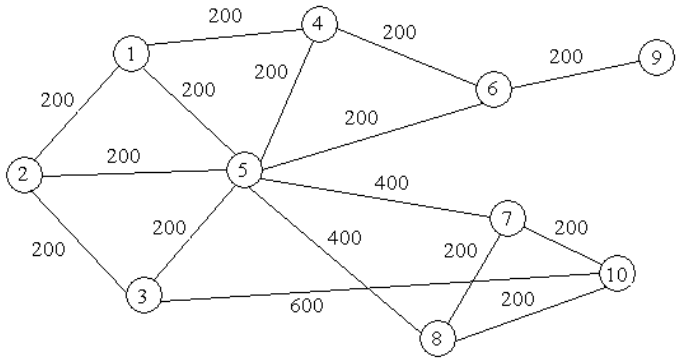

Fig 5 - 2: Irregular topology with link distances in km

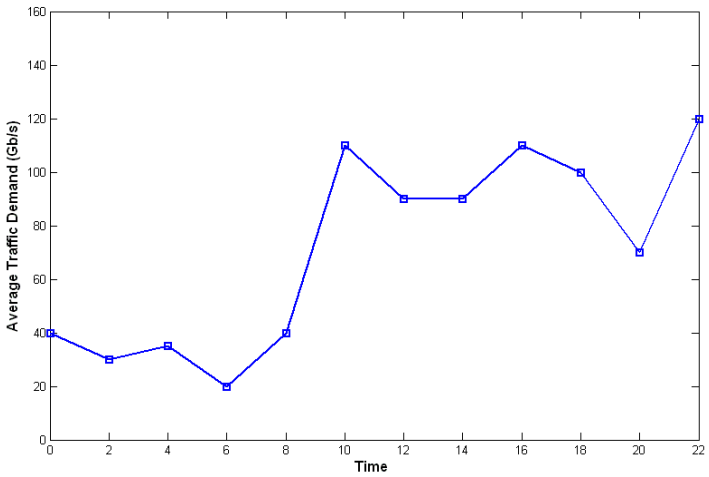

Fig 5 - 3: Average traffic demand between regular nodes

Table 5-1 shows the network parameters in terms of number of wavelengths, wavelength capacity, distance between two neighbouring EDFAs, and the power consumption of different components in the network. The parameters are similar to those in [58] which are derived from Cisco's 8-slot CRS-1 data sheets [144]. The AMPL/CPLEX software was used to solve the MILP model.

The optimal location of the single (in this case) data centre was evaluated through the MILP model. The optimal location under the non-bypass and the multi-hop bypass heuristics in two traffic scenarios were investigated: In the first traffic scenario, the traffic to and from data centres is only considered. In the second

scenario, the traffic between regular nodes in addition to the data centre traffic is considered.

Distance between two neighbouring EDFAs	80 (km)
Number of wavelengths in a fibre (*W*)	16
Capacity of each wavelength (*B*)	40 (Gbit/s)
Power consumption of a router port (*PR*)	1000 (W)
Power consumption of a transponder (*PT*)	73 (W)
Power consumption of an EDFA (*PE*)	8 (W)
Power consumption of an optical switch (*PO*)	85 (W)
Power consumption of a multiplexer or a demultiplexer (*PMD*)	16 (W)

Table 5 - 1: Input data for the network

For the non-bypass approach the MILP model results give the optimal data centre location as node 5 under both traffic scenarios. For the multi-hop bypass heuristic the MILP optimal data centre location is node 7 and node 4 under the first and the second traffic scenarios, respectively. To verify the MILP results, we evaluated, through simulation, the power consumption of the network assuming different locations of the data centre (Fig 5-4 and Fig 5-5). From Fig 5-4 and Fig 5-5, the simulation results confirm the MILP model results for both heuristics under the two traffic scenarios.

In Fig 5-4 where the first traffic scenario (only the traffic to and from data centres) is considered, the optimal location has achieved an average power saving of 37.5% and 11.2% compared to the worst location for the non-bypass and the multi-hop bypass, respectively. It is clear that under the non-bypass approach the power savings introduced by optimising the location of the data centre is more significant compared to the multi-hop bypass heuristic. This is due to the power requirements of the non-bypass approach where an IP router port (the most power consuming component in a node) is required in each intermediate node, therefore reducing the

number of intermediate nodes by optimising the location of the data centre (i.e. reduce the average hop number) has a significant impact on the network power consumption. However, under the multi-hop bypass heuristic, where IP routers are only required at the source and destination nodes, the location optimisation will only affect the power consumption of EDFAs, transponders, wavelength multiplexers and demultiplexers and optical switches at intermediate nodes whose power consumption is much lower than the IP routers ports power consumption.

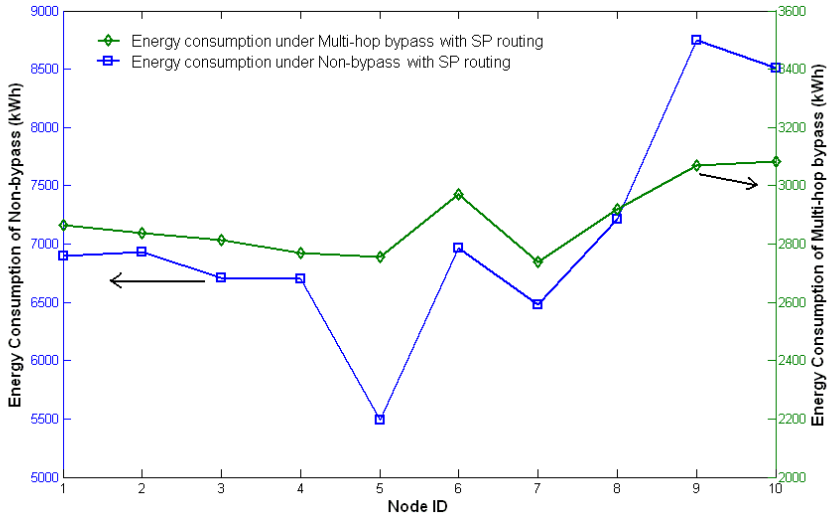

Fig 5 - 4: The total energy consumption of the irregular topology with a single data centre under different data centre locations (x-axis) with different heuristics considering only the data centre traffic

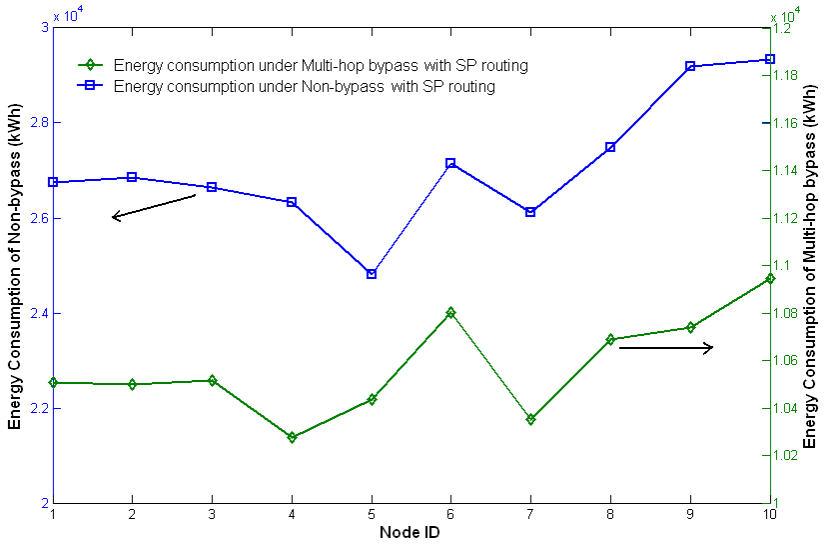

Fig 5 - 5: The total energy consumption of the irregular topology with a single data centre under different data centre locations (x-axis) with different heuristics considering the data centre traffic and regular traffic

In Fig 5-5 the energy consumption reduction achieved by optimising the location of data centres under the second traffic scenario (data centre traffic and regular traffic) decreases to 17.2% and 6.3% for the non bypass and multi-hop bypass, respectively. This is due to the fact that the energy consumption attributed to regular traffic is not affected by optimising the data centre location. Therefore the saving compared to the total energy consumption is lower.

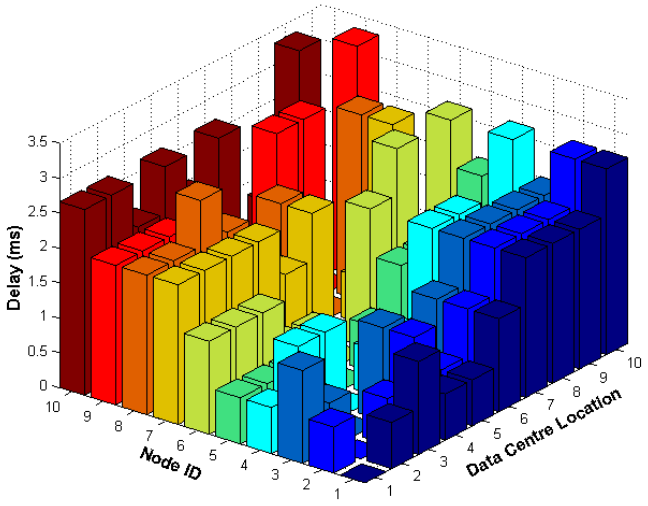

Fig 5 - 6: Propagation delay experienced by each node in the irregular topology under different data centre locations

Fig 5-6 gives the propagation delay experienced by all the nodes in the irregular topology in accessing the data centre under different data centre locations. Note that both the non-bypass and multi-hop bypass heuristics are based on shortest-path routing. It is clear that the optimal (from an energy point of view) data centre location (node 5) has not increased the propagation delay compared to other node choices. It is also clear that nodes at the centre of the network are less affected by a change in the data centre location compared to nodes at the edge as nodes in the centre have a lower average hop count to other nodes in the network.

To evaluate the impact of the optimisation of data centre locations in a realistic network, the same NSFNET network as in Chapter 4 is considered, depicted in Fig 4-4 and MILP models and simulators are used. The NSFNET network consists of 14 nodes and 21 bidirectional links and is considered to be more regular where all the nodes have comparable nodal degrees. Similarly, the same average traffic demand in different time zones as in Chapter 4 is considered, depicted in Fig 4-5.

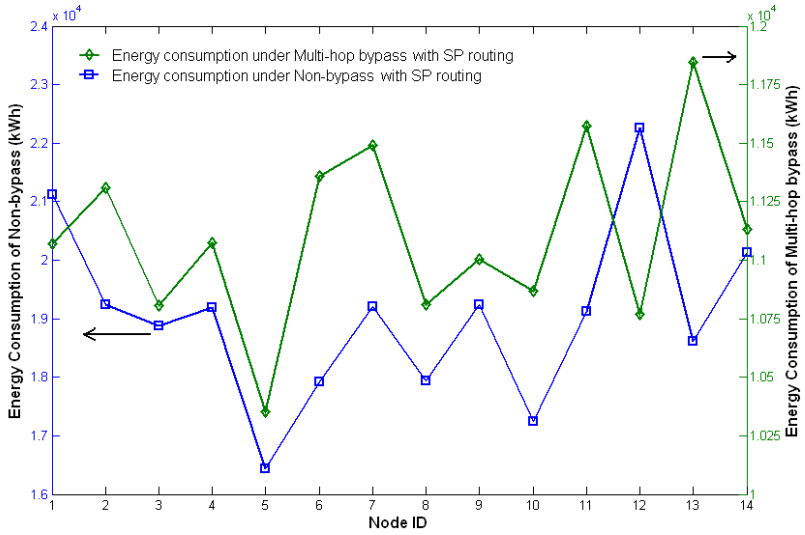

Fig 5 - 7: The total energy consumption of the NSFNET network with a single data centre under different data centre locations (x-axis) with different heuristics considering only the data centre traffic

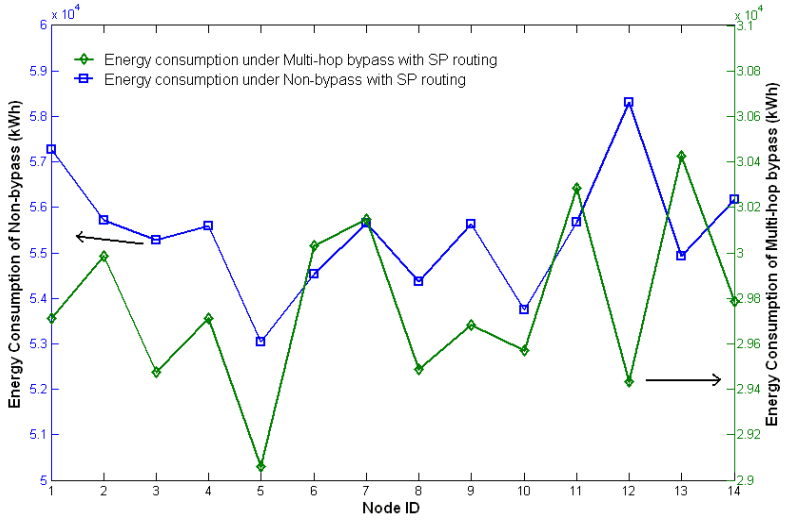

Fig 5 - 8: The total energy consumption of the NSFNET network with a single data centre under different data centre locations (x-axis) with different heuristics considering the data centre traffic and regular traffic

The location of the data centres for the NSFNET with a single data centre was optimised for the same traffic scenarios discussed above and using the parameters in Table 5-1. The optimal location obtained from the MILP model matches the simulator results in Fig 5-7 and Fig 5-8. The optimal data centre location under different heuristics and traffic scenarios is node 5 which is located at the centre of the network. As discussed above, optimising the location of data centres minimises the energy consumption of the network by reducing the total power consumed by IP

router ports; transponders & EDFAs which are related to the number of hops and distance between source and destination, respectively. Therefore data centres should be located to provide optimal number of hops and distance to all nodes. Under the first traffic scenario (only data centre traffic), the optimal data centre location has reduced the energy consumption by 26.6% and 12.7% compared to the worst location for the non bypass and the multi-hop bypass, respectively. The difference between the optimal and the worst location under the second traffic scenario (data centre traffic and regular traffic) decreases to 8.6% and 4.6% for the non bypass and the multi-hop bypass, respectively. Similar trends to those observed in Fig 5-4 and Fig 5-5 can be seen in Fig 5-7 and Fig 5-8 for NSFNET. However, the difference between the different locations under the different heuristics and traffic scenarios is reduced. This is due to the regularity of the NSFNET topology where all nodes have comparable nodal degrees.

In addition to the scenarios evaluated above, a scenario where the NSFNET has a larger number of data centres (*Ndc=5*) was evaluated. Fig 5-9 gives the optimal locations for data centres under the different heuristics and traffic scenarios. The optimal data centre locations are distributed throughout the network to provide optimal number of hops and distance to all nodes. Fig 5-10 shows that the optimal data centre locations for the multi-hop heuristic with data centre and regular traffic are distributed throughout the network under different values of *Ru* and *Rd.*

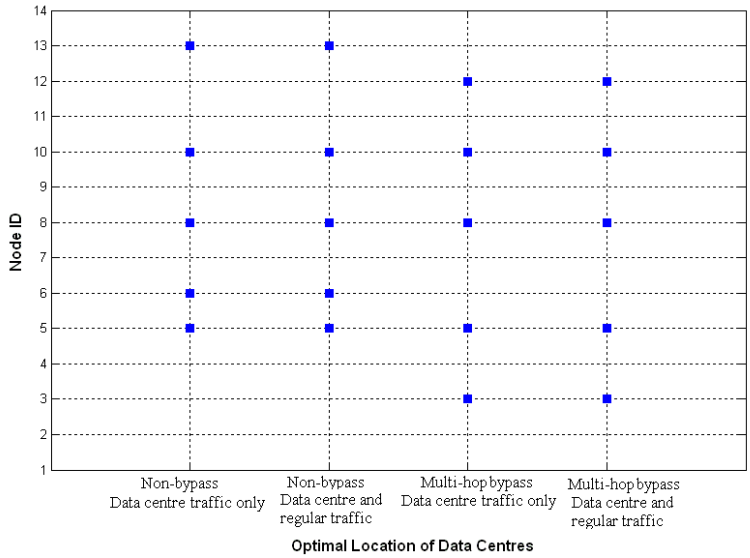

Fig 5 - 9: Optimal data centre locations under different heuristics and traffic scenarios

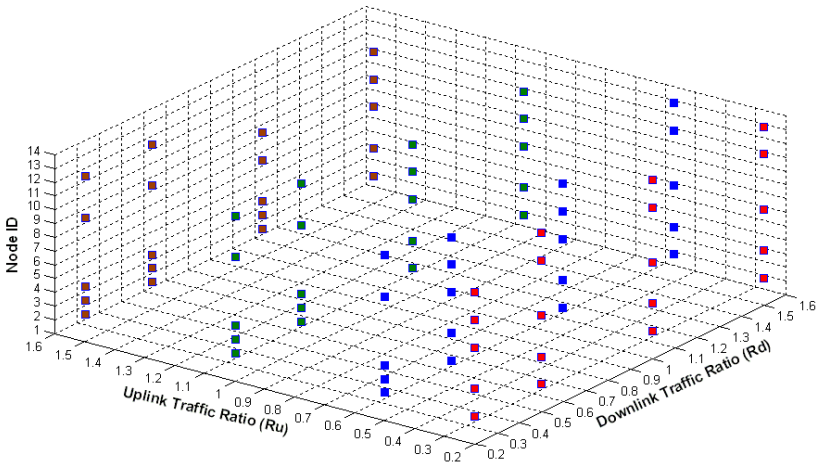

Fig 5 - 10: Optimal data centre locations for the multi-hop bypass heuristic under different *Ru* and *Rd* values with data centre and regular traffic

Fig 5-11, Fig 5-12 Fig 5-13 and Fig 5-14 show the NSFNET power consumption under the optimal data centre locations in Fig 5-9 and Fig 5-10 obtained from the MILP model for the different heuristics and traffic scenarios compared with the case where random nodes are selected to serve as data centres. The power consumption obtained from the MILP model under the optimal locations represents a lower bound on the power consumption.

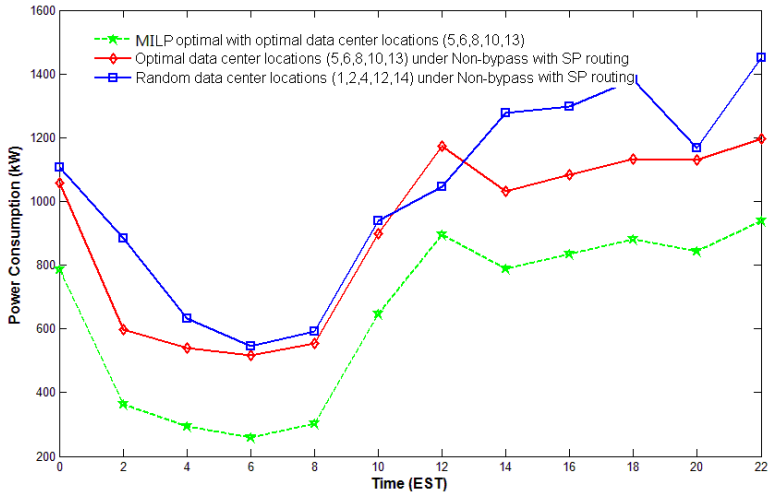

Fig 5 - 11: The power consumption of the NSFNET network with different data centre locations in a 24 hour period under the non-bypass heuristic with 5 data centres considering only the data centre traffic

In Fig 5-11 and Fig 5-12, compared with the random data centre locations under the non-bypass heuristic, the power consumption under the optimal locations has

been reduced by an average of 11.4% and 4.4% under the first and the second traffic scenarios, respectively. The power consumption obtained from the MILP model is lower than the power consumption obtained under the non-bypass with shortest-path routing as shortest-path routing will not necessarily result in the minimum number of hops, and the number of hops determines the number of IP ports used under the non-bypass heuristic. The number of IP ports used has the largest impact on power consumption.

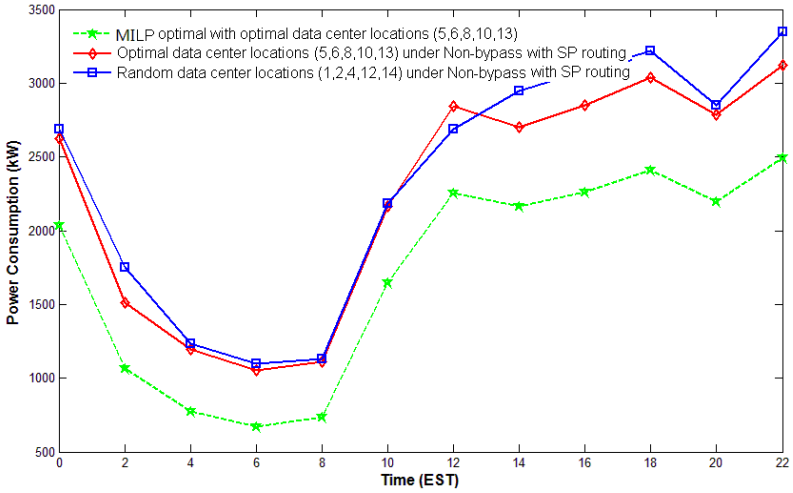

Fig 5 - 12: The power consumption of the NSFNET network with different data centre locations in a 24 hour period under the non-bypass heuristic with 5 data centres considering the data centre traffic and regular traffic

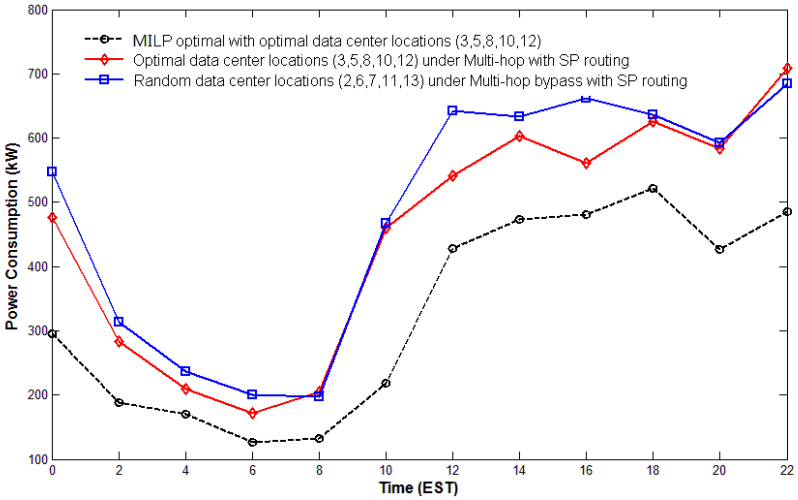

Fig 5 - 13: The power consumption of the NSFNET network with different data centre locations in a 24 hour period under the multi-hop bypass heuristic with 5 data centres considering only the data centre traffic

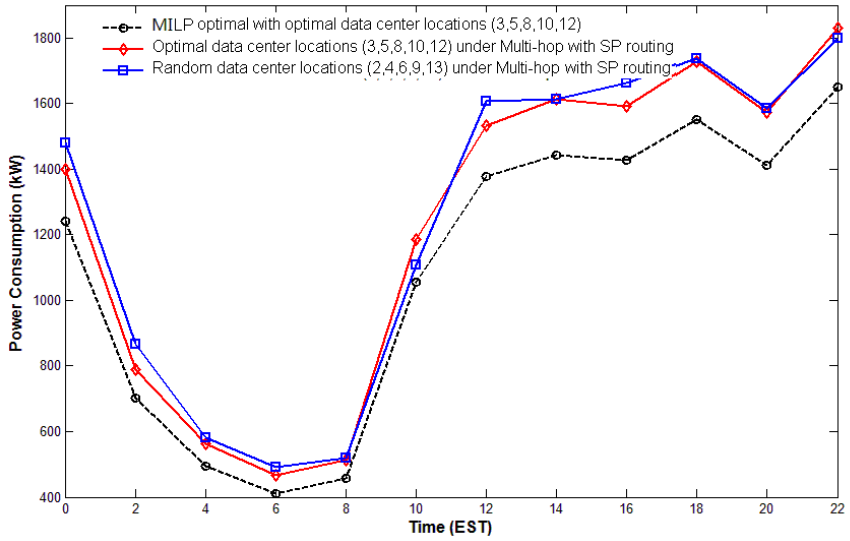

Fig 5 - 14: The power consumption of the NSFNET network with different data centre locations in a 24 hour period under the multi-hop bypass heuristic with 5 data centres considering the data centre traffic and regular traffic

Under multi-hop bypass (Fig 5-13 and Fig 5-14), the power consumption has been reduced to an average of 6.5% and 1.7% under the first and the second traffic scenario, respectively. In a fashion similar to the non-bypass case, shortest path routing results in higher power consumption in the multi-hop bypass heuristic. However, the difference between the MILP model and the multi-hop bypass heuristic is smaller than the difference in the case of the non-bypass heuristic as under the multi-hop bypass heuristic IP router ports are eliminated at intermediate nodes therefore the number of hops becomes less critical.

From the results above, power savings are higher under the non-bypass heuristic. However, compared to the case with one data centre, the power savings achieved by optimising the multiple data centre locations are limited. This is due to the fact that with a larger number of data centres the average distance between a node and a data centre is reduced. Therefore optimising the locations of data centres has a smaller effect on the average number of hops, i.e. the distance between nodes and data centres and therefore it has a limited effect on power consumption. Therefore optimising the location of data centres is more critical if the number of data centres is small or the topology is irregular as seen earlier in this section.

Table 5-2 gives a summary of the power consumption savings obtained under different topologies, heuristics and number of data centres. Similar observations can

be made in relation to delay in the more regular NSFNET topology by comparing Fig 5-15 and Fig 5-6, both under a single data centre. Fig 5-16 compares the propagation delay experienced by different nodes in the NSFNET network with 5 data centres under the optimal data centre locations and under other random locations. The optimal (power consumption minimisation criterion) data centre locations have had limited effect on the average propagation delay experienced by different nodes in accessing data centres and as Fig 5-16 shows, some nodes experience lower delay. Therefore the developed MILP model optimises the data centre locations to minimise the network power consumption while maintaining QoS (propagation delay here).

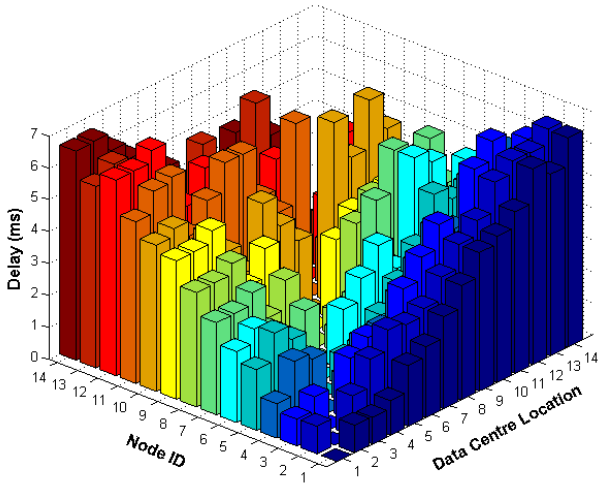

Fig 5 - 15: Delay experienced by each node in the NSFNET network with a single data centre under different data centre locations

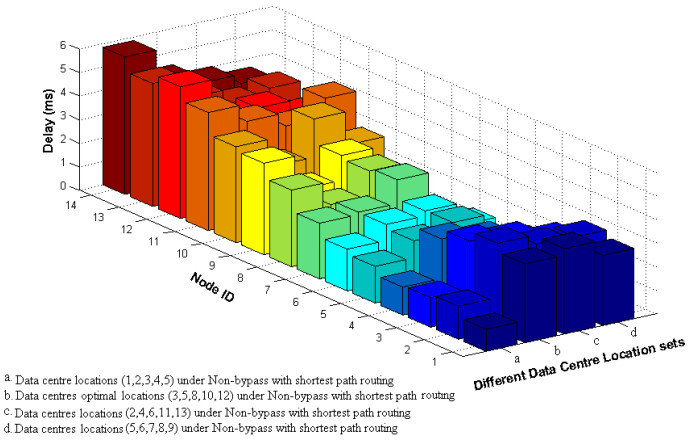

Fig 5 - 16: Delay experienced by each node in the NSFNET network with 5 data centres under the optimal data centre locations

Topology	Data centre traffic only	Data centre traffic and regular traffic
Irregular topology under the non-bypass heuristic	37%	11%
Irregular topology under the multi-hop bypass heuristic	17%	6.3%
NSFNET topology with a single data centre under the non-bypass heuristic	26.6%	12.7%
NSFNET topology with a single data centre under the multi-hop bypass heuristic	8.6%	4.6%
NSFNET topology with 5 data centres under the non-bypass heuristic	11.4%	4.4%
NSFNET topology with 5 data centres under the multi-hop bypass heuristic	6.5%	1.7%

Table 5 - 2: Summary of power consumption savings obtained under optimal data centre locations

5.3 A Replication Scheme for IP over WDM Network with Data Centres

The results in Section 5.2.2 were obtained under the assumption that each data centre has different content i.e. a user interested in that particular content has to access it from the data centre in question. However, in practice large operators (e.g. BBC, YouTube, Amazon...) have multiple data centres where they replicate content (that has different popularity) to reduce the access delay experienced by users. In terms of power consumption, replicating data objects to multiple data centres allows a node to access a data object from a closer data centre and therefore reduces the power consumption by reducing the number of hops and the distance from source to destination. In this section, the power savings introduced by implementing a

replication scheme in the IP over WDM network with data centres is investigated where we assume that data objects are replicated according to their popularity.

5.3.1 Mathematical Model

A MILP model is developed to optimise the selection of data centres to replicate data objects under the lightpath bypass approach. In addition to the assumptions in Section 5.2.1, the MILP model is developed under the following assumptions:

1. The optimal data centre locations are obtained using the MILP model in Section 5.2.1.

2. Data objects in the network are classified into five different popularity groups. A traffic demand between a node and a data centre is distributed among different data object groups according to their popularity. Previous research on content popularity [159-161] has established that the popularity of content can be approximated using a Zipf distribution which states that the relative probability of a request for the *i*'th most popular data object is proportional to 1/*i.* The Zipf's distribution is given by [127]:

$$P(i) = \frac{\varphi}{i} \tag{5-18}$$

where

$$\varphi = \left(\sum_{i=1}^{N} \frac{1}{i} \right)^{-1} \tag{5-19}$$

where N is the number of data objects. In our scenario we assume five data object groups (N=5). Therefore, the popularity of the data object groups P_O, is: 43.7%, 21.8%, 14.5%, 10.9% and 9%.

3. Given that the least popular data object must exist in at least one data centre and assuming that the most popular object exists in all data centres, a relationship can be constructed between content popularity and the number of locations where it is present. This does not however predetermine the location of a data object based on its popularity. Different relationships can be

constructed given the two points (maximum and minimum) discussed and shown in Fig 5-17. The simplest being a linear relationship which is the one selected here (see Fig 5-17). Other Relationships (e.g polynomial) can be investigated as an extension.

The total number of data centres, $NR_O(P)$, used to replicate a data object group, O, is defined as a function of the object's popularity, P_O, as:

$$NR_O(P_O) = \frac{|D| - 1}{P_{max} - P_{min}} P_O + \frac{P_{max} - |D| P_{min}}{P_{max} - P_{min}} \quad (5\text{-}20)$$

where D is the set of data centres, P_{max} and P_{min} are the popularities of the most and least popular data objects, respectively. From equation (5-20) and given that $|D|$=5 and given the popularity values mentioned above we calculate $NR_O(P_O)$ for all data object groups resulting in data object groups with the popularities 43.7%, 21.8%, 14.5%, 10.9% and 9% having to exist in 5, 4, 3, 2 and 1 data centres, respectively.

4. Only data centre traffic is considered (uplink and downlink traffic) when optimising the replication locations (but the mirroring traffic between data centres is also considered). The data centres are assumed to be synchronised.

5. The problem is decomposed by solving the MILP model each time for a particular data centre X and a particular data object O. While such decomposition yields a simplified tractable model, it may not lead to the global optimal solution.

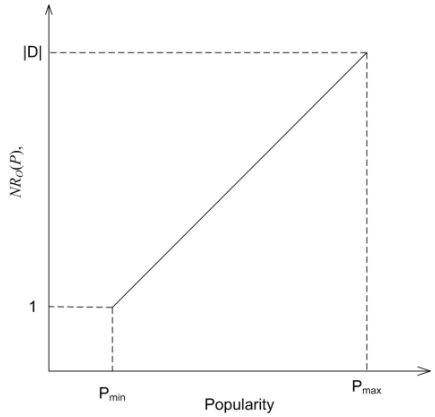

Fig 5 - 17: Popularity vs. total number of data centres

The corresponding optimisation problem is presented in the following which obtain optimal locations of contents replication.

Objective: minimise

$$\sum_{t\in T}\Bigg(\sum_{i\in N}\sum_{j\in N:i\neq j} PR\cdot\left(Cd_{ijt}+Cu_{ijt}\right)+\sum_{m\in N}\sum_{n\in Np_m} PT\cdot\omega_{mnt} + \sum_{m\in N}\sum_{n\in Np_m} PE\cdot EA_{mn}\cdot f_{mn}+\sum_{i\in N} PO_i + \sum_{i\in N} PMD\cdot DM_i\Bigg) \tag{5-21}$$

Note that the power consumption of the aggregation ports is not considered in the objective function as it is related linearly to the traffic demand and therefore will not affect the selection of the optimal replication locations.

Subject to:

$$\sum_{j\in N:i\neq j}\lambda\_d_{ijt}^{nd}-\sum_{j\in N:i\neq j}\lambda\_d_{jit}^{nd}=\begin{cases}\lambda d^{Xdt}\cdot P_O\cdot\delta_n & if\ i=n\\ -\lambda d^{Xdt}\cdot P_O\cdot\delta_n & if\ i=d\\ 0 & otherwise\end{cases} \tag{5-22}$$

$$\forall\ t\in T,\forall\ d\in NN,\forall\ n\in D,$$

$$\sum_{j\in N:i\neq j}\lambda\_u_{ijt}^{dn}-\sum_{j\in N:i\neq j}\lambda\_u_{jit}^{dn}=\begin{cases}\lambda u^{dXt}\cdot P_O\cdot\delta_n & if\ i=d\\ -\lambda u^{dXt}\cdot P_O\cdot\delta_n & if\ i=n\\ 0 & otherwise\end{cases} \tag{5-23}$$

$$\forall\ t\in T,\forall\ d\in NN,\forall\ n\in D,$$

$$\sum_{n\in D}\sum_{d\in NN}\lambda\_d_{ijt}^{nd}\leq Cd_{ijt}\cdot B \tag{5-24}$$

$$\forall\ t\in T,\forall\ i,j\in N:i\neq j,$$

$$\sum_{d\in NN}\sum_{n\in D}\lambda\_u_{ijt}^{dn}\leq Cu_{ijt}\cdot B \tag{5-25}$$

$$\forall\ t\in T,\forall\ i,j\in N:i\neq j,$$

$$\sum_{n\in Np_m} W_{mnt}^{ij} - \sum_{n\in Np_m} W_{nmt}^{ij} = \begin{cases} Cd_{ijt} + Cu_{ijt} & m = i \\ -Cd_{ijt} - Cu_{ijt} & m = j \\ 0 & otherwise \end{cases} \quad (5\text{-}26)$$

$$\forall\ t \in T,\ \forall\ i,j,m \in N: i \neq j,$$

$$\sum_{n\in D} \delta_n = NR_O^{P_o}, \quad (5\text{-}27)$$

$$\sum_{i\in N} \sum_{j\in N: i\neq j} W_{mnt}^{ij} = \omega_{mnt} \quad (5\text{-}28)$$

$$\forall\ t \in T, \forall\ m \in N, n \in Np_m,$$

$$\sum_{i\in N} \sum_{j\in N: i\neq j} W_{mnt}^{ij} \leq W \cdot f_{mn} \quad (5\text{-}29)$$

$$\forall\ t \in T, \forall\ m \in N, n \in Np_m.$$

In addition to the parameters of the MILP model in Section 5.2.1, the following parameters are defined:

X	The data centre with an original data object.
NN	The set of normal nodes.
$NR_O^{P_o}$	The total number of data centres used to replicate a data object group, O, with popularity, P_O.

In addition to the parameters in Section 5.2.1, the following variables are defined:

Cd_{ijt}	The number of wavelength channels used for downlink traffic demand on the virtual link (i, j) at time t.
Cu_{ijt}	The number of wavelength channels used for uplink traffic demand on the virtual link (i, j) at time t.
δ_n	$\delta_n = 1$ if data centre n is chosen to replicate an object present in data centre X, otherwise $\delta_n = 0$.
λ^{xdt}	The downlink traffic demand from data centre X to node d.
λ^{dxt}	The uplink traffic demand from node d to data centre X.

$\lambda\_d_{ijt}^{nd}$ The downlink traffic flow from data centre *n* to node *d* that traverses the virtual link (*i, j*) at time *t.*

$\lambda\_u_{ijt}^{dn}$ The uplink traffic flow from node *d* to data centre *n* that traverses the virtual link (*i, j*) at time *t.*

Constraint (5-22) ensures that the downlink traffic demands from data centre *X* to node *d* in the IP layer are allowed to be replicated to data centre *n*, split and transmitted through multiple flow paths. Constraint (5-23) ensures that the uplink traffic demands from node *n* to the data centre *X* in the IP layer are allowed to be replicated at data centre *n*, split and transmitted through multiple flow paths. Constraints (5-24) and (5-25) show that the downlink and uplink traffic flows cannot exceed the capacity of each virtual link. Constraint (5-26) ensures the flow conservation in the optical layer. Constraint (5-27) states the number of data centres used for replication. Constraint (5-28) gives the relationship between the number of wavelength channels on physical links and virtual links. Constraint (5-29) ensures that the limited number of wavelength channels on each physical link is not exceeded.

From constraints (5-22) and (5-23), it is clear that the original traffic demand between a data centre and nodes is calculated repeatedly for each possible replication data centre in order to keep the model linear. Therefore, the total power consumption of the network calculated from the model has some tolerance. However, this does not affect the results of optimal locations of the replication data centres.

5.3.2 Energy-Delay Optimal Routing Algorithm (EDOR)

Using shortest-path routing to choose a replica of a data object in the IP over WDM network can result in increasing the power consumption of the network as the shortest path may involve more hops (hence IP ports) and furthermore more router ports and transponders may be required to establish a new virtual link if enough capacity is not available on existing virtual links on the shortest path. Therefore we propose a new routing algorithm, Energy-Delay Optimal Routing (EDOR), to route traffic demands to data objects. EDOR aims to minimise the energy consumption

while maintaining QoS (propagation delay). The flow chart associated with the EDOR algorithm is shown in Fig 5-18.

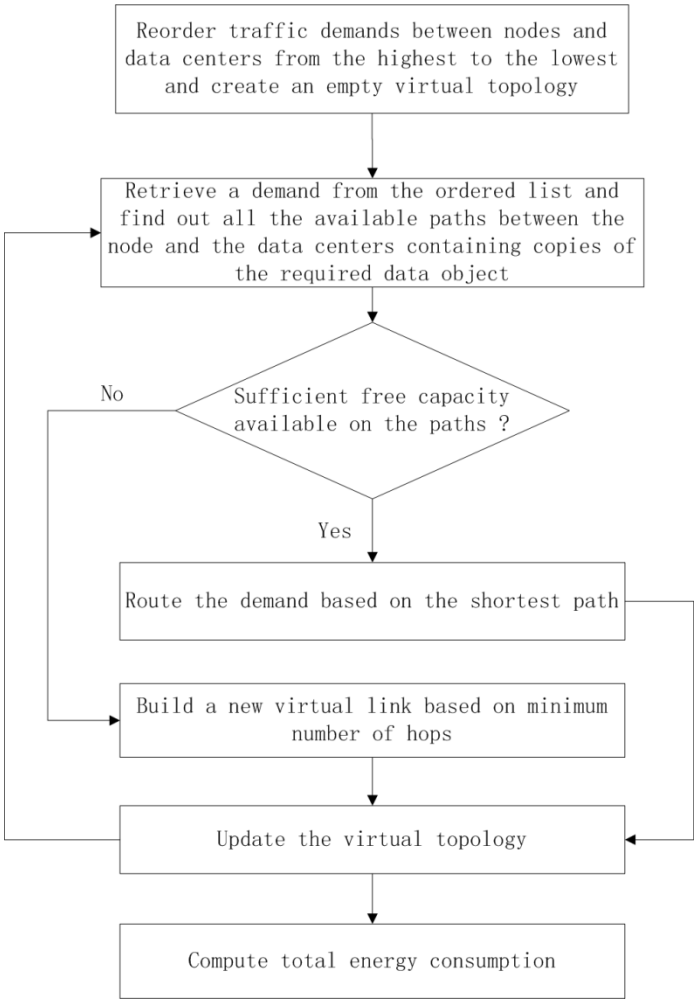

Fig 5 - 18: EDOR algorithm flowchart

In this algorithm, all the traffic demands between data centres and nodes are reordered from the highest to the lowest and an empty virtual topology is created. A traffic demand is then retrieved from the ordered list. All the available paths to all the required data centres are checked. If more than one path has sufficient capacity, the required data centre with the shortest available path is selected in order to reduce the propagation delay. If sufficient capacity is not available in the virtual topology, a new virtual link is established between the node and the data centre with the minimum number of hops in order to minimise the power consumption by reducing the number of transponders in intermediate nodes. After routing the traffic demand, the remaining capacity on all the virtual links is updated. The above process is

repeated for all the traffic demands. After routing all the traffic demands on the virtual topology, the total power consumption of the network is calculated.

Under the EDOR algorithm the same data object exists in multiple data centres, so the data centre routing problem becomes a form of "anycasting" which introduces a degree of freedom in selecting the destination with the minimum energy consumption. The multi-hop bypass heuristic proposed in [58] is a unicasting algorithm, i.e. the destination is pre-determined and only the most energy efficient route is selected.

5.3.3 Simulation and Results

In this section we identify the impact of the replication scheme in the NSFNET network with 5 data centres. The data centre traffic demand and other parameters are similar to the assumptions in Section 5.2.2.

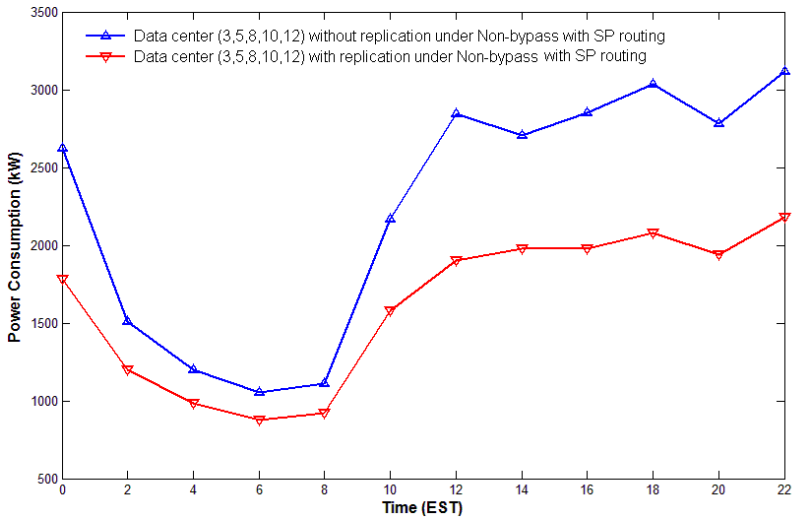

Fig 5 - 19: The power consumption of the IP over WDM network with optimal locations of data centres under the non-bypass heuristic with and without replication

In Fig 5-19, the performance of the replication scheme under shortest-path routing with the non-bypass scheme is evaluated. Simulation results are reported under the optimal data centre locations ((5, 6, 8, 10 and 13) obtained from running the model in Section 5.2.1 for the non-bypass heuristic) considering data centre traffic and regular traffic. The optimal selection of data centres is determined to replicate data objects through the use of the MILP model in Section 5.3.1.

Implementing the replication scheme has resulted in an average power saving of 28%. This significant saving is due to the reduction in the number of hops and the distance between data centres and nodes (as under replication objects are available in multiple data centres).

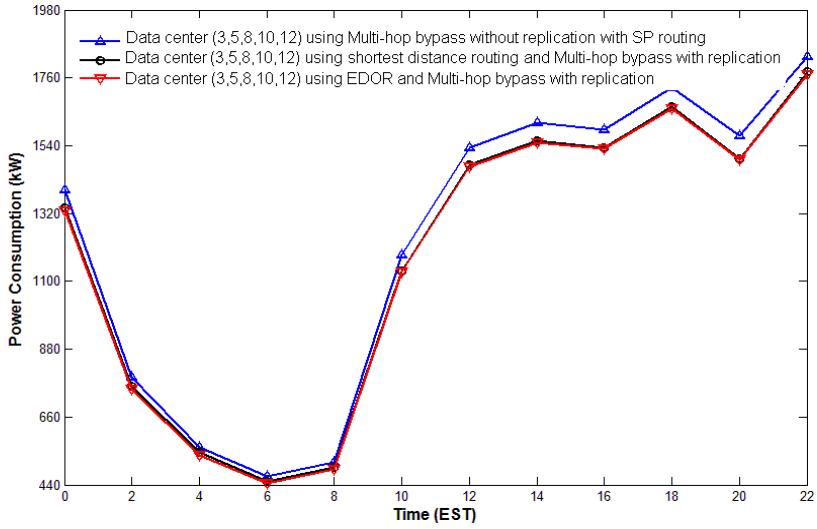

Fig 5 - 20: The power consumption of the IP over WDM network with optimal locations of data centres under the EDOR algorithm and the multi-hop bypass heuristic with shortest path algorithm with and without replication

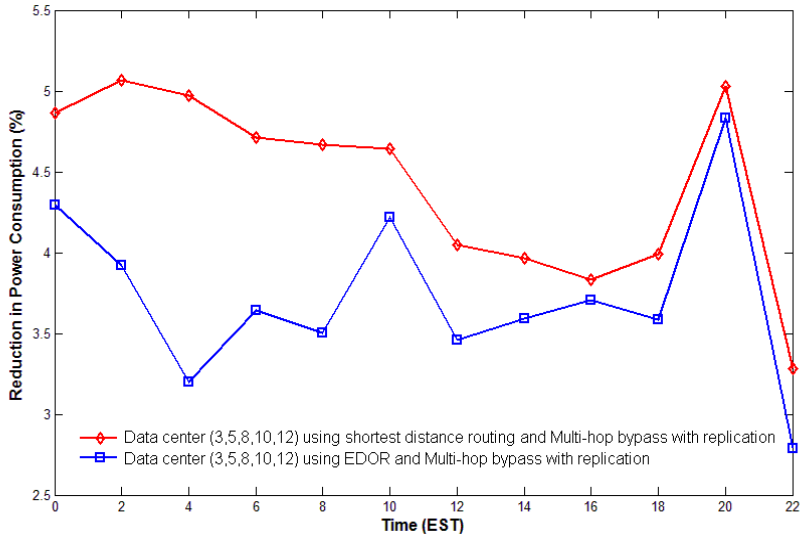

Fig 5 - 21: Reduction in the power consumption of the IP over WDM network with optimal locations of data centres under the EDOR algorithm and the multi-hop bypass heuristic with shortest path routing

The results under EDOR with the optimal data centre locations (3, 5, 8, 10 and 12) have also been evaluated using the model in Section 5.2.1 for the multi-hop

bypass heuristic considering data centre traffic and regular traffic. The optimal selection of data centres to replicate data objects was determined from the MILP model in Section 5.3.1. Fig 5-20 gives the power consumption of the IP over WDM network with data centres with and without the replication scheme. It is clear that implementing the replication scheme has resulted in power savings under both shortest-path routing and the EDOR algorithm. The difference between the EDOR algorithm and the multi-hop bypass heuristic with shortest-path routing can be seen in Fig 5-21 where we show the power saving introduced by the replication scheme under the two algorithms compared to the multi-hop heuristic without replication.

While the EDOR algorithm achieves an average power saving of 4.5%, the multi-hop bypass heuristic with shortest-path routing average power saving is limited to 3.7 %. This is because the EDOR algorithm allows more traffic demands to share the capacity on common virtual links and therefore a smaller number of new virtual links need to be established. It also routes using a minimum hop criterion (minimum number of IP ports, switches, transponders and multiplexers and demultiplexers) when there is no sufficient capacity on established lightpaths. Between 04:00 and 08:00, the difference between the two algorithms reaches its peak as during this time period the average traffic demand is the lowest, and is lower than the capacity of a wavelength. The EDOR algorithm uses all available virtual links with sufficient capacity therefore more traffic demands share the capacity on common virtual links.

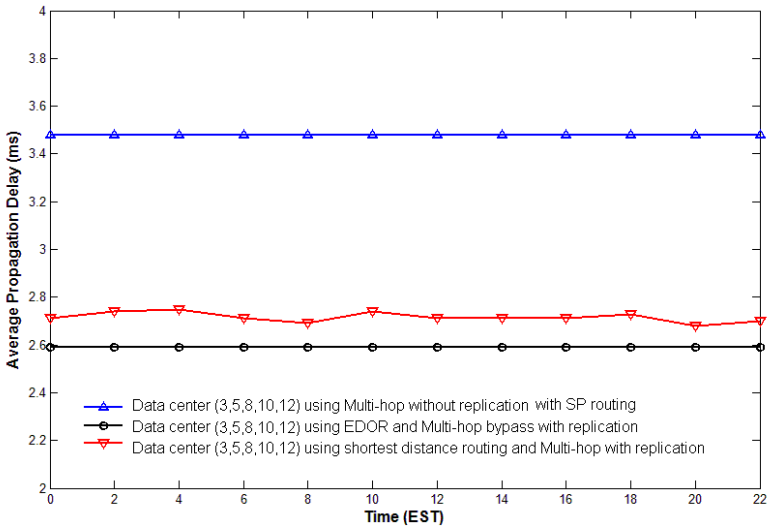

Fig 5 - 22: Average propagation delay of IP over WDM network with optimal locations of data centres under different algorithms

Fig 5-22 gives the average propagation delays under different algorithms. The multi-hop bypass heuristic without the replication scheme gives the upper bound on the propagation delay. The multi-hop bypass heuristic with the shortest path algorithm results in the lowest propagation delay (2.59 ms). With the EDOR algorithm, the propagation delay has not increased significantly (the increase is less than 0.2 ms, i.e. less than 8% compared to the lowest propagation delay) maintaining the QoS. It should be noted that while the propagation delay of the multi-hop bypass heuristic without replication and with the shortest-path algorithm are almost constant in a 24 hour period, the average propagation delay of the EDOR algorithm fluctuates slightly as the routing paths are dynamic.

5.4 Applying Renewable Energy in the IP over WDM Network with Data Centres

In this section, introducing renewable energy sources to the IP over WDM network with data centres is investigated and a scenario where moving bits to where renewable energy is (wind farms) is evaluated and compared to transporting renewable energy to data centres. The impact of the power losses associated with transporting electrical power to data centres on the optimal data centres locations is studied. The impact of the other networking factors including network topology, routing, and traffic is also studied. We further assume that solar energy is employed to partly power regular nodes, 20kW per node and similar solar panel area as in Chapter 4. However, as the power consumption of a data centre is high, due to high traffic demand to and from the data centre and the high consumption of the computing and cooling equipment inside the data centre, the power generated by limited size solar cells built in the local site will not be sufficient to power a data centre. Therefore the data centres are powered by the energy generated from wind farms.

5.4.1 Mathematical Model

The MILP model in Section 5.2.1 is extended to support the objective of minimising the non-renewable energy consumption of data centres by optimising the locations of data centres in the IP over WDM network assuming the lightpath bypass approach but taking into account renewable energy sources and the transmission losses. In addition to the assumptions of the MILP model in Section 5.2.1, the following assumptions are made:

1. Renewable energy is only available to the ports and transponders in regular nodes as these are the most power consuming elements in a node. Renewable energy from wind farms is however also available to power the computing servers, cooling and lighting.

2. Data centres and regular nodes have access to non-renewable energy to guarantee QoS at all time in case the renewable energy is low.

3. Each data centre has access to only a single wind farm. Note that If the data centre is connected to more than a single wind farm, then more than one transmission line will have to be constructed increasing the cost. Alternatively, the power from the wind farm can be injected into the power grid and the data centre can be connected to the power grid, however it is difficult to evaluate of the power losses attributed to the data centre location in a complex power grid network. From a power loss point of view, connecting a data centre to multiple wind farms, e.g. 3 wind farms can reduce the transmission power losses if the power remains the same and the distance, d, to each wind farm (three loss components, each proportional to $I^2/9$) however the installation cost becomes high. Therefore the simplest/lowest cost option has been selected, where each data centre is connected to a single wind farm.

4. A fraction of the total output power of a wind farm k, denoted as U_k, is assumed to be available to power data centres.

5. The power transmission loss (loss_{ki}) is the power lost in transmitting renewable energy from wind farm k to data centre i.

6. To be able to evaluate the non-renewable energy consumption separately from the renewable energy consumption, the variables is redefined by representing the number of wavelength channels and traffic flows.

In addition to the parameters in Section 5.2.1, the following parameters are defined:

K	The set of wind farms,
PWF_{kt}	The output power of wind farm k at time t,
PR^w	The wind power consumption of a router port which is equal to PR,
PR^s	The solar power consumption of a router port which is equal to PR,
PT^w	The wind power consumption of a transponder which is equal to PT,
PT^s	The solar power consumption of a transponder which is equal to PT,
$P\_cooling_i$	The power consumption associated with cooling in a data centre,
$P\_computing_i$	The power consumption associated with computing in a data centre,
S_{it}	The output power of solar cells of node i at time t.

The following variables are defined:

Cd_{ijt}	The number of wavelength channels carrying data centre traffic in the virtual link (i, j) which start or end at a data centre and are powered by non-renewable energy at time t,
Cdw_{ijt}	The number of wavelength channels carrying data centre traffic in the virtual link (i, j) which start or end at a data centre and are powered by wind energy at time t,
Cn_{ijt}	The number of wavelength channels carrying data centre traffic in the virtual link (i, j) which start or end at regular nodes and are powered by non-renewable energy at time t,
Cns_{ijt}	The number of wavelength channels carrying data centre traffic in the virtual link (i, j) which start or end at a regular node and are powered by solar energy at time t,

Cnw_{ijt} The number of wavelength channels carrying data centre traffic in the virtual link (*i, j*) which start or end at a regular node (connected to a data centre) and are powered by wind energy at time *t*,

Cr_{ijt} The number of wavelength channels carrying regular traffic in the virtual link (*i, j*) which are powered by non-renewable energy at time *t*,

Crw_{ijt} The number of wavelength channels carrying regular traffic in the virtual link (*i, j*) which are powered by wind energy at time *t*,

Crs_{ijt} The number of wavelength channels carrying regular traffic in the virtual link (*i, j*) which are powered by solar energy at time *t*,

$\lambda\_ddc_{ijt}^{sd}$ The downlink traffic flow from data centre *s* to node *d* that traverses the virtual link (*i, j*) at time t. This is associated with data centres (*dc*),

$\lambda\_dn_{jit}^{sd}$ The downlink traffic flow from data centre *s* to node *d* (for regular node) that traverses the virtual link (*i, j*) at time *t*. This is associated with regular nodes (*n*),

$\lambda\_ud_{cijt}^{sd}$ The uplink traffic demand from node *s* to data centre *d* (for data centre) that traverses the virtual link (*i, j*) at time *t*. This is associated with data centres (*dc*),

Wd_{mnt}^{ij} The number of wavelength channels carrying data centre traffic in the virtual link (*i, j*) which traverses physical link (*m, n*) that starts or ends at a data centre at time *t*,

Wn_{mnt}^{ij} The number of wavelength channels carrying data centre traffic in the virtual link (*i, j*) which traverses physical link (*m, n*) that starts or ends at a regular node at time *t*,

Wr_{mnt}^{ij} The number of wavelength channels carrying regular traffic in the virtual link (*i, j*) which traverses physical link (*m, n*) at time *t*,

$\lambda\_un_{jit}^{sd}$ The uplink traffic demand from node *s* to data centre *d* (for regular node) that traverses the virtual link (*i, j*) at time *t*. This is associated with regular nodes (*n*),

ωd_{mnt} The number of wavelength channels carrying data centre traffic in the physical link (*m, n*) which start or end at a data centre and are powered by non-renewable energy at time *t*,

ωdw_{mnt} The number of wavelength channels carrying data centre traffic in the physical link (*m, n*) which start or end at a data centre and are powered by wind energy at time *t*,

ωn_{mnt} The number of wavelength channels carrying data centre traffic in the physical link (*m, n*) which start or end at a regular node and are powered by non-renewable energy at time *t*,

ωns_{mnt} The number of wavelength channels carrying data centre traffic in the physical link (*m, n*) which start or end at a regular node and are powered by solar energy at time *t*,

ωnw_{mnt} The number of wavelength channels carrying data centre traffic in the physical link (*m, n*) which start or end at a regular node (connected with a data centre) node and are powered by wind energy at time *t*,

ωr_{mnt} The number of wavelength channels carrying regular traffic in the physical link (*m, n*) powered by non-renewable energy at time *t*,

ωrs_{mnt} The number of wavelength channels carrying regular traffic in the physical link (*m, n*) powered by solar energy at time *t*,

ωrw_{mnt} The number of wavelength channels carrying regular traffic in the physical link (*m, n*) powered by wind energy at time *t*,

Qe_{it} The number of ports in node *i* used for data aggregation powered by non-renewable energy at time *t*,

Qs_{it} The number of ports in regular node i used for data aggregation powered by solar energy at time t,

Qw_{it} The number of ports in data centre i used for data aggregation powered by wind energy at time t,

δ_{ki} $\delta_{\mathrm{ki}} = 1$ if node i is a data centre and has access to wind farm k, otherwise, $\delta_{\mathrm{ki}} = 0$.

The power consumption of optical switches, multiplexers/demultiplexer and EDFAs have the same definition as in Section 5.2.1. However the power consumption of router ports and transponders is redefined as follows:

1) The power consumption of ports in regular nodes and data centres at time t

$$\sum_{i \in N} \sum_{j \in N: i \neq j} PR \cdot \left(Cd_{ijt} + Cn_{ijt} + Cr_{ijt}\right) + \sum_{i \in N} PR \cdot Qe_{it} \tag{5-30}$$

2) The power consumption of transponders in regular nodes and data centres at time t

$$\sum_{m \in N} \sum_{n \in Np_m} (PT \cdot \omega d_{mnt} + PT \cdot \omega n_{mnt} + PT \cdot \omega r_{mnt}) \tag{5-31}$$

The power consumption of the cooling and computing equipment inside the data centre is also included in the total non-renewable energy consumption.

The MILP model is defined as follows and given the optimal locations of data centres:

Objective: minimise

$$\begin{aligned} \sum_{t \in T} \Bigg(& \sum_{i \in N} \sum_{j \in N: i \neq j} PR \cdot \left(Cd_{ijt} + Cn_{ijt} + Cr_{ijt}\right) + \sum_{i \in N} PR \cdot Qe_{it} \\ & + \sum_{m \in N} \sum_{n \in Np_m} (PT \cdot \omega d_{mnt} + PT \cdot \omega n_{mnt} + PT \cdot \omega r_{mnt}) \\ & + \sum_{m \in N} \sum_{n \in Np_m} PE \cdot EA_{mn} \cdot f_{mn} + \sum_{i \in N} PO_i + \sum_{i \in N} PMD \cdot DM_i \Bigg) \end{aligned} \tag{5-32}$$

Subject to:

$$\sum_{j\in N:i\neq j} \lambda\_ddc_{ijt}^{sd} - \sum_{j\in N:i\neq j} \lambda\_dn_{jit}^{sd} = \begin{cases} \lambda^{sdt}\cdot Rd\cdot \sum_{k\epsilon K}\delta_{ks} & if\ i=s \\ -\lambda^{sdt}\cdot Rd\cdot \sum_{k\epsilon K}\delta_{ks} & if\ i=d \\ 0 & otherwise \end{cases} \quad (5\text{-}33)$$

$$\forall\ t\in T, \forall\ s,d,i\in N: s\neq d,$$

$$\sum_{j\in N:i\neq j} \lambda\_un_{ijt}^{sd} - \sum_{j\in N:i\neq j} \lambda\_udc_{jit}^{sd} = \begin{cases} \lambda^{sdt}\cdot Ru\cdot \sum_{k\epsilon K}\delta_{kd} & if\ i=s \\ -\lambda^{sdt}\cdot Ru\cdot \sum_{k\epsilon K}\delta_{kd} & if\ i=d \\ 0 & otherwise \end{cases} \quad (5\text{-}34)$$

$$\forall\ t\in T, \forall\ s,d,i\in N: s\neq d,$$

$$\sum_{j\in N:i\neq j} \lambda r_{ijt}^{sd} - \sum_{j\in N:i\neq j} \lambda r_{jit}^{sd} = \begin{cases} \lambda^{sdt} & if\ i=s \\ -\lambda^{sdt} & if\ i=d \\ 0 & otherwise \end{cases} \quad (5\text{-}35)$$

$$\forall\ t\in T, \forall\ s,d,i\in N: s\neq d,$$

$$\sum_{s\in N}\sum_{d\in N:s\neq d} \left(\lambda\_ddc_{ijt}^{sd} + \lambda\_udc_{ijt}^{sd}\right) \leq \left(Cd_{ijt} + Cdw_{ijt}\right)\cdot B \quad (5\text{-}36)$$

$$\forall\ t\in T, \forall\ i,j\in N: i\neq j,$$

$$\sum_{s\in N}\sum_{d\in N:s\neq d} \left(\lambda\_dn_{ijt}^{sd} + \lambda\_un_{ijt}^{sd}\right) \leq \left(Cn_{ijt} + Cns_{ijt} + Cnw_{ijt}\right)\cdot B \quad (5\text{-}37)$$

$$\forall\ t\in T, \forall\ i,j\in N: i\neq j,$$

$$\sum_{s\in N}\sum_{d\in N:s\neq d} \lambda r_{ijt}^{sd} \leq \left(Cr_{ijt} + Crw_{ijt} + Crs_{ijt}\right)\cdot B \quad (5\text{-}38)$$

$$\forall\ t\in T, \forall\ i,j\in N: i\neq j,$$

$$\sum_{n\in Np_m} Wd_{mnt}^{ij} - \sum_{n\in Np_m} Wd_{nmt}^{ij} = \begin{cases} Cd_{ijt} + Cdw_{ijt} & m = i \\ -\left(Cd_{ijt} + Cdw_{ijt}\right) & m = j \\ 0 & otherwise \end{cases} \quad (5\text{-}39)$$

$$\forall\ t \in T,\ \forall\, i,j,m \in N: i \neq j,$$

$$\sum_{n\in Np_m} Wn_{mnt}^{ij} - \sum_{n\in Np_m} Wn_{nmt}^{ij} = \begin{cases} Cn_{ijt} + Cns_{ijt} + Cnw_{ijt} & m = i \\ -\left(Cn_{ijt} + Cns_{ijt} + Cnw_{ijt}\right) & m = j \\ 0 & otherwise \end{cases} \quad (5\text{-}40)$$

$$\forall\ t \in T,\ \forall\, i,j,m \in N: i \neq j,$$

$$\sum_{n\in Np_m} Wr_{mnt}^{ij} - \sum_{n\in Np_m} Wr_{nmt}^{ij} = \begin{cases} Cr_{ijt} + Crs_{ijt} + Crw_{ijt} & m = i \\ -\left(Cr_{ijt} + Crs_{ijt} + Crw_{ijt}\right) & m = j \\ 0 & otherwise \end{cases} \quad (5\text{-}41)$$

$$\forall\ t \in T,\ \forall\, i,j,m \in N: i \neq j,$$

$$\begin{aligned} &\sum_{j\in N: i\neq j} PR^w \cdot \left(Crw_{ijt} + Cdw_{ijt} + Cnw_{ijt}\right) + PR^w \cdot Qw_{it} \\ &\quad + \sum_{n\in Np_i} PT^w \cdot (\omega dw_{int} + \omega nw_{int} + \omega rw_{int}) \\ &\quad + P\_cooling_i + P\_computing_i \\ &\quad \leq \sum_{k\in K} (\delta_{ki} \cdot PWF_{kt} \cdot (1 - loss_{ki}) \cdot U_k) \end{aligned} \quad (5\text{-}42)$$

$$\forall\ t \in T, \forall\ i \in N,$$

$$\begin{aligned} &\sum_{j\in N: i\neq j} PR^s \cdot \left(Crs_{ijt} + Cns_{ijt}\right) + PR^s \cdot Qs_{it} + \sum_{n\in Np_i} PT^s \cdot (\omega ns_{int} \\ &\quad + \omega rs_{int}) \leq \left(1 - \sum_{k\in K} \delta_{ki}\right) \cdot S_{it} \quad \forall\ t \in T, \forall\ i \in N, \end{aligned} \quad (5\text{-}43)$$

$$\sum_{i\in N}\Bigg((1+loss_{ki})\cdot\Bigg(\sum_{j\in N:i\neq j}PR^{w}\cdot\left(Crw_{ijt}+Cdw_{ijt}+Cnw_{ijt}\right)+PR^{w}\cdot Qw_{it}+\sum_{n\in Np_i}PT^{w}\cdot(\omega dw_{int}+\omega nw_{mnt}+\omega rw_{int})\Bigg)+P_{cooling_i}+P_{computing_i}\Bigg)\leq\sum_{a\in K}PWF_{at}\cdot U_a \tag{5-44}$$

$$\forall\ t\in T,k\in K,$$

$$\sum_{i\in N}\sum_{j\in N:i\neq j}\left(Wd_{mnt}^{ij}+Wn_{mnt}^{ij}+Wr_{mnt}^{ij}\right)\leq W\cdot f_{mn} \tag{5-45}$$

$$\forall\ t\in T,\forall\ m\in N,n\in Np_m,$$

$$\sum_{i\in N}\sum_{j\in N:i\neq j}Wd_{mnt}^{ij}=\omega d_{mnt}+\omega dw_{mnt} \tag{5-46}$$

$$\forall\ t\in T,\forall\ m\in N,n\in Np_m\ ,$$

$$\sum_{i\in N}\sum_{j\in N:i\neq j}Wn_{mnt}^{ij}=\omega n_{mnt}+\omega ns_{mnt}+\omega nw_{mnt} \tag{5-47}$$

$$\forall\ t\in T,\forall\ m\in N,n\in Np_m\ ,$$

$$\sum_{i\in N}\sum_{j\in N:i\neq j}Wr_{mnt}^{ij}=\omega r_{mnt}+\omega rs_{mnt}+\omega rw_{mnt} \tag{5-48}$$

$$\forall\ t\in T,\forall\ m\in N,n\in Np_m\ ,$$

$$\sum_{k\epsilon K}\delta_{ki}\leq 1 \tag{5-49}$$

$$\forall\ i\in N,$$

$$\sum_{i\in N}\sum_{k\in K}\delta_{ki} = Ndc, \tag{5-50}$$

$$\begin{aligned} Qe_{it} + Qs_{it} + Qw_{it} \\ = \Bigg(\sum_{d\in N:d\neq i} \lambda^{idt} + \sum_{s\in N:s\neq i} \lambda^{sit}\cdot Rd \cdot \sum_{k\epsilon K}\delta_{ks} \\ + \sum_{n\in N:n\neq i} \lambda^{int}\cdot Ru \cdot \sum_{k\epsilon K}\delta_{kn} \Bigg)/B \\ \forall\ t\in T, \forall\ i\in N. \end{aligned} \tag{5-51}$$

The above constraints (5-33)-(5-35), (5-36)-(5-38), (5-39)-(5-41), (5-45), (5-46)-(5-47), (5-50) and (5-51) replace constrains (5-7)-(5-9) and (5-10), (5-11), (5-12), (5-13), (5-14) and (5-15), respectively in Section 5.2.1. Constraint (5-42) states that the renewable energy consumption of ports, transponders, cooling and computing in a data centre should not be larger than the power provided by a single wind farm taking into account the transmission losses. Constraint (5-43) ensures that the renewable energy consumption of ports and transponders at a regular node does not exceed the solar power available at the node. Constraint (5-44) ensures that the renewable energy consumption of all data centres does not exceed the power provided by all wind farms. Constraint (5-49) ensures that one data centre can only access one wind farm.

5.4.2 Simulation and Results

The NSFNET network is considered as an example network to identify the optimal location of data centres using the MILP model. Only 3 wind farms have been selected based on their location and maximum output power [162] to power the data centres in the network (see Fig 5-23): 1) WF1: Cedar Creek Wind Farm, 2) WF2: Capricorn Ridge Wind Farm, 3) WF3: Twin Groves Wind Farm, all three in blue. The wind Farms are shown in Fig 5-23. The maximum output power of the three wind farms is 300 MW, 700 MW and 400 MW, respectively.

The solar power [142] available to a node is shown in Fig 5-24. The geographical location of nodes affects the sunset and sunrise time, and therefore has

impact on the solar energy generated in each node. In Chapter 4, the details of the solar power available in each node are given. This is non-zero from 6:00 to 22:00 and the maximum output power occurs at 12:00.

We assume the electric transmission power loss is 15% per 1000 km [163] and the percentage of the power of wind farms allocated to data centres is assumed to be 0.3% (typical level sufficient to power a medium size data centre, see the power consumption values below). The lighting and cooling power consumption of a typical data centre is 150-200W/ft^2. Assuming a 3500 ft^2 data centre, the total power consumed in such a (typical) data centre for lighting and cooling is 700 kW and the computing power consumption is assumed to be 300 kW which is typical for this data centre size. The power allocated by a wind farm to a data centre is known and is assumed here to be 1.4 MW. This corresponds to a power usage efficiency (PUE) of 2 which is typical for a data centre [164]. The renewable energy available to a data centre is a function of the transmission losses and these are location dependent. Furthermore the network topology, traffic, and components' power consumption also play an important role in determining the optimum data centre location as in Section 5.2. Therefore the MILP model in this section takes into account the Section 5.2 trade-offs as well as the trade-offs introduced by the losses associated with the transmission of renewable energy to the data centre location. These losses reduce the renewable power available to a node for communications purposes, hence the MILP model identifies the optimum data centre locations by minimising the non-renewable power consumption of the network.

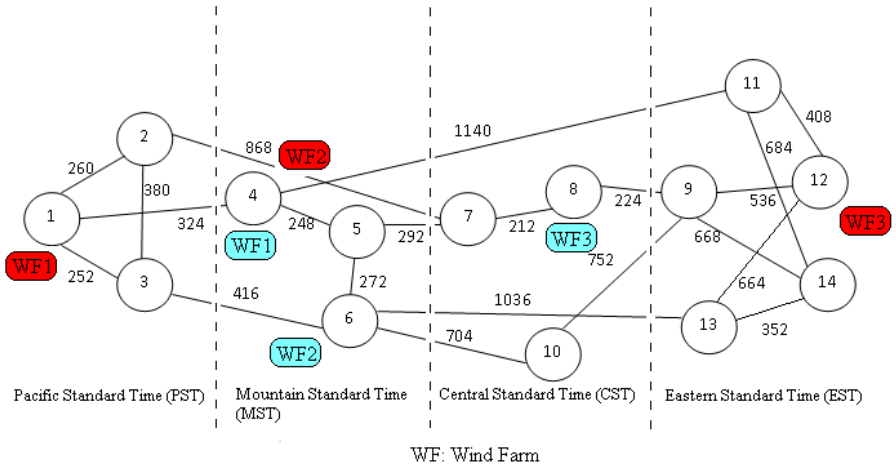

Fig 5 - 23: The NSFNET network with wind farms and time zones

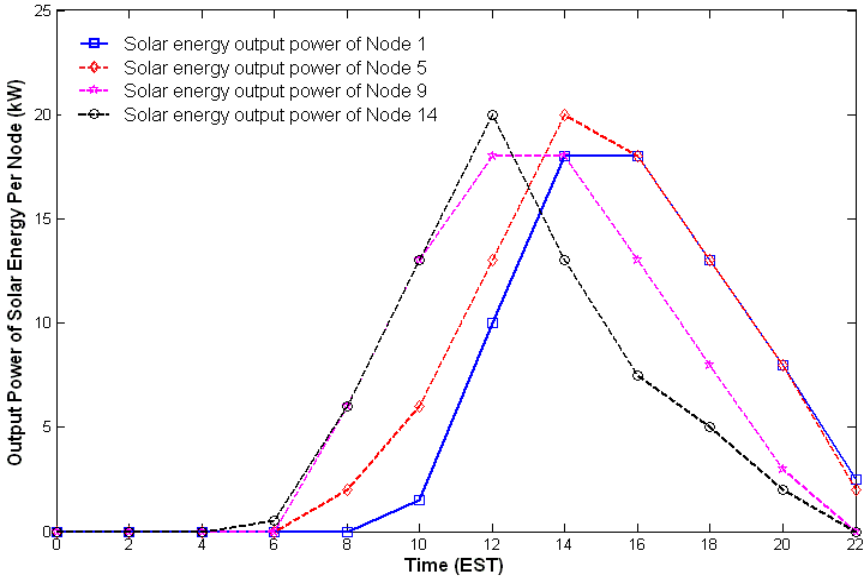

Fig 5 - 24: Solar power in different nodes at different geographic locations

The MILP model is ran with five data centres (*Ndc*=5) under the same assumptions as in Section 5.2.2. The optimal locations of data centres obtained from the MILP model are as follows (4, 5, 6, 7, 8) where data centres 4 and 5 are powered by WF1, data centre 6 and 7 are powered by WF2, and data centre 8 is powered by WF3. The MILP model results are such that all the data centres are located in the centre of the network. Unlike the results in Section 5.2.2 where the data centres selection was only dictated by the number of hops and distance between data centres and nodes, in the presence of renewable energy and transmission losses, the selection of data centres locations is also controlled by the utilisation of the renewable energy resources, as the amount of energy available from wind farms and solar cells at regular nodes is limited. Therefore nodes at the centre of the network are selected to serve as data centres so that they can utilise the wind farm renewable power more efficiently and consequently result in higher reductions in the total non-renewable power consumption compared to the selection of nodes at the edge.

Fig 5-25 shows the non-renewable power consumption under the optimal data centre locations obtained from the MILP model and simulations under the multi-hop bypass heuristic. This is compared to the case where random nodes (1, 2, 4, 6 and 13) are selected to serve as data centres, powered by the nearest wind farm. The non-renewable power consumption obtained from the MILP model under the optimal locations represents a lower bound. Compared with the random locations, the non-

renewable power consumption under the optimal locations has on average reduced the non-renewable power consumption by 26.2% for the MILP model and by 4.9% for the multi-hop bypass with shortest path routing (simulation results). The random locations result in larger hop numbers and distances between data centres and nodes and consequently higher power consumption. In addition the random locations reduce the utilisation of the renewable energy from wind farms and solar cells and consequently increase the non-renewable power consumption. The difference between the MILP model and the multi-hop bypass with shortest path routing (simulation results) is due to the same reasons discussed in Section 5.2.2.

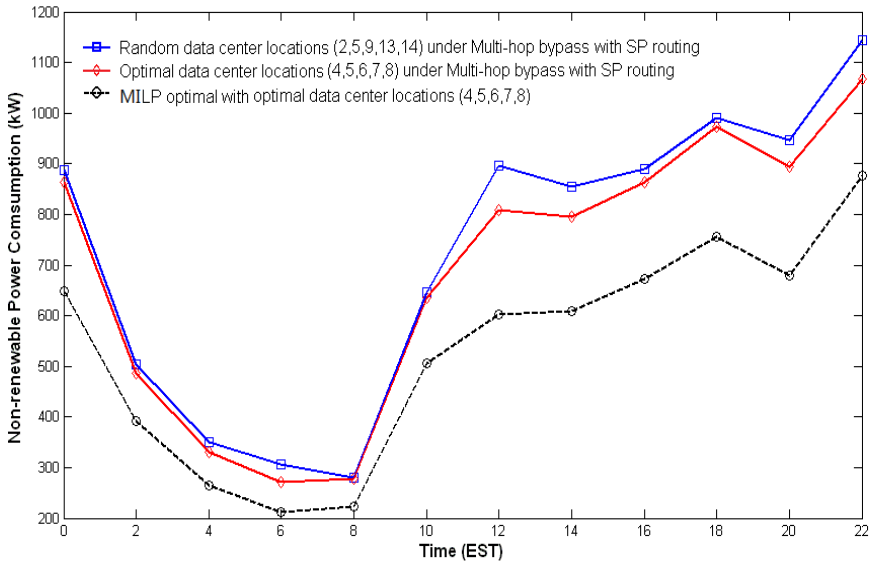

Fig 5 - 25: The non-renewable power consumption of the IP over WDM network with different locations of data centres under the multi-hop bypass heuristic in a 24 hour period.

The MILP model was used to determine the power consumption assuming that the wind farms are located as shown in Fig 5-23 in red. The optimal locations of data centres obtained from the MILP model in this case are as follows (1, 3, 4, 12, 13) where data centres 1 and 3 are powered by WF1, data centre 4 is powered by WF2, and data centres 12 and 13 are powered by WF3. It can be observed that as with the first scenario the optimum data centres locations are next to or near wind farms. In Fig 5-26, the non-renewable power consumption under the optimal locations (1, 3, 4, 12, 13) was evaluated. Compared with random locations, the non-renewable power consumption under the optimal locations has been reduced by an average of 20.8% under the MILP model and by an average of 2.8% for the multi-hop bypass with shortest path routing (simulation results).

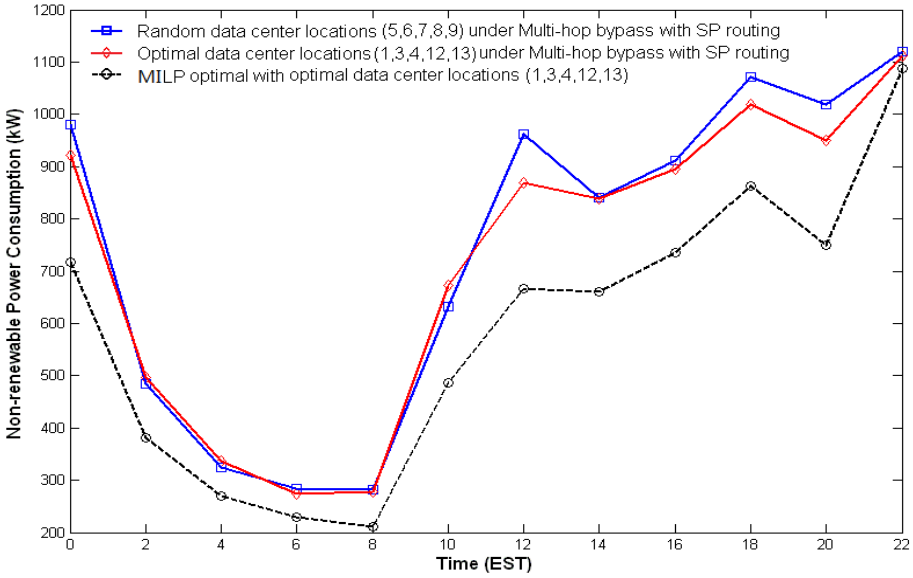

Fig 5 - 26: The non-renewable power consumption under the multi-hop bypass heuristic in the IP over WDM network assuming optimal data centre locations under different wind farm locations

Fig 5-27 shows that under the optimal data centre locations for the first wind farms location scenario, introducing renewable energy to the network (wind farms next to data centres and solar cells in regular nodes) has reduced the non-renewable power consumption under the different heuristics. Fig 5-28 gives the reductions in the non-renewable power consumption under the different heuristics and scenarios. The results are compared with the non-bypass heuristic (with shortest-path routing) without renewable energy representing the upper bound on the non-renewable energy consumption. The multi-hop bypass heuristic (with shortest-path routing) without renewable energy introduces average savings of 46%. The figure also shows that the savings due to introducing renewable energy (non-bypass with renewable energy) has achieved an average reduction of 58%. Combining the multi-hop bypass heuristic with renewable energy increases power saving to an average of 77% obtained from the MILP network design and 71% obtained from the simulation. Introducing the replication scheme increases the average saving to 73% (simulation results).

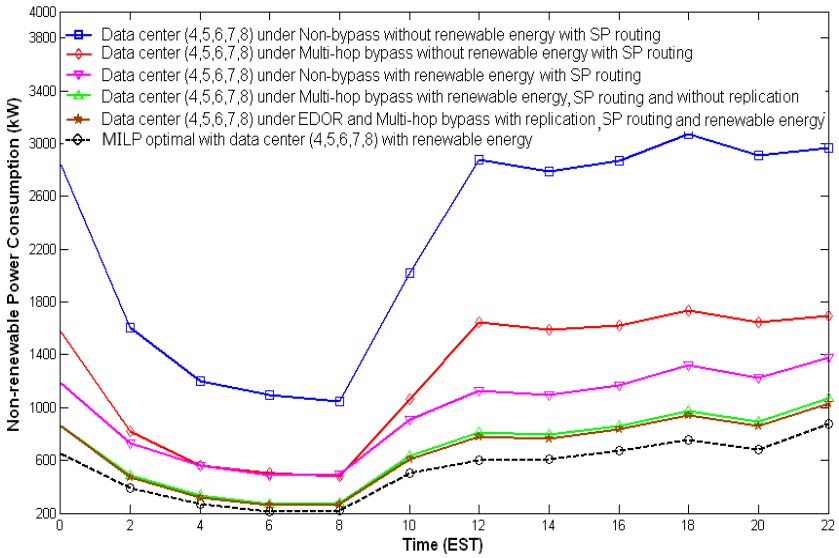

Fig 5 - 27: The non-renewable power consumption of the IP over WDM network under different heuristics with and without renewable power in the IP over WDM network assuming optimal data centre locations.

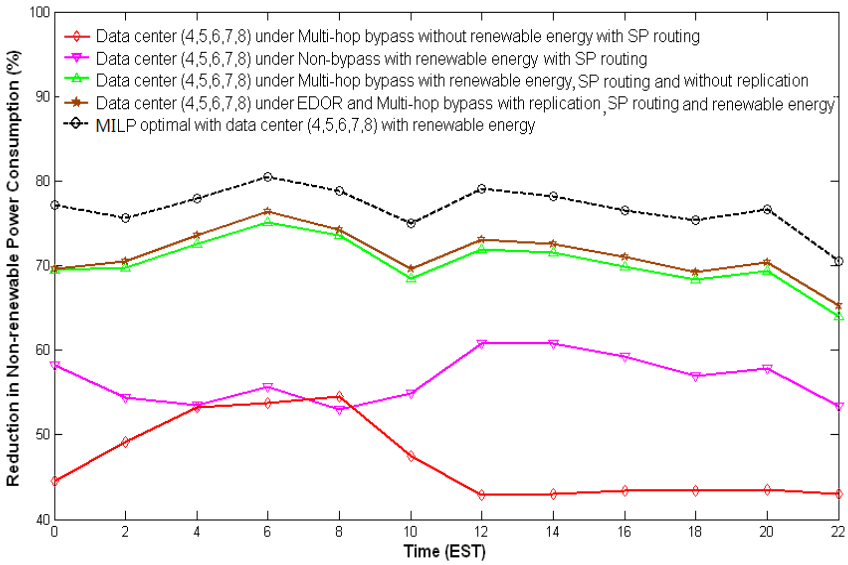

Fig 5 - 28: The reduction in non-renewable power consumption under different heuristics with and without renewable power in the IP over WDM network assuming optimal data centre locations

Fig 5-29 shows the total power consumption of the network under the non-bypass and multi-hop bypass heuristics with and without renewable energy. It is clear that the optimal data centre locations maintain the total power consumption of the network by minimising the power loss due to the transmission of renewable energy from wind farms to data centres. The total transmission loss throughout the day is insignificant compared to the savings in CO_2 emissions.

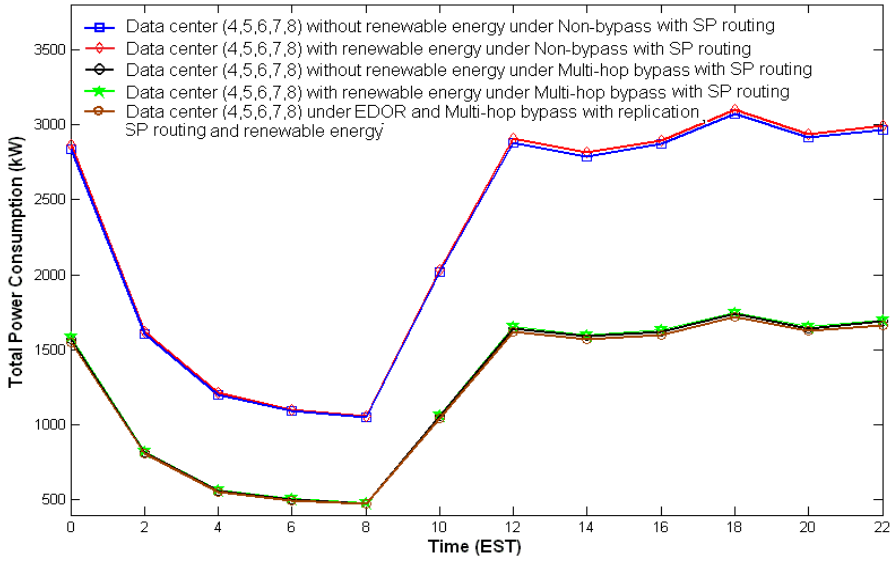

Fig 5 - 29: The total power consumption under different heuristics with and without renewable power in the IP over WDM network assuming optimal data centre locations

5.5 Summary

This chapter has investigated the power consumption of IP over WDM networks with data centres where data centres create a hot node scenario leading to a significant increase in the power consumption. Three problems have been investigated.

In the first problem, the optimisation of the data centre locations with the objective of minimising the power consumption of the network was studied. A MILP model has been developed and simulations have been carried out. The MILP model and simulation results show that the power savings obtained by optimising the data centre locations depend on three factors: the IP over WDM routing approach implemented (lightpath bypass or no-bypass), regularity of the network topology and the number of data centres in the network. Comparing the non-bypass and the multi-hop bypass heuristics shows that while power savings up to 37.5% are obtained under the non-bypass heuristic, the savings under the multi-hop bypass heuristic are limited to 11.2%. The results also show that the location of data centres has significant effect on the power consumption of the network for networks with irregular topologies and fewer number of data centres as optimising the locations of

data centres has significant impact on reducing the average hop number and distance between nodes and data centres and consequently the power consumption. Comparing the results of the irregular topology with the result of the NSFNET topology, it has been observed that the power consumption savings have been reduced by an average of 10% under the non-bypass heuristic. NSFNET network results have shown that while the power saving obtained as a result of optimising the location of a single data centre is up to 26.6%, the savings with 5 data centres are limited to 11.4%.

In the second problem, the power savings introduced by implementing a data replication scheme in the IP over WDM network with data centres have been studied. A novel algorithm, Energy-Delay Optimal Routing (EDOR), has been proposed to minimise the power consumption under the replication scheme while maintaining the QoS. Simulation results show that implementing the replication scheme under the non-bypass heuristic with shortest distance routing has resulted in an average power savings of 28%. The power saving achieved is reduced to 4.5% under the multi-hop bypass with the EDOR algorithm. The results also show that with the EDOR algorithm the increase in the propagation delay is limited to less than 8% compared to the propagation delay with shortest distance routing. However the results show that with a larger number of data centres the data centre location optimisation is less important (savings are limited to 4.4% and 1.7%). Therefore the problem in this case becomes that of optimising the routing and it has been shown that energy consumption results obtained from the simple heuristics are close to the optimal MILP model results.

In the third problem, the use of renewable energy (wind and solar energy) to reduce the non-renewable power consumption and consequently the CO_2 emission of IP over WDM networks with data centres has been evaluated. A MILP model is developed to optimise the location of data centres taking into account the location of renewable energy sources (wind farms) and the transmission power losses. It was determined that following the optimisation all the data centres are located in the centre of the network as the selection of data centres is controlled by the utilisation of the renewable energy resources in addition to the number of hops and distance between data centres and nodes. The results show that moving the data centres closer to renewable energy sources maximises the utilisation of renewable energy sources

and consequently reduces the CO_2 emissions. By combining the multi-hop bypass heuristic with renewable energy and the replication scheme power consumption savings up to 73% have been achieved. The results also show that the optimal data centre locations minimise the power losses associated with the transmission of renewable energy from wind farms to data centres.

Up to here, only virtual topology design (RWA problem) is included by the novel MILP models proposed in this thesis to reduce power consumption of optical networks on top of the reduction from applying renewable energy and optimising data centre locations. In the next chapter, we will investigate the combination of energy efficient physical topology design and energy efficient virtual topology design. Using this combination, we expect further power consumption reduction in optical networks.

Chapter 6: Energy Efficient Physical Topology Design for IP over WDM Networks

6.1 Introduction

A number of major operators and equipment manufacturers are currently interested in the physical topology design of core networks, e.g. partners in the Green Touch initiative [165]. In previous research, the physical topology design problem concentrated on improving the QoS and reducing the cost of networks. For examples, in [166] an analytical framework is developed to optimise the physical connectivity of WDM networks as the network size and traffic volume scale. In [167], the authors give some analytical insights into cost-efficient physical architectures for WDM Metropolitan Area Networks (MAN). The work in [168] gives a node degree-constrained topology optimisation model for the deployment of directional RF or Free Space Optical (FSO) based tactical networks. In [169] the authors investigated the design of large-scale WDM networks of OXCs that provide end-to-end lightpath services. The relationship between the number of wavelengths required and topology design parameters, including connectivity, nodal degrees, and average hop distance, is studied in [170].

In this chapter, energy-efficient physical topologies for IP over WDM networks under different scenarios in terms of IP over WDM approaches (non-bypass and bypass), nodal degree constraints, traffic symmetry and renewable energy availability are investigated. The optimisation of the physical topology of IP over

WDM networks is studied by developing a MILP model with the objective of minimising the total power consumption of the network. The power savings introduced by deploying topologies that eliminate the need for IP routers (the most energy consuming devices in the network) are also investigated, including a full mesh topology and a star topology.

In addition, existing research has not investigated the impact of embodied energy on the energy efficiency of wired network. In this chapter, the impact of taking the embodied energy of network devices into account in the physical topology design is also investigated. In this chapter we consider this topic under different scenarios in terms of IP over WDM approaches (non-bypass and bypass) and traffic symmetry and give a detailed analysis of the embodied energy of the different network devices for the first time.

6.2 Energy Efficient Physical Topology Design Considering Operational Energy

6.2.1 Mathematical Model

In [45] a MILP model was developed to minimise the power consumption of IP over WDM networks by optimising the virtual topology considering a fixed physical topology. In this section, a MILP model to minimise the power consumption of IP over WDM networks is developed by optimising the physical topology. Note that in addition to the physical topology design approach (where the power consumption is minimised over the 24 hours), dynamic approaches can be implemented on the virtual topology to minimise the network power consumption, for example switching off resources at low traffic demands. In this work, a scenario where the node locations are given (for example city locations) is considered and in addition to optimising the virtual topology as in [45], the model optimises the deployment of the physical links connecting these nodes so that the total network power consumption is minimised.

Before introducing the model, the notations used are defined. The following parameters are defined:

EA_{mn} The number of EDFAs on physical link (*m, n*). Typically $EA_{mn} = \lfloor L_{mn}/S - 1 \rfloor + 2$, where *S* is the distance between two neighbouring EDFAs [78],

$Ndgr$ Minimum nodal degree,

$Nlink$ Total number of links,

NF Maximum number of fibres on one physical link,

PR Power consumption of a router port,

PT Power consumption of a transponder,

PE Power consumption of an EDFA,

PO_i Power consumption of the optical switch at node *i*,

PMD Power consumption of a multi/demultiplexer.

The following variables are also defined:

C_{ijt} The number of wavelength channels in the virtual link (*i, j*) at time *t*,

ω_{mnt} The number of wavelength channels in the physical link (*m, n*) at time *t*,

W_{mnt}^{ij} The number of wavelength channels in the virtual link (*i, j*) that traverse physical link (*m, n*) at time *t*,

DM_i The number of multi/demultiplexers in node *i,*

λ_{ijt}^{sd} The traffic flow from node *s* to node *d* that traverses the virtual link (*i, j*) at time *t,*

$link_{mn}$ If there is a physical link between nodes *m* and *n*, $link_{mn} = 1$, otherwise $link_{mn} = 0$,

f_{mn} The number of fibres on physical link (*m, n*).

Under the multi-hop bypass heuristic [45] at time t, the total network power consumption is composed of:

1) The power consumption of ports at time t

$$\sum_{i\in N}\sum_{j\in N:i\neq j} PR\cdot C_{ijt} \tag{6-1}$$

2) The power consumption of transponders at time t

$$\sum_{m\in N}\sum_{n\in N:m\neq n} PT\cdot \omega_{mnt} \tag{6-2}$$

3) The power consumption of EDFAs at time t

$$\sum_{m\in N}\sum_{n\in N:m\neq n} PE\cdot EA_{mn}\cdot f_{mn} \tag{6-3}$$

4) The power consumption of optical switches at time t

$$\sum_{i\in N} PO_i \tag{6-4}$$

5) The power consumption of multiplexers and demultiplexer at time t

$$\sum_{i\in N} PMD\cdot DM_i \tag{6-5}$$

The MILP model with the output of the optimal physical topology is defined as follows:

Objective: minimise

$$\begin{aligned}\sum_{t\in T}\Bigg(&\sum_{i\in N}\sum_{j\in N:i\neq j} PR\cdot C_{ijt}+\sum_{m\in N}\sum_{n\in N:m\neq n} PT\cdot \omega_{mnt}\\ &+\sum_{m\in N}\sum_{n\in N:m\neq n}\left(PE\cdot EA_{mn}\cdot f_{mn}\right)+\sum_{i\in N} PO_i\\ &+\sum_{i\in N} PMD\cdot DM_i\Bigg)\end{aligned} \tag{6-6}$$

Subject to:

1) Flow conservation constraint in the IP layer:

$$\sum_{j\in N:i\neq j}\lambda_{ijt}^{sd}-\sum_{j\in N:i\neq j}\lambda_{jit}^{sd}=\begin{cases}\lambda^{sdt} & if\ i=s\\ -\lambda^{sdt} & if\ i=d\\ 0 & otherwise\end{cases} \tag{6-7}$$

$$\forall\ t\in T,\forall\ s,d,i\in N: s\neq d$$

Constraint (6-7) represents the flow conservation constraint in the IP layer. It ensures that in all nodes the total outgoing traffic is equal to the total incoming traffic except for the source and the destination nodes. It also ensures that traffic flows can be split and transmitted through multiple flow paths in the IP layer.

2) *Virtual link capacity constraint:*

$$\sum_{s\in N}\sum_{d\in N:s\neq d}\lambda_{ijt}^{sd}\leq C_{ijt}\cdot B \tag{6-8}$$

$$\forall\ t\in T,\forall\ i,j\in N: i\neq j$$

Constraint (6-8) ensures that the summation of all traffic flows through a virtual link does not exceed its capacity.

3) *Flow conservation constraint in the optical layer:*

$$\sum_{n\in N:m\neq n}W_{mnt}^{ij}-\sum_{n\in N:m\neq n}W_{nmt}^{ij}=\begin{cases}C_{ijt} & m=i\\ -C_{ijt} & m=j\\ 0 & otherwise\end{cases} \tag{6-9}$$

$$\forall\ t\in T,\qquad \forall\ i,j,m\in N: i\neq j$$

Constraint (6-9) represents the flow conservation constraint in the optical layer. It represents the fact that in all nodes the total outgoing wavelengths in a virtual link should be equal to the total incoming wavelengths except for the source and the destination nodes of the virtual link.

4) *Physical link capacity constraints:*

$$\sum_{i \in N} \sum_{j \in N: i \neq j} W_{mnt}^{ij} \leq W \cdot f_{mn} \qquad (6\text{-}10)$$

$$\forall\ t \in T, \forall\ m \in N, n \in N: m \neq n$$

$$\sum_{i \in N} \sum_{j \in N: i \neq j} W_{mnt}^{ij} \leq W \cdot NF \cdot link_{mn} \qquad (6\text{-}11)$$

$$\forall\ t \in T, \forall\ m \in N, n \in N: m \neq n$$

$$\sum_{i \in N} \sum_{j \in N: i \neq j} W_{mnt}^{ij} = \omega_{mnt} \qquad (6\text{-}12)$$

$$\forall\ t \in T, \forall\ m \in N, n \in N: m \neq n$$

Constraints (6-10), (6-11) and (6-12) represent the physical link capacity constraints. Constraint (6-10) ensures that the total number of wavelength channels in virtual links traversing a physical link does not exceed the capacity of fibres in that physical link. Constraint (6-11) ensures that the total number of wavelength channels in virtual links traversing a physical link does not exceeded the maximum capacity of fibres in the physical link if the physical link exists. Constraint (6-12) ensures that the number of wavelength channels in virtual links traversing a physical link is equal to the number of wavelengths in that physical link.

5) *Nodal degree limit constraint:*

$$\sum_{n \in N: n \neq m} link_{mn} \geq Ndgr \qquad \forall\ m \in N \qquad (6\text{-}13)$$

Constraint (6-13) gives the minimum nodal degree. Note that a limit on the minimum nodal degree is needed to ensure connectivity i.e. the node is not isolated from the network.

6) *Number of links constraint:*

$$\sum_{m\in N}\sum_{n\in N:n\neq m} link_{mn} = 2\cdot Nlink \tag{6-14}$$

Constraint (6-14) ensures that the number of links in the network does not exceed the limit on the number of links.

The model can be extended to represent the non-bypass approach by redefining the power consumption of ports at time *t* as follows:

$$\sum_{m\in N}\sum_{n\in N:m\neq n} PR\cdot\omega_{mnt} \tag{6-15}$$

Therefore the objective function becomes:

$$\begin{aligned}\sum_{t\in T}\Bigg(&\sum_{m\in N}\sum_{n\in N:m\neq n} PR\cdot\omega_{mnt} + \sum_{m\in N}\sum_{n\in N:m\neq n} PT\cdot\omega_{mnt}\\ &+\sum_{m\in N}\sum_{n\in N:m\neq n}\left(PE\cdot EA_{mn}\cdot f_{mn}\right)+\sum_{i\in N} PO_i\\ &+\sum_{i\in N} PMD\cdot DM_i\Bigg)\end{aligned} \tag{6-16}$$

6.2.2 Result under Symmetric Traffic Demand

To optimise the physical topology in a realistic network, the same NSFNET network as in Chapter 4, depicted in Fig 4-4 and the same average traffic demand in different time zones as in Chapter 4, depicted in Fig 4-5 are considered. The simulation environment parameters in terms of number of wavelengths, wavelength capacity, distance between two neighbouring EDFAs, and energy consumption of different components in the network are same as Table 4-3 in Chapter 4.

The MILP model is solved using the AMPL/CPLEX software on a Core2, 2.8 GHz PC with 4GB memory. Note that the MILP model for the NSFNET network utilises about 0.8 million variables in our case and the time needed to run the different scenarios varies from 3 hours to 8 hours. As the NSNET physical topology was not designed taking into account the traffic demand of Fig 4-5, the NSFNET

physical topology is first optimised to minimise the delay considering the traffic demand of Fig 4-5 for a fairer comparison with the power-minimised topologies we obtain later that also use the traffic demand of Fig 4-5. Fig 6-1 shows the delay-optimised NSNET physical topology.

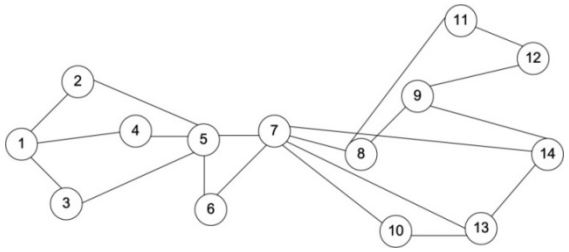

Fig 6 - 1: NSFNET delay-optimised topology considering traffic demand in Fig 4 - 5 and network with time zones

The NSFNET is redesigned with the same number of links (*NLink* =21) and under two nodal degree constraints, *Ndgr*=1 and *Ndgr*=2 (a larger nodal degree is considered later by removing the limitation imposed by constraint (6-14)) considering a symmetric full-mesh connectivity traffic demand (Fig 4-5) where all nodes send to each other with the same probability.

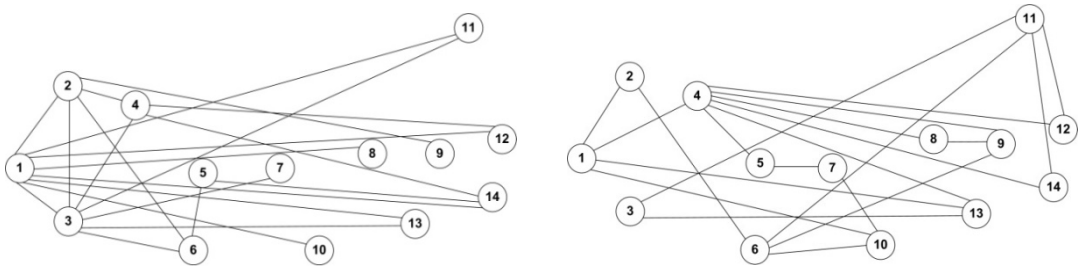

a) *Ndgr*=1 b) *Ndgr*=2

Fig 6 - 2: Optimised physical topology under symmetric traffic demand

Fig 6-2(a) shows the physical topology obtained from the MILP model under the non-bypass approach with *Ndgr*=1. A similar topology is obtained under the multi-hop bypass. A number of long links exist between nodes in one end of the network and nodes in the other end which reduces the number of intermediate hops, i.e. reduces the number of IP router ports and transponders whose power consumption is significantly higher compared to that of EDFAs. However having nodes connected to the network with a single link is not desirable in terms of resilience as the these nodes will be totally disconnected from the network in case of

link fauilure. Therefore in Fig 6-2(b) the optimised physical topology is obtained from the MILP model with *Ndgr*=2.

The power consumption of the optimised physical topologies under *Ndgr*=1 and *Ndgr*=2 is given in Fig 6-3. The optimised topologies under the non-bypass approach have resulted in average power savings of 11% and 10% with *Ndgr*=1 and *Ndgr*=2, respectively compared to the original NSFNET topology. Compared to the delay-minimised topology the average savings are 18% and 17% with *Ndgr*=1 and *Ndgr*=2, respectively. Note that these power savings are due to the physical topology optimisation while the saving achieved in [45], up to 45%, were a result of the virtual topology optimisation. Therefore our saving of 11% and 10% are additional to those in [45]. Increasing the minimum nodal degree while the number of links is fixed increases the average hop count which is related to the number of IP routers and transponders used and therefore the power consumption increases. The figure also shows that higher savings are obtained between 12:00 and midnight where the traffic is higher (see Fig 4-5). Under the multi-hop bypasss approach no IP router ports (the most energy consuming component) are required at intermediate nodes. Therefore the optimisation of the physical topology has an insignificant impact on the power consumption. The power savings is limited to 0.5% in this case.

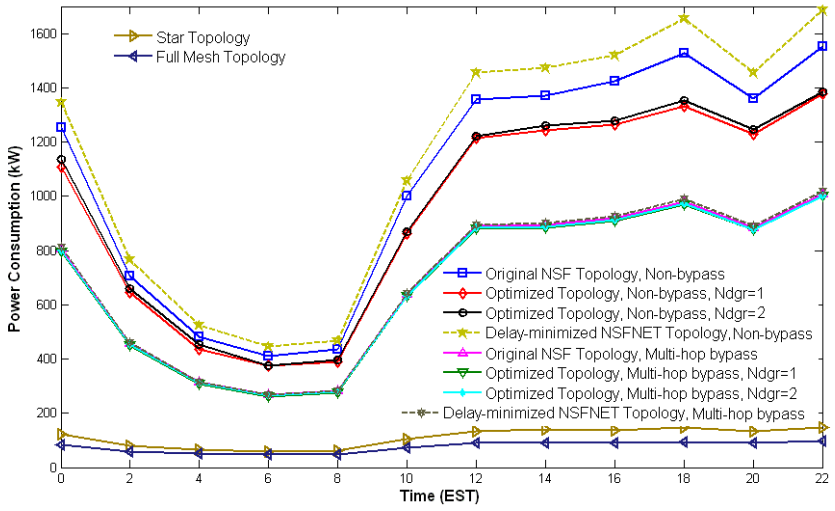

Fig 6 - 3: The power consumption of the NSFNET under different physical topologies under symmetric traffic demand

In the above results the network physical topology is optimised while taking into account a limit on the number of links. Optimising the physical topology

without this constraint resulted in a full mesh topology. According to the network total power consumption in Equation (6-6), the full mesh topology eliminates intermediate nodes which reduces the number of transponders and IP router ports needed to support the full-mesh connectivity traffic demand in the network and consequently the energy consumption decreased by an average of 37% under the non-bypass approach. However, deploying a full mesh topology eliminates the need for IP routers (the most energy consuming components in the network). Note that IP routers can perform other functions in addition to routing and these are not considered here. The total energy consumption of the full mesh topology is calculated without considering IP routers and therefore the full mesh results in saving most of the network power consumption. Fig 6-3 shows the power consumption of the full mesh topology connecting nodes in the NSFNET network. Compared to the original topology under the non-bypass approach, the power consumption has been significantly decreased by 95%. Although the number of links significantly increases under the full mesh topology compared to a regular topology (in case of the NSFNET the number of links increases from 21 to 91) leading to the use of more EDFAs, the power savings obtained from eliminating the IP routers is much more significant.

Another topology that eliminates the need for IP routers is the star topology. In NSFNET, the star is centred at node 8 to give the average minimum distance to all nodes. The star topology saves 92% of the power consumption compared to the original NSFNET topology under a symmetric traffic demand. The number of links in the star topology is significantly lower than the full mesh topology therefore fewer EDFA's are needed compared to the full mesh topology. However, more transponders are needed as a connection between a source destination pair in a star topology will traverse two physical links. Note that the power consumption of the transponder (73 W) is much higher than the EDFA power consumption (8 W) therefore the power consumption of the star topology is slightly higher than the full mesh topology. Note that the power savings produced by the full mesh and star topologies (95% and 92% respectively) are significantly higher than those in [45] (45%).

Optimising the topology has increased the propagation delay experienced by all the nodes under the optimised physical topologies considering shortest path routing.

The average propagation delay has increased from 3.5 ms for the original NSFNET topology to 6.2 ms and 5.6 ms for the optimised topologies with *Ndgr*=1 and *Ndgr*=2, respectively. This significant increase (77% and 60%) comes with no significant power savings. However, as each node is directly connected to other nodes, the full mesh topology has resulted in reducing the average propagation delay by 16% compared to the NSFNET original topology. The star topology has not significantly increased the average propagation delay (the delay has increased by about 17%).

From the results above, it can be seen that physical topology optimisation of existing networks will generally produce limited power savings if the number of links is not to be increased. This can be explained by observing that current network designs minimise delay and although this is not identical to power minimisation, the two are not diametrically opposite (hence 10% to 11% power saving). Shorter routes that minimise delay may also minimise power consumption, but in some cases such short routes pass through many intermediate nodes thus increasing the power consumption and as such the two goals are compatible, but not identical. It can also be observed that both the star and full mesh topologies have resulted in significant power savings and acceptable propagation delay. However, the two topologies may lack practicality due to the large number of links of the full mesh topology and the single point failure of the star topology. Therefore the developed MILP model is used to design power-minimised physical topologies where reliability and practical implementation are taken into account. In the MILP model constraint (6-13) sets a limit on the number of links and constraint (6-14) ensures reliability by setting a minimum nodal degree to 2.

6.2.3 Result under Asymmetric Traffic Demand

In the results above, a symmetric traffic demand scenario is considered. However the presence of data centres (or large cities) in the network may create a hot node scenario where more traffic is destined to or originates from data centres. In this section, physical topology optimisation to minimise the total energy consumption of the network where some nodes serve as data centres is investigated. The traffic demand considered is as follows:

1. In addition to the regular traffic demand, i.e. the traffic demand between regular nodes, the data centre traffic demand which includes the traffic demand between data centres and regular nodes and the traffic demand between data centres is also consider. The traffic demand between data centres and nodes at time t is assumed to be a certain ratio of the regular traffic demand λ^{sdt} [157].

2. The uplink traffic demand ratio from nodes to data centres, R_u, is smaller than the downlink traffic from data centres to nodes ratio, R_d [171].

3. The traffic demand between nodes and data centres is generated based on the regular traffic demand in Fig 4-5 where we assume that R_u=0.3 and R_d=2.5. These values reflect the expected growth in data centre traffic [172].

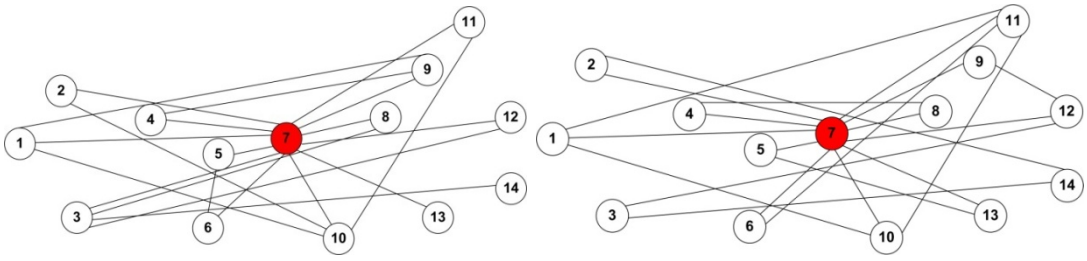

a) *Ndgr*=1 b) *Ndgr*=2

Fig 6 - 4: The optimised physical topologies with node 7 serving as a data centre

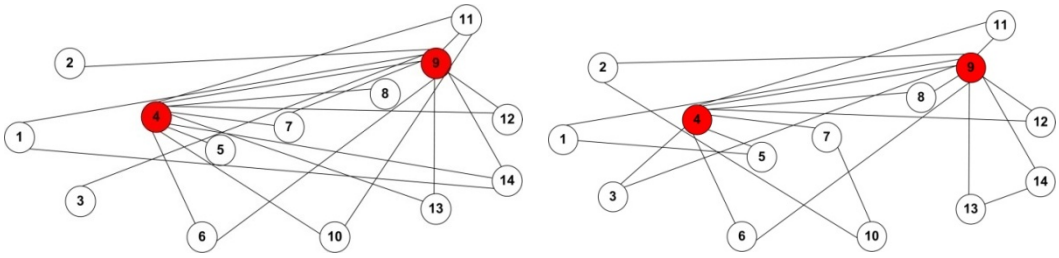

a) *Ndgr*=1 b) *Ndgr*=2

Fig 6 - 5: The optimised physical topologies with nodes 4 and 9 serving as data centres

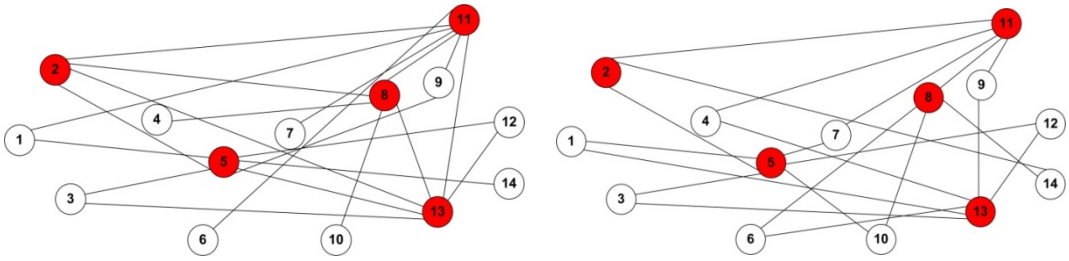

a) *Ndgr*=1 b) *Ndgr*=2

Fig 6 - 6: The optimised physical topologies with nodes 2, 5, 8, 11 and 13 serving as data centres

Fig 6-4, Fig 6-5 and Fig 6-6 show the physical topology optimisation results considering different nodes as data centres and different nodal degree limits. Optimising the topology with node 7 as a data centre (Fig 6-4) has resulted in a physical topology where node 7 has a very high nodal degree of 12. Directly connecting the data centre to nodes will reduce the power consumption of the traffic demands between the data centre and regular nodes (representing 64% of the total traffic demand in the network) by reducing the number router ports and transponders required as intermediate nodes are eliminated. Similarly optimising the physical topology with nodes 4 and 9 serving as data centres (Fig 6-5) has resulted in a physical topology where the nodal degree of nodes 4 and 9 is 9 under *Ndgr*=1. Increasing the nodal degree limit *(Ndgr*=2) has decreased the nodal degree of data centres to 8. Fig 6-6 shows the optimised physical topology with nodes 2, 5, 8, 11 and 13 serving as data centres. Data centre nodes have a high nodal degree.

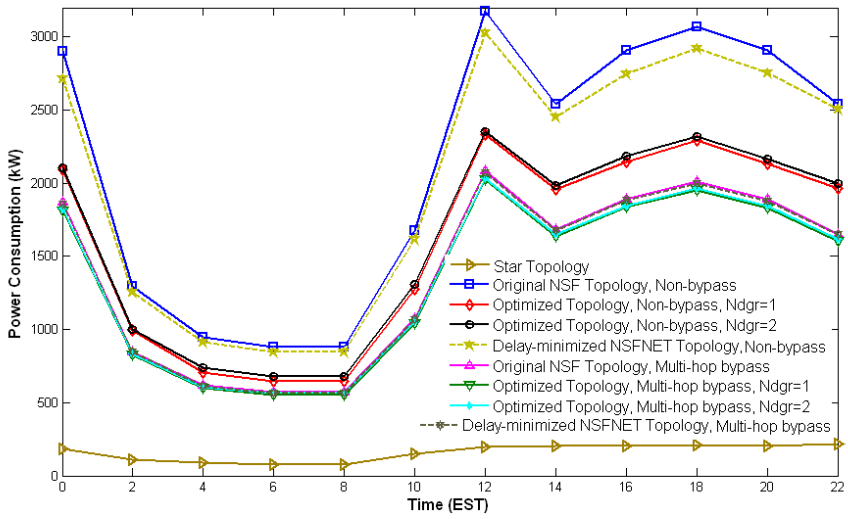

Fig 6 - 7: The power consumption of the NSFNET with node 7 serving as a data centre under different physical topologies

Fig 6-7, Fig 6-8 and Fig 6-9 evaluate the power consumption of the optimized physical topologies with data centres and compare it with the power consumption of the original NSFNET topology with data centres under different asymmetric traffic scenarios and IP over WDM approaches. In Fig 6-7, the optimised physical topology with a single data centre at node 7 under the non-bypass approach has saved an average of 22% and 20% with *Ndgr*=1 and *Ndgr*=2, respectively compared to the original NSFNET. However, compared to the delay minimised topology the avrage savings are 20% and 19% with *Ndgr*=1 and *Ndgr*=2, respectively. As discussed

above increasing the minimum nodal degree while the number of links is fixed has increased the average hop count which is related to the number of IP routers and transponders used and consequecely the power consumption. Using a star topology centred at the data centre node has reduced the energy consumption by 97%.

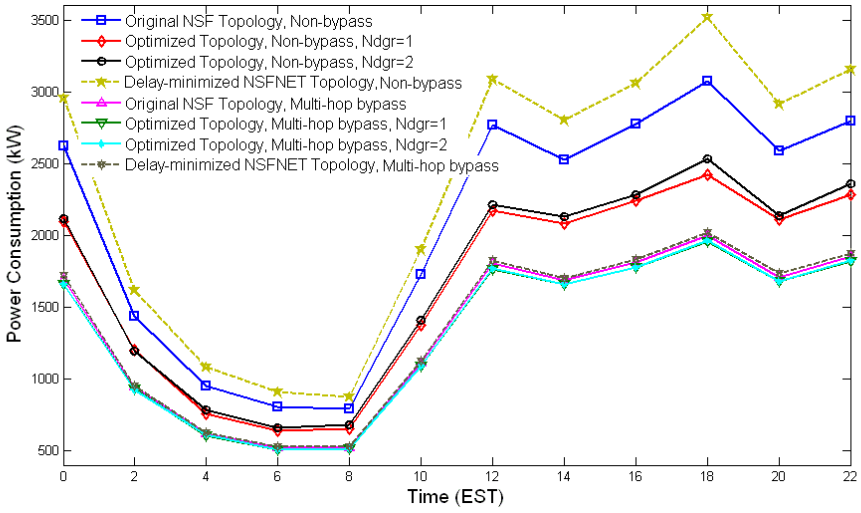

Fig 6 - 8: The power consumption of the NSFNET with nodes 4 and 9 serving as data centres under different physical topologies

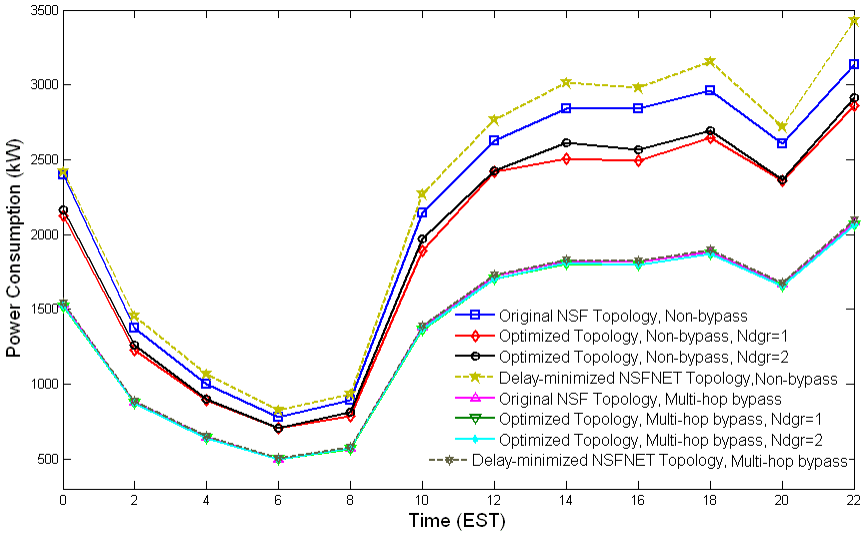

Fig 6 - 9: The power consumption of the NSFNET with nodes 2, 5, 8, 11 and 13 serving as data centres under different physical topologies

Optimising the physical topology considering nodes 4 and 9 as data centres has resulted in saving an average of 20% and 18% of the network total power consumption under the non-bypass approach with *Ndgr*=1 and *Ndgr*=2 respectively compared to the original NSFNET. However, compared to the delay minimised topology the avrage savings are 28% and 25% with *Ndgr*=1 and *Ndgr*=2,

respectively. Power Savings are limited to 1% under the Multi-hop bypass heuristic. Considering a 2-star topology centred at nodes 4 and 9 has resulted in no extra savings.

The physical topology optimisation with 5 data centres (nodes 2, 5, 8, 11 and 13) has resulted in 10% and 8% power savings under the non-bypass approach with *Ndgr*=1 and *Ndgr*=2, respectively compared to the original NSFNET. However, compared to the delay minimised topology the avrage savings are 16% and 13% with *Ndgr*=1 and *Ndgr*=2, respectively.

As in Section 6.2.2, optimising the physical topology has increased the propagation delay. With node 7 serving as a data centre, the average propagation delay has increased by 29% and 50% with *Ndgr*=1 and *Ndgr*=2, respectively. The increase in propagation delay under the optimised topologies is up to 54% and 57% with nodes 4 and 9 and nodes 2, 5, 8, 11 and 13 serving as data centres, respectively.

6.2.4 Energy Efficient Physical Topology Design Considering Renewable Energy

In this section, the physical topology of IP over WDM networks is optimised taking renewable energy sources into account to maximise the utilisation of the renewable energy. Assuming renewable energy in the form of solar energy is available to a limited number of nodes in the network.

The MILP model in Section 6.2.1 is extended to include the renewable enrgy sources. The objective becomes to minimise the total non-renewable enregy consumed by the network. In addition to the parameters defined in Section 6.2.1, the following parameters are defined:

PRS The renewable power consumption of a router port that has access to renewable energy,

PTS The renewable power consumption of a transponder that has access to renewable energy.

In addition to the variables defined in Section 6.2.1, the following variables are defined:

Cn_{ijt} The number of wavelength channels in the virtual link (*i, j*) that are powered by non-renewable energy at time *t*,

ω_{mnt} The number of wavelength channels in the physical link (*m, n*) that are powered by non-renewable energy at time *t*,

W_{mnt}^{ij} The number of wavelength channels in the virtual link (*i, j*) that traverse physical link (*m, n*) at time *t*,

Cs_{ijt} The number of wavelength channels in the virtual link (*i, j*) that are powered by renewable energy at time *t*,

ωs_{mnt} The number of wavelength channels in the physical link (*m, n*) that are powered by renewable energy at time *t*,

y_{it} If the optical switch in node *i* has access to renewable energy at time *t* $y_{it} = 1$, otherwise $y_{it} = 0$,

P_{it} Output power of solar energy in node *i* at time *t.*

The total non-renewable power consumption of the network under the bypass approach at time *t* is composed of:

1) The non-renewable power consumption of ports at time *t*

$$\sum_{i \in N} \sum_{j \in N: i \neq j} PR \cdot Cn_{ijt}, \tag{6-17}$$

2) The non-renewable power consumption of transponders at time *t*

$$\sum_{m \in N} \sum_{n \in N: m \neq n} PT \cdot \omega n_{mnt}, \tag{6-18}$$

3) The non-renewable power consumption of EDFAs at time *t*

$$\sum_{m \in N} \sum_{n \in N: m \neq n} PE \cdot EA_{mn} \cdot f_{mn}, \tag{6-19}$$

4) The non-renewable power consumption of optical switches at time *t*

$$\sum_{i\in N} PO_i(1-y_{it}), \tag{6-20}$$

5) The non-renewable power consumption of multiplexers and demultiplexer at time *t*

$$\sum_{i\in N} PMD \cdot DMn_i. \tag{6-21}$$

The MILP model is defined as follows:

Objective: minimise

$$\sum_{t\in T}\left(\sum_{i\in N}\sum_{j\in N:i\neq j} PR\cdot Cn_{ijt} + \sum_{m\in N}\sum_{n\in N:m\neq n} PT\cdot \omega n_{mnt} + \sum_{m\in N}\sum_{n\in N:m\neq n}\left(PE\cdot EA_{mn}\cdot f_{mnt}\right) + \sum_{i\in N} PO_i(1-y_{it}) + \sum_{i\in N} PMD\cdot DMn_i\right) \tag{6-22}$$

Subject to:

The model is subject to constraints (6-2), (6-5), (6-6), (6-8) and (6-9) in Section 6.2.1. Constraints (6-3), (6-4), (6-7) are replaced with the following equations:

$$\sum_{s\in N}\sum_{d\in N:s\neq d} \lambda_{ijt}^{sd} \leq \left(C_{ijt} + Cs_{ijt}\right)\cdot B, \quad \forall\ t\in T, \forall\ i,j\in N: i\neq j \tag{6-23}$$

$$\sum_{n\in N:m\neq n} W_{mnt}^{ij} - \sum_{n\in N:m\neq n} W_{nmt}^{ij} = \begin{cases} C_{ijt}+Cs_{ijt} & m=i \\ -C_{ijt}-Cs_{ijt} & m=j \\ 0 & otherwise \end{cases} \tag{6-24}$$

$$\forall\ t\in T,\ \forall\ i,j,m\in N: i\neq j$$

$$\sum_{i\in N}\sum_{j\in N:i\neq j} W_{mnt}^{ij} = \omega_{mnt} + \omega s_{mnt} \tag{6-25}$$

$$\forall\ t\in T, \forall\ m\in N, n\in N: m\neq n$$

A constraint is added to ensure the renewable energy consumption at node i does not exceed the solar power available to it.

$$\sum_{j \in N: i \neq j} PRS \cdot Cs_{ijt} + \sum_{n \in N: i \neq n} PTS \cdot \omega s_{int} \leq P_{it} \qquad (6\text{-}26)$$

$$\forall\ t \in T, \forall\ i \in N$$

The NSFNET network is also considered for the physical topology optimisation in the presence of renewable energy sources. Typically a one square meter silicon solar cell can produce about 0.28 kW of power [143]. We assume that the maximum solar energy available to a node is 80 kW, therefore a total solar cell area of about 300 m^2 is required. Solar cell cladding with such surface area can be practically built in a typical core routing node location. The details of the solar power available in nodes are given in Table 4-2. The solar power available to nodes in the NSFNET is shown in Fig 6-10 [142]. This is non-zero from 6:00 to 22:00 and the maximum output power occurs at 12:00.

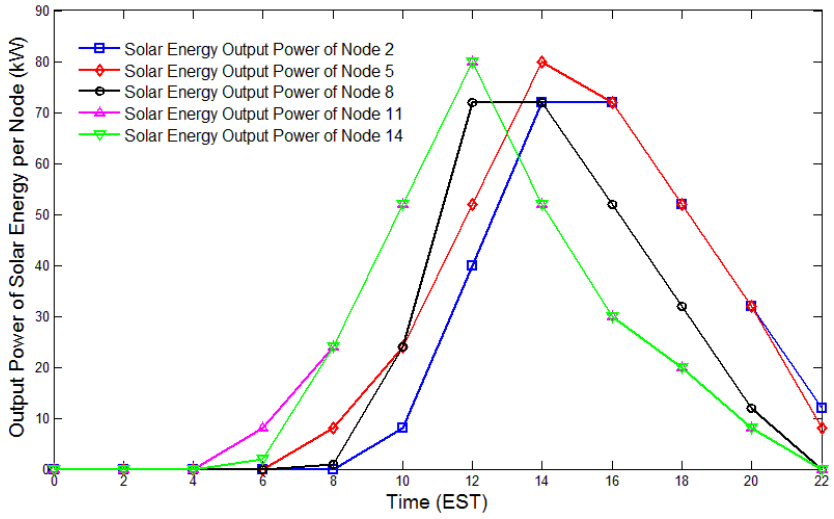

Fig 6 - 10: Solar power in different nodes at different geographic locations

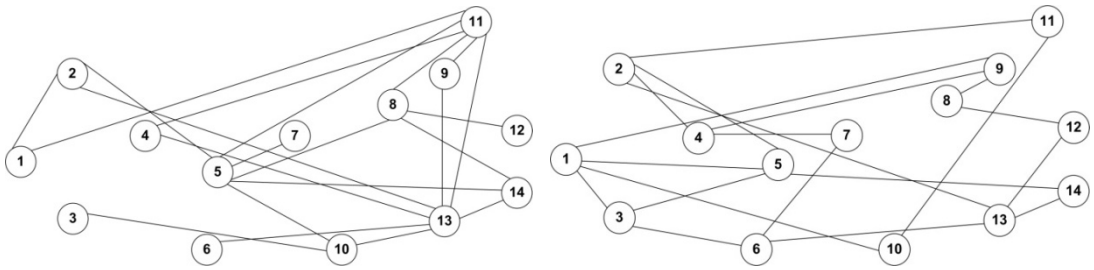

a) *Ndgr*=1 b) *Ndgr*=2

Fig 6 - 11: Optimised physical topology with renewable energy

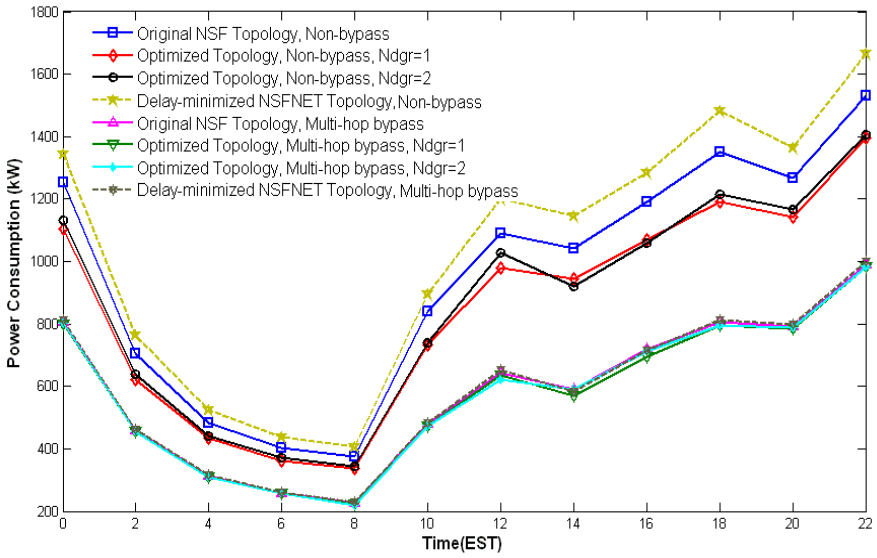

Fig 6 - 12: The power consumption of the NSFNET with nodes 2, 5, 8, 11, 13 employing renewable energy under different physical topologies and heuristics

Fig 6-11 shows the optimisation results for the NSFNET considering five nodes (2, 5, 8, 11 and 13) to employ renewable energy and different nodal degree limits (*Ndgr*=1 and *Ndgr*=2). The physical topologies have changed compared to the topologies in Fig 6-2. The nodal degree of the nodes with solar energy becomes higher to maximise the renewable energy utilisation by allowing more traffic flows to be routed through renewable energy nodes.

Fig 6-12 evaluates the total non-renewable power consumption of the optimised physical topologies in Fig 6-11 where nodes 2, 5, 8, 11 and 13 employ renewable energy and compares it with the non-renewable power consumption of the original NSFNET topology considering the same nodes to employ renewable energy. The optimisation of the physical topology decreases the non-renewable power consumption by increasing the utilisation of the renewable energy sources. Compared to the original NSFNET topology the optimised topology has saved an average of 10% and 9% of the non-renewable energy consumption with *Ndgr*=1 and *Ndgr*=2, respectively under the non-bypass approach. Compared to the delay minimised topology the avrage savings are 18% and 17% with *Ndgr*=1 and *Ndgr*=2, respectively.While the average non-renewable power savings under the bypass approach with *Ndgr*=1 is 2%, the saving is less than 1% with *Ndgr*=2. The propagation delay experienced by nodes in the optimised physical topologies with

renewable energy considering shortest path routing increases by 51% and 57% with *Ndgr*=1 and *Ndgr*=2, respectively compared to the original NSFNET topology.

6.2.5 Cost and Characteristics of Optimised Topologies

The results in the sections above show that the optimised topologies result in higher propagation delays (less than 6.5 ms) compared to the original NSFNET topology. However this increase can be ignored compared to the total network delay including the server response time and electronic layer processing time. Another factor to consider when designing the physical topology is the cost of the network components. Table 6-1 gives the cost of the different network components. The GYTA53 optical fibre cable [173] and solar cells based on the Canadian Solar CS6P-230 design [174] are considered for use by the physical topologies. The cost of the other network components is as given in [45]. Note that the installation cost of the fibre cable is not included as this is region dependent and varies hugely.

40 Gbit/s IP router	80000 $ per port
40 Gbit/s Transponder	25000 $
EDFA	1500 $
Multi/demultiplexer	5000 $
Optical fibre cable (GYTA53)	1500 $ per km (average)
Solar cells (Canadian Solar 230P)	2.12 $ per watt

Table 6 - 1: Cost of network components

Given the traffic and the distances between nodes in the NSFNET network, the cost of the IP router ports and the optical fibre cables will have the major contribution to the total network cost. As the power consumption of the IP routers is the major contributor to the total network power consumption, the power optimised topologies will be supported by the minimum number of IP router ports. In Fig 6-2, Fig 6-4 Fig 6-5 and Fig 6-6, optimising the physical topologies has resulted in topologies with longer links compared to the original NSFNET. These longer links increase the contribution of the optical cable to the total network cost.

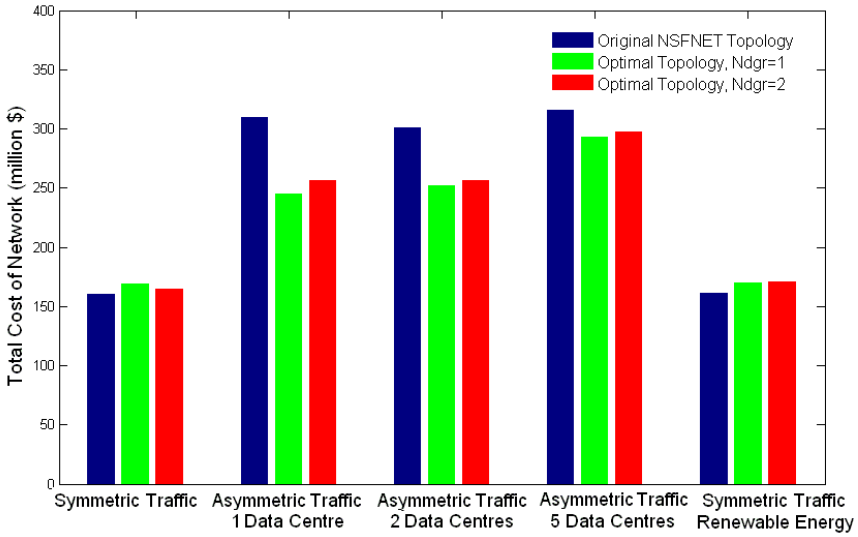

Fig 6 - 13: Cost of different NSFNET physical topologies under the non-bypass approach

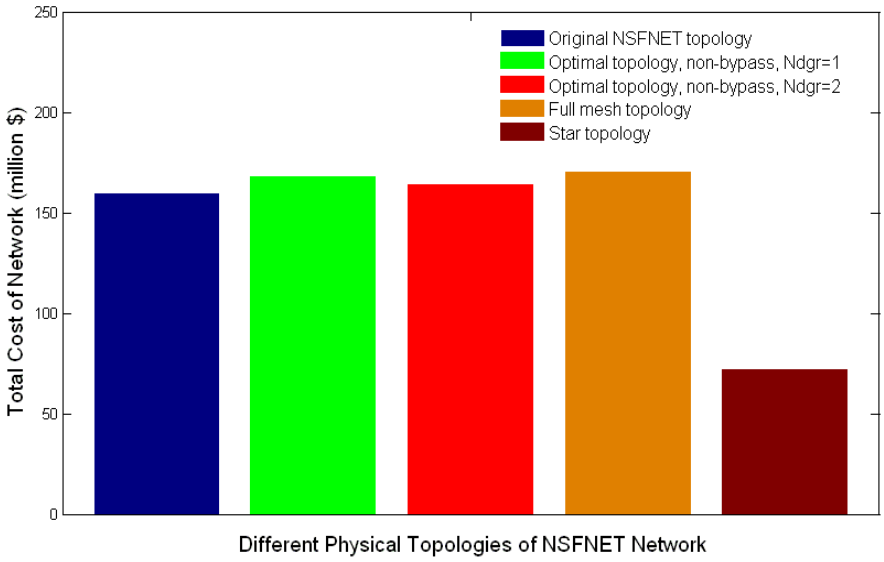

Fig 6 - 14: Cost of the NSNET full mesh and star topologies under the non-bypass approach

Fig 6-13 and Fig 6-14 show the total cost of the different NSFNET topologies. Under symmetric traffic (Fig 6-13), the total cost has slightly increased compared to the original NSFNET topology (maximum increase of 5%) as the increase in the optical cable cost is higher than the savings obtained by optimising the number of IP router ports. Under asymmetric traffic (Fig 6-13), the optimal physical topologies have resulted in up to 21% cost savings compared to the original NSFENT topology. Under asymmetric traffic, the optimised topologies (Fig 6-4, Fig 6-5 and Fig 6-6) have shorter links compared to the symmetric traffic topologies. Therefore the cost

savings obtained by optimising the number of IP router ports to save power is high enough to compensate for the increase in optical fibre cable cost. The total cost of the full mesh and star topologies are shown in Fig 6-14. While the full mesh topology eliminates the IP router ports, it increases the number and length of links resulting in an increase of 7% in the total network cost. The star topology, where IP router ports are eliminated and fewer links are used, saves 55% of the total cost.

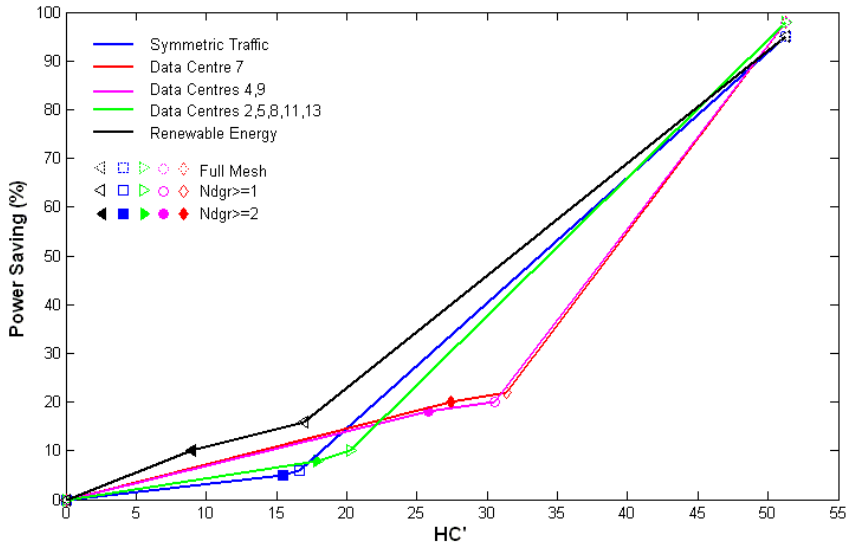

Fig 6 - 15: Relationship between hop count and power savings

Fig 6-15 shows the characteristics of the different energy efficient topologies under the non-bypass approach. It shows how the power savings are related to the topology hop count. We define *HC'* as the percentage reduction in the hop count compared to the original NSFNET topology (NSFNET average hop count is 2.5). The power savings introduced by deploying a topology increase as the reduction in the hop count increases. The maximum reduction is achieved by the full mesh topology with a hop count equal to 1. Power saving in networks through physical topology optimisation can be viewed in many cases as a design process whose goal is to minimise the average hop count between a source and a destination. As shown in Fig 6-15, a given power saving level calls for a higher percentage hop count reduction when there are large users. For example a power saving of 20% calls for hop count reduction of 22% and 32% for the symmetric case and single large user case respectively. The optimisation has shown that with large users stars formed around the large users (Fig 6-4 and Fig 6-5) with the result that nodes "connect themselves to well connected nodes" a parallel with social networks.

6.2.6 Impact of Traffic Variation

In the results above we have chosen to analyze and design the network based on time varying traffic as this represents the realistic conditions in the network. More importantly an increase in the time varying traffic may mean that new network components (e.g. a wavelength) may have to be added to cater for even a slight increase in traffic. This modular jump in power consumption may lead to a different route/link establishment becoming more efficient from the power consumption point of view. Such effects will not be captured if a flat traffic profile is considered. The network topology design faces a number of other challenges, for example the traffic is time zone dependent and the resulting time shifts mean that at certain times of the day (rising and falling traffic), the traffic generated by the nodes becomes uneven. Consider for example 1 a.m. and 9 a.m. where the traffic disparity among the nodes becomes high (due to time zone shifts) causing the symmetric traffic case to appear asymmetric. Under asymmetric traffic the optimal network physical topology changes significantly as earlier parts of this chapter have shown. There is therefore a different optimal network physical topology at different times of the day. Our approach in the chapter so far has been to design the "best" network physical topology that minimises the sum of the power consumption over the 24 hours. Such a physical topology may not be optimal at any time of the day, but minimises the sum power consumption over the whole day.

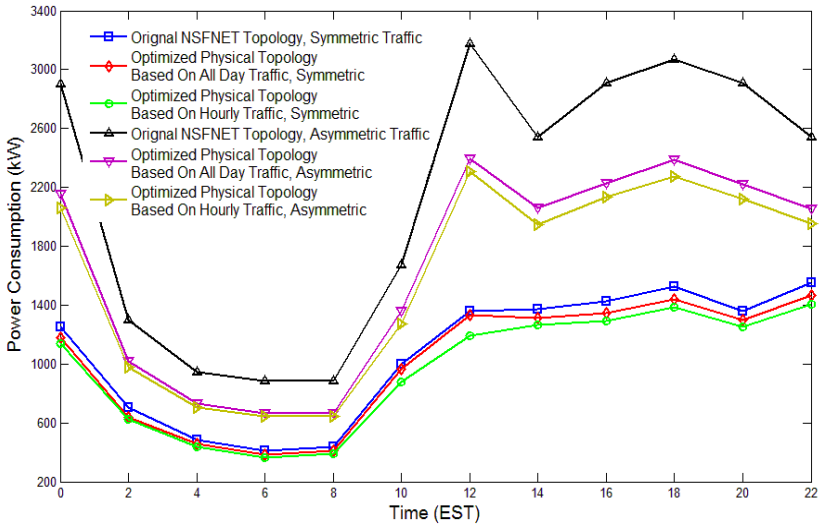

Fig 6 - 16: Power consumption of optimised physical topologies based on hourly traffic or all day traffic

In this section, a best physical topology has been designed for each hour of the day and we have compared the power consumption of such networks (12 topologies in our case, one every 2 hours) to that of our earlier "best" network design and to the NSFNET original topology.

In the symmetric case this approach yields a power saving of 16% compared to the NSFNET original topology, see Fig 6-16. This is to be compared with the 10% saving achieved by our "best" network. In the case of asymmetric traffic the savings compared to the original NSFNET are 26% (Fig 6-16) which is to be compared to the 22% reported in Section 6.2.3 for the single data centre case with the "best" network design. These higher savings although not directly achievable as they stem from different physical topologies motivate further work into "best" physical topology design and subsequent optimal virtual topology implementation.

6.3 Energy Efficient Physical Topology Design Considering Operational and Embodied Energy

The embodied energy, E_{EMB}, of a device is defined as the energy associated with the different processes of its production and maintenance [175]. The production embodied energy $E_{EMB\text{-}P}$ is composed of the energy consumed by the acquirement and processing of raw materials, transportation, manufacturing components, and the assembly and installation the device. The maintenance embodied energy, $E_{EMB\text{-}M}$, is the energy consumed throughout the lifetime of the device to maintain, repair, and replace materials. Network operators are particularly interested in the minimisation of the operational energy as it is directly reflected in the OPEX. On the other hand the embodied energy is not necessary reflected on the CAPEX as CAPEX is controlled by the economic and pricing policies [175].

Embodied energy is already considered in the energy efficiency studies of other fields such as buildings, cars, solar cells, computers [176], mobile phones [177], and network switches [178]. The need to rethink the previous approaches of evaluating the energy efficiency of ICT networks emerge from the sophisticated and energy-intensive process involved in the production of network devices. In [179], [180], the

authors have raised the issue of including both operational and embodied energies in the energy efficiency evaluation of communication networks. The results in [175] have highlighted the importance of considering embodied energy in evaluating the energy efficiency of base-stations in cellular networks. In other fields such as buildings and cars the embodied energy represents a relatively limited percentage of the total energy (7–10 % for buildings [181] and 10–15% for cars [182]) compared to the embodied energy of base-stations which is responsible for 30–40 % of the total energy consumption [175].

6.3.1 Network Devices Embodied Energy

The lack of embodied energy data for devices and systems is a key challenge in optimising networks taking embodied energy into account. A number of methods are used to estimate the embodied energy of a device. In [183], life cycle assessment (LCA) is defined as a technique to assess the environmental impacts associated with all the stages of a product's life from cradle to grave and this progress includes materials processing, manufacture, distribution, use, repair and maintenance, and disposal or recycling. LCA is the most used method where the energy requirement through the different stages of the lifetime of the product is studied. In addition to the fact that LCA involves very extensive time-consuming studies that require data which may not be easily available, LCA results are usually given for an entire system making it not useful in estimating the embodied energy associated with a single device. In here, we consider the most significant factors in LCA: materials processing, manufacture and maintenance to estimate the total embodied energy of optical network devices in their life cycle. Using similar methods as in [184], the considered network devices are disassembled to their basic components and materials, and based on the data available about the embodied energy of these components and materials, we estimate the total embodied energy of the devices. According to [175] the embodied energy of most network devices is mainly composed of: Printed Circuit Board (PCB), semiconductor devices (silicon wafers, integrated circuitry), bulk materials (plastic, glass and rubber) and metal (aluminium, copper, steel, lead and zinc). Table 6-2 gives the embodied energy and the density of these materials in network devices. Because the embodied energy of materials

depends on the manufacturing processing and the same material may have different embodied energy under different processing approaches, firstly the maximum embodied energy of these materials is used, we then investigate the impact of varying the embodied energy per device (sensitivity analysis).

We consider the PCB maximum density (4.5 kg/m^2 [185]) to calculate the weight of PCBs in different network devices given their dimensions. We assume that the density of semiconductor devices on the different optical network components is equal to the density of semiconductor devices on the motherboard of a typical desktop PC. Considering a mATX motherboard with a size of 24.4 cm x 24.4 cm. The manufacturing of the electronics of a desktop PC requires about 2900 MJ, of which 2780 MJ is consumed by the wafer manufacturing/chip packaging [184]. This assumes that 90% of the energy consumed by the wafer manufacturing/chip packaging in a desktop PC is associated with the motherboard. Considering the motherboard to have 6 layers of PCB [185], the embodied energy of the PCB in the motherboard can be calculated. The embodied energy of semiconductors in the motherboard can be calculated as the difference between the embodied energies of the motherboard and the PCB. Therefore, the density of semiconductor devices on a desktop PC motherboard can be calculated as 400 g/m^2.

Materials/Processing	Embodied Energy (MJ/kg)	Density (g/m2)
Semiconductor device	120000 [175]	400 (on PCBs) [175],[186],[187]
Metals	100-400 [175]	Various
Bulk materials	20-400 [175]	Various
PCB	300-500 [175],[185]	2000-4500 [175],[185]

Table 6 - 2: The embodied energy and the density of the different metarials of network devices

Based on the densities in Table 6-2, the dimensions given by the manufacturers and the embodied energy values per unit weight in Table 6-2, the embodied energy of the different network devices and systems were calculated. In particular we have determined the embodied energy of Cisco 16-slot CRS-1 IP router [144], Cisco ONS 15454 10-Gbps multi-rate transponder card [146], Cisco ONS 15501 EDFA [188], Cisco OC-48/STM-16 bidirectional Regenerator [189], Cisco ONS 15454 100-GHz

4-CH Multi/Demultiplexer [190], Glimmerglass Intelligent Optical System 500 [191], and the GYTY53 optical cable [173].

The embodied energy of the solar cells used as the renewable energy sources in Chapter 4 is not considered, as these cells have energy paybacks of 1 to 4 years and life expectancies of 30 years [192], and the ratio $E_R/(E_R + E_E)$ is 87% to 97% over their lifetime, where E_R and E_E are the renewable energy generated and the embodied energy, respectively. The installation embodied energy of the different network devices is also not included in the embodied energy calculations.

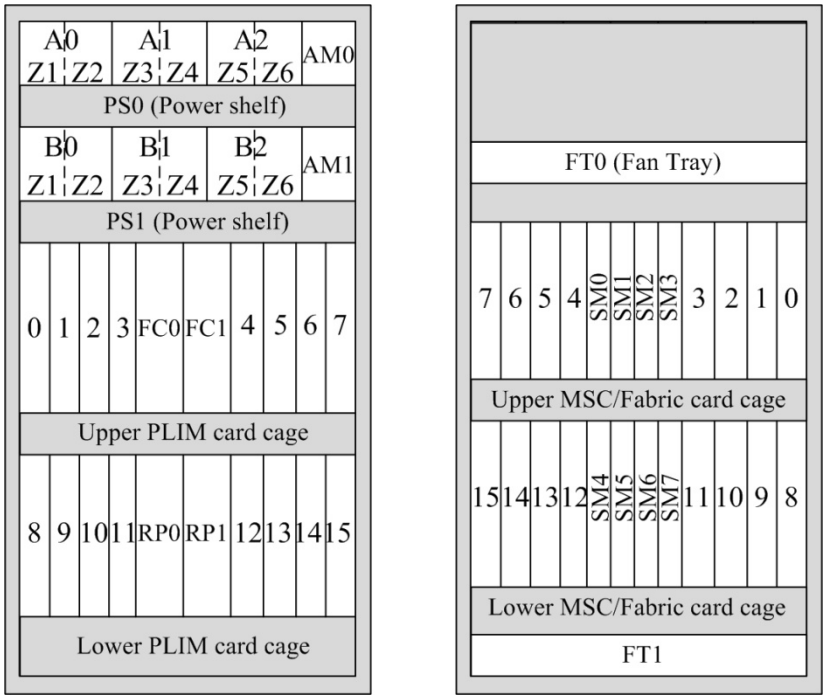

Fig 6 - 17: The structure of CRS-1 16 slots chassis routing system [193]

Considering the Cisco CRS-1 16 Slots Chassis Routing System [193] (795 kg), shown in Fig 6-17. Each IP port is composed of two module cards: Physical Layer Interface Module card (PLIM) and Module Service Card (MSC). In addition to the IP ports, the router has different modules including: power module, Fan Controller (FC), Switch Module (SM) and Router Processor (RP). Given the size of the module cards, we can calculate the weight of PCB and semiconductor devices in each module card. The chassis weight is calculated as the difference between the router total weight and modules weight. Assuming that only 10% of the chassis weight is bulk materials and the remaining is metal. The details of the embodied energy of each module are given in Table 6-3.

Similar to the IP router, we estimate the embodied energy of the Cisco ONS 15454 10-Gbps multi-rate transponder card [146], Cisco ONS 15501 EDFA [188], Cisco ONS 15104 OC-48/STM-16 bidirectional regenerator [189] and CiscoONS 15454 100-GHz 4-CH Multi/Demultiplexer [190]. The details are given in Table 6-4. Note that all the estimations above are subject to uncertainties in terms of the embodied energy of materials and the amount of materials in devices. Variations in data are considered to be ±30 % for bulk materials and semiconductor, ±21% for PCB [176].

CRS-1 16 Slots Chassis Routing System									
Module		Dimension (cm)	Weight (kg)	Embodied energy (MJ)				Units	Total (GJ)
				PCB	Semiconductor	Bulk Materials	Metals		
IP Port	PLIM	H52.3, D47.2, W4.6	3.8	555	9480	144	900	16	177.3
	MSC	H52.3, D47.2, W4.6	6.68	555	8280	200	2000	16	176.6
Power		H50,D46,W90 (estimate)	35	980	1440	1300	11900	1	15.6
RP		H52.3, D28.4, W7.1	5.8	335	7080	228	1800	2	18.9
FC		H52.2, D28.5, W7.1	5.6	223	4920	224	1820	2	14.4
SM		H52.3, D28.5, W3.6	5.4	335	6960	182	1690	8	73.3
Fan Tray		N/A	20	0	0	0	8000	2	16
System Chassis		N/A	486	0	0	19440	174960	1	194.4
Total embodied energy of a full load CRS-1 16 Slots Chassis Routing System									686.5

Table 6 - 3: The embodied energy of CRS-1 16 slots chassis routing system

Device	Dimension (cm)	Weight (kg)	Embodied energy (MJ)				Total (GJ)
			PCB	Semiconductor	Bulk Materials	Metals	
Transponder	H32.1, D22.8, W2.3	1.4	164	3480	40	380	4.1
EDFA	H4.5, D25.9, W48.3	3.08	135	3393	224	899	4.7
Regenerator	H4.4, D30, W43.9	4.4	197	4425	320	1100	6
Multi /Demultiplexer	H32.1, D22.8, W2.3	1.5 (estimated)	64	2446	225	414	3.2

Table 6 - 4: The embodied energy of the network devices

Materials/Processing	Embodied Energy (MJ)	Weight (g)	Total Embodied Energy (MJ)
SCS processing	30.3	0.253	11000
Semiconductor device	4116	34.3	
Metals	5440	13600	
Bulk materials	1200 (Estimated)	3000	
PCB	220.5 (Estimated)	490	

Table 6 - 5: The embodied energy of the 192×192 Glimmerglass optical switch

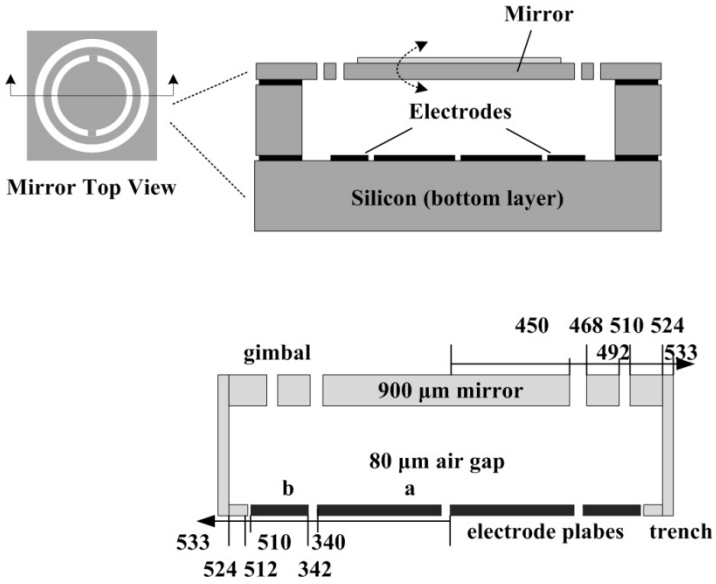

Fig 6 - 18: Schematic cross-section of a MEMS mirror with design dimensions [194]

The Glimmerglass Intelligent Optical System 500 - 192 × 192 optical switch is considered, (17.2 kg, 35.6×43.7×41.0 cm^3) [191]. The Glimmerglass optical switch is based on MEMS mirrors. A single MEMS mirror is made of single-crystal silicon (SCS) with a gold plated layer (3µm thickness) [195]. Fig 6-18 gives the structure of the MEMS mirror. The main contributor to the embodied energy of the MEMS mirror is the SCS processing. Given that the diameter of a single mirror is 900 µm, the total weight of gold used in the Glimmerglass optical switch (192 MEMS mirrors) is less than 0.5 g which can be neglected. As semiconductors are based on SCS, we assume that the SCS embodied energy is equal to that of semiconductor devices (120 GJ/kg). Table 6-5 gives the details of the embodied energy of the 192 × 192 Glimmerglass optical switch. Given the density of silicon (2.3 g/cm^3) and the single MEMS mirror chip size (1.55×1.7×0.5 mm^3) [194], the embodied energies of SCS processing, semiconductor device and metals are calculated. The embodied energies of bulk material and PCB are estimated.

The GYTY53 optical cable [173] is considered for the analysis of the embodied energy of optical fibre cables. Fig 6-19 gives the structure of the GYTY53 optical cable and Table 6-6 gives the embodied energy of its different materials [196]. The strength member in the centre of the cable is considered to be made of steel, the loose tubes to be made of Polybutylene Terephthalate (PBT) [197], and the filling compound to be made of a mixture of different polymers [173]. Given the cable

weight and diameter as 250kg/km and 15.7mm, respectively and the diameter of the fibre as 125 µm, we estimate the thickness and diameter of the different components in Fig 6-19. Table 6-7 gives the details of the embodied energy per km of the GYTY53 optical cable. Given the distances between nodes, the embodied energy of optical fibre cable will be the main contributor to the network embodied energy compared to the other devices.

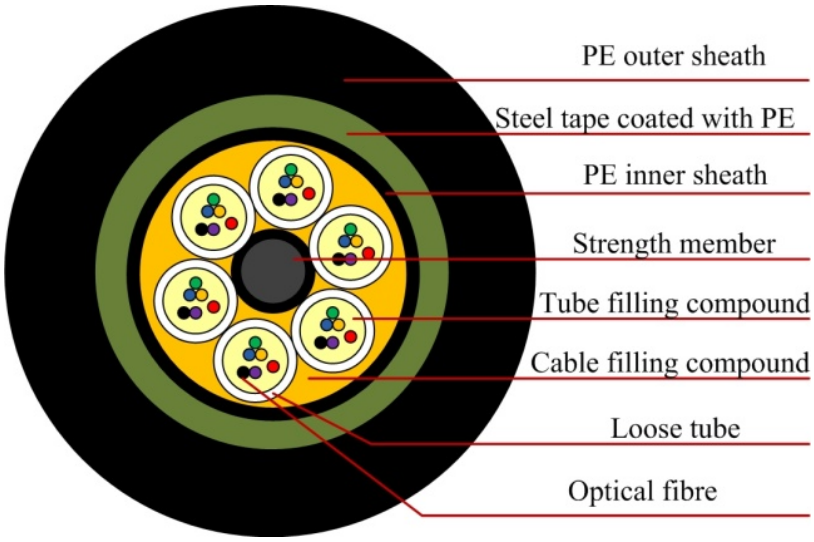

Fig 6 - 19: Structure of the GYTY53 optical cable [173]

Material	Embodied energy	Density kg/m3
PE	80.8 MJ/kg [198]	1000 kg/m3 [198]
Steel	32 MJ/kg [198]	7900 kg/m3 [199]
Glass	71.3 MJ/kg [198]	2550 kg/m3 [200]
PBT (for loose tube)	89.1 MJ/kg [197]	1310 kg/m3 [196]
Polymers (for filling compound)	100 MJ/kg (average) [198]	various

Table 6 - 6: The embodied energy of the different materials of the GYTY53 optical cable

Component	Material	Thickness or Diameter (estimation)	Weight kg/km	Embodied energy MJ/km
PE outer sheath	PE	3mm	122.46 (analysis)	9907
Steel tape	steel	0.5 mm	37.5 (analysis)	1200 MJ/km
PE inner sheath	PE	1 mm	25.12 (analysis)	2302 MJ/km
Strength member	steel	2 mm	24.8 (analysis)	793 MJ/km
Fibers	glass	125 µm	1.73 (analysis)	123 MJ/km
Loose tube (6 items)	PBT	1 mm	25.2 (estimated)	2245 MJ/km
Filling compound	Polymers	--	14.9 (estimated)	1490 MJ/km
Total embodied energy			18059 MJ/km	

Table 6 - 7: The embodied energy per km of the GYTY53 optical cable

6.3.2 Mathematical Model

A MILP model has been developed for the physical topology optimisation where we consider a scenario where the node locations are given (for example city locations) and the objective is to optimise the deployment of the physical links connecting these nodes so that the network operational and embodied energy consumption are minimised. The model considers the commercial lifetime of the network devices to compare the embodied energy with the operational energy. Note that the commercial lifetime is usually substantially shorter than the technical lifetime as devices may be replaced before the end of their lifetimes due to the emergence of new technologies. The average commercial lifetime of network devices (LT) is currently estimated to be 10 years [175], and the maintenance is considered to consume 10% of the device production embodied energy annually [175]. In addition to the parametres of the MILP model which is presented in Section 6.2.1, we define the new parametres EBF, EBR, EBT, EBG, EBO, EBE and EBM as the embodied energy of the optical Finbre cable, IP Router, Transponder, reGenerator, Optical switch, EDFA and Multi/demultiplexer. From equation (6-6), the total operational power consumption is:

$$
\begin{aligned}
&Operational\_Power \\
&= \sum_{t \in T} \Bigg(\sum_{i \in N} \sum_{j \in N: i \neq j} PR \cdot C_{ijt} + \sum_{m \in N} \sum_{n \in N: m \neq n} PT \cdot \omega_{mnt} \\
&+ \sum_{m \in N} \sum_{n \in N: m \neq n} \left(PE \cdot EA_{mn} \cdot f_{mn} + PG \cdot EG_{mn} \cdot f_{mn} \right) + \sum_{i \in N} PO_i \\
&+ \sum_{i \in N} PMD \cdot DM_i \Bigg)
\end{aligned}
\tag{6-27}
$$

The total production embodied energy,E_{EMB-P}, of the network under the bypass approach is given as follows:

$$E_{EMB-P} = \sum_{m\in N}\sum_{n\in N:m\neq n} EBF \cdot L_{mn} \cdot link_{mn} + \sum_{i\in N}\sum_{j\in N:i\neq j} EBR \cdot C_{ijt} + \sum_{m\in N}\sum_{n\in N:m\neq n} EBT \cdot \omega_{mnt} + \sum_{m\in N}\sum_{n\in N:m\neq n}\left(EBE \cdot EA_{mn} \cdot f_{mn} + EBG \cdot EG_{mn} \cdot f_{mn}\right) + \sum_{i\in N} EBO \cdot PO_i + \sum_{i\in N} EBM \cdot DM_i \quad (6\text{-}28)$$

where $t = T_{max}$. The number of devices in the network is based on the maximum traffic demand, therefore T_{max} is the time of a day where the traffic demand is maximum. Therefore, the new objective function can be wirtten as:

$$Operational\_Power \times LT + E_{EMB-P} \quad (6\text{-}29)$$

$$+0.1 \times E_{EMB-P} \times LT$$

The model also can be extended to represent the non-bypass approach by redefining the operational power consumption of router ports at time *t* as:

$$\sum_{m\in N}\sum_{n\in N:m\neq n} PR \cdot \omega_{mnt} \quad (6\text{-}30)$$

and redefining the embodied energy of router ports as:

$$\sum_{i\in N}\sum_{j\in N:i\neq j} EBR \cdot \omega_{mnt} \quad (6\text{-}31)$$

6.3.3 Simulation and Results

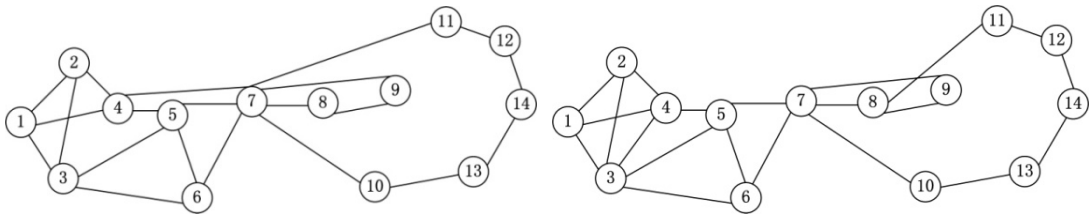

(a) Symmetric traffic, non-bypass (b) Symmetric traffic, bypass

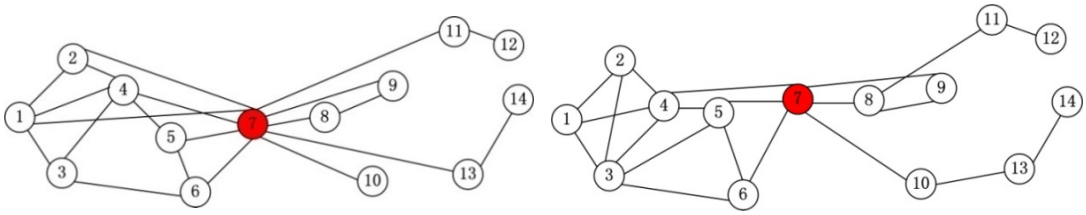

(c) Asymmetric traffic, non-bypass (d) Asymmetric traffic, bypass

Fig 6 - 20: Optimised physical topologies considering operational and embodied energies under symmetric traffic demand and asymmetric traffic demand (Data centre at node 7)

The same NSFNET topology and simulation environment parametres in Section 6.2.2 are used in here. Fig 6-20 shows the optimised physical topologies considering both the operational and embodied energies under symmetric and asymmetric (node 7 as a data centre) traffic demands. Compared to the operational-power-minimised topologies, considering both energies has resulted in topologies with shorter links. This is due to the large embodied energy of the optical fibre cable compared to the operational and embodied energies of other network devices. Note that optimising the physical topology without a constraint on the number of links has resulted in a topology of 14 links.

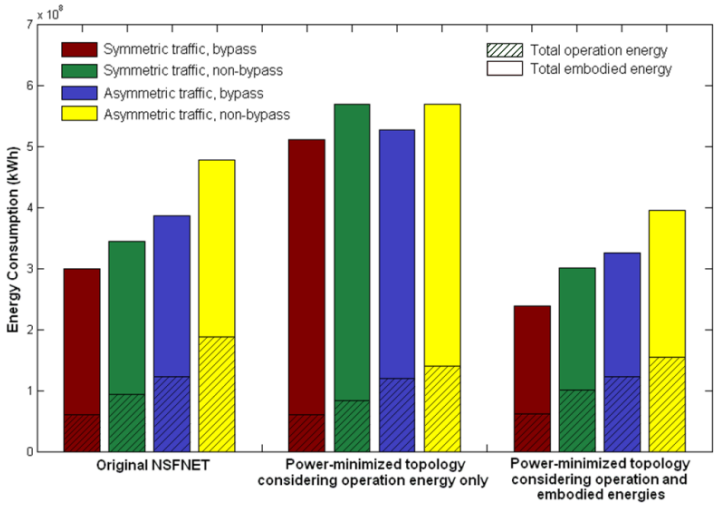

Fig 6 - 21: The operational and embiodied energy consumption of different NSFNET physical topologies over the network lifetime (Ndgr=1)

Fig 6-21 shows the total energy consumption (operational energy and embodied energy) of the original NSFNET topology and the optimised topologies over the network lifetime. For the different topologies the embodied energy is the major contributor to the total network energy consumption. This is due to the relatively low operational energy consumption of the network, and the relatively short commercial

lifetimes of network devices due to the technological advances. The embodied energy represents 80% and 73% of the total energy consumption of the original NSFNET topology under the symmetric traffic demand for the bypass approach and the non-bypass approach, respectively. These percentages decrease to 68% and 61% under asymmetric traffic.

Although optimising the physical topology considering the operational energy only under the non-bypass approach and symmetric traffic has resulted in operational energy savings of 12%, the embodied energy has significantly increased by 93% as a result of deploying longer fibre links, resulting in an increase of 65% in the total energy consumption. Optimising the physical topology considering both the operational and embodied energies has increased the operational energy by 7% and 20% under the non-bypass approach compared to the original NSFNET topology and the operational-power-optimised topology, respectively. The operational energy has increased as the optimised topology tries to minimise the number of devices used. For example in order to minimise the embodied and operational energies the MILP may employ fewer routers, but with a larger number of line cards (larger than the sum of the cards used in the separate routers prior to optimisation). This increases the operational energy, reduces the embodied energy and reduces the overall energy. Therefore, significant embodied energy savings of 20% and 59% are achieved compared to the original NSFNET topology and the operational-power-optimised topology, respectively resulting in a total energy saving of 47% and 13%.

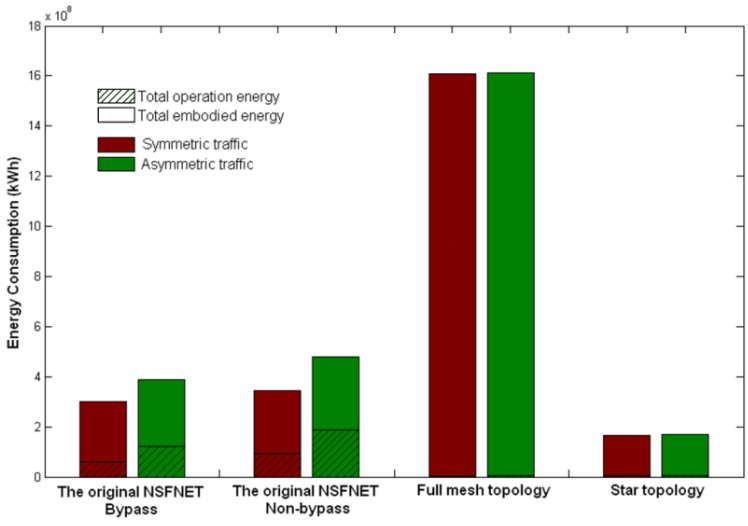

Fig 6 - 22: The operational and embiodied energy consumption of of the full mesh and star topologies

Compared to the original NSFNET topology, the full mesh has significantly decreased the operational power consumption by 95% (Section 6.2). Another topology that eliminates the need for IP routers is the star topology. The star topology saves 92% of the operational power consumption compared to the original NSFNET topology under a symmetric traffic demand (Section 6.2). Fig 6-22 shows the total energy consumption of the full mesh and star topologies. As the optical cable is the main contributor to the network embodied energy, deploying the full mesh has resulted in a huge increase in the embodied energy (more than 500% compared to the original NSFNET topology) diminishing the 95% operational energy savings. In addition to the operational energy savings (92%) (Section 6.2), the star topology has saved 31% of the embodied energy resulting in a total saving of 44%.

As mentioned previously the network devices embodied energy estimations are subject to uncertainties in terms of the embodied energy of materials and the amount of material in devices. Furthermore technological advances the embodied energy of optical cables is anticipated. Fig 6-23 and Fig 6-24 investigate the variations in the physical topology and the energy consumption as the embodied energy of network devices changes. We examine 20%, 60% and 80% reduction in embodied energy.

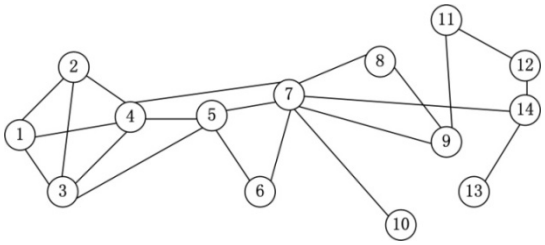

(a) Symmetric traffic, non-bypass 20% reduction

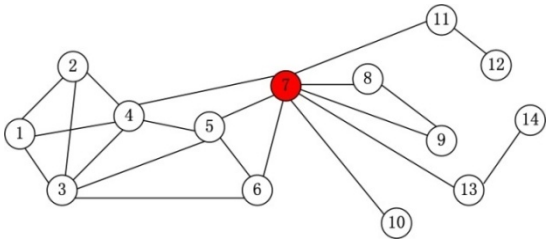

(b) Asymmetric traffic, non-bypass 20% reduction (Data centre at node 7)

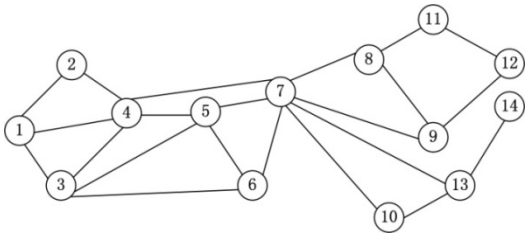

(c) Symmetric traffic, non-bypass 60% reduction

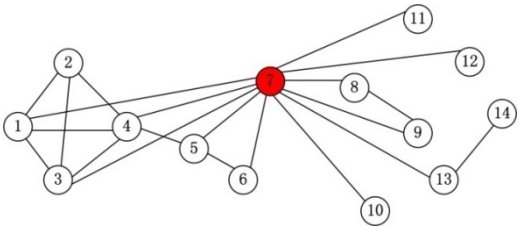

(d) Asymmetric traffic, non-bypass 60% reduction (Data centre at node 7)

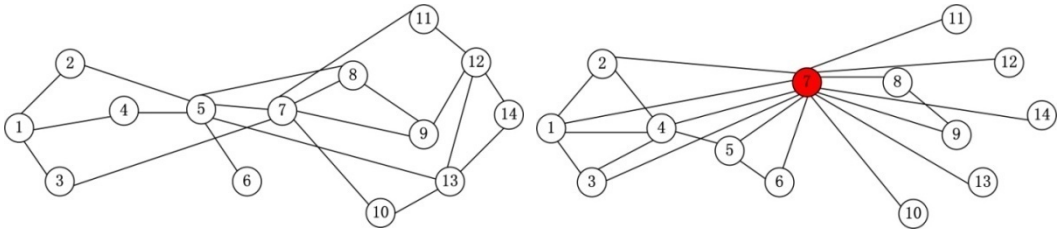

(c) Symmetric traffic, non-bypass 80% reduction

(d) Asymmetric traffic, non-bypass 80% reduction (Data centre at node 7)

Fig 6 - 23: Optimised physical topologies for different embodied energy reduction degrees of optical network devices

Fig 6-23 shows the physical topologies associated with different embodied energy reduction degrees with non-bypass scenario under symmetric and asymmetric traffic respectively. It can be observed that as the embodied energy of the network devices is reduced, longer links are deployed in the optimised physical topologies. This is because the proportion attributed to the embodied energy in the total energy consumption of the network is reduced and the operational energy impact on the final optimised physical topology increases. However, compared with operation energy of network, the major contribution to the total energy consumption saving of the network comes from the embodied energy, even in the case when only 20% of the initial estimate value for the embodied energy is taken into account.

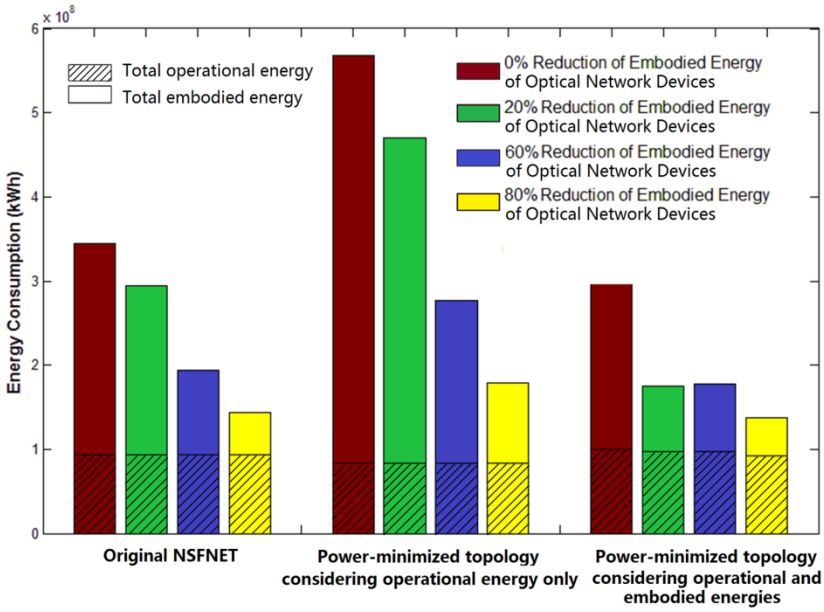

(a) Symmetric traffic

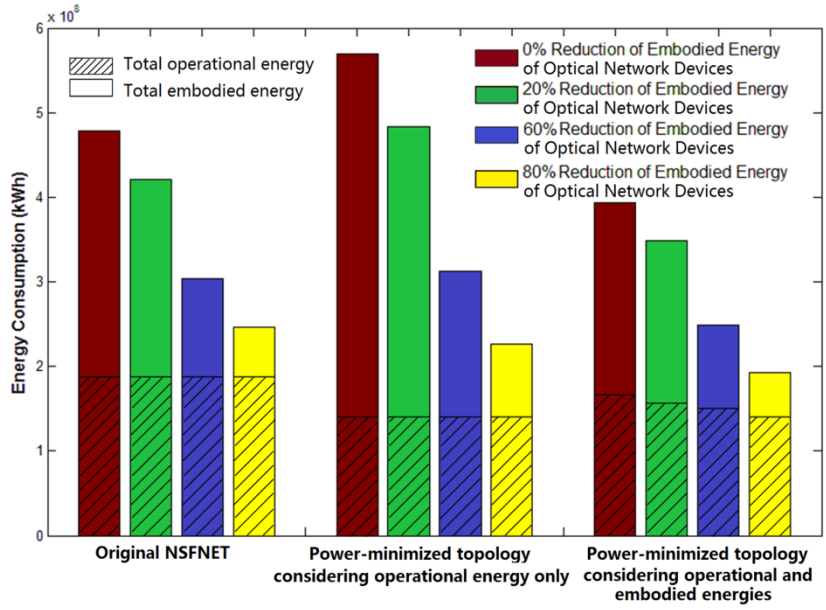

(b) Asymmetric traffic

Fig 6 - 24: operation and embodied energy of the network under non-bypass scenario with symmetric and asymmetric traffic with different reductions in the optical network devices' embodied energy

Fig 6-24 shows the operational and embodied energy of the optimised physical topology when the estimates of the value of the embodied energy of the devices is reduced to varying extents. It is particularly worth noting that under asymmetric traffic, when the reduction in the embodied energy of optical network devices reaches 80%, the operational energy of optimised physical topology considering both of embodied and operational energy is almost same as that of the optimised physical topology considering operational energy only.

The results above show that the embodied energy of the optical cable is the main factor in designing energy-efficient physical topologies. Note that other optical cables may have higher embodied energy than the GYTY53 optical cable considered. However, with technological advances the embodied energy of optical cables is anticipated to be reduced, making the embodied energy contribution of other network devices more significant. In the following we investigate energy-efficient topology design without considering the embodied energy of the optical cable to highlight the impact of the embodied energy of the other network devices. The topologies in Fig 6-25 show similar trends to the operational-power-optimised

topologies where a number of long links exist between the nodes at the two ends of the network.

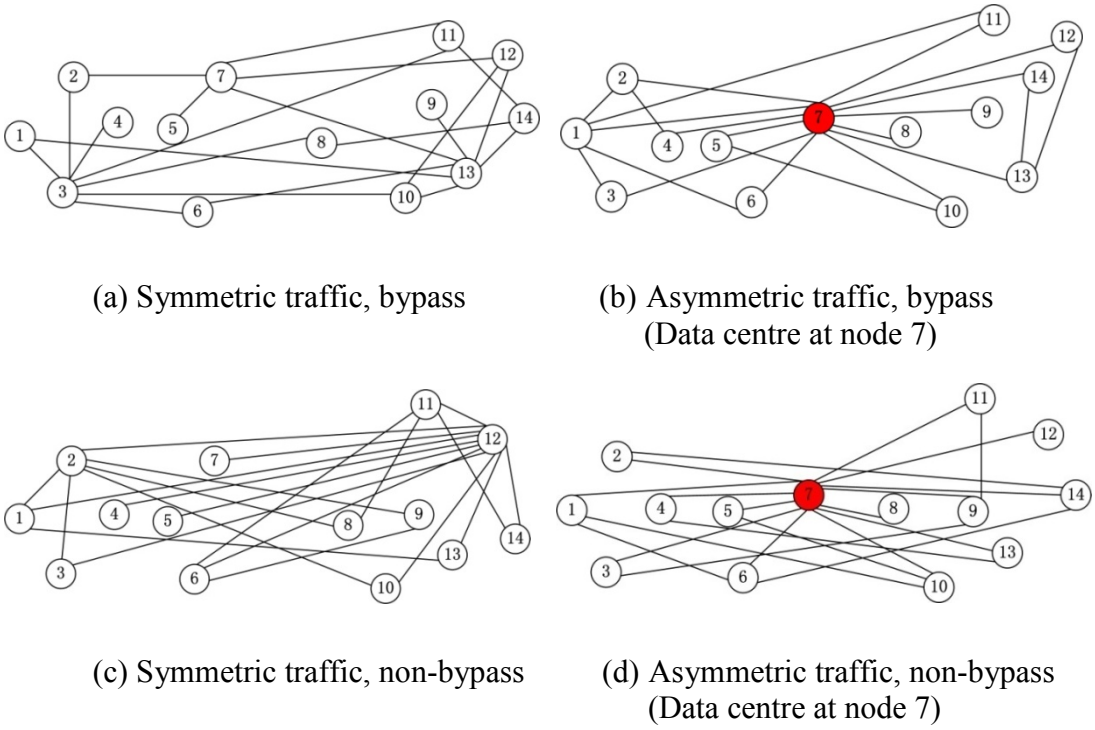

(a) Symmetric traffic, bypass

(b) Asymmetric traffic, bypass (Data centre at node 7)

(c) Symmetric traffic, non-bypass

(d) Asymmetric traffic, non-bypass (Data centre at node 7)

Fig 6 - 25: Optimised physical topologies without considering the embodied energy of the optical cables

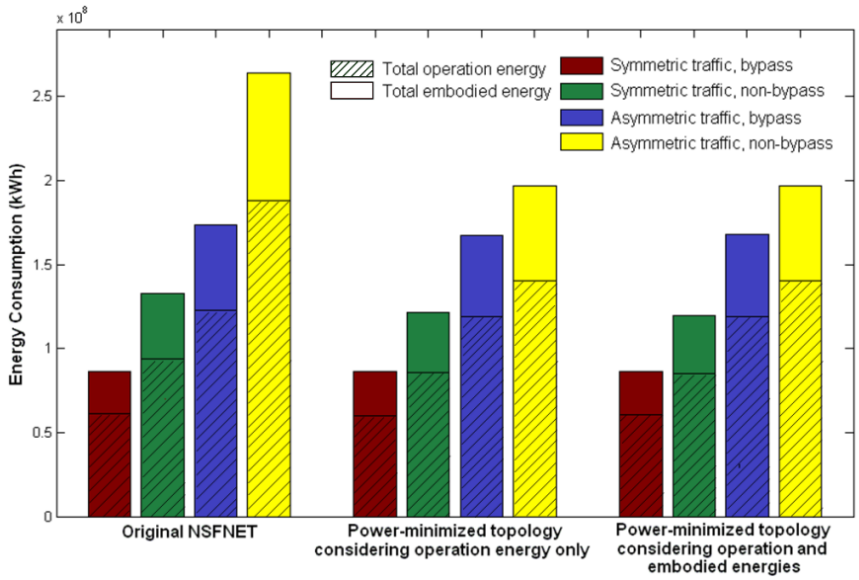

Fig 6 - 26: The total operational energy and embodied energy (without the embodied energy of optical cable) of different NSFNET physical topologies over the network lifetime (Ndgr=1)

Fig 6-26 shows that the embodied energy of network devices not including the optical cable represents only 30% and 29% of the total energy consumption of the original NSFNET topology under symmetric traffic and the bypass approach and the non-bypass approach, respectively. These percentages decrease to 29% and 28% under asymmetric traffic. Compared with the original NSFNET, operational-power-optimised topologies under symmetric traffic and the non-bypass approach have saved 12% of the total energy consumption (here 28% of the total energy is contributed by embodied energy (without optical cable)). Optimising the physical topology considering the operational and embodied energies of other network devices not including the optical cable has resulted in a very limited energy saving (less than 1%), compared to optimising with respect to operational energy only.

6.4 Summary

Firstly, in this chapter, the power savings obtained by optimising the physical topology of IP over WDM networks using a MILP model have been investigated. The NSFNET network has been considered and its original topology was compared with power-optimised topologies considering different IP over WDM approaches (bypass and non-bypass) and nodal degree constraints (*Ndgr*=1 and *Ndgr*=2). The physical topology has been optimised under a symmetric full-mesh connectivity traffic matrix considering a limited number of links. The optimised topologies resulted in limited power savings of 10%. It has been shown that optimising the physical topology without a limit on the number of links results in a full mesh topology. The full-mesh topology has resulted in significant power savings of 95% compared to the original NSFNET topology as it promotes switching and transmission instead of IP routing. Another topology that eliminates IP routing is the star topology with power savings of 92%. However, the two topologies have limitations due to the large number of links in the full mesh and the single point failure of the star topology. These limitations have to be taken into account and future work can consider placing a constraint on the maximum number of links (to reduce the links compared to full mesh) and a constraint on the formation of single stars. In addition, physical topology optimisation has been studied under asymmetric

traffic demands where data centres create a hot node scenario. The results show that physical topology (and virtual topology) optimisation become important if there are dominant or larger users which is almost always the case as cities vary in size. The single data centre case resulted in 22% power saving (instead of 10% for symmetric traffic) even without an increase in the number of physical links. The optimisation of the physical topology taking into account the presence of renewable energy sources in the network has also been investigated. The results show that physical topology optimisation increases the utilisation of the renewable energy sources. Compared to the original NSF topology, the optimised topologies have resulted in average power savings up to 10%. The power savings obtained from the optimised topologies under different scenarios come at the cost of an increase in the propagation delay, however this increase can be ignored compared to the total network delay. The cost of the network components has been evaluated when designing the physical topology. The results show that optimising the physical topology with respect to power consumption does not result in significant increase in the total network cost under symmetric traffic, however, under asymmetric traffic the cost of the power optimised topologies even decreases. It has been shown through analysing the characteristics of the different topologies that physical topology optimisation can be viewed in many cases as a design process whose goal is to minimise the average hop count. The optimisation results also show that nodes "connect themselves to well connected nodes" a parallel with social networks.

Secondly, the energy savings gained by optimising the physical topology of IP over WDM networks considering both the operational and embodied energies has been investigated. The analysis of the embodied energy of network devices shows that the embodied energy accounts for up to 80% of the total energy consumption of the IP over WDM network over the network commercial lifetime. Considering both the operational and embodied energies in the physical topology optimisation has resulted in topologies with shorter links as the embodied energy of the optical fibre cable is the main contributor to the network total energy. The operational energy of these topologies has increased by up to 20% compared to the operational-power-optimised topologies, however significant embodied energy savings of up to 59% are achieved, resulting in a total energy saving of 47%. With technological advances the embodied energy of optical devices is anticipated to be reduced. However the

optimised topologies have barely changed that except longer links are employed. Without considering the embodied energy of optical cables the results show that the embodied energy of the other devices has a limited effect on the physical topology optimisation.

In the previous chapters, the optimisation of energy efficient optical networks was only concentrated on minimising the power consumption. However, propagation delay and electricity cost are also important. In the next chapter, we will jointly optimise all the above mentioned factors and investigate the associated trade-offs.

Chapter 7: Joint Optimisation of Power, Delay and Electricity Cost in IP over WDM Networks

7.1 Introduction

Given the ecological and economic drivers, significant research efforts are increasingly being focused on reducing the energy consumption of ICT networks. In addition, some researchers are concentrating on reducing the cost and delay of networks. For examples, in [201], the authors investigated the benefit of making use of the electricity price difference between time intervals of the day for networks covering different time-zones and showed that up to 13 % savings in the electricity bill can be achieved compared to conventional routing. In [202] an end-to-end delay problem in overlay networks is investigated for multicast services by using a Tabu search heuristic. In [203], the authors proposed a new algorithm to minimise the maximum delay for individual flows while meeting demand requirements for multiple source-sink pairs.

In the previous chapters, the optimisation of renewable energy utilisation, data centre locations and physical topology for energy efficient IP over WDM networks were investigated individually. However, to the best of our knowledge, no work in the literature has considered jointly minimising energy, electricity cost and propagation delay. In this chapter, we investigate the impact of optimising each of the three parameters individually on the others and show how jointly minimising them compares to individual minimisation.

7.2 Optimisation of Power, Delay and Electronic Cost under a Unicasting Scenario

7.2.1 Mathematical Model

In this section, we build a MILP model to jointly minimise the non-renewable power consumption, electricity cost and delay in hybrid-power IP over WDM networks under a unicasting scenario. With similar assumption to those in Chapter 4 where we assumed that the renewable energy is available to power IP router ports and transponder in a limited number of nodes in the networks. We also assume that the nodes that have access to renewable energy can also be powered by non-renewable energy to guarantee QoS when the renewable energy output becomes low.

To keep the model linear, the delay is represented as a function of the length of the lightpaths the traffic demands travel through instead of the length of the physical links. Therefore, the traffic demands are not allowed to split.

The model defines the following parameters:

T	Set of time points,
N	Set of nodes,
Np_i	The set of neighbour nodes of node *i* in the optical layer,
i and j	Denote end points of a virtual link in the IP layer,
s and d	Denote source and destination of a traffic demand,
m and n	Denote end points of a physical link in the optical layer,
α	The weight of the non-renewable power consumption in the objective function,
β	The weight of electricity cost in the objective function,
γ	The weight of the propagation delay in the objective function,
L_{mn}	The length of the link between nodes *m* and *n,*

S Distance between neighbouring EDFAs ,

W The number of wavelengths in a fibre,

B The capacity of a wavelength,

λ^{sdt} Traffic demand between source *s* and destination *d* at time *t,*

EA_{mn} The number of EDFAs on physical link (*m, n*). Typically $EA_{mn} = \lfloor L_{mn}/S - 1 \rfloor + 2$, where S is the distance between two neighbouring EDFAs,

PR Power consumption of a router port,

PT Power consumption of a transponder,

PE Power consumption of an EDFA,

PS_{it} The maximum output power of the renewable energy source in node *i* at time *t*,

$Price_{it}$ The price of electricity in node *i* at time *t.*

The following variables are also defined:

C_{ijt} The number of wavelength channels in the virtual link (*i, j*) at time *t* in the IP layer which use non-renewable energy,

Cs_{ijt} The number of wavelength channels in the virtual link (*i, j*) at time *t* in the IP layer which use renewable energy,

ω_{mnt} The number of wavelength channels on physical link (*m, n*) at time *t* in the optical layer which use non-renewable energy,

ωs_{mnt} The number of wavelength channels on physical link (*m, n*) at time *t* in the optical layer which use renewable energy,

W_{mnt}^{ij} The number of wavelength channels in the virtual link (*i, j*) that traverse physical link (*m, n*) at time *t,*

λ_{ijt}^{sd} λ_{ijt}^{sd}=1 if traffic flow from node *s* to node *d* traverses the virtual link (*i, j*) at time *t*, otherwise λ_{ijt}^{sd}=0,

f_{mn} The number of fibres on physical link (*m,n*).

As mentioned above the MILP model objective function jointly minimises the non-renewable power consumption, electricity cost and delay. Under the lightpath bypass approach, these parameters are defined as:

1) The non-renewable power consumption of the network at time *t* (NRE_t):

$$NRP_t = \sum_{i\in N}\sum_{j\in N:i\neq j} PR \cdot C_{ijt} + \sum_{m\in N}\sum_{n\in Np_m} PT \cdot \omega_{mnt} + \sum_{m\in N}\sum_{n\in Np_m} (PE \cdot EA_{mn} \cdot f_{mn}) \quad (7\text{-}1)$$

2) The electricity cost at time *t* (EC_t):

$$EC_t = \sum_{i\in N}\sum_{j\in N:i\neq j} Price_{it} \cdot PR \cdot C_{ijt} + \sum_{m\in N}\sum_{n\in Np_m} Price_{mt} \cdot PT \cdot \omega_{mnt} + \sum_{m\in N}\sum_{n\in Np_m} (Price_{mt} \cdot PE \cdot EA_{mn} \cdot f_{mn}) \quad (7\text{-}2)$$

3) The delay given as the total lightpath length of the network at time *t* (DL_t):

$$DL_t = \sum_{s\in N}\sum_{d\in N:s\neq d}\sum_{i\in N}\sum_{j\in N:i\neq j} \left(\lambda_{ijt}^{sd} \cdot L_{ij}\right) \quad (7\text{-}3)$$

The MILP model is defined as follows:

Objective: minimise

$$\alpha \cdot \sum_{t\in T} NRP_t + \beta \cdot \sum_{t\in T} EC_t + \gamma \cdot \sum_{t\in T} DL_t \quad (7\text{-}4)$$

We introduce the factors α, β and γ to scale the three parameters to reflect their importance in the design.

Subject to:

$$\sum_{j\in N:i\neq j}\lambda_{ijt}^{sd}-\sum_{j\in N:i\neq j}\lambda_{jit}^{sd}=\begin{cases}1 & if\ i=s\\ -1 & if\ i=d\\ 0 & otherwise\end{cases} \tag{7-5}$$

$$\forall\ t\in T,\forall\ s,d,i\in N: s\neq d,$$

$$\sum_{s\in N}\sum_{d\in N:s\neq d}(\lambda_{ijt}^{sd}\cdot\lambda^{sdt})\leq(C_{ijt}+Cs_{ijt})\cdot B \tag{7-6}$$

$$\forall\ t\in T,\forall\ i,j\in N: i\neq j,$$

$$\sum_{n\in Np_m}W_{mnt}^{ij}-\sum_{n\in Np_m}W_{nmt}^{ij}=\begin{cases}C_{ijt}+Cs_{ijt} & if\ m=i\\ -C_{ijt}-Cs_{ijt} & if\ m=j\\ 0 & otherwise\end{cases} \tag{7-7}$$

$$\forall\ t\in T,\forall\ i,j,m\in N: i\neq j,$$

$$\sum_{j\in N:i\neq j}PR\cdot Cs_{ijt}+\sum_{n\in Np_i}PT\cdot\omega s_{int}\leq PS_{it} \tag{7-8}$$

$$\forall\ t\in T,\forall\ i\in N,$$

$$\sum_{i\in N}\sum_{j\in N:i\neq j}W_{mnt}^{ij}\leq W\cdot f_{mn} \tag{7-9}$$

$$\forall\ t\in T,\forall\ m\in N,n\in Np_m,$$

$$\sum_{i\in N}\sum_{j\in N:i\neq j}W_{mnt}^{ij}=\omega_{mnt}+\omega s_{mnt} \tag{7-10}$$

$$\forall\ t\in T,\forall\ m\in N,n\in Np_m.$$

Constraint (7-5) represents the flow conservation constraint in the IP layer. It ensures that in all nodes the outgoing traffic is equal to the incoming traffic except for the source and the destination nodes. It also ensures that a traffic flow is transmitted through a single route (traffic flows are not allowed to split). Constraint (7-6) ensures that the summation of all traffic flows through a virtual link does not exceed its capacity. Constraint (7-7) represents the flow conservation constraint in the optical layer. It represents the fact that in all nodes the total outgoing

wavelengths of a virtual link should be equal to the total incoming wavelengths except for the source and the destination nodes of the virtual link. Constraint (7-8) ensures that at each node the renewable power consumption of router ports and transponders does not exceed the maximum output power of the renewable energy source. Constraints (7-9) and (7-10) represent the physical link capacity constraints. Constraint (7-9) ensures that the total number of wavelength channels in virtual links traversing a physical link does not exceeded the maximum capacity of fibres in the physical link. Constraint (7-10) ensures that the number of wavelength channels in virtual links traversing a physical link is equal to the number of wavelengths in that physical link.

The model can be extended to represent the non-bypass approach by redefining the non-renewable power consumption of IP ports at time *t* as follows:

$$\sum_{m \in N} \sum_{n \in Np_m} PR \cdot \omega_{mnt} \tag{7-11}$$

Therefore the network non-renewable power consumption at time *t* (equations (7-1)) and the electricity price at time *t* (equation (7-2)) become:

$$NRP_t = \sum_{m \in N} \sum_{n \in Np_m} PR \cdot \omega_{mnt} + \sum_{m \in N} \sum_{n \in Np_m} PT \cdot \omega_{mnt} + \sum_{m \in N} \sum_{n \in Np_m} (PE \cdot EA_{mn} \cdot f_{mn}) \tag{7-12}$$

$$EC_t = \sum_{m \in N} \sum_{n \in Np_m} Price_{mt} \cdot PR \cdot \omega_{mnt} + \sum_{m \in N} \sum_{n \in Np_m} Price_{mt} \cdot PT \cdot \omega_{mnt} + \sum_{m \in N} \sum_{n \in Np_m} (Price_{mt} \cdot PE \cdot EA_{mn} \cdot f_{mn}) \tag{7-13}$$

and the constraint (7-8) is replaced by:

$$\sum_{m \in N} \sum_{n \in Np_m} PR \cdot \omega s_{mnt} + \sum_{n \in Np_i} PT \cdot \omega s_{mnt} \leq PS_{mt} \quad \forall\ t \in T, \forall\ m \in N \tag{7-14}$$

7.2.2 Simulation and Results

The same NSFNET network topology as in Chapter 4, depicted in Fig 4-4, is considered as an example of a real world network to evaluate our proposed scenarios. The same average traffic demand as in Chapter 4, shown in Fig 4-5, is used here.

Similar to Chapter 4, solar energy is considered as the renewable energy source. We consider the maximum output power of solar energy to be 120 kW. A solar panel area of 375 m^2 [143] is needed to generate such a value. Due to the high cost of manufacturing and installing the solar panels, it is assumed that the solar energy is available only at 5 nodes. The optimal locations of these nodes are given as nodes 4, 5, 6, 7 and 9 using the work in Chapter 4. Fig 7-1 gives the output power of the solar energy source. Table 7-1 shows the input parameters in terms of number of wavelengths, wavelength capacity, distance between two neighbouring EDFAs, and the power consumption of different components in the network. The power consumption values are derived from Cisco 8-slot CRS-1 data sheets [193], Cisco ONS 15454 data sheets [146] and others are derived from Table 4-3 in Chapter 4.

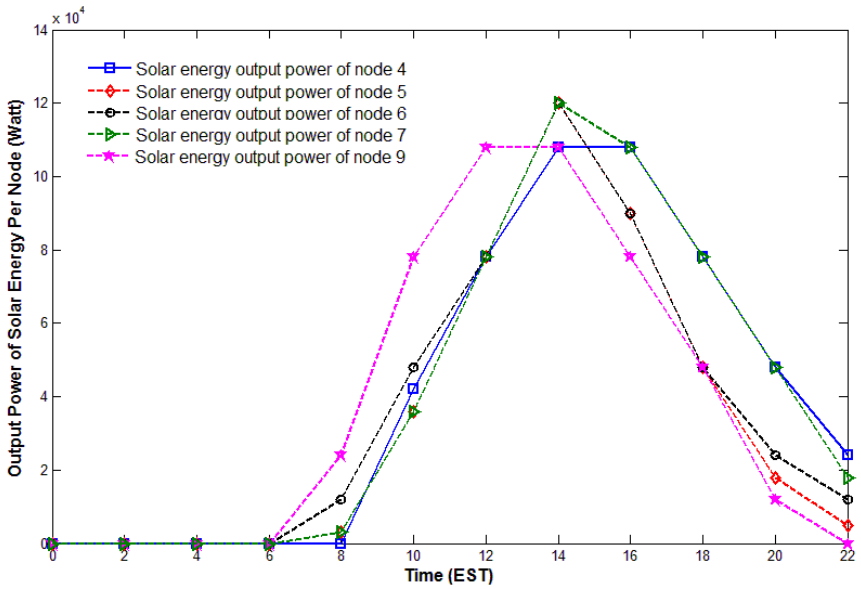

Fig 7 - 1: Output power of solar energy of different nodes in different time zones

Distance between two neighbouring EDFAs (*S*)	80 (km)
Capacity of each wavelength (*B*)	40 (Gbit/s)
Energy consumption of a router port (*PR*)	1000 (W)
Energy consumption of a transponder (*PT*)	73 (W)
Energy consumption of an EDFA (*PE*)	8 (W)

Table 7 - 1: Input parameters for MILP model

As in [201], the electricity price is considered to vary throughout the day. The day is divided into three tiers. In Tier 1 (22:00-6:00), the price is half of the base price, in Tier 2 (6:00-18:00), the price is the base price and in Tier 3 (18:00-22:00), the price is 1.75 times of the base price. The electricity price for different nodes of NSFNET is given in [204]. Table 7-2 gives the details of the electricity price of different node in NSFNET at different time of day.

Note that because of the high cost of solar panels, the cost of electricity produced by solar panels is considered to be relatively high (0.38 $/kWh [205]) compared to electricity from non-renewable sources. However, we do not consider this cost in the optimisation problem as we assume that the solar cells are already installed so using electricity produced by them will not create extra cost. An interesting extension of this work will be to consider the cost of electricity produced by renewable energy sources by optimising the number and location of nodes deploying renewable energy sources.

Node ID / Time	1	2	3	4	5	6	7	8	9	10	11	12	13	14
Tier 1	6.5	3.8	6.5	3.5	4.6	4.9	3.8	3.9	3.9	4.7	8.2	7.4	5.3	4.4
Tier 2	22.8	13.3	22.8	12.2	16	17	13.2	13.4	13.5	16.4	28.8	25.7	18.6	15.2
Tier 3	13	7.6	13	7	9.2	9.7	7.6	7.7	7.7	9.4	16.5	14.7	10.6	8.7

Table 7 - 2: Electricity price at different nodes of NSFNET at different times of the day (Cent/kWh)

To solve the MILP model, the AMPL/CPLEX software on a Core2 2.8 GHz PC with 4GB memory is used. In the following results, four optimisation scenarios are considered. The routing is optimised over IP over WDM networks to individually

minimise the non-renewable power consumption, electricity cost and delay by setting $(\alpha = 1,\ \beta = 0,\ \gamma = 0)$, $(\alpha = 0,\ \beta = 1, \gamma = 0)$ and delay $(\alpha = 0,\ \beta = 0,\ \gamma = 1)$, respectively. We compare the results of the individual optimisation scenarios with the case when we jointly optimise the three parameters. In this case the exact values used are $(\alpha = 1,\ \beta = 0.1\ Watt/\$, \gamma = 2\ Watt/second)$.

Fig 7-2, Fig 7-3 and Fig 7-4 give the non-renewable power consumption, electricity cost and propagation delay of the NSFNET network under the different optimisation scenarios considering the bypass approach. In Fig 7-2 and Fig 7-3, the non-renewable power consumption and electricity cost show similar trends for the different optimisation scenarios. Compared to optimising considering delay only, the other optimisation scenarios achieve power consumption and electricity cost savings up to 66% and 55%, respectively. In Fig 7-4, the non-renewable power-minimised and the electricity cost-minimised models have increased the average propagation delay by 7% compared to the delay-minimised model. However, the joint optimisation of the three parameters has limited the increase in the propagation delay to 2% while, as seen in Fig 7-2 and Fig 7-3, it has maintained the non-renewable power consumption and the electricity cost achieved by the power-minimised and the cost-minimised models, respectively.

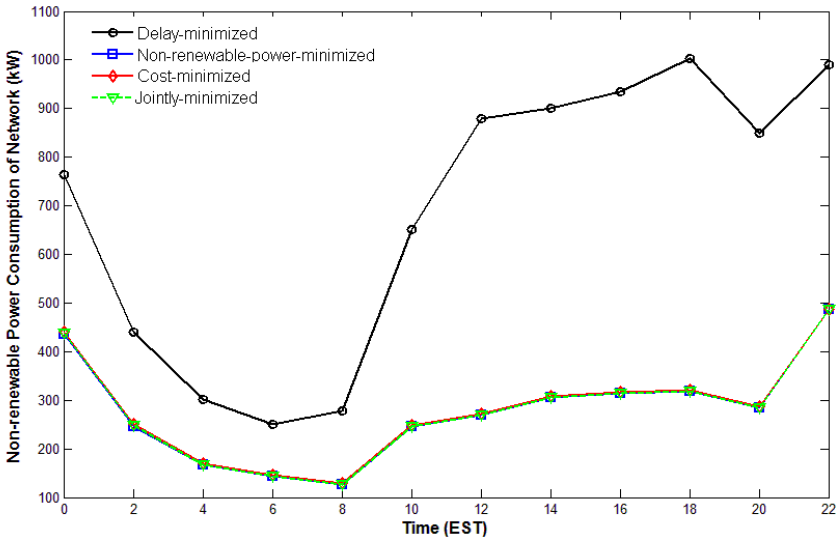

Fig 7 - 2: The non-renewable power consumption under different optimisation scenarios with the bypass approach

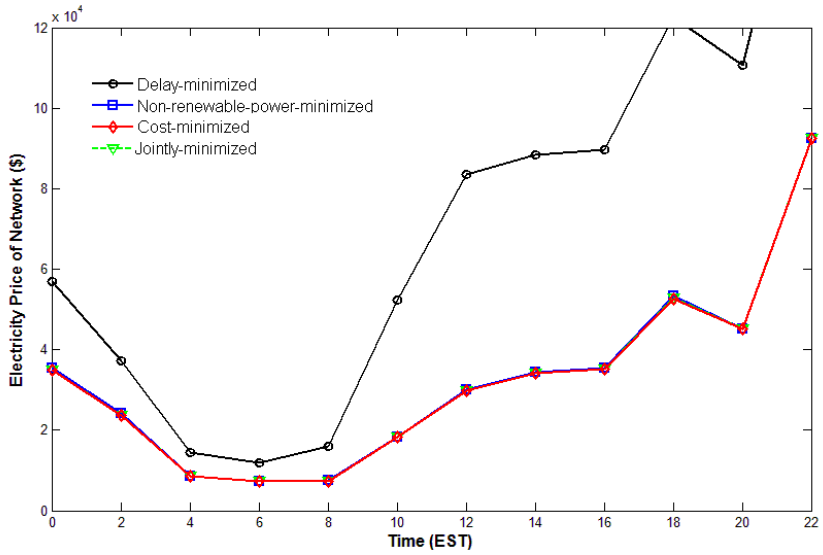

Fig 7 - 3: The electricity cost under different optimisation scenarios with bypass approach

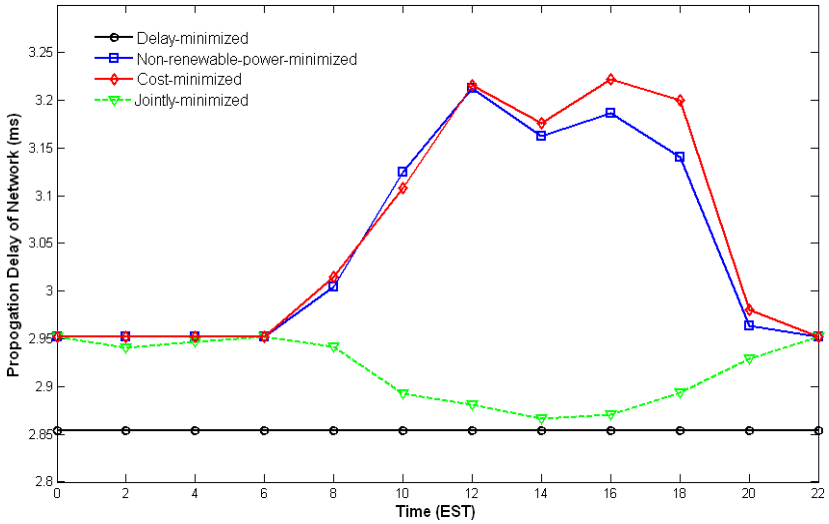

Fig 7 - 4: The propagation delay under different optimisation scenarios with the bypass approach

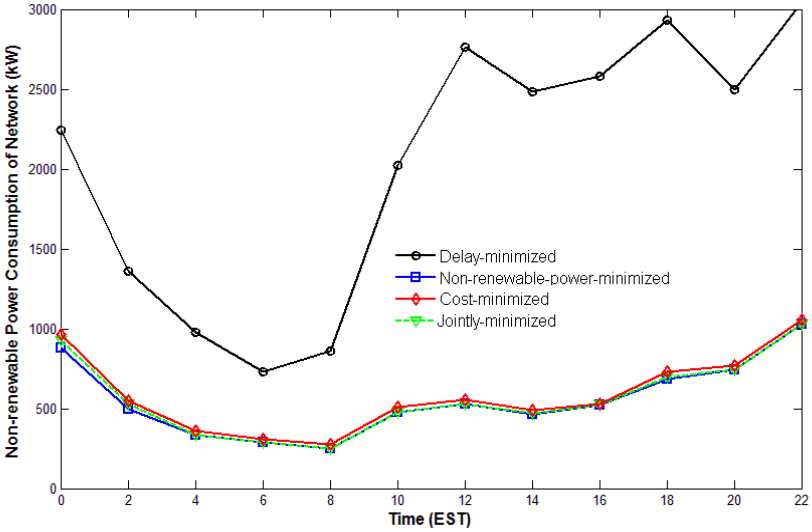

Fig 7 - 5: The non-renewable power consumption under different optimisation scenarios with the non-bypass approach

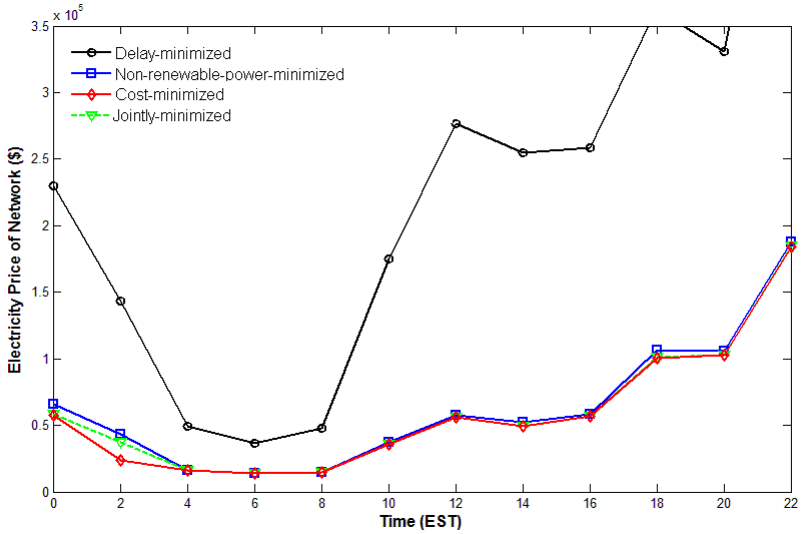

Fig 7 - 6: The electricity cost under different optimisation scenarios with the non-bypass approach

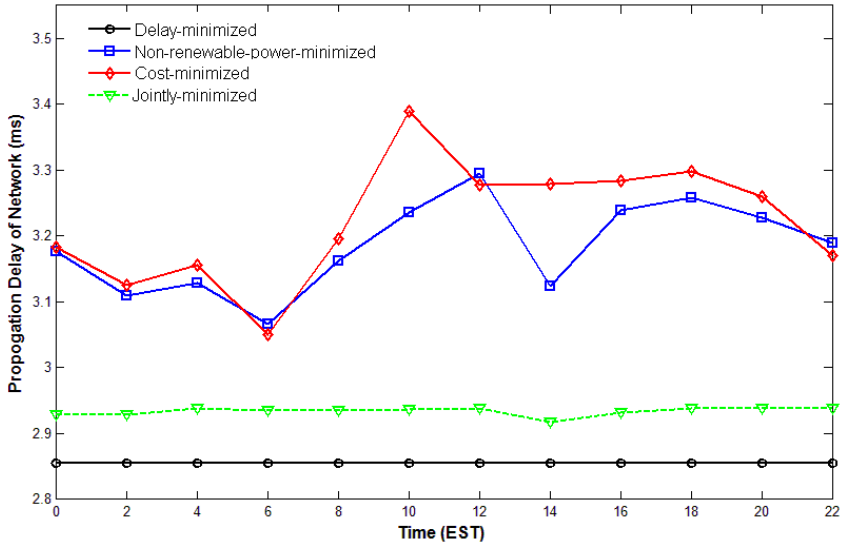

Fig 7 - 7: The propagation delay under different optimisation scenarios with the non- bypass approach

Fig 7-5, Fig 7-6 and Fig 7-7 give the results under the different optimisation scenarios considering the non-bypass approach. Similar trends to those of Fig 7-2 ~ Fig 7-4 are observed. Compared to the delay-minimised model the power consumption and electricity cost savings achieved by the joint optimisation increase to 73% and 74% respectively while hardly affecting the delay.

7.3 Optimisation of Power, Delay and Electricity Cost under an Anycasting Scenario

7.3.1 Mathematical Model

The above results are obtained under a unicasting traffic scenario. In the following results we investigate the savings achieved by jointly minimising the three parameters under an anycasting scenario where a number of data centres with replicated content exist in the network and nodes can download data from any of them. We extend the MILP model in Section 7.2.1 to support an anycasting scenario. In addition to the parameters in Section 7.2.1, the following parameters are introduced:

NN Set of regular node,

D Set of data centre.

In addition to the variables in Section 7.2.1, we define the following variable:

σ^{ksgt} $\sigma^{kst} = 1$ if regular node *s* downloads data from data centre k instead of data centre g at time *t,* otherwise $\sigma^{ksgt} = 0$,

and the variable λ_{ijt}^{sd} in Section 7.2.1 is replaced by:

λ_{ijt}^{ksg} $\lambda_{ijt}^{ksg} = 1$ if regular node *s* downloads data from data centre k instead of data centre g and traverses the virtual link (*i, j*) at time *t*, otherwise $\lambda_{ijt}^{ksg} = 0$.

The extended model has the same objective function and constraints as the model in Section 7.2.1 except that the constraint (7-5) is replaced by:

$$\sum_{j \in N: i \neq j} \lambda_{ijt}^{ksg} - \sum_{j \in N: i \neq j} \lambda_{jit}^{ksg} = \begin{cases} \sigma^{ksgt} & if\ i = k \\ -\sigma^{ksgt} & if\ i = s \\ 0 & otherwise \end{cases} \quad (7\text{-}15)$$

$$\forall\ t \in T, \forall\ s \in NN, k, g \in D$$

and a new constraint is added:

$$\sum_{k \in D} \sigma^{ksgt} = 1 \qquad (7\text{-}16)$$

$$\forall\ t \in T, \forall\ s \in NN, g \in D$$

Constraint (7-16) implies that a regular node can only download from one data centre.

7.3.2 Simulation and Results

We consider the same NSFNET network in Section 7.2.2 to evaluate the optimisation problem under the anycasting traffic profile. Only the download traffic between regular nodes and data centre nodes is considered. The traffic demand between data centres and nodes is assumed to be 1.5 times the regular traffic demand in Fig 4-5. We assume data centres are located in nodes 3, 5, 8, 10 and 12.

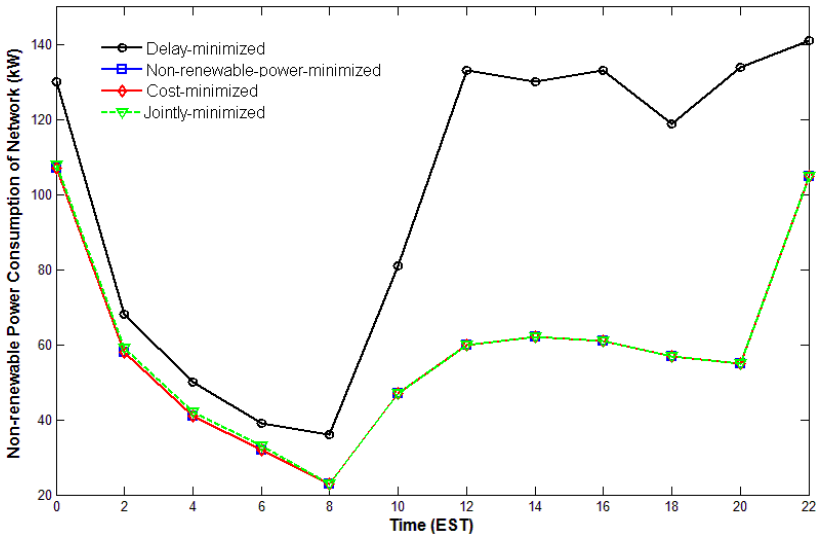

Fig 7 - 8: The non-renewable power consumption under different optimisation scenarios with the bypass approach considering anycasting traffic profile

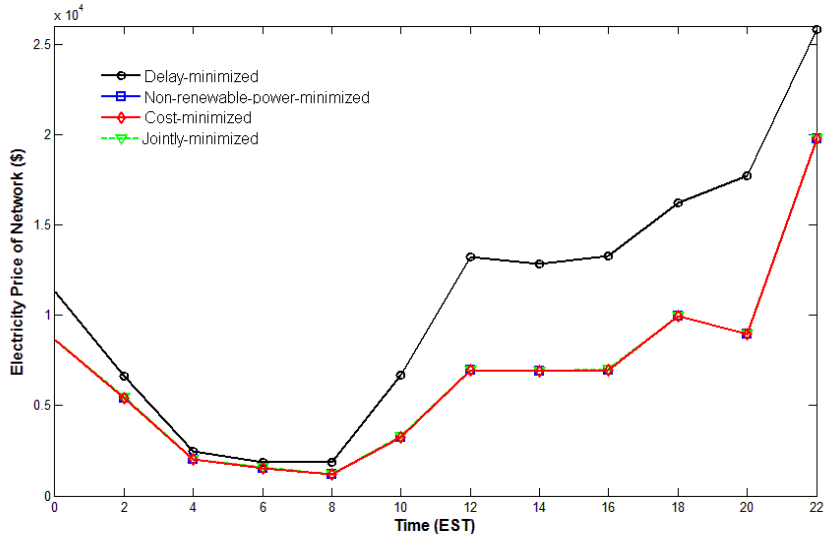

Fig 7 - 9: The electricity cost under different optimisation scenarios with the bypass approach considering anycasting traffic profile

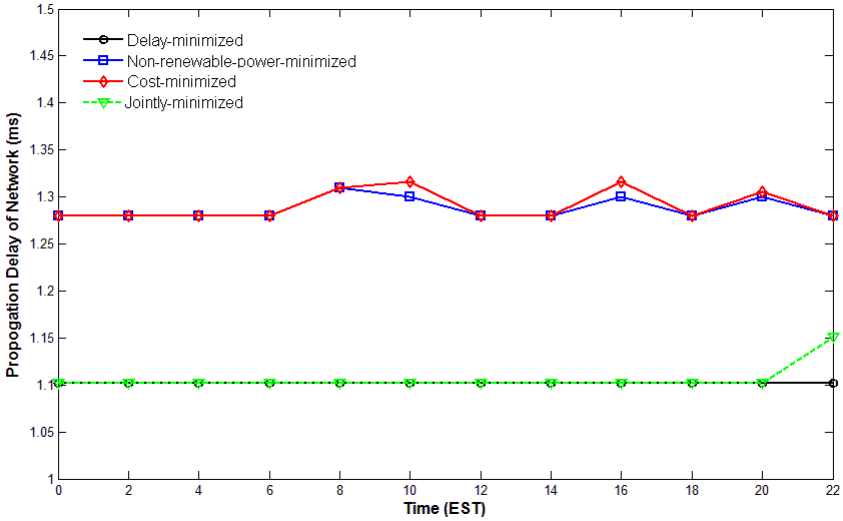

Fig 7 - 10: The propagation delay under different optimisation scenarios with the bypass approach considering anycasting traffic profile

Fig 7-8, Fig 7-9 and Fig 7-10 give the non-renewable power consumption, electricity cost and propagation delay of the NSFNET network under the different optimisation scenarios considering anycasting traffic profile with the bypass approach. Compared to optimising considering delay only, the other optimisation scenarios achieve power consumption and electricity cost savings up to 34% and 31%, respectively. In Fig 7-10, the non-renewable power-minimised and the electricity cost-minimised models have increased the average propagation delay by 25% compared to the delay-minimised model. However, the joint optimisation of the three parameters has hardly increased the propagation delay compared to optimising considering delay only.

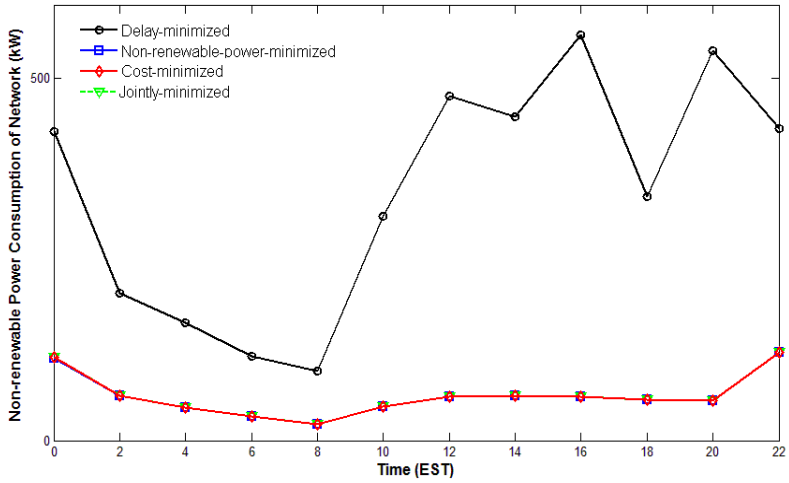

Fig 7 - 11: The non-renewable power consumption under different optimisation scenarios with the non-bypass approach considering anycasting traffic profile

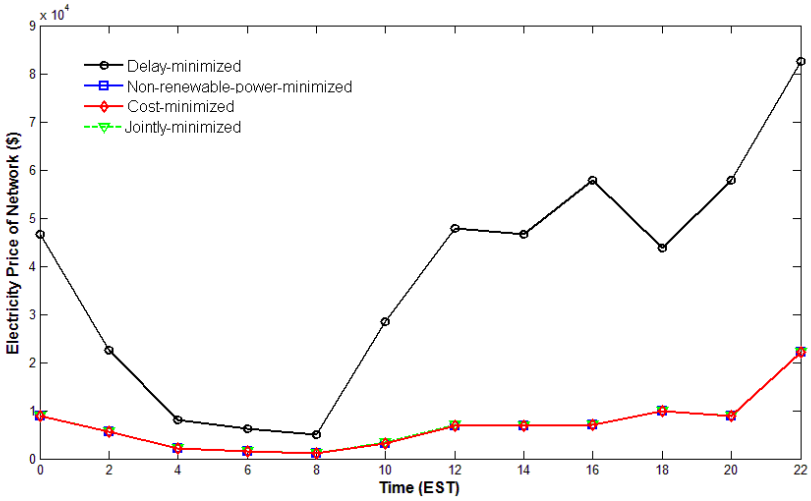

Fig 7 - 12: The electricity cost under different optimisation scenarios with the non-bypass approach considering anycasting traffic profile

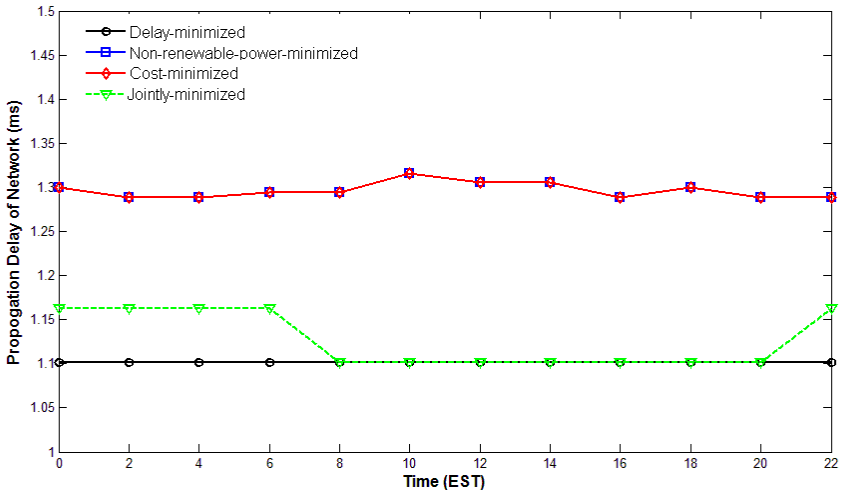

Fig 7 - 13: The propagation delay under different optimisation scenarios with the non-bypass approach considering anycasting traffic profile

Fig 7-11, Fig 7-12 and Fig 7-13 give the non-renewable power consumption, electricity cost and propagation delay of the NSFNET network considering the anycasting traffic profile under the different optimisation scenarios and non-bypass approach. Similar trends to those observed for the unicasting traffic scenario are observed for the anycasting traffic profile. The power consumption and electricity cost savings achieved by the joint optimisation increase to 82%.

7.4 Summary

This chapter has studied the joint optimisation of power, electricity cost and propagation delay in IP over WDM networks. A MILP model was developed to jointly minimise the three parameters considering unicasting and anycasting traffic profiles. The results show that, considering a unicasting traffic profile, the joint optimisation model achieves power consumption and electricity cost savings of 73% and 74%, respectively compared to the delay-minimised model under the non-bypass approach while hardly affecting the delay. Similar trends are obtained under the anycasting traffic profile with power and cost savings up to 82%.

In the previous discussion of energy efficient optical networks, we assumed the traffic demand is not changed during the transmission process. One extension would be the case in which the traffic demand is managed by data compression in which we expect more reduction in power. In the next chapter, we will investigate energy efficient data compression in optical networks.

Chapter 8: Energy Efficient IP over WDM Networks Employing Data Compression

8.1 Introduction

With the increasing popularity of data-intensive application in modern communication such as high-definition IPTV, data compression is becoming a widely used technique to save bandwidth and can result in energy savings. To achieve energy saving, data compression should achieve a trade-off between the energy consumption of computational resources and memory required to compress and decompress data and the network energy savings. A number of papers in the literature have investigated the energy efficiency of data compression in Wireless Sensor Networks (WSNs) and mobile networks. In wireless networks, the transmission energy consumption per bit can be over 1000 times more than the energy consumption of a single 32-bit computation, therefore net energy savings will be obtained by performing significant computation to reduce the number of bits transmitted.

For examples, in [206], the authors significantly reduce the power consumption in modern mobile networks by implementing content-aware compression schemes. In [207], the average power consumption is minimised by implementing a dynamic algorithm for joint compression and transmission. In [208], energy savings up to 57% are achieved for visiting popular web sites on the N810 in IEEE 802.11 WLAN environment by carefully choosing and applying compression schemes. In [209] the

sensor network lifetimes for different network sizes with various data compression and flow balancing strategies are investigated by developing a Linear Programming (LP) model. In [210], the data compression and network energy consumption of optical networks are discussed.

In this chapter, the power consumption savings introduced by implementing data compression in IP over WDM networks are investigated. We optimise the data compression ratio for traffic flows by developing a MILP model considering different IP over WDM approaches. The relationship between the incorrect rate of characters in original information source (ICR_c), data compression and the Bit Error Rate (BER) of the optical channel is analysed. In addition, we also evaluate the power consumption of the IP over WDM networks with data compression when using fixed line rate and Mixed Line Rate (MLR), respectively.

8.2 Data Compression, Bit Error Rate and Incorrect Rate of Original Information Source Characters

Data compression algorithms are classified as lossless and lossy. Compared to lossless data compression algorithms, lossy data compression algorithms, however, may result in some difference between the original data and reconstructed data. Lossy data compression has the advantage of achieving higher compression ratios while maintaining the quality of the application. Different algorithms and typical values of compression ratios for different types of data are given in Table 8-1. Cisco forecasts that 90% of the Internet traffic will be video by 2015 [211]. Video compression algorithms are classified as inter-frame and intra-frame. In the inter-frame compression, a number of frames are described based on their differences from an earlier or later frame. If the next frame is significantly different from the previous frame, a new reference frame is created. Inter-frame algorithms include MPEG-1, MPEG-2…etc. On the other hand, Intra-frame algorithms compress each frame separately and independently from other frames in the sequence [212].

In networks, all the video traffic is compressed before transmission using video compression approaches such as MPEG-4, H.264 etc. If video files can be further

compressed, the network traffic will be significantly reduced and consequently significant energy consumption savings will be achieved. In [213], the authors considered semantic compression to reduce the video storage space by decreasing the low-level descriptors to a small number of dimensions while preserving most of the semantic information. They adapted topic models, which have been used to represent still images, to consider the temporal structure of a video and the multi-modal components such as motion information. Experiments on a large-scale collection of YouTube videos showed that a compression ratio of 20:1 can be achieved by using the topic model compared to ordinary histogram representations. Using the topic model in [213] to compress the video traffic before transmission means that we can obtain a further compression ratio of 20:1.

Traffic type	Compression algorithm	Compression rate
Text	bzip2, ppmd, gzip (lossless)	4:1 [214]
Image	JPEG, GIF, PNG (lossy)	10:1 [215]
Video	MPEG-4, H.264(lossy)	20:1 [213]

Table 8 - 1: Algorithms and compression ratios for different types of data

8.2.1 Power Consumption of Data Compression

In practice, the power consumption of data compression relates to many factors, such as, data type, compression algorithm, compression ratio and implementation (software implementation and hardware implementation). Currently lossless data compression (such as gzip, zlib and ppmd, etc.) is the mainly used data compression method for IP core networks. In [214], the power consumption of lossless data compression based on software implementation is divided among CPU, memory, and peripherals. If we only consider the power consumption by CPU and memory, the power consumption details of different lossless data compression algorithms in [214] can be summarised as below:

Compression algorithm	Compression rate	Power consumption
ppmd	3~4.5:1	96 μW/bit
bzip	2.5~4:1	102 μW/bit
zlib	1.5-2.8:1	95 μW/bit
compress	2~2.5:1	87 μW/bit

lzo	1.5:1	100 μW/bit

Table 8 - 2: Data compression algorithms and power consumption by software implementation

With hardware implementation methods, typically using 100 MHz ASIC can achieve lossless data compression with compression ratios from 2.5:1 to 3.5:1 [216]. According to the power consumption of an ASIC in [217] and [218], the power consumption for hardware implementation of lossless data compression with 2.5~3.5:1 data compression ratio can be estimate as 7 nW/bit. Compared to the software implementation for lossless data compression, hardware implementation has much higher power efficiency. Therefore, hardware implementation of lossless data compression by ASIC or FPGA is widely used in core networks.

For higher data compression ratios, lossy data compression algorithms which are commonly used by image and video processors have to be considered. In [219], an image data compression algorithm 'Consultative Committee on Space Data Systems Image Data Compression' (CCSDS-IDC) is proposed which can offer adjustable data compression ratios or image quality (up to lossless). Because of the low power efficiency associated with software implementations, hardware implementations are the main methodology to achieve lossy data compression in practice. In [220], the authors introduced Xilinx Virtex II Pro FPGA technology to implement CCSDC-IDC (encoding a 512x512x8 bit image in 0.015s at 100 MHz) which nearly has rate-distortion performance similar to JEPG2000 but reduces on-board implementation complexity. Based on the Xilinx Virtex II Pro data sheet [221] (5.5V input with 2.2 A current for XC2VP100), the power consumption of lossy data compression based on hardware implementation can be estimate at up to 40 nW/bit. Similarly, if we want to implement a data compression ratio 20:1 of [213] in hardware, it can be expected that the on-board complexity and the power consumption will increase.

From the above discussion, it can be seen that the power consumption of data compression is subject to variation for different types of data, data compression algorithms and implementations, and therefore is difficult to generalise. However, there is a trend amongst these independent approaches indicating that the power

consumption rises with increase in the data compression ratio. In networks we have to consider the network power saving as a result of transmitting fewer bits following compression versus the power consumption of data compression. Therefore, it is necessary to build a general relationship between the power consumption of data compression and data compression ratio; and also relate them to the power consumption of the network.

In [210] the relationship between the compression ratio and the power consumption of different data compression processors is give as:

$$P_c = A(\eta - 1)^{\beta}$$
$$\eta = \frac{1}{1 - R_c}, \quad A, \beta > 0 \tag{8-1}$$

where P_c is the data compression power consumption per bit, R_c is the data compression ratio, and A and β are parameters. Note that data compression ratio R_c is defined as:

$$R_c = \frac{original\_data\_size - data\_size\_after\_compression}{original\_data\_size}, 0 \leq R_c < 1.$$

The power consumption of the data compression is a function of the algorithm used for the compression and the type of data. According to early discussion in this section, we define β as the efficiency of the data compression algorithm. Different data compression algorithms use different computational resources and memory to achieve a certain compression ratio, resulting in different levels of power consumption. In [222], the authors give the total cost of computational resources for different algorithms as a function of compression ratio.

In Fig 8-1, as the compression ratio increases, the power consumed per bit by data compression processors increases and the network power consumption (transmission, switching, routing etc) per bit decreases. The total power consumption of the network per bit is given as the sum of the compression processors power consumption, P_c , and the power consumption of the network P_{Net}. The optimal compression ratio is the ratio associated with the minimum total power consumption [210].

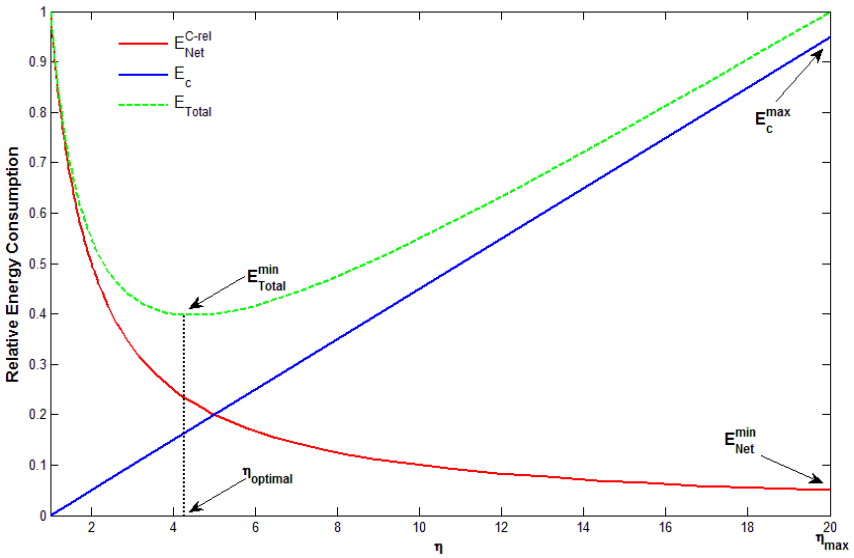

Fig 8 - 1: Data compression processors power consumption and network power consumption vs. data compression ratio (ε=1, β=1)

To obtain the power consumption of a data compression algorithm, the parameter A needs to be calculated. The maximum power consumption saving in the network $P_{Netsaved}^{max}$ is considered to be related to the power consumption P_c^{max} and the maximum data compression ratio(R_c^{max}) based on hardware implementation as follows:

$$P_c^{max} = \varepsilon \cdot P_{Net\ Saved}^{max}$$

where ε is a scaling parameter which can represent the degree of power efficiency for the implementation of data compression and $P_{Net\ Saved}^{max}$ is calculated as

$$P_{Net\ Saved}^{max} = R_c^{max} P_{Net}$$

Note that the value of R_c^{max} depends on the data compression algorithm implemented. Therefore

$$P_c^{max} = \varepsilon\, R_c^{max} P_{Net} = A\left(\frac{1}{1 - R_c^{max}} - 1\right)^{\beta} \tag{8-2}$$

From (8-1) and (8-2), the parameter A can be calculated as:

$$A = \varepsilon\, R_c^{max} P_{Net} \left(\frac{1}{1 - R_c^{max}} - 1\right)^{-\beta} \tag{8-3}$$

Therefore the power consumption of data compression can be given as:

$$P_c = A(\eta - 1)^{\beta} = \varepsilon R_c^{max\,1-\beta}(1 - R_c^{max})^{\beta} P_{Net}(\eta - 1)^{\beta}$$

It is to be expected that the power consumption of data compression per bit based on hardware implementation will be lower than that of data transmission in networks with the development of CMOS processing technology and the value of ε can be expected to be equal to or lower than 1. Note that ε =1 represents the point at which the power consumption of compression is equal to the savings in the network power consumption resulting from data compression, i.e. no further power savings will be achieved from further compression [210]. Fig 8-2 gives the relationship between P_c and η for different value of β assuming ε=1 and $R_c^{max} = 0.95$ ($\eta^{max} = 20$) [213].

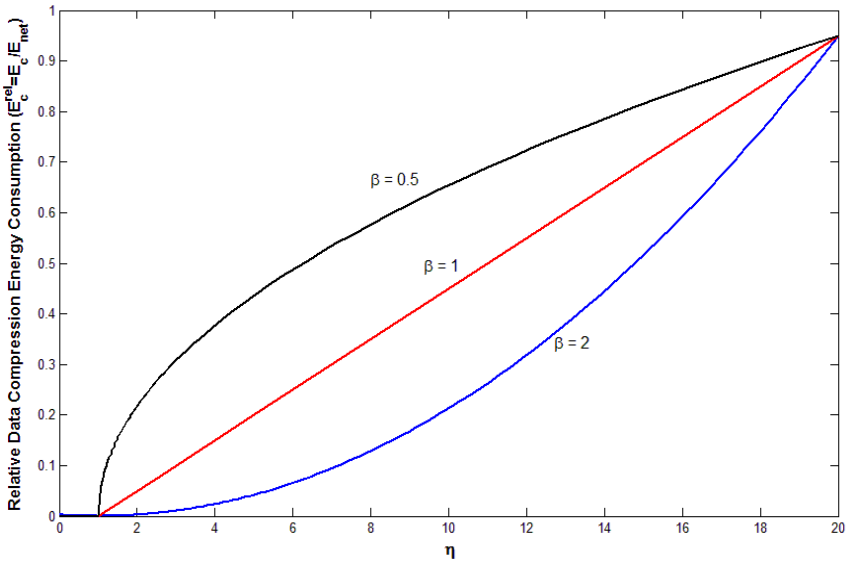

Fig 8 - 2: Relationship between the data compression ratio and data compression power consumption

8.2.2 Bit Error Rate of Optical Channel

The Shannon lossless source coding theorem established that the source entropy rate is the rate of the optimal lossless data compression code, R [223] given as:

$$R = \frac{1}{n}\sum p(B_n)\, l(B_n) \quad bit/character \tag{8-4}$$

where n is the number of characters in the original data, $p(B_n)$ is the probability of the character block B_n in the original data and $l(B_n)$ is the length of the codeword for block B_n in bits. The shorter the length of the codeword the higher the compression rate. With a certain channel *BER*, the higher compression rate will result in higher incorrect rate of characters in the original information source (ICR_c). Therefore, it is necessary to identify the relationship between ICR_c, *BER* and data compression ratio.

The *BER* of an optical receiver is given as [224]:

$$BER = Q\left(\frac{I_1 - I_0}{\sigma_0 + \sigma_1}\right) \tag{8-5}$$

$$Q(x) = \frac{1}{\sqrt{2\pi}} \int_x^{\infty} e^{-y^2/2} dy \tag{8-6}$$

$$r = Q^{-1}(BER) = \frac{I_1 - I_0}{\sigma_0 + \sigma_1} \tag{8-7}$$

where I_1 and I_0 are the photocurrents of logic '1' and logic '0' in the optical receiver, respectively. σ_1 and σ_0 are the the noise standard deviations when the receiver detects logic '1' and logic '0', respectively. The noise signals are considered to be Gaussian.

Neglecting the receiver thermal noise and shot noise, the optical signal-to-noise ratio (*OSNR*) is defined as:

$$OSNR = \bar{P}_{rec}/P_{ASE}$$

where $\bar{P}_{rec}$ is the average received signal power and P_{ASE} is the amplified spontaneous noise power at the output of the amplifier. In the case of deploying optical amplifiers, the total received optical noise power for a link of length L with a distance S between two neighbouring amplifiers is given as:

$$P_{ASE} = P_{noise}^{amp} B_o (G - 1)\, L/S \tag{8-8}$$

where P_{noise}^{amp} is the noise power of an optical amplifier, B_o is the bandwidth of optical receiver, and G is the gain of the amplifier.

Assuming that receivers on different links receive the same optical signal power, the $OSNR_L$ of a link of length L is given as:

$$OSNR_L = \frac{\bar{P}_{rec}}{P_{noise}^{total}} = OSNR \cdot S/L \tag{8-9}$$

The relationship between r and *OSNR* is given as [224]:

$$r = \frac{2\sqrt{\frac{B_o}{B_e}}OSNR}{1+\sqrt{1+4OSNR}} \tag{8-10}$$

where B_e is the bandwidth of the electrical filter.

In practice, optical receivers should have BER better than 10^{-9} $(r = 6)$. For $r > 5$, equation (8-3) can be approximated as follows:

$$Q(x) = \frac{1}{\sqrt{2\pi}}\int_x^{\infty} e^{-y^2/2}dy \cong \frac{e^{-\frac{x^2}{2}}}{x\sqrt{2\pi}}, \text{for } x = r > 5 \tag{8-11}$$

Therefore, from equations (8-11) (8-5), (8-7), (8-8) and (8-10), the BER_L of an optical receiver on a link of length L is given as:

$$BER_L = \frac{e^{-\frac{x^2}{2}}}{x\sqrt{2\pi}},$$

$$\text{where } x = \frac{2\sqrt{\frac{B_o}{B_e}}OSNR \cdot S/L}{1+\sqrt{1+4\,OSNR \cdot S/L}} \tag{8-12}$$

8.2.3 Data Compression Ratio, Incorrect Rate of Characters in Original Information Source and Bit Error Rate of Optical Channel

As discussed in previous sections, higher data compression ratios will result in increasing ICR_c with a certain channel *BER*. A number of source coding algorithms have been developed to achieve high efficiency and data compression ratio in

wireless networks while maintaining the BER [225-227]. In the following we will obtain a relationship between the data compression ratio, ICR_c and the BER of the optical channel.

The ICR_c can be related to the data compression ratio and BER of optical channel as follows:

$$ICR_c = \eta^{\tau} BER \tag{8-13}$$

The parameter τ represents the sensitivity of the ICR_c to the data compression ratio.

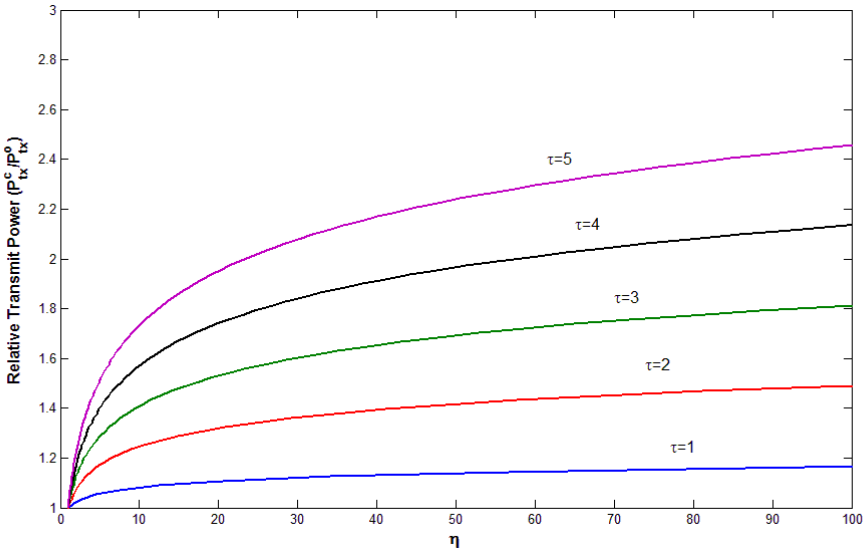

Fig 8 - 3: Relationship between the data compression ratio and the transmit power (P_{tx}^o and P_{tx}^c are the transmit power before and after compression, respectively)

Fig 8-3 shows the relationship between the transmit power and data compression ratio, where the $ICR_c \leq 10^{-12}$ with BER=10^{-12} and $OSNR$=20 dB. For $\tau = 1$, the ICR_c is linearly related to the data compression ratio. Higher values of τ imply that the ICR_c is more sensitive to the data compression ratio. This occurs for example in inter-frame compression of video where one or more of the earlier or later frames in the sequence are used to compress the current frame [228].

There are two approaches to compensate for the growth of the ICR_c resulting from data compression: increasing the transmit power or limiting the data compression ratio. For lower values of τ (τ<=3) considering P_{tx}^o of 1 Watt or less, an increase in the transmit power by a factor of 1.5 or less to maintain the ICR_c (Fig

8-3) will result in a negligible increase in the transmit power in comparison to the power consumption of the network components. However, for higher value of τ (τ>3), increasing in the transmit power will increase the nonlinear effects of associated with the optical channel such as self-phase modulation (SPM) and cross-phase modulation (CPM), or even cause damage to the optical fibre [229]. In this case, we have to limit the data compression ratio to maintain the ICR_c. Such high values of τ can occur in inter-frame video compression where a large number of frames are compressed with reference to a single reference frame, such as security video (CCTV). In Section 8.5, the power consumption of optical networks with data compression will be investigated under the two approaches.

8.3 Mathematical Model

In this section, a MILP model is built to optimise the data compression ratio for the traffic demands in IP over WDM networks to minimise the network power consumption. Compressing traffic demands will result in reducing the traffic and hence the power used by the network devices and/or their number. The decision on whether to compress a traffic demand or not and the compression ratio used depends also on the available capacity on existing virtual links.

The model defines the following parameters:

i and j	Denote end points of a virtual link in the IP layer,
s and d	Denote source and destination of a traffic demand,
m and n	Denote end points of a physical link in the optical layer,
L_{mn}	The length of the physical link between nodes m and n,
T	Set of time points,
S	Distance between neighbouring EDFAs,
N	Set of nodes,
K	Index for the set of equations that approximate the convex/concave

function that describes the relationship between data compression ratio and power consumption of the data compression,

Np_i The set of neighbour nodes of node *i* in the optical layer,

W The number of wavelengths in a fibre,

B The capacity of each wavelength,

λ^{sdt} Traffic demand between source *s* and destination *d* at time *t,*

EA_{mn} The number of EDFAs on physical link (*m, n*). Typically $EA_{mn} = \lfloor L_{mn}/S - 1 \rfloor + 2$, where *S* is the distance between two neighbouring EDFAs [58],

EG_{mn} The number of regenerators on physical link (*m, n*). Typically $EG_{mn} = \lfloor L_{mn}/5S - 1 \rfloor$[58],

PR Power consumption of a router port,

PT Power consumption of a transponder,

PE Power consumption of an EDFA,

PG Power consumption of a regenerator,

PO_i Power consumption of the optical switch at node *i,*

PMD Power consumption of a multi/demultiplexer,

R_c^{max} The maximum data compression ratio,

a_k and b_k Elements of the approximation vectors used in equation *k* in set *K*.

The following variables are also defined:

C_{ijt} The number of wavelength channels in the virtual link (*i, j*) at time *t,*

ω_{mnt} The number of wavelength channels in the physical link (*m, n*) at time *t,*

W_{mnt}^{ij} The number of wavelength channels in the virtual link (*i, j*) that traverse physical link (*m, n*) at time *t,*

DM_i The number of multi/demultiplexers in node *i,*

λ_{ijt}^{sd} The traffic flow from node *s* to node *d* that traverses the virtual link (*i, j*) at time *t,*

R_c^{sdt} Data compression ratio for the traffic from source node *s* to destination node *d* at time *t,*

P_c^{sdt} Data compression power consumption per bit of the traffic from source node *s* to destination node *d* at time *t,*

f_{mn} The number of fibres on physical link (*m, n*).

Under the lightpath bypass approach, the total network power consumption is composed of:

1) The power consumption of ports at time *t*

$$\sum_{i \in N} \sum_{j \in N: i \neq j} PR \cdot C_{ijt} \tag{8-14}$$

2) The power consumption of transponders at time *t*

$$\sum_{m \in N} \sum_{n \in Np_m} PT \cdot \omega_{mnt} \tag{8-15}$$

3) The power consumption of EDFAs and regenerators at time *t*

$$\sum_{m \in N} \sum_{n \in Np_m} (PE \cdot EA_{mn} \cdot f_{mn} + PG \cdot EG_{mn} \cdot f_{mn}) \tag{8-16}$$

4) The power consumption of optical switches at time *t*

$$\sum_{i \in N} PO_i \tag{8-17}$$

5) The power consumption of multiplexers and demultiplexer at time *t*

$$\sum_{i \in N} PMD \cdot DM_i \tag{8-18}$$

6) The power consumption of the data compression processors at time *t*

$$\sum_{s \in N} \sum_{d \in N: s \neq d} \lambda^{sdt} \cdot P_c^{sdt} \tag{8-19}$$

The MILP model is defined as follows:

Objective: minimise

$$\begin{aligned} \sum_{t \in T} \Bigg(& \sum_{s \in N} \sum_{d \in N: s \neq d} \lambda^{sdt} \cdot P_c^{sdt} \\ & + \sum_{i \in N} \sum_{j \in N: i \neq j} PR \cdot C_{ijt} + \sum_{m \in N} \sum_{n \in Np_m} PT \cdot \omega_{mnt} \\ & + \sum_{m \in N} \sum_{n \in Np_m} \left(PE \cdot EA_{mn} \cdot f_{mn} + PG \cdot EG_{mn} \cdot f_{mn} \right) \\ & + \sum_{i \in N} PO_i + \sum_{i \in N} PMD \cdot DM_i \Bigg) \end{aligned} \tag{8-20}$$

Subject to:

1) *Flow conservation constraint in the IP layer:*

$$\sum_{j \in N: i \neq j} \lambda_{ijt}^{sd} - \sum_{j \in N: i \neq j} \lambda_{jit}^{sd} = \begin{cases} \lambda^{sdt} \cdot (1 - R_c^{sdt}) & if\ i = s \\ -\lambda^{sdt} \cdot (1 - R_c^{sdt}) & if\ i = d \\ 0 & otherwise \end{cases} \tag{8-21}$$

$$\forall\ t \in T, \forall\ s, d, i \in N: s \neq d$$

Constraint (8-21) represents the flow conservation constraint in the IP layer. It ensures that in all nodes the total outgoing traffic is equal to the total incoming traffic except for the source and the destination nodes. It also ensures that traffic flows can be split and transmitted through multiple flow paths in the IP layer. Note that we consider the compressed traffic demands.

2) *Virtual link capacity constraint:*

$$\sum_{s\in N}\sum_{d\in N:s\neq d}\lambda_{ijt}^{sd} \leq C_{ijt}\cdot B \qquad (8\text{-}22)$$

$$\forall\ t\in T, \forall\ i,j\in N: i\neq j$$

Constraint (8-22) ensures that the summation of all traffic flows through a virtual link does not exceed its capacity.

3) *Flow conservation constraint in the optical layer:*

$$\sum_{n\in Np_m} W_{mnt}^{ij} - \sum_{n\in Np_m} W_{nmt}^{ij} = \begin{cases} C_{ijt} & if\ m=i \\ -C_{ijt} & if\ m=j \\ 0 & otherwise \end{cases} \qquad (8\text{-}23)$$

$$\forall\ t\in T, \forall\ i,j,m\in N: i\neq j$$

Constraint (8-23) represents the flow conservation constraint in the optical layer. It represents the fact that in all nodes the total outgoing wavelengths of a virtual link should be equal to the total incoming wavelengths except for the source and the destination nodes of the virtual link.

4) *Physical link capacity constraints:*

$$\sum_{i\in N}\sum_{j\in N:i\neq j} W_{mnt}^{ij} \leq W\cdot f_{mn} \qquad (8\text{-}24)$$

$$\forall\ t\in T, \forall\ m\in N, n\in Np_m$$

$$\sum_{i\in N}\sum_{j\in N:i\neq j} W_{mnt}^{ij} = \omega_{mnt} \qquad (8\text{-}25)$$

$$\forall\ t\in T, \forall\ m\in N, n\in Np_m$$

Constraints (8-24) and (8-25) represent the physical link capacity constraints. Constraints (8-24) ensures that the total number of wavelength channels in virtual links traversing a physical link does not exceeded the maximum capacity of fibres in the physical link. Constraint (8-25) ensures that the number of wavelength channels in virtual links traversing a physical link is equal to the number of wavelengths in that physical link.

5) *Power consumption of data compression constraint:*

$$P_c^{sdt} \begin{cases} \leq a_k \cdot R_c^{sdt} + b_k & for\ a\ convex\ function \\ \geq a_k \cdot R_c^{sdt} + b_k & for\ a\ concave\ function \end{cases} \quad (8\text{-}26)$$

$$\forall\ t \in T, k \in K, \forall\ s, d \in N: s \neq d$$

Constraint (8-26) is the linear approximation of the relationship between power consumption of data compression and data compression ratio.

6) *Maximum data compression ratio constraint:*

$$R_c^{sdt} \leq R_c^{max} \quad (8\text{-}27)$$

$$\forall\ t \in T, k \in K, \forall\ s, d \in N: s \neq d$$

Constraint (8-27) gives the limit on the maximum data compression ratio.

The model can be extended to represent the non-bypass approach by redefining the power consumption of ports at time *t* as follows:

$$\sum_{m \in N} \sum_{n \in N: m \neq n} PR \cdot \omega_{mnt} \quad (8\text{-}28)$$

8.4 Energy Efficient Data Compression Algorithm

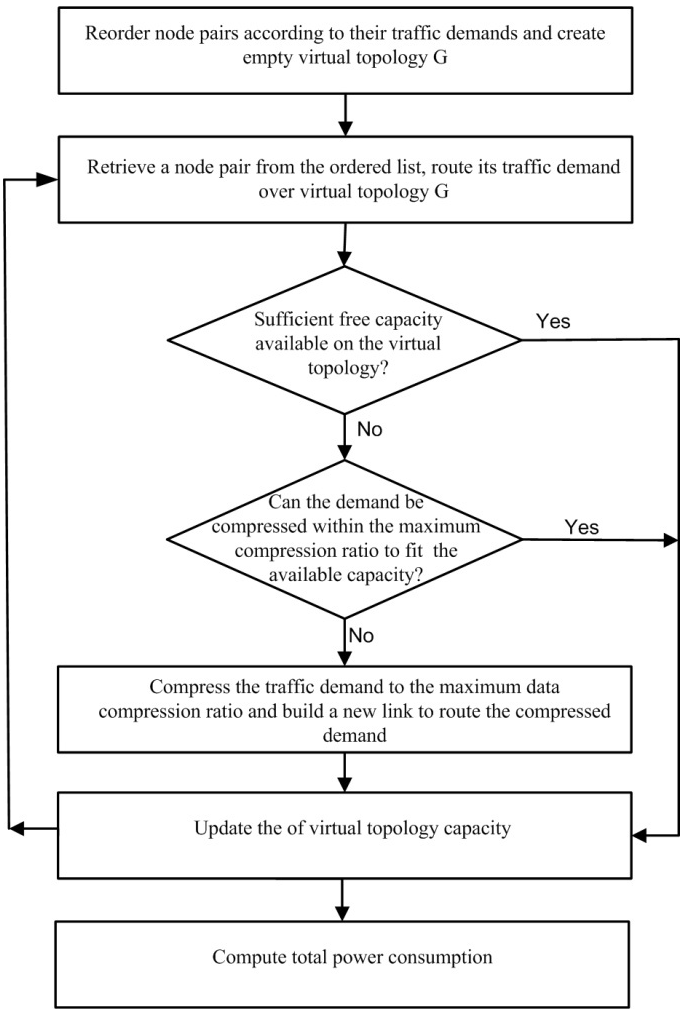

Fig 8 - 4: The energy-efficient data compression and routing heuristic flow chart

In this section we propose an energy-efficient heuristic to compress and route traffic demands in real time. The flow chart of the heuristic is shown in Fig 8-4. Node pairs are reordered from highest to lowest based on their traffic demands and an empty virtual link topology *G* is created. A node pair is then retrieved from the ordered list and its traffic demand is routed over virtual topology *G* if enough capacity is available. If virtual topology *G* cannot accommodate the traffic demand, it will be compressed within the maximum compression ratio to be accommodated in the available capacity. If the required data compression ratio exceeds the maximum compression ratio, the traffic demand is compressed by the maximum data compression ratio and a new virtual link is built to route the compressed demand. After routing all the traffic demands, the network total power consumption is calculated using Equation (8-20).

8.5 Results and Analysis

In this section we evaluate the power consumption of IP over WDM networks with data compression considering the two approaches discussed in Section 8.2.3 to maintain the ICR_c. The same NSFNET network topology as in Chapter 4, depicted in Fig 4-4, is considered. The same average traffic demand as in Chapter 4, shown in Fig 4-5, is used here.

Distance between two neighbouring EDFAs	80 (km)
Distance between two neighbouring regenerators	400 (km)
Capacity of each wavelength (*B*)	40 (Gbit/s)
Power consumption of a router port (*PR*)	1000 (W)
Power consumption of an optical switch in node *i* (PO_i)	85 (W)
Power consumption of a multiplexer or a demultiplexer (*PMD*).	16 (W)
Power consumption of a transponder (*PT*)	73 (W)
Power consumption of a regenerator (*PG*)	100 (W)
Power consumption of an EDFA (*PE*)	8 (W)

Table 8 - 3: Input parameters for MILP model and simulation

Table 8-3 shows the input parameters in terms of number of wavelengths, wavelength capacity, distance between two neighbouring EDFAs, and power consumption of different components in the network derived from Cisco's 16-slot CRS-1 data sheets [193], Cisco's OC-48/STM-16 bidirectional Regenerator data sheets [189], Cisco ONS 15501 EDFA data sheets [188], Cisco ONS 15454 100-GHz 4-CH Multi/Demultiplexer data sheets [190], Cisco ONS 15454 10-Gbps multi-rate transponder card data sheets [190], and Glimmerglass Intelligent Optical System 500 data sheets [191].

We assume that the power consumption of decompression is equal to the power consumption of compression. Considering a mixture of traffic (video, images, text) to reflect the global Internet traffic where 91% of the global Internet traffic is projected to be a form of video by 2015 [211]. Considering the compression ratios in Table 8-1, the maximum data compression ratio for the traffic mixture is 90%. For the NSFNET network, $P_{Net} = 25$ nW/bit as calculated under the bypass approach.

Parameter A, which is used to derive the piecewise linear relations in Equation (8-26) to linearise the MILP, can be determined from P_{Net} as in Equation (8-3).

8.5.1 Increasing Transmit Power

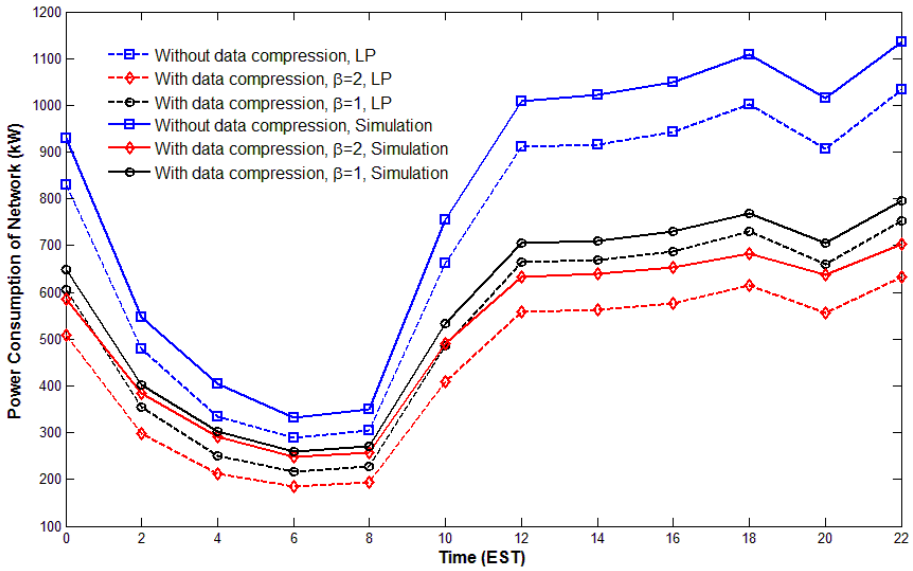

Fig 8 - 5: The network power consumption with and without compression under the bypass approach for different values of β (shortest path routing)

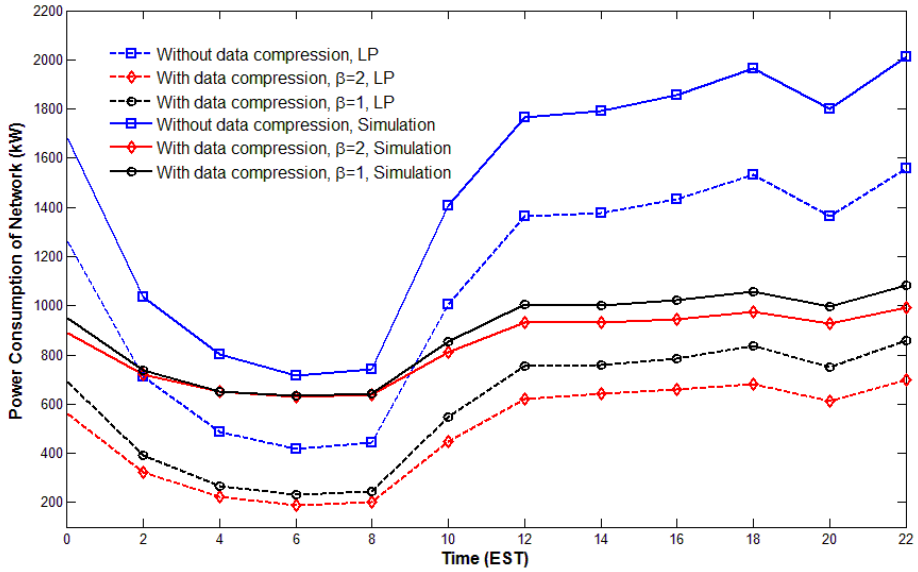

Fig 8 - 6: The network power consumption with and without compression under the non-bypass approach for different values of β (shortest path routing)

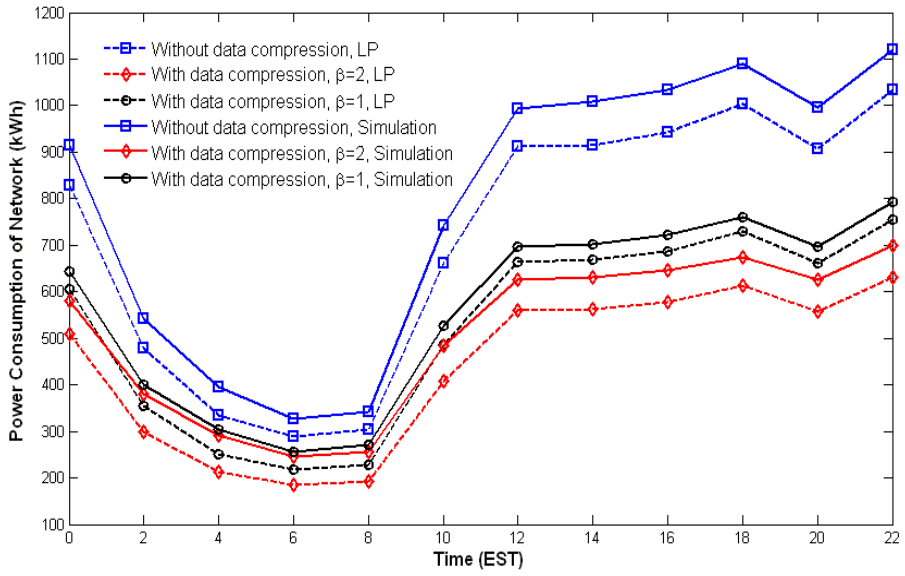

Fig 8 - 7: The network power consumption with and without compression under the bypass approach for different values of β (minimal hop routing)

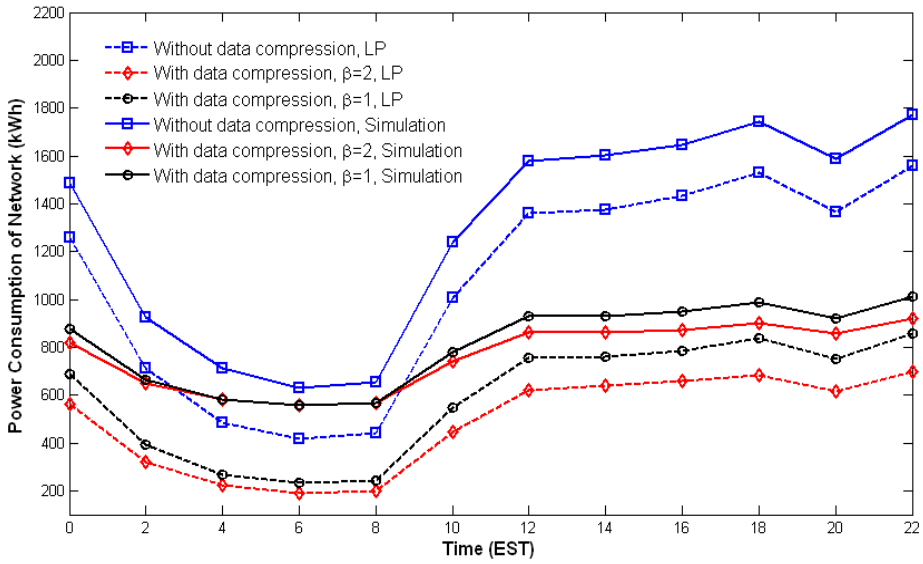

Fig 8 - 8: The network power consumption with and without compression under the non-bypass approach for different values of β (minimal hop routing)

Fig 8-5, Fig 8-6, Fig 8-7 and Fig 8-8 give the power consumption of the network with and without compression for different values of β under the bypass and non-bypass approaches using shortest path routing scenario and minimal hop routing scenario. We consider increasing the transmit power to maintain the ICR_c under the bypass approach. Note that under the non-bypass approach ICR_c is always maintained. Because the traffic always goes up to IP layer in each intermediate node

and the length of optical channel is shorter than that in bypass, the *BER* of optical channel is higher than bypass.

Using shortest path routing scenario, average power savings of 29% are achieved by the data compression MILP model under the bypass approach for $\beta = 1$ (Fig 8-5). More efficient data compression algorithms represented by $\beta = 2$ can achieve an average power saving of 39%. Comparable power savings of 29% and 36% for $\beta = 1$ and $\beta = 2$, respectively, are achieved the energy-efficient data compression and routing heuristic. High power savings of 45% and 55% for $\beta = 1$ and $\beta = 2$, respectively, are achieved under the non-bypass approach (Fig 8-6) as under the non-bypass approach data compression reduces the number of router ports (the most energy consuming devices in the network) at intermediate nodes.

Power savings in the network in simulations can be obtained by using minimal hop routing, especially under the non-bypass approach. Compared to Fig 8-5 minimal hop routing under bypass approach (Fig 8-7) does not result in significant difference. However, in Fig 8-8, under the non-bypass approach, the simulation results using the minimal hop routing scenario are closer to the results from linear programming, compare to Fig. 8-6. The power savings for $\beta = 1$ and $\beta = 2$ are 37% and 41% compared to the power consumption of the network without data compression.

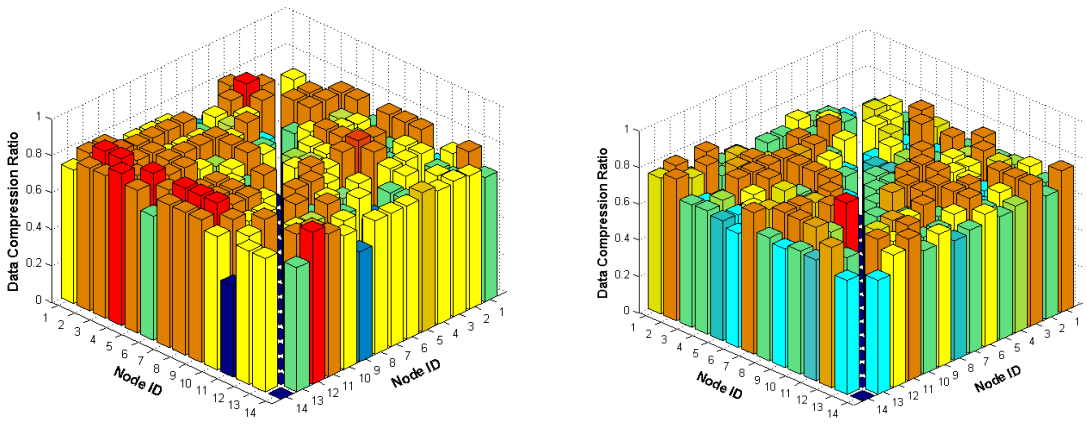

(a) Low Traffic Demand (6 am) (b) High Traffic Demand (10 pm)

Fig 8 - 9: The optimal data compression ratio of each node pair traffic demand under the bypass approach at 6 am and 10 pm (increasing transmit power)

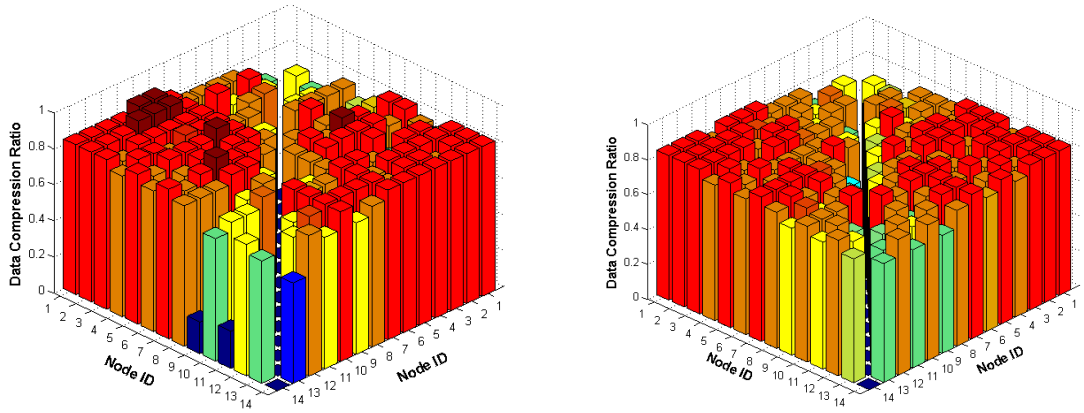

(a) Low Traffic Demand (6 am) (b) High Traffic Demand (10 pm)

Fig 8 - 10: The optimal data compression ratio of each node pair traffic demand under the non-bypass approach at 6 am and 10 pm (increasing transmit power)

Fig 8-9 and Fig 8-10 show the optimal data compression ratio of each node pair traffic demand obtained from the MILP at 6 am (minimum traffic) and 10 pm (maximum traffic) under the bypass and non-bypass approaches, respectively. Under both approaches, the optimal data compression ratio for most of the node pairs varies slightly (between 70%-80%) for the different node pair traffic demand under both the maximum and minimum traffic demands. The average compression ratio is 0.71. Under the non-bypass approach the average optimal data compression ratio is slightly higher compared to the bypass approach (0.77). This is because we calculate the maximum data compression ratio power consumption P_c^{max} based on the P_{Net} associated with the bypass approach.

8.5.2 Limiting the Data Compression Ratio

As discussed in Section 8.2.3, to maintain ICR_c with higher values of τ under the bypass approach, we have to limit the data compression ratio. If we want to maintain the $ICR_c \leq 10^{-12}$ after data compression, Equation (8-13) can be given as:

$$\eta^{\tau} BER \leq 10^{-12}$$

$$R_c \leq 1 - \sqrt[\tau]{\frac{BER}{10^{-12}}}$$

The above equation is added as a constraint to the MILP model in Section 8.3 as follows:

$$R_c^{sdt} \leq 1 - \sqrt[\tau]{\frac{BER^{sd}}{10^{-12}}} \tag{8-29}$$

where

$$BER^{sd} = \frac{e^{-\frac{x^2}{2}}}{x\sqrt{2\pi}}$$

$$x = \frac{2\sqrt{\frac{B_o}{B_e}}OSNR \cdot S/L_{sd}}{1 + \sqrt{1 + 4\,OSNR \cdot S/L_{sd}}}$$

The *BER* of each optical link BER^{sd} is calculated from Equation (8-29) assuming that the longest link in the network has the maximum *BER* of 10^{-12} with *OSNR*=50 dB.

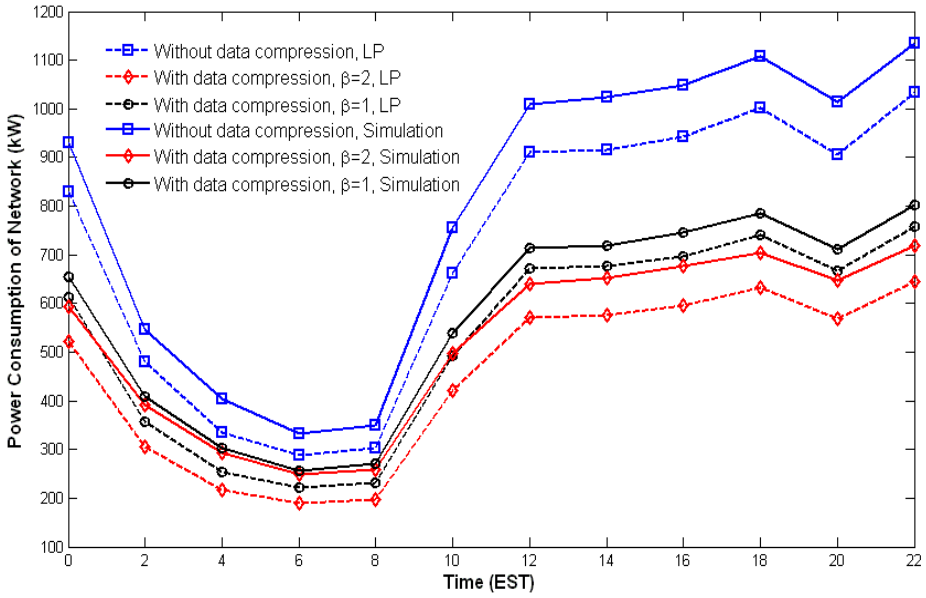

Fig 8 - 11: The network power consumption with and without compression under the bypass approach for different values of β (limiting data compression ratio)

Fig 8-11 shows that limiting the data compression ratio to maintain ICR_c for τ=4, has a limited effect on the achieved power savings under the bypass approach as only few long links exist in the NSFNET. The power saving of the MILP model under the bypass approach is 27% and 37% for $\beta = 1$ and $\beta = 2$, respectively. The

heuristic achieves a power saving of 27% and 34% for $\beta = 1$ and $\beta = 2$, respectively. Fig 8-12 shows that the optimal data compression ratios decrease slightly by an average of 3% as a result of limiting the data compression ratio to maintain the ICR_c. The decreased compression ratios are associated with traffic demands routed through longer links.

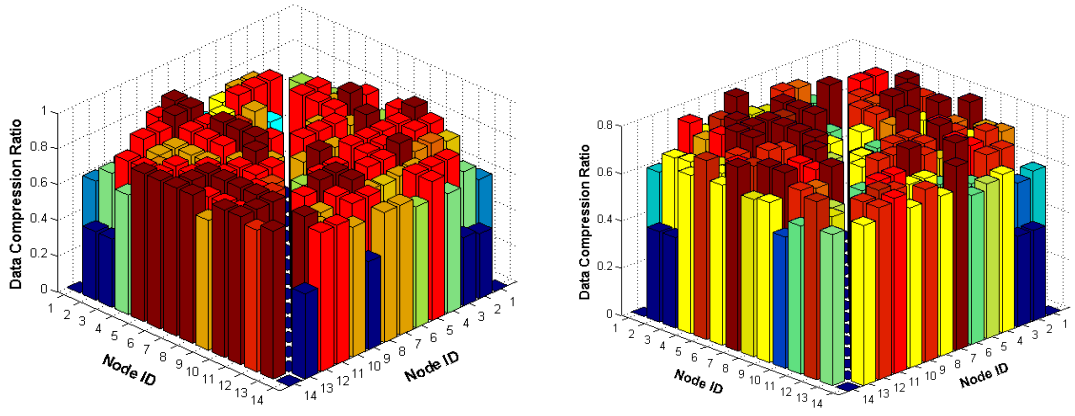

(a) Low Traffic Demand (6 am) (b) High Traffic Demand (10 pm)

Fig 8 - 12: The optimal data compression ratio of each node pair traffic demand under the bypass approach at 6 am and 10 pm (limiting data compression ratio).

8.6 Mixed Line Rate and Data Compression

In the previous sections of this chapter, the power consumption of the network with data compression under a fixed line rate (40 Gbit/s) has been studied. However, after data compression, the traffic demand is reduced significantly and most of the traffic demand between node pairs may be less than the capacity of physical links. Although grooming can be used to combine some low traffic demands into one lightpath, a fixed line rate scenario cannot provide capacity flexibility and may lead to lower bandwidth utilisation. To improve the utilisation of bandwidth after data compression, MLR is proposed here which in itself can lead to added energy efficiency in optical networks.

8.6.1 Mathematical Model

Since a regenerator is used on the 40 Gbit/s line rate physical links in Section 8.5, the impact of different line rates on the maximum reach distance can be neglected in here. We use *R* as the set of the possible line rates and the MILP model in Section 8.3 is extended to support the MLR replacing the parameters *PR*, *PT, B* with:

PR_r Power consumption of a router port with line rate *r,*

PT_r Power consumption of a transponder with line rate *r,*

B_r The capacity of wavelength of line rate *r,*

and the variables C_{ijt}, ω_{mnt}, W_{mnt}^{ij} with

C_{ijtr} The number of wavelength channels in the virtual link (*i, j*) at time *t* and line rate *r,*

ω_{mntr} The number of wavelength channels in the physical link (*m, n*) at time *t* and line rate *r,*

W_{mntr}^{ij} The number of wavelength channels in the virtual link (*i, j*) that traverse physical link (*m, n*) at time *t* and line rate *r.*

Therefore, the new MILP model with data compression and MLR can be defined as:

Objective: minimise

$$\sum_{t\in T}\Bigg(\sum_{s\in N}\sum_{d\in N:s\neq d}\lambda^{sdt}\cdot P_c^{sdt} + \sum_{i\in N}\sum_{j\in N:i\neq j}\sum_{r\ in\ R}PR_r\cdot C_{ijtr} + \sum_{m\in N}\sum_{n\in Np_m}\sum_{r\ in\ R}PT_r\cdot\omega_{mntr} + \sum_{m\in N}\sum_{n\in Np_m}\Big(PE\cdot EA_{mn}\cdot f_{mn} + PG\cdot EG_{mn}\cdot f_{mn}\Big) + \sum_{i\in N}PO_i + \sum_{i\in N}PMD\cdot DM_i\Bigg) \tag{8-30}$$

Subject to:

Constraints (8-15), (8-20) and (8-21)

$$\sum_{s\in N}\sum_{d\in N:s\neq d}\lambda_{ijt}^{sd} \leq \sum_{r\ in\ R}B_r\cdot C_{ijtr} \tag{8-31}$$

$$\forall\ t\in T, \forall\ i,j\in N: i\neq j$$

$$\sum_{n\in Np_m}W_{mntr}^{ij} - \sum_{n\in Np_m}W_{nmtr}^{ij} = \begin{cases} C_{ijtr} & if\ m=i \\ -C_{ijtr} & if\ m=j \\ 0 & otherwise \end{cases} \tag{8-32}$$

$$\forall\ t\in T, r\in R, \forall\ i,j,m\in N: i\neq j$$

$$\sum_{i\in N}\sum_{j\in N:i\neq j}\sum_{r\ in\ R}W_{mntr}^{ij} \leq W\cdot f_{mn} \tag{8-33}$$

$$\forall\ t\in T, \forall\ m\in N, n\in Np_m$$

$$\sum_{i\in N}\sum_{j\in N:i\neq j}W_{mntr}^{ij} = \omega_{mntr} \tag{8-34}$$

$$\forall\ t\in T, r\in R, \forall\ m\in N, n\in Np_m$$

8.6.2 Results and Analysis

To evaluate the power consumption of the network when data compression and MLR are used, we assume that there are three possible line rates: 10 Gbit/s, 40 Gbit/s and 100 Gbit/s. The power consumption of the network devices according to different line rate are discussed in [230].

At first, we study the optimal data compression ratio in optical networks with different fixed line rates. Fig 8-13, Fig 8-14 and Fig 8-15 give the average optimal data compression ratio at different times of the day at different line rates under the bypass and non-bypass approaches when β has different values. From these three figures the variation of the optimal data compression ratio at different times of the day increases with the line rate, especially at times when the traffic demand is low. For example, in Fig 8-15, from 2 am to 10 am, the variation of the optimal data compression ratio is larger than other times of the day. When the line rate is large the data compression ratio is more sensitive to capacity sharing of the optical link and a slight increase in the data compression ratio has more affect on the traffic grooming, especial when traffic demand is low.

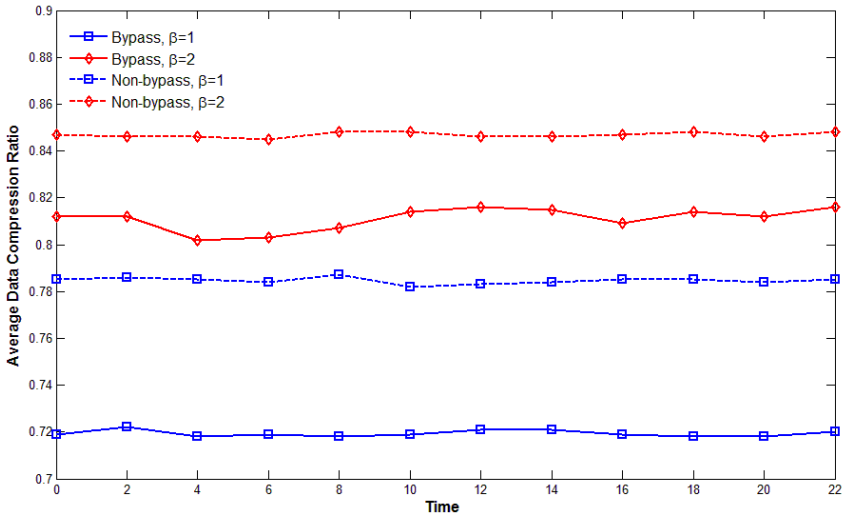

Fig 8 - 13: The average optimal data compression ratio of the network at different times of a day under the bypass and non-bypass approaches when line the rate is 10 Gbit/s

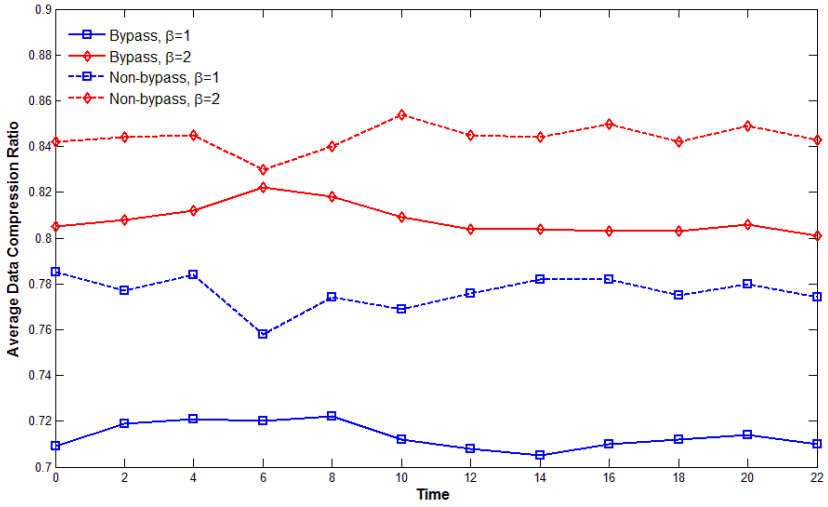

Fig 8 - 14: The average optimal data compression ratio of the network at different times of a day under the bypass and non-bypass approaches when the line rate is 40 Gbit/s

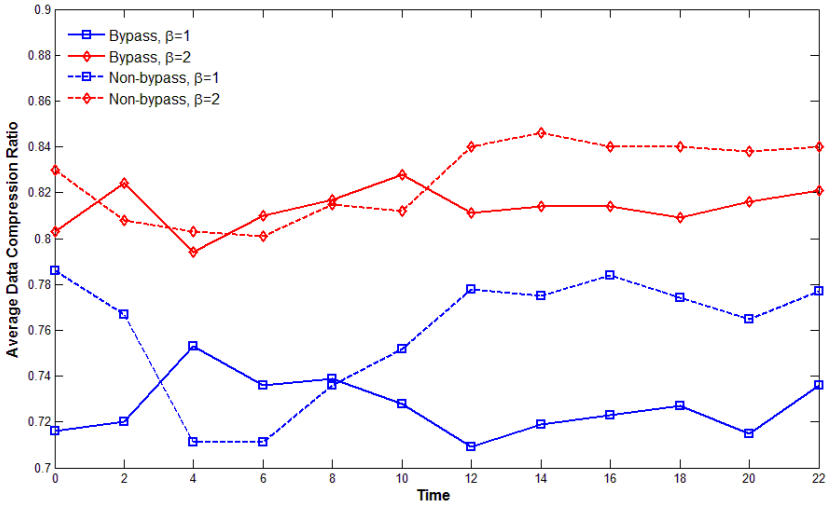

Fig 8 - 15: The average optimal data compression ratio of the network at different times of a day under the bypass and non-bypass approaches when the line rate is 100 Gbit/s

In Fig 8-16, the optimal data compression ratio of the optical network with MLR is evaluated. Compared to the optimal data compression ratio of the network with fixed line rate in Fig 8-13, Fig 8-14 and Fig 8-15, the variation of the optimal data compression ratio of the network with MLR is smaller. This is because after data compression, the MILP model can find the most suitable line rate for each node pair traffic demand consequently reducing the sensitivity of traffic grooming on the data compression ratio.

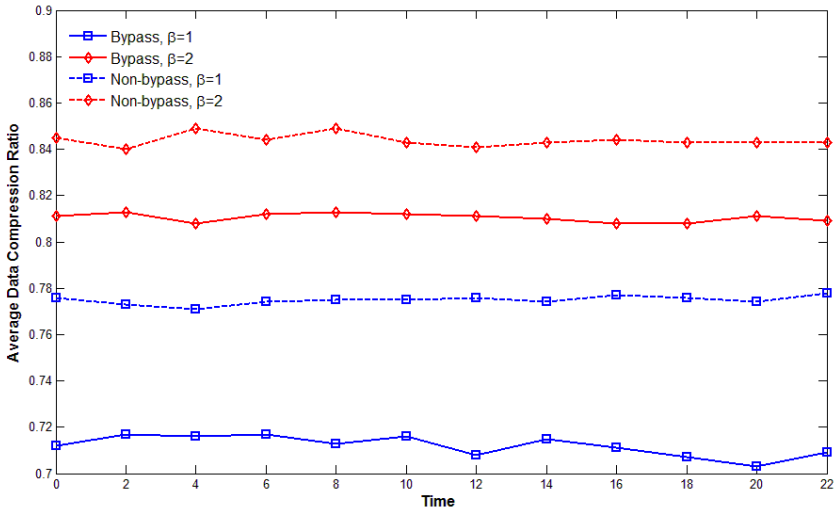

Fig 8 - 16: The average optimal data compression ratio of the network at different time of a day under the bypass and non-bypass approaches with MLR

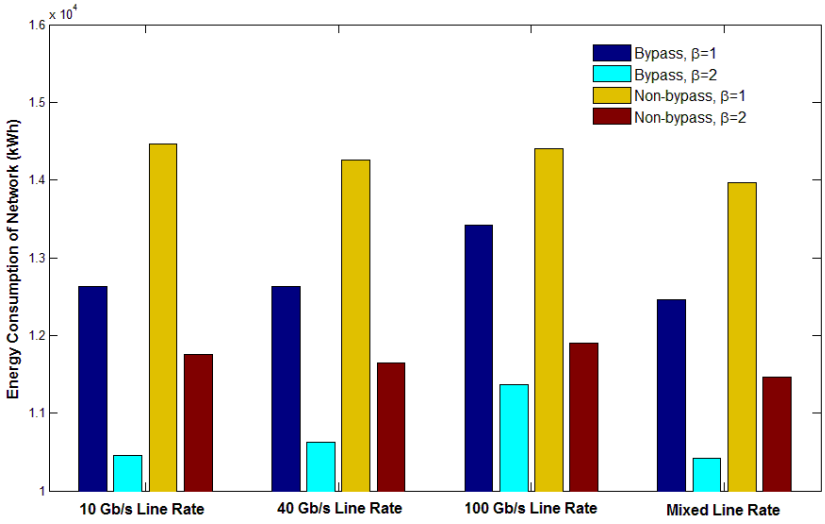

Fig 8 - 17: The energy consumption of the network with data compression under the bypass and non-bypass approach using fixed line rate and MLR

Fig 8-17 gives the energy consumption of the network with data compression under the bypass and non-bypass approach using fixed line rate and MLR. When using fixed line rate the low utilisation of bandwidth in the 100 Gbit/s line rate results the highest energy consumption of the network compared to 10 Gbit/s and 40 Gbit/s with increasing the energy consumption of the network up to 9% and 7%, respectively. With using MLR, the energy consumption of the network under the bypass and non-bypass approach is lower than that of the fixed line rate. Especially compared to the energy consumption of the network using 100 Gbit/s line rate, the maximum saving is up to 8%.

8.7 Summary

This chapter has investigated the energy efficiency of data compression in IP over WDM networks. The power consumption of data compression was given as a function of the compression ratio and the compression algorithm efficiency represented by β. Through analysing the relationship among ICR_c, data compression ratio and BER of optical channel, it has been shown that the increase in the ICR_c caused by data compression can be compensated by either increasing the transmit power or limiting the data compression ratio. A MILP model was proposed to minimise the network power consumption by optimising the data compression ratio for traffic demands considering different IP over WDM approaches (bypass and non-bypass). An energy-efficient data compression approach and a routing heuristic have also been proposed.

We have analysed the power consumption of IP over WDM networks considering a mixture of traffic (video, images and text) to reflect the global Internet traffic. The results also show that optimising data compression in bypass IP over WDM networks and increasing the transmit power to maintain for the ICR_c has saved up to 29% and 39% of the network power consumption for $\beta = 1$ and $\beta = 2$, respectively. Under the non-bypass approach the power savings have increased to 55%. The energy-efficient data compression heuristic has achieved comparable power savings. Limiting the data compression ratio to maintain the ICR_c has resulted in limited reduction in the power savings associated with data compression.

Finally, we evaluated the energy consumption of the IP over WDM network with data compression using fixed line rate and MLR. The results show that with MLR, the energy consumption of the network is the lowest and the variation of the optimal data compression ratio is the smallest.

The energy efficient optical networks proposed in previous chapters were based on the standard ITU WDM technology with low spectrum efficiency. If we can improve spectrum efficiency, the power consumption of network devices will be reduced by improving their bandwidth utilisation. In the next chapter, we will introduce a new energy efficient optical network architecture which is based on Orthogonal Frequency-Division Multiplexing (OFDM) technology.

Chapter 9: Energy Efficient Elastic Optical Networks

9.1 Introduction

Although WDM technologies introduce several desirable features, the rigid nature and coarse granularity of WDM networks results in inefficient capacity utilisation because of the bandwidth mismatch between the application layer with bandwidth requirements varying from several Mbit/s to hundreds of Gbit/s, and the wavelength channels with data rates of 10 Gbit/s and beyond. Current WDM networks address this mismatch by allowing sub-wavelength granularity connections to be groomed onto a single lightpath which results in extra cost and power consumption [231], or by allocating multiple wavelengths to a connection if the requested bandwidth is higher than that of a single wavelength, however, such an approach suffers from low spectral efficiency as adjacent wavelengths must be separated by guard bands.

A promising solution to address this bandwidth mismatch is to support fine granularity through elastic spectrum allocation [232], [233] where connection requests are allocated the minimum spectral resources required. Recently, Orthogonal Frequency-Division Multiplexing (OFDM) has been proposed as an enabling technique for elastic optical networks [234]. OFDM is a multi-carrier modulation technique where data is distributed over multiple orthogonal low rate subcarriers [235]. Optical OFDM helps alleviate many of the drawbacks associated with single carrier systems. Fig 9-1 compares the spectrum utilisation of WDM networks and OFDM-based optical networks. Optical OFDM-based networks

support a higher spectral efficiency as they can exactly provide the bandwidth needed to cater for the requirement of building a link of a certain traffic rate and consequently, the relevant network components can work at the required rate. In contrast to the conventional WDM where frequency guard bands are required between adjacent subcarriers, OFDM improves the spectrum utilisation by allowing the spectrum of adjacent subcarriers to overlap as orthogonality ensures the separation of subcarriers at the receiver side [235].

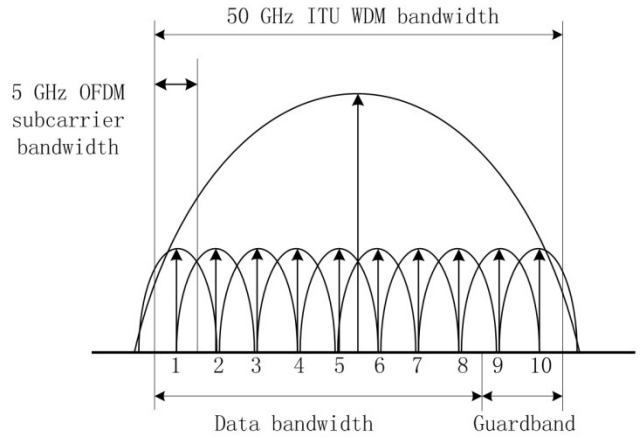

Fig 9 - 1: Spectrum utilisation of WDM networks and optical OFDM-based networks

In conventional optical networks the available capacity is limited to the worst-case optical path design to ensure Quality of Transmission (QoT). However, optical paths of higher Optical Signal-to-Noise Ratios (OSNR) (usually associated with shorter reach) can support significantly higher capacities. Optical OFDM supports distance-adaptive spectrum allocation by adapting the modulation format according to the end-to-end physical conditions of the optical path [236], [237]. Moreover, OFDM is an effective solution to the Inter-Symbol Interference (ISI) caused by a dispersive channel. The parallel transmission of data results in a longer symbol period compared to single carrier systems with similar total data rates, limiting the ISI effect to a small fraction of a symbol period.

A number of papers in the literature have studied the energy-efficiency of OFDM-based wireless systems, e.g. [238], [239]. However, the power savings introduced by optical OFDM-based networks is not a well investigated topic. In this chapter, the energy efficiency of optical OFDM-based networks is investigated. Optical OFDM-based networks are compared to conventional IP over WDM networks with different wavelength rates (10/40/100Gbit/s). Optical OFDM-based

networks are also compared to Mixed Line Rate (MLR) networks where wavelengths of different rates are deployed over the same fibre. In addition to the symmetric traffic profile, the energy efficiency of optical OFDM-based networks in an asymmetric traffic scenario where more traffic is destined to or originates from popular nodes, e.g. data centres, is also considered.

9.2 OFDM-based Optical Networks

9.2.1 Optical OFDM System

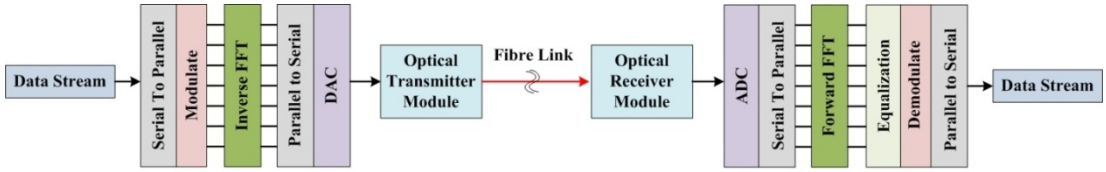

Fig 9 - 2: Block diagram of a typical optical OFDM communication system

Fig 9-2 illustrates the block diagram of a typical optical OFDM system. At the transmitter side, the serial-to-parallel (S/P) module converts the incoming high-bit-rate data stream to low-bit-rate parallel blocks of symbols. The symbols are mapped by some type of Quadrature Amplitude Modulation (QAM) or Phase-Shift Keying (PSK) onto orthogonal carriers with equally spaced frequencies. The time-domain OFDM symbols are obtained by Inverse Fast Fourier Transformation (IFFT). To mitigate ISI between OFDM symbols, a guard time, known as Cyclic Prefix (CP), is added to each OFDM symbol by copying the end of the block generated by the IFFT to the beginning of the block. A Cyclic Prefix (CP) longer than the channel impulse response or multipath delay can eliminate the ISI, maintaining the orthogonality between subcarriers [235]. After adding of the CP, the discrete parallel symbols go through parallel-to-serial (P/S) conversion and Digital-to-Analog Conversion (DAC) to generate a continuous time domain signal. In the Optical Transmitter Module (OTM), electrical OFDM signals are modulated over an optical carrier using a Directly Modulated Laser (DML) or an Externally Modulated Laser (EML) [240]. EML is used to support high data rate and long-distance communication systems. The most used EML is the Mach-Zehnder Modulator (MZM) [241]. There are two

main methods for modulating the optical OFDM signal: Intensity Modulation (IM) and Linear Field Modulation (LFM) [235], [241]. IM is used for systems with different optical modes, e.g. multimode fibre systems and optical wireless systems, while LFM is used for system where only one mode of the optical signal is received, e.g. signal mode fibre.

At the Optical Receiver Module (ORM), the optical OFDM signal detection systems can be classified as: Direct Detection (DD) and Coherent Detection (CO-D) [235], [242], [240]. Typically, DD is used for IM systems and CO-D is used for LFM systems. DD-OOFDM is a suitable solution for cost-effective short-reach systems. Compared to CO-D based optical OFDM (CO-D-OOFDM), DD based optical OFDM (DD-OOFDM) has a simpler receiver, however, the spectral efficiency is reduced with DD-OOFDM as guard bands between the optical carrier and the OFDM subcarriers are needed to eliminate the interference caused by unwanted mixing products. In addition, DD-OOFDM requires extra optical power for the transmitted carrier. On the other hand CO-D-OOFDM performs better in terms of optical signal-to-noise ratio (OSNR) requirements and has higher spectral efficiency. In addition, CO-D-OOFDM has been proved by to be a simple and effective way to eliminate chromatic dispersion for long-haul single-mode fibre systems. However, CO-D requires a laser oscillator and polarisation control and needs to generate the carrier locally. Also it is very sensitive to phase noise of the oscillator. The performance of both detection systems is further investigated in [243], [244] to mitigate their limitations.

To recover data from the orthogonal subcarriers, the serial signal is converted to parallel data blocks, the CP is removed and the OFDM signal is converted back to the frequency domain using forward FFT. At the receiver side, the information symbols are affected by signal phase and amplitude level shifting caused by chromatic dispersion of the optical channel. Therefore, equalisation is needed after the forward FFT to obtain an OFDM signal without forward error [235], [240]. Note that equalisation is simpler in OFDM systems compared to single carrier systems. This is because OFDM symbols are typically longer than the maximum channel delay spread and therefore can be easily equalised. After equalisation, each subcarrier is demodulated and data is converted to serial.

9.2.2 Modulation Level and QoT

As mentioned in Section 9.1, OFDM supports distance-adaptive spectrum allocation. This advantage stems from the fact each OFDM subcarrier can be processed individually. Unlike conventional fixed hardware implementations, in OFDM the signal properties can be easily changed by software as digital signal processing is implemented at both the receiver and the transmitter ends. Therefore, the modulation format can be adapted according to the end-to-end physical condition of the optical path [236]. In terms of OSNR, which is mostly associated with distance, we can add an extra bit per symbol for every 3 dB gain in OSNR. Therefore we can make use of the flexibility offered by OFDM to adapt the modulation level of subcarriers to increase the available capacity. The link capacity (C) is given as a function of the link length [236]:

$$C = \frac{C_0}{2}\left(1 + \log_2 \frac{2 \cdot l_0}{l}\right) \quad l \leq 2 \cdot l_0 \tag{9-1}$$

where l_0 is the maximum distance, C_0 is the capacity associated with the worst-case optical path (path with the maximum distance) and l is the link length. Note that the OSNR improves by 3 dB as the transmission distance decreases to half, allowing the modulation format to increase by 1 bit/symbol, e.g. 8-QAM (3 bit per symbol) can be used instead of QPSK (2 bit per symbol) or 16-QAM (4 bit per symbol) can be used instead of 8-QAM.

9.2.3 Power Consumption of optical OFDM-based Network Devices

As discussed in the previous sections, optical OFDM-based networks provide flexible bandwidth by supporting the allocation of a variable number of subcarriers and adapting the modulation level of subcarriers to increase the available capacity, resulting in significant reduction in the power consumption of the whole network. To enable bandwidth flexible transmissions, the fixed-bandwidth components used for WDM networks need to be replaced with network components that can work at flexible rates. In this section, we study the power consumption of the different network components in an optical OFDM-based network and compare it to the power consumption of the same components in IP over WDM networks. We

consider the three most power consuming components: IP ports, transponders and erbium doped fibre amplifiers (EDFAs).

As the electronic processing of OFDM signals is implemented in the transponder, the IP over optical OFDM network can use IP router ports in the IP layer similar to those used in IP over WDM networks.

The large gain bandwidth of EDFAs makes them useful for WDM networks as a single EFDA can simultaneously amplify many data channels at different wavelengths within its gain region [245]. Similarly EDFAs can be used in OFDM-based optical networks.

In addition to the ability to allocate variable number of subcarriers and modulate each subcarrier individually, OFDM transponders need to perform IFFT and FFT processes. The power consumption of the OFDM transponder mainly depends on the electronic processing, modulation level and the number of subcarriers. The highest power consumption of the OFDM transponder occurs when an optical OFDM signal uses the maximum number of subcarriers with the highest modulation level. The power consumption of the OFDM transponder is calculated by adding the power consumption of the different modules in Fig 9-2. In Section 9.4, the details of the OFDM transponder power consumption are given. We assume OFDM transponders to have an ALR power profile [126].

9.3 Mathematical Model for Optical OFDM-based Networks

In this section we develop a MILP model to minimise the power consumption of the IP over optical OFDM networks. The MILP model is based on the following assumptions:

1. Traffic demands utilise a continuous spectrum, i.e. a contiguous set of subcarriers (spectrum continuity constraint) [237]. To maintain the spectrum continuity constraint, the traffic between a node pair is not allowed to split.

2. The maximum number of subcarriers that the OFDM transponder can process is limited.

3. As discussed in Section 9.2.2, the maximum modulation level of the traffic demand between different node pairs depends on the OSNR which is mostly associated with transmission distance. In this model, we assume that optical OFDM-based networks support three modulation levels: BPSK, QPSK and 8QAM. To achieve the maximum spectrum efficiency, OFDM transponders modulate the subcarriers of a traffic demand using the highest modulation level allowed.

4. There is no need to do the grooming in the IP layer as the flexibility of OFDM can provide each traffic demand with the exact data rate needed [242].

Before introducing the model, the following parameters are defined:

λ^{sdt} The traffic demand between node pair (*s, d*) at time *t,*

EA_{mn} The number of EDFAs on physical link (*m, n*) Typically $EA_{mn} = \lfloor L_{mn}/S - 1 \rfloor + 2$, where S is the distance between two neighbouring EDFAs [58],

C_r The capacity of a single subcarrier using modulation level *r,*

Np_i The neighbouring nodes set of node *i,*

PR Power consumption of an IP router port per 1 Gbit/s,

PE Power consumption of an EDFA,

B The maximum number of wavelengths on an optical fibre,

NSC The maximum number of subcarriers supported by an OFDM-transponder,

Pt^r The power consumption of the single subcarrier of OFDM transponder using modulation level *r,*

R The set of modulation levels.

The following variables are also defined:

ns_r^{sdt} The number of OFDM subcarriers using modulation level *r* of the traffic demand (*s, d*) at time *t,*

NS_{mnr}^{sdt} The number of OFDM subcarriers using modulation level *r* of demand (*s, d*) that traverse physic link *(m, n)* at time *t,*

ω_{mnt}^{sd} $\omega_{\mathrm{mnt}}^{\mathrm{sd}}$=1 if the OFDM subcarriers of traffic demand (*s, d*) traverse physical link (*m, n*) at time *t*, otherwise $\omega_{\mathrm{mnt}}^{\mathrm{sd}}$=0,

NF^{mnt} The number of fibres on physical link (*m,n*) at time *t.*

The network total power consumption is composed of:

1) The power consumption of router ports:

$$\sum_{s\in N}\sum_{d\in N:s\neq d}\lambda^{sdt}\cdot PR \tag{9-2}$$

2) The power consumption of EDFAs:

$$\sum_{m\in N}\sum_{n\in Np_m}NF^{mnt}\cdot EA_{mn}\cdot PE \tag{9-3}$$

3) The power consumption of OFDM transponders:

$$\sum_{s\in N}\sum_{d\in N:s\neq d}\left(\sum_{m\in N}\sum_{n\in Np_m}\left(ALR\left(\frac{\sum_{r\in R}NS_{mnr}^{sdt}\cdot C_r}{LR_{\max}}\right)\cdot PT_{\max}\right)\right) \tag{9-4}$$

where the *ALR()* means the energy profile function of ALR.

Following the discussion in Section 9.2.3, we consider OFDM transponders to have an ALR power consumption profile where the power consumption is dependent on the load, i.e. number of subcarriers used. The maximum power consumption of transponders is PT_{max} working at the maximum line rate LR_{max}. For example, a traffic demand of 100 Gbit/s with BSK modulation will require 2 OFDM

transponders working at the maximum line rate (40 Gbit/s) and 1 transponder working at 20Gbit/s. As discussed in Section 9.2.2, the maximum line rate the OFDM transponder can support depends on the distance between source and destination node pair.

The model is defined as follows:

Objective Function:

Minimise

$$\sum_{t\in T}\left(\sum_{s\in N}\sum_{d\in N:s\neq d}\lambda^{sdt}\cdot PR + \sum_{s\in N}\sum_{d\in N:s\neq d}\left(\sum_{m\in N}\sum_{n\in Np_m}\left(ALR\left(\frac{\sum_{r\in R}NS_{mnr}^{sdt}\cdot C_r}{LR_{\max}}\right)\cdot PT_{\max}\right)\right)+\sum_{m\in N}\sum_{n\in Np_m}NF^{mnt}\cdot EA_{mn}\cdot PE\right) \quad (9\text{-}5)$$

Subject to:

1) *Flow conservation constraint in the optical layer:*

$$\sum_{n\epsilon Np_m}\omega_{mnt}^{sd}-\sum_{n\epsilon Np_m}\omega_{nmt}^{sd}=\begin{cases}1 & m=s\\ -1 & m=d\\ 0 & otherwise\end{cases} \quad (9\text{-}6)$$

$$\forall\, s,d,m\epsilon N: s\neq d, t\epsilon T$$

Constraint (9-6) gives the flow conversion in optical layer and ensures that traffic demands are not allowed to split.

2) Capacity constraints:

$$\lambda^{sdt}\leq\sum_{r\in R}ns_r^{sdt}\cdot C_r \quad (9\text{-}7)$$

$$\forall\, s,d\epsilon N: s \neq d, t\epsilon T \text{ (Power-minimised)}$$

$$\lambda^{sdt} \leq \sum_{r\in Rmax} ns_r^{sdt} \cdot C_r$$

$$\forall\, s,d\epsilon N: s \neq d, t\epsilon T \text{ (Spectrum-minimised)}$$

Constraint (9-7) ensures that the capacity of the subcarriers allocated to a traffic demand is large enough to support the traffic demand. In this constraint, we differentiate between two optimisation problems: power-minimised and spectrum-minimised optical OFDM-based networks. In power-minimised optical OFDM-based networks, the MILP model will select the modulation level that minimises the power consumption of the network. However, this will lead the model to choose the lowest possible modulation level to fit the traffic demand with best granularity. In spectrum-minimised optical OFDM-based networks, the highest modulation level will always be used, and then the total bandwidth of the subcarriers will be minimised.

3) Number of transponders constraint:

$$\sum_{n\epsilon Np_m} NS_{mnr}^{sdt} - \sum_{n\epsilon Np_m} NS_{nmr}^{sdt} = \begin{cases} ns_r^{sdt} & m = s \\ -ns_r^{sdt} & m = d \\ 0 & otherwise \end{cases} \quad (9\text{-}8)$$

$$\forall\, s,d,m\epsilon N: s \neq d, r \in R, t\epsilon T$$

Constraint (9-8) ensures that for each traffic demand, the number of OFDM subcarriers of modulation level *r* entering node *m* is equal to the number of the subcarriers of modulation level *r* leaving from node *m*. This is the conversion for the number of OFDM subcarriers of modulation level *r*.

4) *Physical link capacity constraints:*

$$NS_{nmr}^{sdt} \geq 0 \quad (9\text{-}9)$$

$$\forall\, s,d,m\epsilon N, n\epsilon Np_m: s \neq d, r \in R, t\epsilon T$$

$$NS_{nmr}^{sdt} \leq \omega_{nmt}^{sd} \cdot NMAX$$

$$\forall\, s, d, m \epsilon N, n \epsilon N p_m : s \neq d, r \in R, t \epsilon T \tag{9-10}$$

$$NF^{mnt} \cdot B \geq \sum_{s \in N} \sum_{d \in N: s \neq d} \left(\sum_{r \in R} NS_{nmr}^{sdt} / NSC \right)$$

$$\forall\ t \epsilon T, m \epsilon N, n \epsilon N p_m \tag{9-11}$$

Constraints (9-9) and (9-10) guarantee that the value of the variable NS_{nmr}^{sdt} is related to the value of the binary variable, where NMAX is a large enough number. Constraint (9-11) ensures that the number of OFDM wavelengths allocated to a traffic demand does not exceed the number of wavelength in an optical fibre.

9.4 Results and Analysis

The NSFNET network is considered, depicted in Fig 4-4 in Chapter 4, to evaluate the power consumption of the optical OFDM-based network. The same average traffic demand as Chapter 4, shown in Fig 4-5, is used.

We compare the power consumption of optical OFDM-based networks to conventional WDM networks. We assume that both systems have a channel bandwidth of 50 GHz (as in Fig 9-1). The maximum number of subcarriers for each OFDM channel is 10 each of 5 GHz and 2 of the channels are used as guard bands. We consider 8 QAM as the highest modulation level for optical OFDM, therefore, the maximum line rate for an OFDM transponder LR_{max} is: 5 (GHz)×3 (Bit/Hz) × 8=120 Gbit/s.

For the WDM network, we consider three different wavelength capacities: 10 Gbit/s, 40 Gbit/s and 100 Gbit/s and assume BPSK as the modulation level associated with the maximum transmission distance l in the NSFNET network between node 1 and node 14.

For the optical OFDM-based network the maximum capacity of each subcarrier for different transmission distance C_r is calculated from Equation (9-1) considering C_o as the capacity of BPSK. Note that C_r can only be the capacity associated with BPSK, QPSK and 8 QAM, and the C calculated from Equation (9-1) gives the upper bound.

Table 9-1 shows the network parameters in terms of number of wavelengths, wavelength rate, distance between two neighbouring EDFAs, and power consumption of different components in the WDM network. Given the power consumption of the 40 Gbit/s Cisco's 8-slot CRS-1 [144] as 1 kW per port and considering a linear power consumption profile based on DVFS [246], the router port power consumption per Gbit/s is calculated as 25 W/Gbit/s. This value is used to calculate the power consumption of the 10 Gbit/s and 40 Gbit/s WDM router ports and the OFDM router ports working at flexible rates.

The power consumption of the 10 Gbit/s and 40 Gbit/s WDM transponders is derived from Cisco ONS 15454 10 Gbps Multirate Transponder Card [247] and Cisco ONS 15454 40 Gbps multi-rate transponder card [248], respectively. The power consumption of the 100 Gbit/s WDM transponder is calculated based on the ratio between the power consumption of the 40 Gbit/s WDM transponder and the 100 Gbit/s WDM transponder given in [249]. The power consumption of EDFAs is derived from Cisco ONS 15501 EDFA [188].

Distance between two neighbouring EDFAs	80 (km)
Capacity of each wavelength	40 (Gbit/s)
Power consumption of a WDM router port	25 (W/Gbit/s)
Power consumption of a WDM transponder (10Gbit/s)	45 (W)
Power consumption of a WDM transponder (40Gbit/s)	73 (W)
Power consumption of a WDM transponder (100Gbit/s)	135 (W)
Power consumption of an EDFA	8 (W)

Table 9 - 1: Input data for the simulation

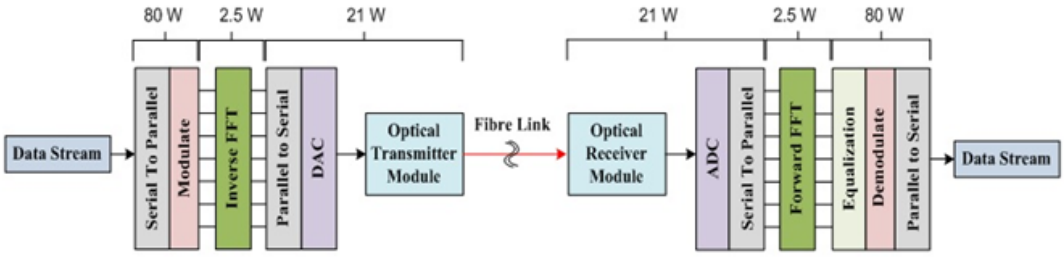

Fig 9 - 3: Power consumption of different parts of an OFDM transponder

We calculate the power consumption of an OFDM transponder working at the maximum rate of 120 Gbit/s based on the structure shown in Fig 9-3. A DSP module performs S/P conversion and modulation at the transmitter side and another DSP module performs equalisation, demodulation and P/S conversion at the receiver side. As shown in Fig 9-3, the power consumption of the DSP module is estimated as 80W [250]. In addition, state-of-the-art parallel optical interconnects were shown to operate with less than 5 mW/Gbit/s total power consumption [251]. The power consumption of the IFFT and FFT modules is estimated as 0.4 mW/Gbit/s [252]. The power consumption of the P/S, DAC and the optical transmitter module is estimated as 21 W [253]. Also the power consumption of the optical receiver module and the ADC and S/P is estimated as 21 W. We estimate the power consumption of OFDM transponders working at lower rates by assuming ALR power consumption profiles: linear and cubic [126]. Table 9-2 gives the details of the OFDM transponder according to different modulation levels with linear energy profile.

Reach	Modulation format	Data Rate	Power Consumption			
			DSP	IFFT/FFT	DAC/ADC	Total
500 km [254]	8QAM	120 Gbit/s	160 W	2448 mW	42 W	204.4 W
1000 km [254]	QPSK	80 Gbit/s	106 W	1632 mW	28 W	136.3 W
2000 km [254]	BPSK	40 Gbit/s	53 W	816 mW	14 W	68.1 W

Table 9 - 2: Power consumption of OFDM transponder

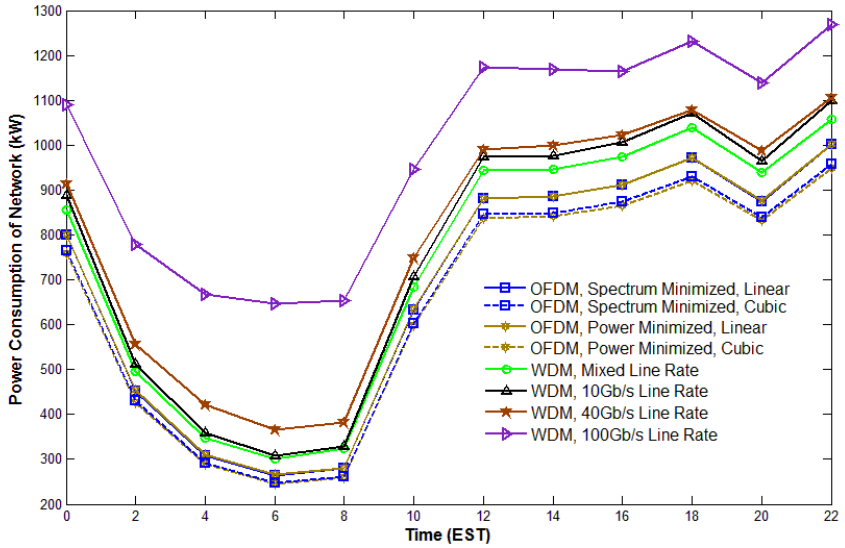

Fig 9 - 4: The network total power consumption considering optical OFDM and conventional WDM under a symmetric traffic demand and the bypass approach

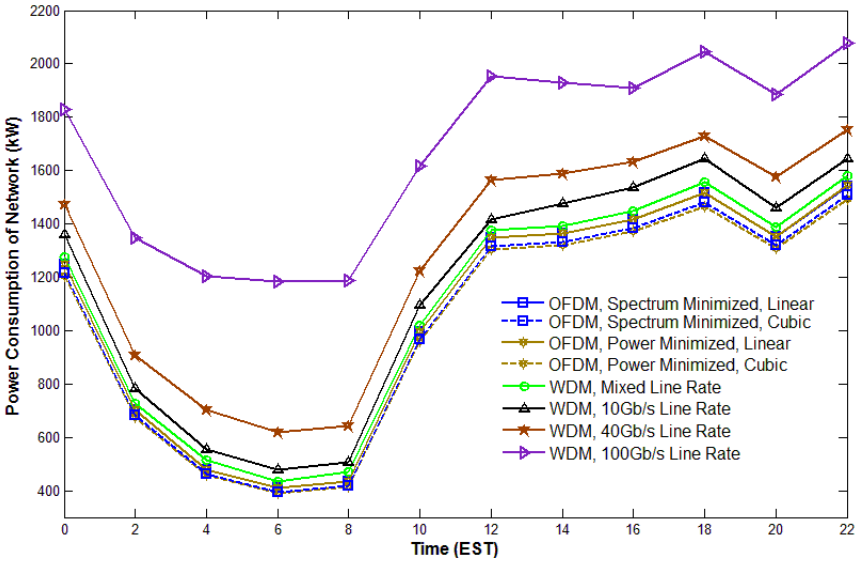

Fig 9 - 5: The network total power consumption considering optical OFDM and conventional WDM under a symmetric traffic demand and the non-bypass approach

Considering the symmetric traffic profile in Fig 4-5 the network power consumption is shown in Fig 9-4 and Fig 9-5. Under the bypass approach (Fig 9-4), the power minimised optical OFDM-based network with linear energy profile for OFDM transponders saves 10%, 14% and 31% of the network power consumption compared to WDM networks deploying wavelength capacities of 10 Gbit/s, 40 Gbit/s and 100Gbit/s, respectively. Similar power savings are achieved by the spectrum-minimised with linear energy profile scheme. The maximum saving is achieved compared to the IP over WDM network with the 100 Gbit/s wavelength

rate as the larger wavelength granularity results in lower utilisation of the IP router ports and transponders and consequently lower power consumption as the power consumption of IP router ports the most energy consuming devices in the network) increases linearly as the capacity increases. However this is not the case for transponders as discussed below.

As a result of the higher efficiency of MLR networks compared to WDM networks deploying a single wavelength rate, the power savings achieved by the optical OFDM-based network compared to MLR networks is limited to 7% and 12% with linear and cubic energy profiles for OFDM transponders respectively.

Compared to linear energy profile for OFDM transponders, the power minimised optical OFDM-based network with cubic energy profile for OFDM transponders saves more power compared to WDM networks deploying wavelength capacities of 10 Gbit/s, 40 Gbit/s and 100 Gbit/s, with savings respectively of 15%, 18% and 34% of the network total power consumption. Similar power savings are achieved by spectrum-minimised with cubic energy profile OFDM transponders.

Similar savings are obtained under the non-bypass approach as seen in Fig 9-5. The total network power consumption is higher under the non-bypass approach as IP routers are required at intermediate nodes.

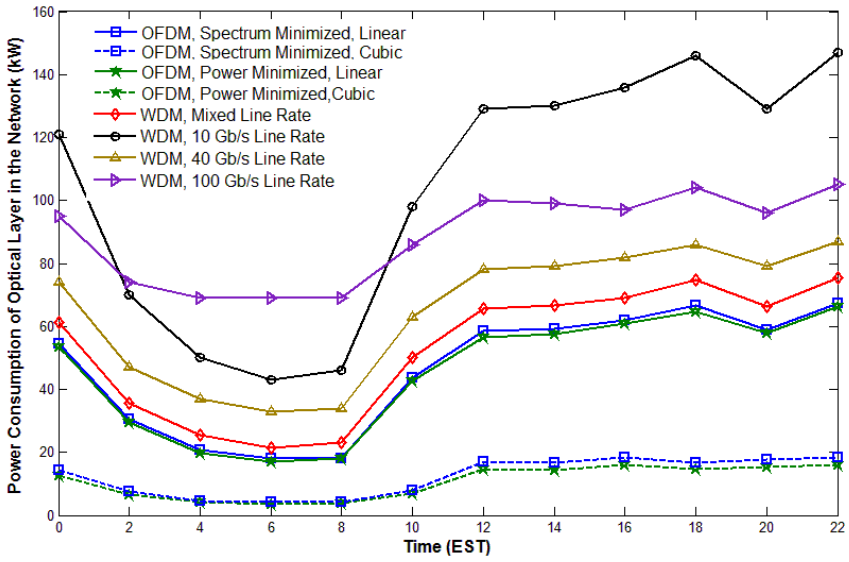

Fig 9 - 6: The optical layer power consumption considering optical OFDM and conventional WDM under a symmetric traffic demand and the bypass approach

To emphasise the power savings achieved by optical OFDM-based networks, Fig 9-6 shows the power consumption of the optical layer. The optical OFDM-based network with linear energy profile for OFDM transponders saves 55%, 29% and 48% of the optical layer power consumption compared to WDM networks deploying wavelength capacities of 10 Gbit/s, 40 Gbit/s, 100 Gbit/s, respectively, and with cubic energy profile for OFDM transponders, the savings are 89%, 83% and 88%. In the optical layer, the maximum saving is achieved compared to the WDM network with the 10 Gbit/s wavelength rate. This is because the power consumption of transponders does not increase linearly as the wavelength rate increases (see Table 9-1). Therefore deploying a 10 Gbit/s wavelengths to support a traffic demand with an average of 80 Gbit/s is less energy-efficient than deploying wavelengths of 40 Gbit/s and 100 Gbit/s. The difference in power consumption between the power-minimised and spectrum-minimised optical OFDM-based networks is limited to 1%.

In Fig 9-7 and Fig 9-8, we investigate the impact of the presence of data centres in the network (which creates a hot node scenario, where more traffic is destined to or originates from data centres) on the power saving achieved by optical OFDM-based networks. The following assumptions are considered:

1. Each node writes and retrieves data from all data centres equally and different data centres have different content.

2. In addition to the regular traffic demand, i.e. the traffic demand between regular nodes, we consider the traffic demand between data centres and regular nodes. The traffic demand between data centres and nodes at time *t* is assumed to be a certain ratio of the regular traffic demand λ^{sdt}.

3. The uplink traffic demand (from nodes to data centres) ratio, R_u, is smaller than the downlink traffic demand (from data centres to nodes) ratio, R_d. The traffic demand between nodes and data centres is generated based on the regular traffic demand in Fig 4-5 where we assume that R_u=0.3 and R_d=2.5. These values reflect the expected growth in data centre traffic.

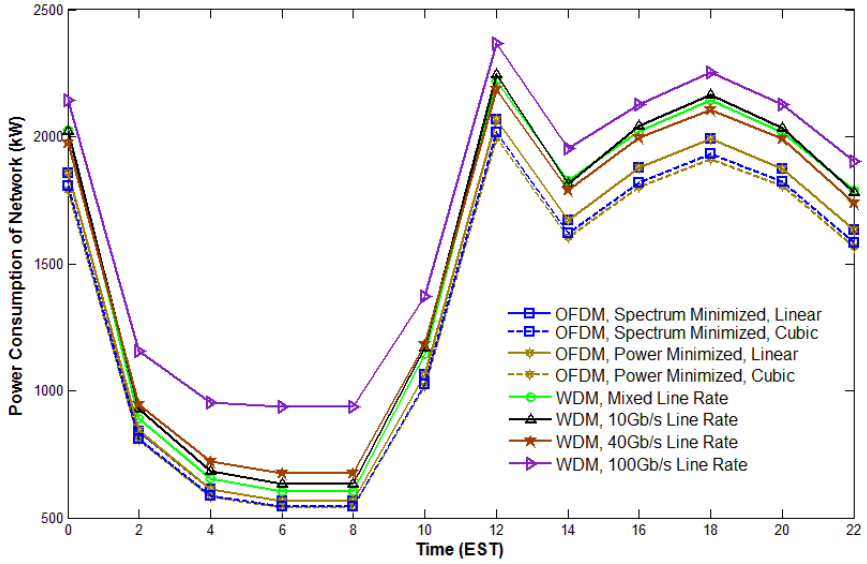

Fig 9 - 7: The network total power consumption considering optical OFDM and conventional WDM networks under an asymmetric traffic demand and the bypass approach

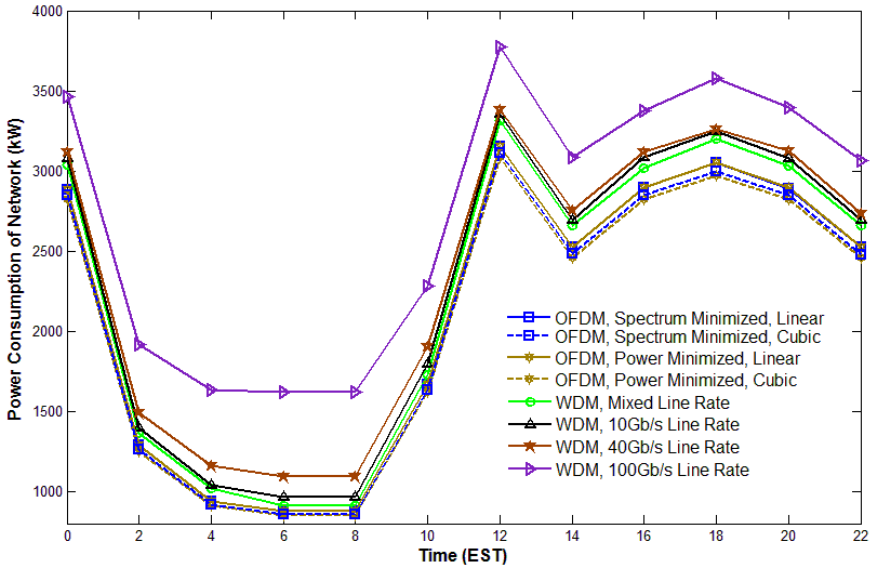

Fig 9 - 8: The network total power consumption considering optical OFDM and conventional WDM networks under an asymmetric traffic demand and the non-bypass approach

In Fig 9-7, the optical OFDM-based network with linear energy profile for OFDM transponders has saved 8%, 8%, 18% and 7% compared to WDM networks deploying wavelength capacities of 10 Gbit/s, 40 Gbit/s, 100 Gbit/s and MLR, respectively, under the bypass approach. The power consumption savings of the optical OFDM-based network with cubic energy profile for the OFDM transponder are 12%, 11%, 21% and 11%. The higher traffic demands between data centres and other nodes reduces the bandwidth wastage associated with the rigid bandwidth

allocation of conventional WDM networks and therefore the benefit the network gets from implementing flexible bandwidth allocation is limited. Similar savings are achieved under the non-bypass approach in Fig 9-8.

The total power savings achieved by optical OFDM depends on the assumptions made to calculate the power consumption of the OFDM transponders. As discussed above we estimated the power consumption of a 120 Gbit/s OFDM transponder based on the power consumption of different module parts with a linear and cubic ALR.

Fig 9-9 shows the network energy consumption versus a range of power consumptions for the 120 Gbit/s OFDM transponder. This figure can guide manufactures to the acceptable levels of power consumption for OFDM transponders after which the optical OFDM-based network will lose its advantage over conventional WDM networks. Assuming a linear profile to estimate the power consumption of elastic bandwidth OFDM transponders, the power consumption of the 120 Gbit/s OFDM transponder should not exceed 425 W.

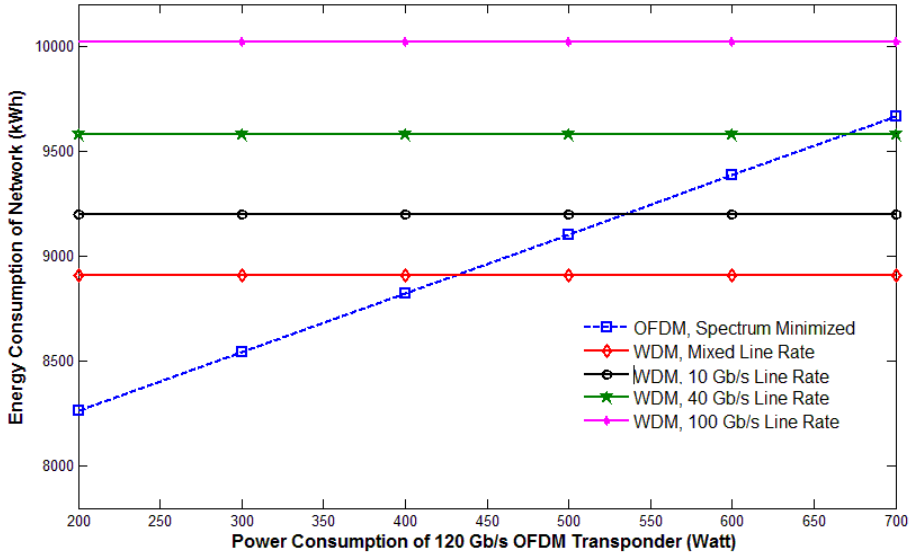

Fig 9 - 9: Network total energy consumption versus a range of OFDM transponder power consumptions

In Fig 9-10 and Fig 9-11, we investigate the spectral efficiency of optical OFDM-based networks. Under symmetric traffic (Fig 9-10), the spectrum-minimised optical OFDM uses 34% less subcarries compared to the power-minimised optical

OFDM. Under asymmetric traffic (Fig 9-11), the spectrum-minimised OFDM MILP model uses 45% less subcarries compared to the power–minimised.

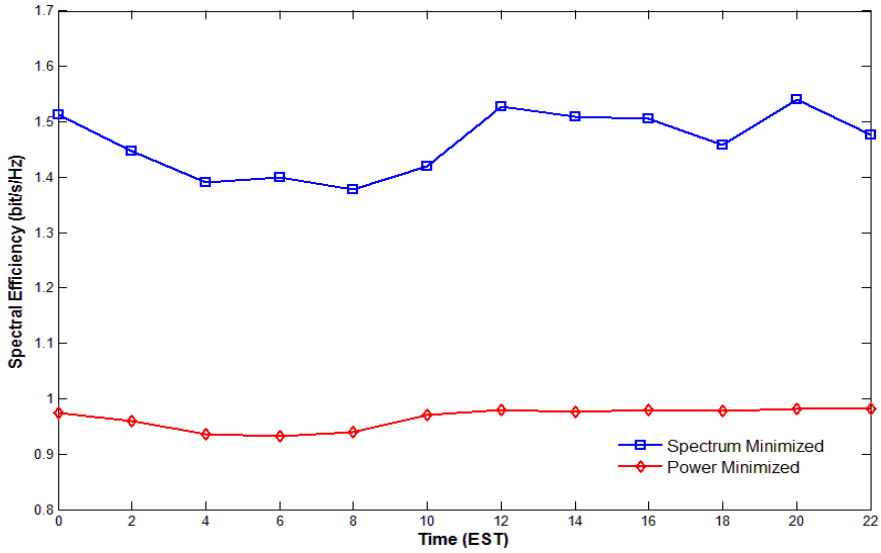

Fig 9 - 10: Spectral efficiency of optical OFDM-based networks under symmetric traffic demand

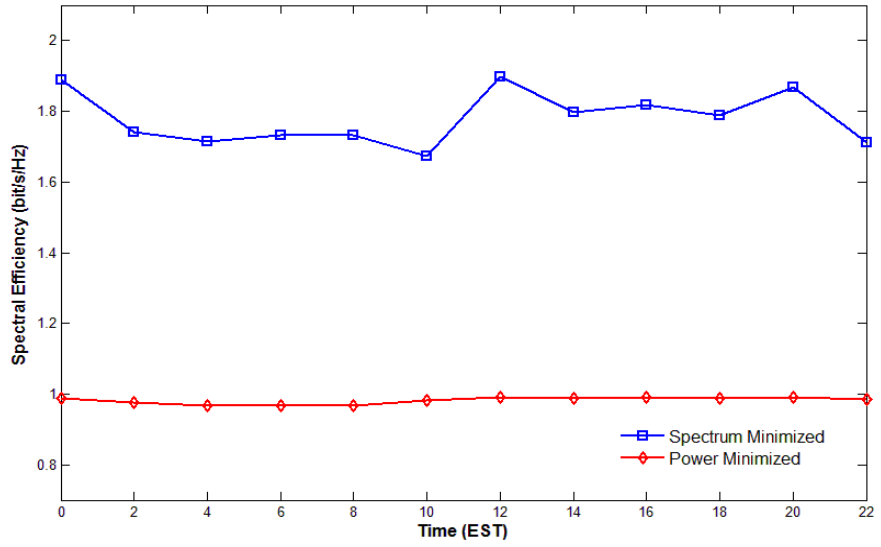

Fig 9 - 11: Spectral efficiency of optical OFDM-based networks under asymmetric traffic demand

Under symmetric traffic (Fig 9-10), the spectrum-minimised optical OFDM has 51% higher spectral efficiency compared to the power–minimised, however, as mentioned the spectrum-minimised consumes less than 1% more power compared to the power-minimised OFDM. Under asymmetric traffic (Fig 9-11) the difference in spectral efficiency between the two approaches increased to 81%.

9.5 Summary

In this chapter, we have studied the energy efficiency of optical OFDM-based networks. We have developed a MILP model to minimize the total power consumption of optical OFDM-based networks. In addition to flexible spectrum allocation, we have also considered distance-adaptive spectrum allocation. Considering a linear profile to estimate the OFDM transponder power consumption, the results show that optical OFDM-based networks under a symmetric traffic demand with linear energy profile for OFDM transponders have saved 10%, 14% and 31% of the network power consumption compared to conventional IP over WDM networks with 10 Gbit/s, 40 Gbit/s and 100 Gbit/s wavelength rate, respectively. With cubic energy profile for OFDM transponders, the saving are 15%, 18% and 34%. We have also compared optical OFDM-based networks to MLR networks and savings of 12% are achieved. Similar power savings are achieved by both the spectrum-minimised and power-minimised optical OFDM-based networks. Considering the power consumption of the optical layer, optical OFDM-based networks save up to 89%, of the optical layer power consumption. The results also show that the spectrum-minimised optical OFDM-based network is 51% and 81% more efficient than the power-minimised network under symmetric traffic and asymmetric traffic, respectively

Chapter 10: Conclusions and Future Work

This chapter summarises the main contributions and states the main conclusions of this thesis. In this thesis, we have investigated the problems of power consumption in optical networks to minimise the power consumption and the carbon emissions. The energy efficient optical network studies have been done mainly based on IP over WDM networks that are the major architecture used in current core networks. Different energy efficient architectures, routing protocols, physical topologies data transmission methods and relative novel MILP models have been proposed.

It has been shown that the use of renewable energy can reduce the non-renewable power consumption and consequently carbon emissions in the network. In Chapter 4, a hybrid-power IP over WDM network architecture was investigated. A novel MILP optimisation model was developed with the objective of minimising the non-renewable power consumption of the network rather than the conventional objective of minimising the total power consumption of the network. The nodes that have access to renewable energy can also be powered by non-renewable energy to guarantee QoS when the renewable energy output becomes low. The renewable energy can power the ports, transponders, optical switches, multiplexers and demultiplexers in a node. To overcome the drawback of using Multi-hop bypass heuristic in the hybrid-power IP over WDM network, we have proposed a new heuristic 'REO-hop' where the traffic flows are allowed to traverse as many nodes as possible that have access to renewable energy. This constraint may increase the propagation delay, to maintain QoS, only the two shortest-path routes are

considered. Due to the changing traffic pattern and the fact that the output power of renewable energy sources varies during different times of the day, the routing paths are dynamic. A simulator has been developed to evaluate the performance of the proposed routing heuristic and network architecture. Details of the design and implementation of the network simulator have been presented. Simulations have evaluated different scenarios: maximum solar power per node: 20 kW, 40 kW, 60 kW and 80 kW; scale of networks: NSFNET and USNET; and power profile of network devices: on-off, linear, cubic, $\log_{10}$ and $\log_{100}$.

We have also investigated the impact of the location of nodes that use renewable energy on the total non-renewable energy consumption. A novel MILP optimisation model was developed to optimise the selection of nodes using renewable energy. The results show that selecting nodes with higher solar power and non-renewable power consumption to locate renewable energy resources results in higher reductions in the total non-renewable energy consumption of the network. Furthermore, the effects caused by seasonal and weather conditions have been investigated. The results show that the non-renewable energy consumption of a network in December has increased compared to June, and on a cloudy day it increases compared to a clear sky day in June.

Chapter 5 investigated the power consumption associated with transporting data between data centres and end-users. Firstly, we have determined the optimal location of a single data centre or multiple data centres in an IP over WDM network so as to minimise the network's power consumption through novel MILP models. The optimal location of data centres was determined using MILP models and verified by simulations. We have considered different scenarios to optimise the data centres location and have considered the impact of network topology (regular and irregular), traffic profile (regular traffic and data centre traffic), upload and download rates (low rate and high rate), number of data centres (single data centre and multiple data centres). The impact of power minimisation on delay has also been investigated.

Secondly, we studied a replication scheme for content that has different popularity to minimise the power consumption through the use of a novel MILP model. Here we have considered 5 classes of content that have different levels of popularity and considered multiple data centres. The optimisation identified where to

store a data object that has a given popularity so that the network's power consumption is minimised. We have also developed a novel routing algorithm, Energy-Delay Optimal Routing (EDOR), to minimise the power consumption of the network under replication while maintaining QoS. In this routing algorithm, all the available paths to all the required data centres are checked and the required data centre with the shortest available path is selected in order to reduce the propagation delay. If sufficient capacity is not available in the virtual topology, a new virtual link is established between the node and the data centre with the minimum number of hops in order to minimise the power consumption by reducing the number of transponders at intermediate nodes.

Thirdly we have investigated the problem of whether to locate data centres next to renewable energy or to transmit renewable energy to data centres in a given network topology under different traffic conditions and taking into account the network components' power consumption through a novel MILP model. We have identified the optimal location of data centres, so that the network's power consumption is minimised given a number of wind farms whose locations are known together with the electrical power transmission losses. We considered a network where the nodes that are not connected to wind farms have access to solar power. The results have shown that the optimal data centre locations are close to renewable energy sources. Combining optimal data centre locations with the multi-hop bypass heuristic, renewable energy and the replication scheme, power consumption savings of up to 73% have been achieved.

In Chapter 6, we have investigated energy efficient physical topology design for backbone IP over WDM networks. We have developed a novel MILP model to optimise the physical topology of IP over WDM networks with the objective of minimising the network power consumption. We have considered the NSFNET topology and compared its energy consumption with the energy consumption of optimised physical topologies under different traffic scenarios: symmetric full-mesh connectivity traffic matrix and asymmetric traffic demand where data centres create a hot node scenario in the network; and different nodal degree constraints. The power savings obtained were also investigated by deploying topologies that eliminate the need for IP routers, including a full mesh topology and a star topology. Furthermore the optimisation of the physical topology has been investigated

considering the presence of renewable energy sources in the network. The results have shown that optimising the physical topology increases the utilisation of the renewable energy sources.

Taking into account the embodied energy of the network devices in addition to the operational energy, we have reconsidered the energy efficiency of the physical topology of IP over WDM networks. We have disassembled the considered network devices to their basic components and materials, and we have estimated the total embodied energy of the devices based on the data available about the embodied energy of these components and materials. A novel MILP model has been developed to optimise the physical topology of IP over WDM networks with the objective of minimising both the operational and embodied energies in the network's commercial life time. Physical topology optimisation considering both operational and embodied energies has resulted in topologies with shorter links compared to operational-power-minimised topologies as the embodied energy of the optical fibre cable is the main contributor to the network total energy. Although optimising the physical topology considering both the operational and embodied energies has resulted in increasing the operational energy compared to the operational-power-minimised topologies, significant embodied energy savings have been achieved, resulting in a total energy saving of 47%.

In Chapter 7, we have investigated the joint optimisation of power, electricity cost and propagation delay in IP over WDM networks employing renewable energy. We have developed a novel MILP model to jointly minimise the three parameters and compared the results to the results of optimisation models that consider these parameters individually. The models results have shown that the joint optimisation maintains the power consumption and electricity cost savings obtained by the non-renewable power-minimised and the electricity cost-minimised models while hardly affecting the propagation delay. In addition, we also have investigated the energy savings achieved by jointly minimising the three parameters under an anycasting scenario where a number of data centres with replicated content exist in the network and nodes can download data from any of them. The NSFNET network with data centres at nodes 3, 5, 8, 10 and 12 has been considered to evaluate the optimisation problem under an anycasting access scenario. Compared to the delay-minimised

model, the power and cost savings under an anycasting scenario have increased to 82%.

In Chapter 8, the power consumption savings introduced by implementing data compression in IP over WDM networks was investigated. We have optimised the data compression ratio for traffic flows by developing a novel MILP model considering different IP over WDM approaches (bypass and non-bypass). For a real-time implementation, we have also developed a novel energy-efficient data compression and routing heuristic. The relationship between the incorrect rate of the original information source characters (ICR_c), data compression ratio and the bit error rate (BER) of the optical channel has been analysed and two approaches have been considered to maintain the ICR_c under the bypass approach: increasing the transmit power and limiting the data compression ratio. The results of the MILP model have shown that optimising the data compression ratios for bypass IP over WDM networks has saved up to 39% of the network power consumption where the transmit power is increased to maintain the ICR_c. Limiting the data compression ratio to maintain the ICR_c has slightly reduced the power savings achieved compared to the first approach. The results have also shown that higher power savings of 55% are obtained under the non-bypass approach and comparable power savings have been achieved by the heuristic. In addition, we have also evaluated the power consumption of the IP over WDM networks with data compression when using fixed line rate and Mixed Line Rate (MLR), respectively. The results have shown that joint use of MLR and data compression results in the energy consumption of the network being lower than that with the fixed line rate and data compression.

In Chapter 9, we have investigated the energy efficiency of optical OFDM-based networks. A novel MILP model was developed to minimise the total power consumption of optical OFDM networks. In this model, we have assumed that optical OFDM-based networks support three modulation levels: BPSK, QPSK and 8 QAM. We have also differentiated between two optimisation problems: power-minimised and spectrum-minimised optical OFDM-based networks. In power-minimised optical OFDM-based networks, the MILP model selects the modulation level that minimises the power consumption of the network. In spectrum-minimised optical OFDM-based networks, the highest modulation level will always be used, and as such the total bandwidth of the subcarrier is minimised. Simulation results

have shown that considering a symmetric traffic, the optical OFDM-based networks have saved up to 31% of the network total power consumption compared to conventional IP over WDM networks. Emphasising the power consumption of the optical layer, the optical OFDM-based network saves up to 55%, of the optical layer power consumption. The results have also shown that under an asymmetric traffic scenario, where more traffic is destined to or originates from popular nodes e.g. data centres, the power savings achieved by the optical OFDM-based networks are limited as the higher traffic demands to and from data centres reduce the bandwidth wastage associated with conventional WDM networks.

The topic of energy efficient optical networks is a hot research topic with several areas to be investigated. The energy efficient architectures, energy efficient routing heuristics, energy efficient physical topologies, energy efficient data compression proposed and results obtained in this thesis motivate the investigation of further issues in energy efficient optical networks.

The evaluation of the proposed architectures, physical topologies, routing heuristics and data compression has been limited to mathematical models and computer simulations. However, experimental demonstration is another method to evaluate the performance and verify the accuracy of the developed simulators and mathematical models by comparing the results obtained from the demonstrations with those obtained from simulations and models.

OBS based networks have attracted considerable attention in recent years. Compared to other current network switching technologies, OBS gives a possible solution to provide all-optical architectures which have a high potential to save energy in next generation optical core networks. Therefore, it is interesting to investigate the implementation of OBS with the energy efficient architectures proposed in this thesis.

Another interesting topic to investigate the energy savings associated with the use of forwarding and delay tolerant mechanism in optical networks. Usually these mechanisms are used in mobile networks and extreme environments lacking continuous connectivity. However they can potentially improve the performance of wavelength grooming in optical networks, which results in lower network resources usage and lower energy consumption.

Furthermore, network coding scheme is widely using in wireless network to eliminate the interference between uploading and downloading links and improve the throughput of wireless router by combining different traffic flows together. Therefore, it is very interesting to investigate that applying network coding scheme in optimal networks to further reduce the power consumption.

References

1. *"Growing Pains: Bandwidth on the Internet"*. 2010; Available from: http://www.isoc.org/isoc/conferences/bwpanel/docs/bp-growingp-201003-en.pdf.

2. K.G.Coffman and A.M.Odlyzko. *"Internet growth: Is there a "Moore's Law" for data traffic?"*. 2001; Available from: http://citeseerx.ist.psu.edu/.

3. U. Barth, et al. *"GreenTouch Roadmap: Strategic Research Areas and Project Portfolio"*. 2012; Available from: http://www.greentouch.org/uploads/documents/GreenTouch%20Strategic%20Research%20Areas%20and%20Project%20Portfolio.pdf.

4. Hecht, J. *"Ultrafast fibre optics set new speed record "*. 2011; Available from: http://www.newscientist.com/article/mg21028095.500-ultrafast-fibre-optics-set-new-speed-record.html.

5. Athineos, M. *"Realize the Goal of Reducing Energy Consumption and CO2 Emissions"*. 2010; Available from: http://www.emersonnetworkpower.com/en-US/Brands/EnergySystems/Documents/eSure/Shared/eSure%20White%20Paper.pdf.

6. *"BT Announces Major Wind Power Plans"*. 2007; Available from: http://www.commsbusiness.co.uk/News_Article_JS1.cfm?NewsID=3985&YearViewed=2007&Newsmonth=10&EndDay=31&StartDay=16&NoNews=0 .

7. Etoh, M., T. Ohya, and Y. Nakayama. *"Energy Consumption Issues on Mobile Network Systems"*. in *Applications and the Internet, 2008. SAINT 2008. International Symposium on*. 2008.

8. Plepys, A., *"The grey side of ICT"*. Environmental Impact Assessment Review, 2002. **22**(5): p. 509-523.

9. Baliga, J., K. Hinton, and R.S. Tucker. *"Energy Consumption of the Internet"*. in *Optical Internet, 2007 and the 2007 32nd Australian Conference on Optical Fibre Technology. COIN-ACOFT 2007. Joint International Conference on*. 2007.

10. Yamada, M., et al. *"Power Efficient Approach and Performance Control for Routers"*. in *Communications Workshops, 2009. ICC Workshops 2009. IEEE International Conference on*. 2009.

11. *SMART 2020 Report, Enabling the low carbon economy in the information age*. 2008; Available from: http://www.theclimategroup.org.

12. *"Green ICT Handbook: A Guide to Green ICT"*. 2009; Available from: http://www.globalactionplan.org.uk/sites/gap/files/Green%20ICT%20Handbook.pdf.

13. *"Wind farms to power BT"*. 2009; Available from: http://www.btplc.com/sharesandperformance/Annualreportandreview/Shareholdermagazine/May2009/windfarms.htm.

14. Gupta, M. and S. Singh, *"Greening of the Internet"*, in *SIGCOMM*2003, Proc. ACM.

15. Hamilton, J. *"Where Does Power Go and What to do about it?"*. 2008; Available from: http://www.scribd.com/doc/8940309/James-Hamilton-Where-Does-The-Power-Go.

16. ASSOCIATES, E.M., *"Data Center Management: The Key Ingredient for Reducing Server Power While Increasing Data Center Capacity"*, 2010.

17. Nanda, S. and T. Chiueh, *"A survey of virtualization technologies"*, in *Department of Computer Science, SUNY at Stony Brook*2005.

18. Hecht, J. *"A Short History of Fibre Optics"*. Available from: http://www.sff.net/people/jeff.hecht/history.html.

19. Lee, K.J. and T.J. Aprille. *"SONET evolution: the challenges ahead"*. in *Global Telecommunications Conference, 1991. GLOBECOM '91. 'Countdown to the New Millennium. Featuring a Mini-Theme on: Personal Communications Services*. 1991.

20. El-Gorashi, T.E.H., *"Optical Storage Area Networks"*, in *Electronic and Electrical Engineering*2009, Leeds. p. 175.

21. Tucker, R.S., G. Eisenstein, and S.K. Korotky, *"Optical time-division multiplexing for very high bit-rate transmission"*. Lightwave Technology, Journal of, 1988. **6**(11): p. 1737-1749.

22. Kawanishi, S., *"Ultrahigh-speed optical time-division-multiplexed transmission technology based on optical signal processing"*. Quantum Electronics, IEEE Journal of, 1998. **34**(11): p. 2064-2079.

23. Nakazawa, M., T. Yamamoto, and K. Tamura. *"Ultra high speed OTDM transmission using femtosecond pulses"*. in *Lasers and Electro-Optics, 2001. CLEO/Pacific Rim 2001. The 4th Pacific Rim Conference on*. 2001.

24. Wuth, T., M.W. Chbat, and V.F. Kamalov. *"Multi-rate (100G/40G/10G) Transport Over Deployed Optical Networks"*|. in *Optical Fiber*

communication/National Fiber Optic Engineers Conference, 2008. OFC/NFOEC 2008. Conference on. 2008.

25. Motorala. *"WDM/CWDM/DWDM: Segmentation Primer - Maximizing Capacity for Revenue"* 2008; Available from: http://www.motorola.com/staticfiles/Video-Solutions/_Documents/static%20files/WDM%20CWDM%20DWDM%20Segmentation%20Primer.pdf.

26. ITU-T. *"Recommendation G.694.2,Spectral grids for WDM applications: CWDM wavelength grid"*. 2003; Available from: http://www.itu.int/rec/T-REC-G.694.2-200312-I/en.

27. Pranggono, B. and J.M.H. Elmirghani. *"A novel optical storage area network implemented in a metro WDM setting"*. in *High Performance Switching and Routing, 2005. HPSR. 2005 Workshop on*. 2005.

28. Su Hwan, O., et al., *"Multiwavelength Lasers for WDM-PON Optical Line Terminal Source by Silica Planar Lightwave Circuit Hybrid Integration"*. Photonics Technology Letters, IEEE, 2007. **19**(20): p. 1622-1624.

29. Vasilyev, M., et al., *"Broadcast and select" OADM in 80 x 10.7 Gb/s ultra-longhaul network"*. Photonics Technology Letters, IEEE, 2003. **15**(2): p. 332-334.

30. Tonguz, O.K. and F.A. Flood, *"EDFA-based DWDM lightwave transmission systems with end-to-end power and SNR equalization"*. Communications, IEEE Transactions on, 2002. **50**(8): p. 1282-1292.

31. Sabella, R. and E. Iannone, *"Modular optical path cross-connect"*. Electronics Letters, 1996. **32**(2): p. 125-126.

32. Nakano, Y., et al., *"Optical Network Systems for Next-generation Networks"*. Hitachi Review, 2009. **58**: p. 31-35.

33. Finnie, G., *"DSL Acceleration: Making It Work"*, 2012.

34. Parrish, K. *"100 Mbps Could Finally Be Possible on DSL Lines"*. 2010; Available from: http://www.tomsguide.com/us/DSL-Broadband-NodeScale-Vectoring-Ikanos-VDSL,news-8459.html.

35. *"The 2012 FTTH European conference of Munich gives the European FTTx latest progress informations"*. 2012; Available from: http://www.china-pof.org/news/The-2012-FTTH-European-conference-of-Munich-gives-the-European-FTTx-latest-progress-informations-26.html.

36. *"ITU-T G.987.1 Telecommunication Standardization Sector of ITU"*. 2010; Available from: http://www.itu.int/rec/dologin_pub.asp?lang=e&id=T-REC-G.987.1-201001-I!!PDF-E&type=items.

37. Davey, R., et al., *Options for Future Optical Access Networks*, 2006.

38. Farahmand, F. and Q. Zhang. *"Circuit Switching"*. 2007; Available from: http://web.ccsu.edu/technology/farahmand/ccsu/courses/cet543/resources/ch69_circuit_switcing.pdf.

39. Hui, Z., et al., *"Dynamic lightpath establishment in wavelength routed WDM networks"*. Communications Magazine, IEEE, 2001. **39**(9): p. 100-108.

40. Lee, K.C. and V.O.K. Li, *"A wavelength rerouting algorithm in wide-area all-optical networks"*. Lightwave Technology, Journal of, 1996. **14**(6): p. 1218-1229.

41. Barry, R.A. and P.A. Humblet, *"On the number of wavelengths and switches in all-optical networks"*. Communications, IEEE Transactions on, 1994. **42**(234): p. 583-591.

42. Banerjee, A., et al., *"Generalized multiprotocol label switching: an overview of signaling enhancements and recovery techniques"*. Communications Magazine, IEEE, 2001. **39**(7): p. 144-151.

43. Jajszczyk, A. *"The ASON approach to the control plane for optical networks"*. in *Transparent Optical Networks, 2004. Proceedings of 2004 6th International Conference on*. 2004.

44. Yang, J., et al., *"All-Optical Contention Resolution with TTL-Aware Selective 3R Regeneration in Optical-Label Switching Router Networks"*, in *OFC/NFOEC 2008*2008: San Diego p. 1-3.

45. Bourzac, K. *"Optical memory could ease Internet bottlenecks"*. 2012; Available from: http://www.nature.com/news/optical-memory-could-ease-internet-bottlenecks-1.10108.

46. Guillemot, C., et al., *Transparent Optical Packet Switching: The European ACTS KEOPS Project Approach.* J. Lightwave Technol., 1998. **16**(12): p. 2117.

47. Chlamtac, I., et al., *"CORD: contention resolution by delay lines"*. Selected Areas in Communications, IEEE Journal on, 1996. **14**(5): p. 1014-1029.

48. Carena, A., et al., *"OPERA: an optical packet experimental routing architecture with label swapping capability"*. Lightwave Technology, Journal of, 1998. **16**(12): p. 2135-2145.

49. Hunter, D.K., et al., *"WASPNET: a wavelength switched packet network"*. Communications Magazine, IEEE, 1999. **37**(3): p. 120-129.

50. Guillemot, C., et al., *"Transparent optical packet switching: the European ACTS KEOPS project approach"*. Lightwave Technology, Journal of, 1998. **16**(12): p. 2117-2134.

51. Blumenthal, D.J., R.J. Feuerstein, and J.R. Sauer, *"First demonstration of multihop all-optical packet switching"*. Photonics Technology Letters, IEEE, 1994. **6**(3): p. 457-460.

52. Develder, C., et al. *"Optical Packet/Burst Switching"*. 2008; Available from: http://citeseerx.ist.psu.edu/viewdoc/summary?doi=10.1.1.68.5649.

53. Maier, M., *"Optical Switching Networks"*2008: Cambridge University Press

54. Battestilli, T. and H. Perros, *"An introduction to optical burst switching"*. Communications Magazine, IEEE, 2003. **41**(8): p. S10-S15.

55. Xiang, Y., et al., *"Traffic statistics and performance evaluation in optical burst switched networks"*. Lightwave Technology, Journal of, 2004. **22**(12): p. 2722-2738.

56. Vokkarane, V.M. and J.P. Jue, *"Prioritized burst segmentation and composite burst-assembly techniques for QoS support in optical burst-switched networks"*. Selected Areas in Communications, IEEE Journal on, 2003. **21**(7): p. 1198-1209.

57. Armitage, G.J. and K.M. Adams, *"How Inefficient is IP over ATM anyway"*, 1995: IEEE Network.

58. Gangxiang, S. and R.S. Tucker, *"Energy-Minimized Design for IP Over WDM Networks"*. Optical Communications and Networking, IEEE/OSA Journal of, 2009. **1**(1): p. 176-186.

59. Karamitsos, I.P. and E. Varthis. *"Routing mechanisms for IP over OBS-WDM optical networks"*. in *Electrotechnical Conference, 2004. MELECON 2004. Proceedings of the 12th IEEE Mediterranean*. 2004.

60. Yijun, X., M. Vandenhoute, and H.C. Cankaya, *"Control architecture in optical burst-switched WDM networks"*. Selected Areas in Communications, IEEE Journal on, 2000. **18**(10): p. 1838-1851.

61. Ferguson, T.S. *"Linear Programming"*. Available from: http://www.math.ucla.edu/~tom/LP.pdf.

62. Dantzig, G.B. and M.N. Thapa, *Linear Programming*1997: Springer.

63. Dantzig, G.B. and M.N. Thapa, *"Linear Programming 2: Theory and Extensions"*2003: Springer.

64. Brahma, S. *"The Ellipsoid Algorithm for Linear Programming"*. 2005; Available from: http://www.cs.princeton.edu/courses/archive/fall05/cos521/ellipsoid.pdf.

65. Hamad, A.M. and A.E. Kamal. *"Routing and wavelength assignment with power aware multicasting in WDM networks"*. in *Broadband Networks, 2005. BroadNets 2005. 2nd International Conference on*. 2005.

66. Ahmad, A., et al. *"Power-aware logical topology design heuristics in Wavelength-Routing networks"*. in *Optical Network Design and Modeling (ONDM), 2011 15th International Conference on*. 2011.

67. Larrosa, J., A. Oliveras, and E. Rodr´ıguez-Carbonell. *"Problem Solving and Constraint Programming"*. Available from: https://www.lsi.upc.edu/~erodri/webpage/rpar/s6.pdf.

68. Cornuejols, G. *"Valid Inequalities for Mixed Integer Linear Programs"*. 2006; Available from: http://integer.tepper.cmu.edu/webpub/integerRioMPSjuly.pdf.

69. Land, A.H. and A.G. Doig, *"An Automatic Method for Solving Discrete Programming Problems"*, in *"50 Years of Integer Programming 1958-2008"*2010, Springer. p. 105-132.

70. Mitchell, J.E. *"Branch-and-Cut Algorithms for Combinatorial Optimization Problems"*. 1999; Available from: http://128.113.2.9/~mitchj/papers/bc_hao.pdf.

71. Santi, P., *"Topology control in wireless ad hoc and sensor networks"*. ACM Computing Surverys, 2005. **37**(2): p. 164-194.

72. Mukherjee, B., *"Optical Communication Networks"*1997: McGraw-Hill.

73. Rodoplu, V. and T.H. Meng, *"Minimum energy mobile wireless networks"*. Selected Areas in Communications, IEEE Journal on, 1999. **17**(8): p. 1333-1344.

74. Jeng, A.A.K. and J. Rong-Hong, *"The r-Neighborhood Graph: An Adjustable Structure for Topology Control in Wireless Ad Hoc Networks"*. Parallel and Distributed Systems, IEEE Transactions on, 2007. **18**(4): p. 536-549.

75. Komali, R.S., A.B. MacKenzie, and R.P. Gilles, *"Effect of Selfish Node Behavior on Efficient Topology Design"*. Mobile Computing, IEEE Transactions on, 2008. **7**(9): p. 1057-1070.

76. Jeng, A.A. and J. Rong-Hong, *"Adaptive Topology Control for Mobile Ad Hoc Networks"*. Parallel and Distributed Systems, IEEE Transactions on, 2011. **22**(12): p. 1953-1960.

77. Ying, C. and A. Jaekel. *"Energy efficient grooming of scheduled sub-wavelength traffic demands"*. in *Optical Fiber Communication Conference and Exposition (OFC/NFOEC), 2011 and the National Fiber Optic Engineers Conference*. 2011.

78. Coiro, A., et al., *"Power-Aware Routing and Wavelength Assignment in Multi-Fiber Optical Networks"*. Optical Communications and Networking, IEEE/OSA Journal of, 2011. **3**(11): p. 816-829.

79. Bonetto, E., et al. *"Exploiting traffic dynamics in Power-Aware Logical Topology Design"*. in *Optical Communication (ECOC), 2011 37th European Conference and Exhibition on*. 2011.

80. Chiaraviglio, L., M. Mellia, and F. Neri. *"Reducing Power Consumption in Backbone Networks"*. in *Communications, 2009. ICC '09. IEEE International Conference on*. 2009.

81. Coiro, A., M. Listanti, and A. Valenti. *"Dynamic Power-Aware Routing and Wavelength Assignment for Green WDM Optical Networks"*. in *Communications (ICC), 2011 IEEE International Conference on*. 2011.

82. Zhu, Z. *"Mixed regenerator placement and routing and wavelength assignment for energy-efficient optical transport networks"*. in *Optical Communications and Networks (ICOCN 2011), 10th International Conference on*. 2011.

83. Ricciardi, S., et al. *"Energy-Aware RWA for WDM Networks with Dual Power Sources"*. in *Communications (ICC), 2011 IEEE International Conference on*. 2011.

84. Fernandez, N., et al. *"Cognition to design energetically efficient and impairment aware virtual topologies for optical networks"*. in *Optical Network Design and Modeling (ONDM), 2012 16th International Conference on*. 2012.

85. Tubaishat, M. and S. Madria, *"Sensor networks: an overview"*. Potentials, IEEE, 2003. **22**(2): p. 20-23.

86. Heinzelman, W.R., A. Chandrakasan, and H. Balakrishnan. *"Energy-efficient communication protocol for wireless microsensor networks"*. in *System Sciences, 2000. Proceedings of the 33rd Annual Hawaii International Conference on*. 2000.

87. Manjeshwar, A. and D.P. Agrawal. *"TEEN: a routing protocol for enhanced efficiency in wireless sensor networks"*. in *Parallel and Distributed Processing Symposium., Proceedings 15th International*. 2001.

88. Lindsey, S. and C.S. Raghavendra. *"PEGASIS: Power-efficient gathering in sensor information systems"*. in *Aerospace Conference Proceedings, 2002. IEEE*. 2002.

89. Ruay-Shiung, C. and K. Chia-Jou. *"An energy efficient routing mechanism for wireless sensor networks"*. in *Advanced Information Networking and Applications, 2006. AINA 2006. 20th International Conference on*. 2006.

90. Song, Y. and F. Kuipers. *"Energy-aware path selection for scheduled lightpaths in IP-over-WDM networks"*. in *Communications and Vehicular Technology in the Benelux (SCVT), 2011 18th IEEE Symposium on*. 2011.

91. Chabarek, J., et al. *"Power Awareness in Network Design and Routing"*. in *INFOCOM 2008. The 27th Conference on Computer Communications. IEEE*. 2008.

92. Wiatr, P., P. Monti, and L. Wosinska. *"Green lightpath provisioning in transparent WDM networks: Pros and cons"*. in *Advanced Networks and*

Telecommunication Systems (ANTS), 2010 IEEE 4th International Symposium on. 2010.

93. Cavdar, C., A. Yayimli, and L. Wosinska. *"Cutting the electric bill by routing and wavelength assignment with time-zones and time-of-use prices"*. in *Communications and Photonics Conference and Exhibition, 2011. ACP. Asia*. 2011.

94. Yong, W., et al. *"Power-Aware Routing and Wavelength Assignment in optical networks"*. in *Optical Communication, 2009. ECOC '09. 35th European Conference on*. 2009.

95. Wang, J., et al. *"Green-aware routing in GMPLS networks"*. in *Computing, Networking and Communications (ICNC), 2012 International Conference on*. 2012.

96. Wang, J., et al. *"Energy-aware routing optimization in dynamic GMPLS controlled optical networks"*. in *Transparent Optical Networks (ICTON), 2012 14th International Conference on*. 2012.

97. Verchere, D., et al. *"Routing protocol enhancements for power state engineering of green network elements"*. in *Networks and Optical Communications (NOC), 2012 17th European Conference on*. 2012.

98. Ramos, F.M.V., et al. *"Power Excursion Aware Routing in GMPLS-based WSONs"*. in *Optical Fiber Communication - incudes post deadline papers, 2009. OFC 2009. Conference on*. 2009.

99. Mingui, Z., et al. *"GreenTE: Power-aware traffic engineering"*. in *Network Protocols (ICNP), 2010 18th IEEE International Conference on*. 2010.

100. Athanasiou, G., et al. *"Introducing energy-awareness in Traffic Engineering for Future Networks"*. in *Network and Service Management (CNSM), 2011 7th International Conference on*. 2011.

101. Puype, B., et al. *"Power reduction techniques in multilayer traffic engineering"*. in *Transparent Optical Networks, 2009. ICTON '09. 11th International Conference on*. 2009.

102. Puype, B., et al. *"Energy efficient multilayer traffic engineering"*. in *Optical Communication, 2009. ECOC '09. 35th European Conference on*. 2009.

103. Poellabauer, C. and K. Schwan. *"Energy-aware traffic shaping for wireless real-time applications"*. in *Real-Time and Embedded Technology and Applications Symposium, 2004. Proceedings. RTAS 2004. 10th IEEE*. 2004.

104. Schoenen, R., et al. *"Green communications by demand shaping and user-in-the-loop tariff-based control"*. in *Online Conference on Green Communications (GreenCom), 2011 IEEE*. 2011.

105. Schoenen, R. and A. Otyakmaz. *"QoS and Flow Management for Future Multi-Hop Mobile Radio Networks"*. in *Vehicular Technology Conference Fall (VTC 2010-Fall), 2010 IEEE 72nd*. 2010.

106. Tucker, R.S. *"A green internet"*. in *IEEE Lasers and Electro-Optics Society, 2008. LEOS 2008. 21st Annual Meeting of the*. 2008.

107. Bathula, B.G. and J.M.H. Elmirghani. *"Green networks: Energy efficient design for optical networks"*. in *Wireless and Optical Communications Networks, 2009. WOCN '09. IFIP International Conference on*. 2009.

108. Idzikowski, F., et al. *"Saving energy in IP-over-WDM networks by switching off line cards in low-demand scenarios"*. in *Optical Network Design and Modeling (ONDM), 2010 14th Conference on*. 2010.

109. Warip, M.N.M., I. Glesk, and I. Andonovic. *"GMPLS energy efficiency scheme for Green Photonic Networks"*. in *Transparent Optical Networks (ICTON), 2010 12th International Conference on*. 2010.

110. Cerutti, I., N. Sambo, and P. Castoldi, *"Sleeping Link Selection for Energy-Efficient GMPLS Networks"*. Lightwave Technology, Journal of, 2011. **29**(15): p. 2292-2298.

111. De Turck, K., et al. *"Performance of the IEEE 802.16e Sleep Mode Mechanism in the Presence of Bidirectional Traffic"*. in *Communications Workshops, 2009. ICC Workshops 2009. IEEE International Conference on*. 2009.

112. PalChaudhuri, S. and D.B. Johnson. *"Power mode scheduling for ad hoc networks"*. in *Network Protocols, 2002. Proceedings. 10th IEEE International Conference on*. 2002.

113. Baldi, M. and Y. Ofek, *"Fractional Lambda Switching-Principles of Operation and Performance Issues"*. Transactions of The Society for Modeling and Simulation International, 2004. **80**(10): p. 527-544.

114. Baldi, M. and Y. Ofek. *"Time for a "Greener" Internet"*. in *Communications Workshops, 2009. ICC Workshops 2009. IEEE International Conference on*. 2009.

115. Van Heddeghem, W., et al. *"Energy-efficiency in telecommunications networks: Link-by-link versus end-to-end grooming"*. in *Optical Network Design and Modeling (ONDM), 2010 14th Conference on*. 2010.

116. Feng, M.Z., et al. *"Energy efficiency in optical IP networks with multi-layer switching"*. in *Optical Fiber Communication Conference and Exposition (OFC/NFOEC), 2011 and the National Fiber Optic Engineers Conference*. 2011.

117. Baliga, J., et al., *"Energy Consumption in Optical IP Networks"*. Lightwave Technology, Journal of, 2009. **27**(13): p. 2391-2403.

118. Palkopoulou, E., D.A. Schupke, and T. Bauschert. *"Energy efficiency and CAPEX minimization for backbone network planning: Is there a tradeoff?"*. in *Advanced Networks and Telecommunication Systems (ANTS), 2009 IEEE 3rd International Symposium on*. 2009.

119. Jingjing, Z. and N. Ansari, *"Toward energy-efficient 1G-EPON and 10G-EPON with sleep-aware MAC control and scheduling"*. Communications Magazine, IEEE, 2011. **49**(2): p. s33-s38.

120. Jingjing, Z., W. Ting, and N. Ansari. *"Designing energy-efficient optical line terminal for TDM passive optical networks"*. in *Sarnoff Symposium, 2011 34th IEEE*. 2011.

121. Skubic, B., et al., *"Energy-efficient next-generation optical access networks"*. Communications Magazine, IEEE, 2012. **50**(1): p. 122-127.

122. Osman, N.I., T. El-Gorashi, and J.M.H. Elmirghani. *"Reduction of energy consumption of Video-on-Demand services using cache size optimization"*. in *Wireless and Optical Communications Networks (WOCN), 2011 Eighth International Conference on*. 2011.

123. Chowdhury, P., et al., *"On the Design of Energy-Efficient Mixed-Line-Rate (MLR) Optical Networks"*. Lightwave Technology, Journal of, 2012. **30**(1): p. 130-139.

124. Yi, Z. and J.P. Jue. *"Energy-efficient flow aggregation for IPTV program delivery in optical backbone networks with multiple line rates"*. in *Optical Fiber Communication Conference and Exposition (OFC/NFOEC), 2011 and the National Fiber Optic Engineers Conference*. 2011.

125. Clemm., A., *"Network Management Fundamentals"*. 1st ed2006: Cisco Press.

126. Restrepo, J.C.C., C.G. Gruber, and C.M. Machuca. *"Energy Profile Aware Routing"*. in *Communications Workshops, 2009. ICC Workshops 2009. IEEE International Conference on*. 2009.

127. Mandviwalla, M. and T. Nian-Feng. *"Energy-efficient scheme for multiprocessor-based router linecards"*. in *Applications and the Internet, 2006. SAINT 2006. International Symposium on*. 2006.

128. Burd, T.D. and R.W. Brodersen. *"Design issues for Dynamic Voltage Scaling"*. in *Low Power Electronics and Design, 2000. ISLPED '00. Proceedings of the 2000 International Symposium on*. 2000.

129. Lahiri, A., N. Bussa, and P. Saraswat. *"A Neural Network Approach to Dynamic Frequency Scaling"*. in *Advanced Computing and Communications, 2007. ADCOM 2007. International Conference on*. 2007.

130. Tolle, G. and D. Culler. *"Design of an application-cooperative management system for wireless sensor networks"*. in *Wireless Sensor Networks, 2005. Proceeedings of the Second European Workshop on*. 2005.

131. Furthmuller, J., S. Kessler, and O.P. Waldhorst. *"Energy-efficient management of wireless sensor networks"*. in *Wireless On-demand Network Systems and Services (WONS), 2010 Seventh International Conference on*. 2010.

132. Hyunchul, K. and K. Jungsuk. *"Energy-efficient resource management in Wireless Sensor Network"*. in *Wireless Sensors and Sensor Networks (WiSNet), 2011 IEEE Topical Conference on*. 2011.

133. Kwang-Jin, P., et al. *"An Energy-Efficient Key Management Protocol For Large-Scale Wireless Sensor Networks"*. in *Multimedia and Ubiquitous Engineering, 2007. MUE '07. International Conference on*. 2007.

134. Cai, L.X., et al., *"Dimensioning network deployment and resource management in green mesh networks"*. Wireless Communications, IEEE, 2011. **18**(5): p. 58-65.

135. Sharma, P., et al. *"NEEM: Network energy efficiency manager"*. in *Network Operations and Management Symposium (NOMS), 2012 IEEE*. 2012.

136. Bashar, A., et al. *"Employing Bayesian Belief Networks for energy efficient Network Management"*. in *Communications (NCC), 2010 National Conference on*. 2010.

137. Lee, S.S.W., T. Po-Kai, and A. Chen. *"A Distributed Link Management Algorithm for Energy Efficient IP Networks"*. in *Global Telecommunications Conference (GLOBECOM 2011), 2011 IEEE*. 2011.

138. Jain, V., et al. *"Intelligent energy efficient network management across the access networks to CPE pathway"*. in *Integrated Network Management (IM), 2011 IFIP/IEEE International Symposium on*. 2011.

139. Youn-Kwae, J., H. Intark, and P. Kwang-Roh. *"A Network Level Power Management for Home Network Devices"*. in *Consumer Electronics, 2008. ICCE 2008. Digest of Technical Papers. International Conference on*. 2008.

140. Keyao, Z. and B. Mukherjee, *"Traffic grooming in an optical WDM mesh network"*. Selected Areas in Communications, IEEE Journal on, 2002. **20**(1): p. 122-133.

141. Yen-Wen, C. and C. Chung-Chi. *"Traffic modeling of a sub-network by using ARIMA"*. in *Info-tech and Info-net, 2001. Proceedings. ICII 2001 - Beijing. 2001 International Conferences on*. 2001.

142. He, W., Y. Hong, and W. Hongcai. *"A Fine Model for Evaluating Actual Output Performance of Crystalline Silicon Solar Modules"*. in *Photovoltaic Energy Conversion, Conference Record of the 2006 IEEE 4th World Conference on*. 2006.

143. Jianhua, Z., et al. *"24% efficient silicon solar cells"*. in *Photovoltaic Energy Conversion, 1994., Conference Record of the Twenty Fourth. IEEE*

Photovoltaic Specialists Conference - 1994, 1994 IEEE First World Conference on. 1994.

144. *"Cisco CRS-1 specification data sheet"*. Available from: http://www.cisco.com.

145. *"Glimmerglass System-600 data sheet"*. Available from: http://www.glimmerglass.com.

146. *"Cisco ONS 15454 data sheet"*. Available from: http://www.cisco.com.

147. Ye, T.T., L. Benini, and G. De Micheli. *"Analysis of power consumption on switch fabrics in network routers"*. in *Design Automation Conference, 2002. Proceedings. 39th*. 2002.

148. *IEEE802.3az*. Available from: http://www.ieee802.org/3/az/index.html.

149. Aber, J.D. and R. Freuder, *"Variation among solar radiation data sets for the Eastern US and its effects on predictions of forest production and water yield"*. Climate Research, 2000. **15**(1): p. 33-43.

150. Jewell, W. and R. Ramakumar, *"The Effects of Moving Clouds on Electric Utilities with Dispersed Photovoltaic Generation"*. Energy Conversion, IEEE Transactions on, 1987. **EC-2**(4): p. 570-576.

151. Group, I.E.E.E.S.; Available from: http://grouper.ieee.org/groups/802/3/eee_study/index.html.

152. *U.S. Environmental Protection Agency's Data Center Report to Congress*. Available from: http://tinyurl.com/2jz3ft.

153. Heller, B., et al., *"ElasticTree: saving energy in data center networks"*, in *Proceedings of the 7th USENIX conference on Networked systems design and implementation*2010, USENIX Association: San Jose, California. p. 17-17.

154. Loukopoulos, T. and I. Ahmad. *"Static and adaptive data replication algorithms for fast information access in large distributed systems"*. in *Distributed Computing Systems, 2000. Proceedings. 20th International Conference on*. 2000.

155. Rabinovich, M., et al. *"A dynamic object replication and migration protocol for an Internet hosting service"*. in *Distributed Computing Systems, 1999. Proceedings. 19th IEEE International Conference on*. 1999.

156. Wolfson, O., S. Jajodia, and Y. Huang, *"An adaptive data replication algorithm"*. ACM Trans. Database Syst., 1997. **22**(2): p. 255-314.

157. Sun, Z., et al., *"Internet QoS and traffic modelling"*. Software, IEE Proceedings -, 2004. **151**(5): p. 248-255.

158. sheet, Y.f.; Available from: http://www.youtube.com/t/fact_sheet.

159. Paneda, X.G., et al. *"Popularity analysis of a video-on-demand service with a great variety of content types: influence of the subject and video characteristics"*. in *Advanced Information Networking and Applications, 2006. AINA 2006. 20th International Conference on*. 2006.

160. Zhe, X., et al., *"Peer-to-peer based multimedia distribution service"*. Multimedia, IEEE Transactions on, 2004. **6**(2): p. 343-355.

161. Breslau, L., et al. *"Web caching and Zipf-like distributions: evidence and implications"*. in *INFOCOM '99. Eighteenth Annual Joint Conference of the IEEE Computer and Communications Societies. Proceedings. IEEE*. 1999.

162. *Drilling Down: What Projects Made 2008 Such a Banner Year for Wind Power?* ; Available from: http://www.renewableenergyworld.com/rea/news/article/2009/02/drilling-down-what-projects-made-2008-such-a-banner-year-for-wind-power?cmpid=WNL-Friday-February27-2009.

163. Rabinowitz, M., *"Advanced Power Transmission of the Future"*. Power Engineering Review, 2003. **20**(1): p. 5-21.

164. Labs, L.B.N. *"Benchmarking: Data Centers"*. 2007.

165. Kilper, D.C., G. Atkinson, and S. Korotky. *"Optical transparency and network energy efficiency"*. in *Transparent Optical Networks (ICTON), 2010 12th International Conference on*. 2010.

166. Chi, G. and V. Chan. *"Efficient physical topologies for regular WDM networks"*. in *Optical Fiber Communication Conference, 2004. OFC 2004*. 2004.

167. Guan, K.C. and V.W.S. Chan, *"Cost-Efficient Fiber Connection Topology Design for Metropolitan Area WDM Networks"*. Optical Communications and Networking, IEEE/OSA Journal of, 2009. **1**(1): p. 158-175.

168. Guan, K., et al. *"Topology formation for tactical networks with directional RF and free-space optical links"*. in *Military Communications Conference, 2008. MILCOM 2008. IEEE*. 2008.

169. Yufeng, X., G.N. Rouskas, and H.G. Perros, *"On the physical and logical topology design of large-scale optical networks"*. Lightwave Technology, Journal of, 2003. **21**(4): p. 904-915.

170. Baroni, S. and P. Bayvel. *"Key topological parameters for the wavelength-routed optical network design"*. in *Optical Communication, 1996. ECOC '96. 22nd European Conference on*. 1996.

171. Lodha, A., et al. *"CAVALIER architecture for metro Data Center Networking"*. in *Broadband Communications, Networks and Systems, 2008. BROADNETS 2008. 5th International Conference on*. 2008.

172. *Cisco Visual Networking Index: Forecast and Methodology, 2009 - 2014*. 2011; Available from: http://www.slideshare.net/jimkaskade/cisco-visual-networking-index-forecast-and-methodology-200914.

173. *Antenna Systems & Solutions, Inc*. Available from: http://www.antennasystems.com/af-fiberopticcable.html.

174. *Data sheet of Canadian Solar CS6P-230*. Available from: http://www.canadiansolar.com.

175. Humar, I., et al., *"Rethinking energy efficiency models of cellular networks with embodied energy"*. Network, IEEE, 2011. **25**(2): p. 40-49.

176. Williams, E., *"Energy Intensity of Computer Manufacturing: Hybrid Assessment Combining Process and Economic Input−Output Methods"*. Environmental Science & Technology, 2004. **38**(22): p. 6166-6174.

177. Singhal, P., *"Life Cycle Environmental Issues of Mobile Phones"*, in *Integrated Product Policy Pilot Project*2005: Finland.

178. Mahadevan, P., A. Shah, and C. Bash. *"Reducing lifecycle energy use of network switches"*. in *Sustainable Systems and Technology (ISSST), 2010 IEEE International Symposium on*. 2010.

179. Forster, C., et al., *"Understanding the Environmental Impact of Communication Systems"*, in *Ofcom Final Report*2009.

180. Badic, B., et al. *"Energy Efficient Radio Access Architectures for Green Radio: Large versus Small Cell Size Deployment"*. in *Vehicular Technology Conference Fall (VTC 2009-Fall), 2009 IEEE 70th*. 2009.

181. Manish Kumar Dixit, et al., *"Identification of Parameters for Embodied Energy Measurement: A Literature Review"*. Energy and Buildings, 2010. **42**(8): p. 1238-1247.

182. Yan, X., *"Energy Demand and Greenhouse Gas Emissions During the Production of A Passenger Car in China"*. Energy Conversion and Management, 2009. **50**(12): p. 2964-2966.

183. Scott, B. *"A gate-to-gate life-cycle inventory of solid hardwood flooring in the EasternUS"*. Wood and Fiber Science 2010; Available from: http://www.corrim.org/pubs/reports/2010/swst_vol42/79.pdf.

184. Duque Ciceri, N., T.G. Gutowski, and M. Garetti. *"A tool to estimate materials and manufacturing energy for a product"*. in *Sustainable Systems and Technology (ISSST), 2010 IEEE International Symposium on*. 2010.

185. Kemna, R., et al. *"Methodology study eco-design of energy-using products – MEEuP methodology report"*. 2005; Available from: http://ec.europa.eu/energy/demand/legislation/doc/2005_11_28_finalreport1_en.pdf.

186. Li, J., Z. Wu, and H.-C. Zhang, *"Application of neural network on environmental impact assessment tools"*. International Journal of Sustainable Manufacturing, 2008. **1**(1): p. 100-121.

187. *The monster footprint of digital technology*. Available from: http://www.lowtechmagazine.com/2009/06/embodied-energy-of-digital-technology.html.

188. *Data sheet of Cisco ONS 15501 EDFA*.

189. *Cisco ONS 15104 OC-48/STM-16 bidirectional regenerator data sheet*. Available from: http://www.cisco.com.

190. *Data sheet of Cisco ONS 15454 100-GHz 4-CH Multi/Demultiplexer*. Available from: http://www.cisco.com.

191. *Data sheet of Glimmerglass Intelligent Optical System 500*. Available from: http://www.glimmerglass.com/products/intelligent-optical-system-500/.

192. *PV FAQ: What is the energy payback for PV?* 2004; Available from: http://www.nrel.gov/docs/fy04osti/35489.pdf.

193. *Data sheet of CRS-1 16 slots chassis power systems*.

194. Wu, L., et al. *"A 2.8-MM imaging probe based on a high-fill-factor MEMS mirror and wire-bonding-free packaging for endoscopic optical coherence tomography"*. in *Micro Electro Mechanical Systems (MEMS), 2011 IEEE 24th International Conference on*. 2011.

195. Chu, P.B., et al., *"Design and nonlinear servo control of MEMS mirrors and their performance in a large port-count optical switch"*. Microelectromechanical Systems, Journal of, 2005. **14**(2): p. 261-273.

196. *Fiber Cable Design*. Available from: www.addison-tech.com.

197. *Data sheet of polybutylene terephthalate (PBT)*. Available from: http://www.dlftrade.com/files/PBT-GC.pdf.

198. *Emboided Energy*. Available from: http://www.greenspec.co.uk/embodied-energy.php.

199. *Mass, Weight, Density or Specific Gravity of Different Metals*. Available from: http://www.simetric.co.uk/si_metals.html.

200. Ericsson. *"Sustainable Energy Use in Mobile Communications"*. 2007; Available from: www.connectedurbandevelopment.org.

201. Cavdar, C., A. Yayimli, and L. Wosinska. *"How to cut the electric bill in optical WDM networks with time-zones and time-of-use prices"*. in *Optical Communication (ECOC), 2011 37th European Conference and Exhibition on*. 2011.

202. Lee, C.Y., P. Hyo Jung, and B. Jin woo. *"An Overlay Multicast to Minimize End-to-end Delay in IP Networks"*. in *Communication Technology, 2006. ICCT '06. International Conference on*. 2006.

203. Devetak, F., et al. *"Minimizing Path Delay in Multipath Networks"*. in *Communications (ICC), 2011 IEEE International Conference on*. 2011.

204. *Average Retail Price of Electricity to Ultimate Customers by End-use Sector, by State, EIA*. Available from: http://www.eia.doe.gov.

205. *Information and analysis on the economics of solar and alternative energies*. Available from: http://greenecon.net/understanding-the-cost-of-solar-energy/energy_economics.html.

206. Barr, K.C. and K. Asanovi, *"Energy-aware lossless data compression"*. ACM Trans. Comput. Syst., 2006. **24**(3): p. 250-291.

207. Neely, M.J. *"Dynamic data compression for wireless transmission over a fading channel"*. in *Information Sciences and Systems, 2008. CISS 2008. 42nd Annual Conference on*. 2008.

208. Le, W. and J. Manner. *"Evaluation of data compression for energy-aware communication in mobile networks"*. in *Cyber-Enabled Distributed Computing and Knowledge Discovery, 2009. CyberC '09. International Conference on*. 2009.

209. Tavli, B., I.E. Bagci, and O. Ceylan, *"Optimal data compression and forwarding in wireless sensor networks"*. Communications Letters, IEEE, 2010. **14**(5): p. 408-410.

210. Kilper, D. *"Insights on Coding and Transmission Energy in Optical Networks"*. in *2nd International Conference on Energy-Efficient Computing and Networking*. 2011.

211. *Cisco Visual Networking Index: Forecast and Methodology*. 2010-2015; Available from: http://www.cisco.com.

212. *Video Compression*. Available from: http://www.studiocodegroup.com/.

213. Wanke, J., et al., *"Topic models for semantics-preserving video compression"*, in *Proceedings of the international conference on Multimedia information retrieval*2010, ACM: Philadelphia, Pennsylvania, USA. p. 275-284.

214. Barr, K., K. Asanovi, and #263, *"Energy aware lossless data compression"*, in *Proceedings of the 1st international conference on Mobile systems, applications and services*2003, ACM: San Francisco, California. p. 231-244.

215. *Optimizing Web Graphics*. Available from: http://www.webreference.com/dev/graphics/compress.html.

216. *CebaTech Launches CebaRIP Library of Rapidly Tunable Intellectual Property Cores*. Available from: http://www.cebatech.com/news/press-

releases/110-cebatech-launches-cebarip-library-of-rapidly-tunable-intellectual-property-cores.html.

217. Leibo, L., et al. *"An ASIC implementation of JPEG2000 codec"*. in *Custom Integrated Circuits Conference, 2005. Proceedings of the IEEE 2005*. 2005.

218. Raul San Martin, J.P.K. *"Power-Profiler: Optimizing ASICs Power Consumption at the Behavioral Level"*. in *Design Automation, 1995. DAC '95. 32nd Conference on*. 1995.

219. *Image Data Compression Recommendation for space data system standards*, 2005, CCSDS 122.0-B-1. Blue Book.

220. Xiaodong, X. and Z. Yiqi. *"Design of Image Data Compression IP Core Based on Processor Local Bus"*. in *Database Technology and Applications (DBTA), 2010 2nd International Workshop on*. 2010.

221. *Data sheet of Xilinx Virtex II Pro*. Available from: http://www.xilinx.com/support/documentation/data_sheets/ds083.pdf.

222. Jaspers, E.G.T. and J. Groenenboom. *"Quantification of the optimal video-coding complexity for cost-efficient storage"*. in *Consumer Electronics, 2005. ICCE. 2005 Digest of Technical Papers. International Conference on*. 2005.

223. *Theory of Data Compression*. Available from: http://www.data-compression.com/theory.html.

224. Ramaswami, R. and K.N. Sivarajan, *"Optical Networks, A Practical Perspective"*. second edition ed2002: Morgan Kaufmann Publishers.

225. Boggia, G., P. Camarda, and V.G. Squeo. *"ROHC+: a new header compression scheme for TCP streams in 3G wireless systems"*. in *Communications, 2002. ICC 2002. IEEE International Conference on*. 2002.

226. Camarda, P. and S. Petrizzelli. *"Performance analysis of a new header compression scheme for TCP streams in IP based wireless networks"*. in *MILCOM 2002. Proceedings*. 2002.

227. Couvreur, A., et al., *"Performance analysis of a header compression protocol: The ROHC Unidirectional Mode Telecommunication Systems"*. Telecommunication Systems, Vol. 31, No. 1. (January 2006), pp. 85-98, doi:10.1007/s11235-006-5524-z Key: citeulike:524745, 2006. **31**(1): p. 85-98.

228. Girod, B., et al., *"Distributed Video Coding"*. Proceedings of the IEEE, 2005. **93**(1): p. 71-83.

229. Seo, K., et al., *"Evaluation of High-power Endurance in Optical Fiber Links"*. Furukawa Review, 2003. **24**(24): p. 17-22.

230. Menglin, L., M. Tornatore, and B. Mukherjee, *"New Strategies for Connection Protection in Mixed-Line-Rate Optical WDM Networks"*. Optical

Communications and Networking, IEEE/OSA Journal of, 2011. **3**(9): p. 641-650.

231. Jinno, M., et al., *"Spectrum-efficient and scalable elastic optical path network: architecture, benefits, and enabling technologies"*. Communications Magazine, IEEE, 2009. **47**(11): p. 66-73.

232. Takagi, T., et al. *"Algorithms for maximizing spectrum efficiency in elastic optical path networks that adopt distance adaptive modulation"*. in *Optical Communication (ECOC), 2010 36th European Conference and Exhibition on*. 2010.

233. Armstrong, J. *"OFDM: From Copper and Wireless to Optical"*. in *Optical Fiber communication/National Fiber Optic Engineers Conference, 2008. OFC/NFOEC 2008. Conference on*. 2008.

234. Armstrong, J., *"OFDM for Optical Communications"*. Lightwave Technology, Journal of, 2009. **27**(3): p. 189-204.

235. Rohling, M., et al., *"Broad-band OFDM radio transmission for multimedia applications"*. Proceedings of the IEEE, 1999. **87**(10): p. 1778-1789.

236. Bocoi, A., et al. *"Reach-dependent capacity in optical networks enabled by OFDM"*. in *Optical Fiber Communication - incudes post deadline papers, 2009. OFC 2009. Conference on*. 2009.

237. Christodoulopoulos, K., I. Tomkos, and E.A. Varvarigos, *"Elastic Bandwidth Allocation in Flexible OFDM-Based Optical Networks"*. Lightwave Technology, Journal of, 2011. **29**(9): p. 1354-1366.

238. Papandreou, N. and T. Antonakopoulos, *"Bit and power allocation in constrained multicarrier systems: the single-user case"*. EURASIP J. Adv. Signal Process, 2008. **2008**: p. 11.

239. Luschi, C., et al., *"Advanced signal-processing algorithms for energy-efficient wireless communications"*. Proceedings of the IEEE, 2000. **88**(10): p. 1633-1650.

240. Benlachtar, Y., et al., *"Generation of optical OFDM signals using 21.4 GS/s real time digital signal processing"*. Optics Express, 2009. **17**(20): p. 17658-17668.

241. Lowery, A.J., D. Liang Bangyuan, and J. Armstrong, *"Performance of Optical OFDM in Ultralong-Haul WDM Lightwave Systems"*. Lightwave Technology, Journal of, 2007. **25**(1): p. 131-138.

242. Jinno, M., et al., *"Distance-adaptive spectrum resource allocation in spectrum-sliced elastic optical path network [Topics in Optical Communications]"*. Communications Magazine, IEEE, 2010. **48**(8): p. 138-145.

243. Dischler, R. and F. Buchali. *"Experimental Assessment of a Direct Detection Optical OFDM System Targeting 10Gb/s and beyond"*. in *Optical Fiber communication/National Fiber Optic Engineers Conference, 2008. OFC/NFOEC 2008. Conference on*. 2008.

244. Goebel, B., et al. *"On the Effect of FWM in Coherent Optical OFDM Systems"*. in *Optical Fiber communication/National Fiber Optic Engineers Conference, 2008. OFC/NFOEC 2008. Conference on*. 2008.

245. Mahad, F. and A. Supaat, *"EDFA gain optimization for WDM system"*. Journal of Electrical Engineering, 2009. **11**(1): p. 34-37.

246. Kolpe, T., A. Zhai, and S.S. Sapatnekar. *"Enabling improved power management in multicore processors through clustered DVFS"*. in *Design, Automation & Test in Europe Conference & Exhibition (DATE), 2011*. 2011.

247. *Cisco ONS 15454 10-Gbps Multirate Transponder Card*. Available from: http://www.cisco.com.

248. *Cisco ONS 15454 40-Gbps Multirate Transponder Card*. Available from: http://www.cisco.com.

249. Chowdhury, P., M. Tornatore, and B. Mukherjee. *"On the energy efficiency of mixed-line-rate networks"*. in *Optical Fiber Communication (OFC), collocated National Fiber Optic Engineers Conference, 2010 Conference on (OFC/NFOEC)*. 2010.

250. Anderson, J. and M. Traverso, *"Optical transceivers for 100 gigabit Ethernet and its transport"*. Communications Magazine, IEEE, 2010. **48**(3): p. S35-S40.

251. Schares, L., et al., *"Terabus: Terabit/Second-Class Card-Level Optical Interconnect Technologies"*. Selected Topics in Quantum Electronics, IEEE Journal of, 2006. **12**(5): p. 1032-1044.

252. Glick, M., Y. Benlachtar, and R.I. Killey. *"Performance and power consumption of digital signal processing based transceivers for optical interconnect applications"*. in *Transparent Optical Networks, 2009. ICTON '09. 11th International Conference on*. 2009.

253. Poulton, K., et al. *"A 20 GS/s 8 b ADC with a 1 MB memory in 0.18 μm CMOS"*. in *Solid-State Circuits Conference, 2003. Digest of Technical Papers. ISSCC. 2003 IEEE International*. 2003.

254. Carena, A., et al., *"Maximum Reach Versus Transmission Capacity for Terabit Superchannels Based on 27.75-GBaud PM-QPSK, PM-8QAM, or PM-16QAM"*. Photonics Technology Letters, IEEE, 2010. **22**(11): p. 829-831.